CONDENSATION HEAT TRANSFER AND PRESSURE DROP OF PROPANE IN VERTICAL MINICHANNELS

A Thesis
Presented to
The Academic Faculty

By

Daniel Murphy

In Partial Fulfillment
Of the Requirements for the Degree
Master of Science in Mechanical Engineering

Georgia Institute of Technology

May 2014

CONDENSATION HEAT TRANSFER AND PRESSURE DROP OF PROPANE IN
VERTICAL MINICHANNELS

Approved by:

Dr. Srinivas Garimella, Adviser
School of Mechanical Engineering
Georgia Institute of Technology

Dr. S. Mostafa Ghiaasiaan
School of Mechanical Engineering
Georgia Institute of Technology

Dr. Sheldon M. Jeter
School of Mechanical Engineering
Georgia Institute of Technology

Date Approved: January 9, 2014

To my family

ACKNOWLEDGEMENTS

TABLE OF CONTENTS

LIST OF TABLES

LIST OF FIGURES

NOMENCLATURE

Latin Variables

A	Area, [m^2], Regression Coefficient, [-]
a	Regression Coefficient, [-]
B	Coefficient, [-]; Baffle Spacing, [m]
b	Regression Coefficient, [-]
Bo	Bond Number $= g\,(\rho_l - \rho_v)\,D^2 / (4\sigma)$, [-]
C	Chisholm Parameter, [-]; Terms in correlations; Tube Clearance, [m]
c	Regression Coefficient, [-]
C_0	Distribution Parameter, [-]
c_p	Specific Heat, [J kg^{-1} K^{-1}]
D	Diameter, [m]
E	Ratio of eddy conductivity to eddy viscosity, [-]
f	Darcy Friction Factor, [-]
F	Parameter in model, [-]
F_g	Correction coefficient for stratification, [-]
Fr	Froude Number $= G^2 / (gD\rho^2)$, [-]
G	Mass flux, [kg m^{-2} s^{-1}]
g	Acceleration due to gravity $= 9.81$ m s^{-2}
Gr	Grashof Number $= g\beta\varDelta TD^3 / \nu^2$, [-]
h	Heat Transfer Coefficient, [W m^{-2} K^{-1}]

H	Height, [m]
i	Specific Enthalpy, [kJ kg^{-1}]
i_{fg}	Latent Heat, [kJ kg^{-1}]
j	Superficial Velocity, [m s^{-1}]; Volumetric flux density, [m s^{-1}]
j^*	Dimensionless velocity, [-]
k	Thermal Conductivity, [W m^{-1} K^{-1}]; Slug length ratio correlating parameter, [-]
L	Length, [m]
m	Fin Parameter, [-]
$\dot{m}$	Mass Flow Rate, [kg s^{-1}]
n	Number of data points, [-]; Exponent in Blasius' Equation, [-]
N	Number of units, [-]
Nu	Nusselt Number $= hD / k$, [-]
P	Pressure, [kPa]
Pr	Prandtl Number $= c_p \mu / k$, [-]
P_r	Reduced Pressure, [-]
p_t	Tube Pitch, [m]
q	Regression Coefficient, [-]
$\dot{Q}$	Heat Duty, [W]
q''	Heat Flux, [W m^{-2}]
R	Thermal Resistance, [K W^{-1}]; Radius, [m]
r	Regression Coefficient, [-]; Correlation Coefficient, [-]
r^*	Radius Ratio of an Annulus, [-]

R^2	Coefficient of Determination, [-]
Ra	Rayleigh Number $= \rho g \beta \Delta T D^3 / \mu \alpha$, [-]
Ra^*	Modified Rayleigh Number, [-]
Re	Reynolds Number $= GD / \mu$, [-]
Re_l	Liquid Reynolds Number $= G(1-x)D / \mu_l$, [-]
Re_v	Vapor Reynolds Number $= GxD / \mu_v$, [-]
s	Regression Coefficient, [-]
Su	Suratman Number $= (\rho_v \sigma D)/\mu_v^2$, [-]
T	Temperature, [°C], [K]
U	Uncertainty, [%]
u	Velocity, [m s^{-1}]
UA	Heat Exchanger Conductance, [W K^{-1}]
$\dot{V}$	Volumetric Flow Rate, [L min^{-1}], [ft^3 min^{-1}]
$V_{g,j}$	Drift Velocity, [-]
v_z	Liquid film velocity, [m s^{-1}]
W	Width, [m]
We	Weber Number $= G^2 D / (\sigma \rho)$, [-]
x	Quality, [-]
X	Martinelli Parameter, [-]
z	Height, [m], Vertical Coordinate, [m], Exponent Parameter, [-]
Z	Shah's correlating dimensionless parameter

Greek Symbols

α	Void Fraction, [-]; Thermal Diffusivity [$m^2 s^{-1}$]
β	Constant, [-]; Volumetric Thermal Expansion Coefficient [K^{-1}]
Γ	Physical Property Coefficient, [-]
Δ	Change in quantity
δ	Film thickness, [m]
ε	Emissivity, [-]
ϵ_m, ϵ_h	Eddy Viscosity, Eddy Conductivity, [$m^2 s^{-1}$]
$\varepsilon_{\Delta P(b)}$	Dimensionless two-phase parameter, [-]
ζ	Natural convection parameter, [-]
η	Efficiency, [-]
θ	Liquid Pool Angle, [rad]; Ratio of the liquid-vapor pressure gradient, [-]
λ	Surface Tension Parameter, [-]
μ	Dynamic Viscosity, [$kg\ m^{-1} s^{-1}$]
ν	Kinematic Viscosity, [$m^2 s^{-1}$]
ρ	Density, [$kg\ m^{-3}$]
σ	Stefan-Boltzmann Constant = 5.67×10^{-8} W m^{-2} K^{-4}; Surface Tension, [$N\ m^{-1}$]
τ	Shear Stress, [Pa]
ϕ	Two-phase Multiplier, [-]
ψ	Surface Tension Parameter, [-]; Two-phase multiplier, [-]
Ω	Correction Factor, [-]
ω	Humidity ratio, [-]; Frequency, [$rad\ s^{-1}$]

Subscripts and Superscripts

+	Dimensionless quantity
adj	Adjusted
air	Air
Al	Aluminum
annulus	Annulus Section of the test section
bubble	Bubble in slug flow
C	Contraction
contraction	Contraction
deceleration	Deceleration Component
eff	Effective
eq	Equivalent
expansion	Expansion
f, frictional	Frictional Component
film bubble	Film-Bubble interface in slug flow
fin	Fin
flow	Open flow area
g	Gravity Component
h	Hydraulic Diameter
H	Homogeneous model
HT	Heat Transfer Length
in	Inner, Inlet
l	Liquid

line	Pressure tap lines
literature	Value from a published correlation
LM	Log Mean
lo	Liquid Only
loss	Ambient loss
m	Momentum Component
measured	Measured Value
OT	Outer Tube
out	Outer, Outlet
post	Post-Condenser
pre	Pre-Condenser
Propane	Propane
ratio	Ratio of two quantities
reducer	Reducer fitting in the test section
S	Separated Model
sat	Saturated conditions
single-phase	Single-Phase Conditions
slug	Liquid Slug
static	Static Head Component
T15	Turbulent conditions at Re = 15,000
tee	Tee fitting in the test section
test	Test Section
tp	Homogeneous two-phase property value

tt	Turbulent-turbulent flow conditions
two-phase	Two-Phase Conditions
unit cell	Consisting of one bubble and one liquid slug
v	Vapor
vo	Vapor Only
wall	Wall
water	Water
wetted	Wetted

Abbreviations

AAD	Average Absolute Deviation
AD	Average Deviation
LMTD	Log Mean Temperature Difference
STD	Standard Deviation

SUMMARY

Heat transfer coefficients and frictional pressure drops during vertical downward condensation of propane in minichannels are investigated. The main source of propane production in the US is in gas refineries. An understanding of the mechanisms of propane condensation will result in the design of better heat exchangers for use in gas separation processes. Also, hydrocarbons such as propane are promising as refrigerants because they have favorable thermal and transport properties along with low global warming potential. The literature on vertical condensation, especially of hydrocarbons for the tube sizes and flow conditions of interest to the present study, is limited.

An experimental facility is designed and constructed to measure the frictional pressure drop and local heat transfer coefficient of propane condensing in 1.93 mm diameter tubes. Measurements are taken over the entire quality range at approximately $\Delta x \approx 0.25$ increments. Two saturation temperatures are considered: 47°C and 74°C for mass fluxes ranging from 75 to 150 kg m^{-2} s^{-1}. Pressure drop increases with increasing mass flux and quality, and decreases with increasing saturation temperature. Heat transfer coefficients also shows similar trends, although there is a slight negative trend with increasing saturation temperature. None of the relevant correlations from the literature are able to satisfactorily predict the data from the present study over the entire operational range.

The data from this study are used to develop correlations for frictional pressure drop and local heat transfer coefficient based on the measurements and the underlying physical mechanisms of condensation. The pressure drop correlation predicts 85% of the

data to within ±25%, while the heat transfer coefficient correlation predicts 93% of the data to within ±25%.

The results from this study contribute to the understanding of condensation of hydrocarbons in vertical minichannels. The proposed models may be used to design heat exchangers and condensers for applications using propane as the working fluid.

CHAPTER 1: INTRODUCTION

An investigation of heat transfer and pressure drop during condensation of propane flowing in a vertically downward orientation in minichannels is conducted in this study. While condensation in minichannels has received considerable attention in recent years, there remains a scarcity of data on condensation of hydrocarbons in these geometries. Propane in particular is of interest due to its widespread use. This chapter briefly introduces the use of propane as a working fluid, applications in the petrochemical and refrigeration industries, current technologies employing propane, and a summary of the organization of this thesis.

1.1. The Need for Propane Condensation Studies

Heat transfer and pressure drop characteristics of propane are needed for a variety of applications. Propane is an important energy source with many uses in residential, commercial, industrial and agricultural sectors (Sloan and Wilczewski, 2013). Residential use constitutes about 60% of the total propane consumption in the US, primarily for space heating and cooking. Propane is an attractive alternative fuel source because it burns cleaner and is less expensive than heavier hydrocarbon mixtures. Propane-driven internal combustion engines are projected to see an increase in demand from less than 5000 vehicles sold in 2011 to over 40,000 vehicles sold in 2020. Petroleum product production is also increasingly making use of propane.

Related to the demand for propane in these diverse industries is a shift in propane production methods. In recent years, propane production from gas processing plants has increased significantly, making up 70% of the total US supply. Propane production from natural gas processing is projected to increase by 35% between 2012 and 2020. It is important for the petrochemical and process industries to be able to maximize propane production capacities to keep up with the demand.

Condensation studies are especially of interest to the petrochemical industry. Many processes in gas refineries rely on condensation to separate and liquefy petroleum gas (LPG) and its components. To produce propane, raw natural gas is heated and separated into its components through preferential condensation, which in many cases takes place in arrays of air-coupled heat exchangers. By predicting the condensation heat transfer and pressure drop in single channels, this study addresses tube-side phase change in such air-coupled cross-flow heat exchanger arrays used for LPG processes. Minichannel designs are being explored to take advantage of the high heat transfer coefficients experienced during condensation in such small diameter channels. By dividing the flow into a large number of small diameter tubes, higher working pressures can be accomodated with smaller tube wall thickness.

Condensers with small diameter tubes designed based on available correlations from the literature may not yield optimal performance, in particular because there are limited data for condensation of hydrocarbons in the vertically downward flow configuration. Data from the present study will contribute to correlations more relevant to such geometries, which can be used in minichannel heat exchanger design.

1.2. Propane (R290) as a Refrigerant

Since its inception, refrigeration technology has employed a wide variety of refrigerants that have continually evolved due to scientific, economic and social stimuli (Reif-Acherman, 2012). Although various hydrocarbons from petroleum distillation were introduced in the late 1800s as refrigerants, these were soon replaced by other, less flammable working fluids. Until the 1980s and 1990s, chlorofluorocarbons (CFCs, e.g. R12) have been the dominant refrigerants used due to their stability, low toxicity, and low flammability. Although CFCs have excellent thermal and transport properties, these fluids have a high ozone depletion potential (ODP). In the stratosphere, UV radiation decomposes CFCs to release chlorine (Cl_2), which reacts with ozone (O_3) and causes the depletion of the ozone layer leading to the phase-out of such refrigerants. Hydrochlorofluorocarbons (HCFCs, e.g. R22) decompose more before reaching the stratosphere and thus have a lesser effect on the ozone layer.

Although HCFCs have significantly lower ODP than CFCs, the global warming potential of these fluids has been a growing concern. This has led to efforts to find drop-in replacements to make use of existing equipment and infrastructure. Some hydrofluorocarbons (HFCs, e.g. R134a) have been able to accomplish this goal. However, there has been a push to regulate and eventually eliminate HFCs as well due to their high global warming potential. Due to these factors, natural refrigerants are being considered again as viable alternatives. Toxicity and flammability of these refrigerants are concerns for which new approaches are being developed. Table 1.1 shows a comparison of fluid and thermal properties between R22, R134a, and R290 (propane) at the two saturation temperatures of interest to the present study: 47°C and 74°C. These

Table 1.1: Refrigerant Property Comparison (EPA, 2010; Lemmon *et al.*, 2010)

	T_{sat} (°C)	P_{sat} (kPa)	i_{fg} (kJ kg^{-1})	σ (N m^{-1} × 10^3)	ODP	GWP	ρ (kg m^{-3}) liquid	vapor	μ (Pa·s × 10^6) liquid	vapor	k (W m^{-1} K^{-1} × 10^3) liquid	vapor
R22	47.0	1812	158.1	5.12	0.055	1810	1097	79.50	127.6	13.83	73.32	13.79
R22	74.0	3252	115.1	1.92			941.8	163.4	87.42	16.80	59.83	20.06
R134a	47.0	1221	155.3	5.26	0	1430	1116	60.97	147.5	12.74	71.72	16.32
R134a	74.0	2313	117.7	2.20			970.8	129.7	99.83	14.93	59.87	21.59
R290	47.0	1604	291.8	4.42	0	3.3	454.7	35.87	76.65	9.24	83.88	22.81
R290	74.0	2795	214.4	1.65			392.4	71.15	54.00	11.29	72.64	31.21

saturation temperatures correspond to pressures used in some gas separation processes. Propane has a higher latent heat and lower density than conventional refrigerants while maintaining a comparable saturation pressure and thermal conductivity. With the proper safety precautions, propane can be a promising choice as a low-GWP refrigerant.

1.3. Objectives of the Present Study

In view of the needs to understand condensation of hydrocarbons described above, the objectives of the study can be summarized as follows:

- Experimentally determine heat transfer coefficient and frictional pressure drop during condensation of propane flowing vertically downward in a single round tube with a 1.93 mm internal diameter. These parameters are measured for two saturation temperatures, 47°C and 74°C, over the mass flux range

$75 < G < 150$ kg m^{-2} s^{-1} and over the quality range from saturated liquid to saturated vapor.

- Compare the heat transfer and pressure drop data with predictions of the relevant correlations from the literature and provide explanations for agreement or disagreement between the present data and those predictions.

- Develop correlations to predict heat transfer and pressure drop for this flow orientation to serve as a basis for heat exchanger design tools.

1.4. Organization of the Thesis

The thesis is organized as follows:

- Chapter 2 provides a review of the relevant research on condensation heat transfer and pressure drop with special attention to studies on mini- and microchannels, vertical condensation, and hydrocarbon refrigerants. Deficiencies in the literature are highlighted.

- Chapter 3 describes the experimental methodology for all tests. The experimental facility is described in detail. The testing and validation procedures are described as well.

- Chapter 4 describes the analysis of the data and estimations of experimental uncertainties in key variables.

- Chapter 5 presents the experimental results of the validation and single-tube condensation experiments. The data are compared with predictions of relevant models and correlations from the literature. New correlations are also developed for vertical condensation based on these data.

- Chapter 6 summarizes the findings and draws conclusions from the results, and provides recommendations for future work.

CHAPTER 2: LITERATURE REVIEW

This chapter presents an overview of the relevant studies of in-tube condensation of refrigerants and hydrocarbons. The categories of study of interest to this work are primarily frictional pressure drop and heat transfer. However, because studies of the flow regimes and mechanisms are fundamentally relevant to understanding the experimental results, a brief review of some of those studies is presented as well.

2.1. Flow Regimes

The flow patterns in two-phase flow are governed by the influence of forces such as surface tension, inertia and gravity. Factors including tube diameter, orientation, geometry and fluid properties determine the forces that are dominant and thus, the flow regimes that will prevail. Much research on identifying flow regimes and transition criteria has been conducted for horizontal and vertical upward flow; however, the literature on vertical downward flow, which is of interest to the present study, is limited. A summary of the literature on flow regimes reviewed in this study is provided in Table 2.1.

Some of the commonly used flow regime maps for horizontal flow include Mandane *et al.* (1974), Taitel and Dukler (1976), Triplett *et al.* (1999), El Hajal *et al.* (2003) and Coleman and Garimella (2000b, 2003). The primary flow regimes observed in horizontal channels are bubble, plug, stratified, wavy, slug and annular flow. The flow regimes observed in vertical flow, however are somewhat different because of the different influence of gravitational forces on the flow pattern, and the absence of stratification. The most common vertical flow regimes are dispersed bubble (many small

Table 2.1: Summary of In-Tube Condensation Literature: Flow Regime Studies

Author	Fluids	D_h (mm)	Velocity Range (m s^{-1})	Operating Conditions	Orientation
Hewitt and Roberts (1969)	Air-Water	10 – 30	$0.17 < u_v < 45.02$ $0.08 < u_l < 2.77$	Adiabatic	Vertical, upward
Taitel *et al.* (1980)	Theoretical Study: claims general applicability			Adiabatic	Vertical, upward
Barnea *et al.* (1982)	Air-Water	25 – 51	$0.01 < u_v < 100$ $0.001 < u_l < 10$	Adiabatic	Vertical, downward
Mishima and Hibiki (1996)	Air-Water, Steam-Water	1 – 4	$0.0896 < u_v < 79.3$ $0.0116 < u_l < 1.67$	Adiabatic	Vertical, upward
Liu *et al.* (2005)	Air-Water, Air-Ethanol, Air-Oil	0.9 – 3	$0.008 < u_v < 1$ $0.008 < u_l < 1$	Adiabatic	Vertical, upward
Chen *et al.* (2006)	R134a	1.10 – 4.26	$u_v < 10$ m s^{-1} $u_l < 5$ m s^{-1}	Adiabatic	Vertical, upward
Dalkilic and Wongwises (2010a)	R134a	8.1	$300 – 515$ kg m^{-2} s^{-1}	Condensing $40 – 50°C$	Vertical, downward
Julia *et al.* (2013)	Air-Water	50.8	$0.01 < u_v < 10$ $0.1 < u_l < 2.5$	Adiabatic	Vertical, downward

bubbles in continuous liquid phase), bubbly (bubble size not as large as the channel), slug (long bullet shape), churn (distortion in bullet bubbles), and annular (continuous vapor core). Figure 2.1 shows a series of photographs depicting the various flow regimes observed in vertical flow (Chen *et al.*, 2006). Some of the relevent studies on vertical two-phase flow patterns are summarized here.

Hewitt and Roberts (1969) studied flow regimes and transitions for adiabatic upward flow. They used visual and x-ray photography to identify the distinct flow patterns of the air-water working fluid and developed a flow regime map based on data for tube diameters between 10 and 30 mm. The superficial velocity ranged from 0.17 to 45.02 m s^{-1} for the gas and 0.08 to 2.77 m s^{-1} for the liquid. The flow regime map is based on the superficial momentum flux of the liquid and gas phases defined as $\rho_l j_l^2$ and $\rho_v j_v^2$, respectively. The flow regimes identified were plug, churn, annular and wispy annular.

Dispersed Bubble | Bubbly | Slug | Churn | Annular | Annular - Mist
Ugs=0.25m/s Uls=1.90m/s | Ugs=0.01m/s Uls=0.28m/s | Ugs=0.13m/s Uls=0.07m/s | Ugs=0.65m/s Uls=0.07m/s | Ugs=6.62m/s Uls=0.11m/s | Ugs=6.74m/s Uls=0.03m/s
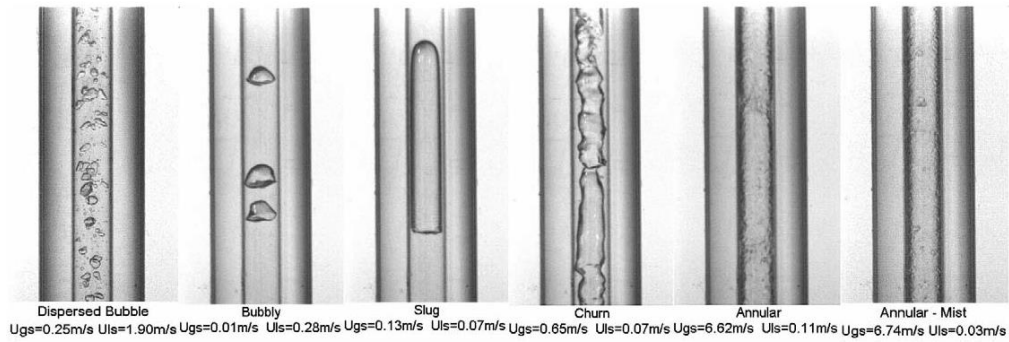
Figure 2.1: Photographs of upward two-phase flow regimes in 2 mm diameter channels (Chen et al., 2006)

They emphasize that this flow regime map is a first approximation that should be refined with more extensive data.

Taitel *et al.* (1980) developed flow regime transition criteria for vertical upward flow based on the underlying physical mechanisms. They note that most flow regime maps are empirically based and correlated to somewhat arbitrary coordinates. The physical parameters they considered in developing transition criteria included fluid properties, pipe size, flow rates, bubble packing density, and surface tension. They designated four flow regimes: bubble flow, slug flow, churn flow and annular flow. For the transition from bubbly to slug flow, the void fraction is compared to the packing density of the bubbles to determine when coalescence to a Taylor bubble will occur. They note that for tubes smaller than 5 cm diameter, bubbly flow cannot exist at low liquid superficial velocities. In modeling the transition between slug and churn flow, they propose that churn flow is an entrance effect to slug flow further downstream. The proposed transition to annular flow is independent of liquid velocity and diameter. The proposed transition criteria are reportedly valid for any pipe size and fluid properties. The superficial gas velocity above which the flow is annular is a function of the surface

9

tension and fluid densities. They compare their models with experimental results for air-water and natural gas-crude oil in tube diameters from $25 - 51$ mm. Their criteria show qualitative agreement with experimental results.

Barnea *et al.* (1982) developed a flow regime map for adiabatic vertical downward flow. They note that fewer studies have been conducted for vertical downward flow compared to horizontal or vertical upward flow. The tube diameters considered in this study were 25 and 51 mm. Three flow regimes were observed experimentally: annular flow, slug flow and dispersed bubble flow. They begin their analysis from the annular flow regime, described as the most natural in vertical downward flow. The transition from annular to slug flow was determined based on the liquid holdup (the cross sectional area of the liquid) in the tube and waviness in the fluid film. The transition from slug to bubble flow is due to the greater significance of turbulent forces compared to interfacial tension. This transition was shown to follow a mechanism similar to upward flow (Taitel *et al.*, 1980). It was observed that for smaller tube diameters, bubble flow cannot exist at higher gas superficial velocity. It should be noted that although this study investigates vertical downward flow, the diameters considered are considerably larger than those in the present study; therefore, the flow mechanisms and transitions between them may be different.

Mishima and Hibiki (1996) investigated several characteristics of two-phase flow in vertical capillary (small diameter) tubes with diameters between 1 and 4 mm. The goal in examining tubes of this size was to determine the effect of the increased influence of surface tension on the flow regime transitions, void fraction, bubble rise velocity and frictional pressure drop. The experimental apparatus consisted of a vertical Pyrex test

section with air and demineralized water as the working fluids. The flow regimes were observed using a high-speed video camera. They reported five major flow regimes for vertical upward flow along with four subcategories seen in capillary tubes but not in conventional tubes. The regimes observed were bubbly flow, slug flow, churn flow, annular flow and annular-mist flow. In bubbly flow, they reported that smaller bubbles formed a spiral, and larger bubbles collected into intermittent trains without coalescing. In slug flow, they observed longer slugs than those formed in conventional tubes. The flow regime transitions they identified agreed qualitatively with the criteria developed by Mishima and Ishii (1984).

Liu *et al.* (2005) studied two-phase adiabatic upward flow in vertical capillary tubes. They examined single tubes with diameter ranging from 0.9 mm to 3 mm and three working fluid combinations: air-water, air-ethanol and air-oil. The flow regimes were observed and bubble rise velocity measurements were taken using a high speed video camera. Five flow regimes were observed: bubbly flow, Taylor flow (slug flow), slug-bubbly flow, churn flow and annular flow. The bubbly flow regime was observed at high liquid and low gas velocities. Annular flow was expected to occur at higher gas and lower liquid superficial velocities than were considered in their experimental study.

Chen *et al.* (2006) examined two-phase flow regime patterns and transition criteria for R134a in adiabatic vertical upward flow. Tube diameter was varied from 1.10 mm to 4.26 mm to determine the effect of channel diameter on the observed flow regimes and transitions. Liquid and vapor superficial velocities were varied up to 5 and 10 m s^{-1}, respectively. Flow patterns in small channels are known to exhibit different characteristics due to the increased significance of surface tension and confinement. This

study proposed a critical diameter of about 2 below which "small tube characteristics" were observed. They note that while some researchers suggest that tube orientation has a smaller effect on flow patterns at small diameters, there is disagreement in the literature. The major flow regimes observed in this study were dispersed bubble, bubbly, slug, churn, and annular. In addition to these regimes, mist flow was observed in the larger channels and confined bubble flow, where the bubble size was the same as the tube diameter, was seen in the small diameter channels. Most of the existing flow regime maps did not predict the data well. They present a flow regime map based on their data and suggest that the Weber number may be a more appropriate parameter than superficial velocity for small diameter tubes.

Dalkilic and Wongwises (2010a) studied downward condensation of R134a in vertical tubes of 8.1 mm diameter. They used the annular flow model of Barnea *et al.* (1982) to determine the film thickness and void fraction in their experiments. By inspection through sight glasses at the inlet and outlet of the test section, they ensured that all of their experiments were conducted in the annular flow regime. The data were compared with multiple flow regime maps developed for vertical and horizontal orientations by Barnea *et al.* (1982), Hewitt and Roberts (1969), Baker (1954), Thome (2005), Kattan *et al.* (1998) and Chen *et al.* (2006). Based on the agreement of the data with these maps, it was determined that flow in the annular regime is independent of tube orientation.

Julia *et al.* (2013) studied global and local flow regimes in adiabatic vertical downward flow. They observe that understanding the differences in flow phenomena for vertical downward flow can be significant for applications in the process industry.

Experiments were conducted for air-water mixtures in vertical 50.8 mm diameter round tubes with a height of 3.8 m. These results for the larger diameter channels may not completely describe the phenomena observed in smaller diameter tubes. The superficial velocity ranged from 0.01 to 10 m s^{-1} for the gas and 0.1 to 2.5 m s^{-1} for the liquid. The flow regime was identified using three double-sensor conductivity probes positioned radially in the tube. These probes measured the bubble chord length. An artificial neural network was used to identify the flow regime at each probe based on the cumulative probability distribution function of the measurements. They identified five global flow regimes that are also seen in upward flow: bubbly flow, cap-bubbly flow, slug flow, churn-turbulent flow, and annular flow. They found that bubbly flow is similar to that seen in upward flow, but for downward flow, the bubbles tend to be located more toward the center of the tube. The higher concentration of bubbles in the center of the tube leads to a transition to cap-bubbly flow at lower gas fraction and containing larger cap bubbles than what is seen in upward flow. Slug flow looks significantly different in downward flow, characterized by an off-center Taylor bubble with the nose facing opposite the flow direction. Churn-turbulent flow is an unstable oscillatory regime. In downward flow, the annular regime can be subdivided to include falling-film flow and annular drop flow. They found the local flow regime combinations for bubbly and churn-turbulent flow to be similar for upward and downward flow. However, the local flow regimes observed in the cap-bubbly, slug and annular global regimes were different in downward flow.

The conditions of interest in the present study are vertical downward condensation in small channels. Although most of the literature addresses upward flow for adiabatic conditions, several conclusions can be drawn from these studies. As

diameter decreases, surface tension effects become more important. The differences between vertical upward and downward flow seem to mainly be in the local flow pattern behavior rather than the broader flow regime categories. It is expected that at small tube diameters, even the upward flow studies will provide reasonable estimates of the flow, but further study is needed in this area.

2.2. Frictional Pressure Drop

The two-phase frictional pressure drop is an important design parameter in many systems; therefore, it is desireable to be able to predict it accurately. Pressure drop depends on several factors including the flow mechanisms, interfacial shear stress, fluid properties and flow geometries. Several methods have been proposed to calculate the frictional pressure drop, but as with the flow regime studies, most studies have been performed for horizontal or vertical upward flow as opposed to vertical downward flow. This section provides a brief overview of the relevant literature on classical and multi-regime models. Many of the classical models make use of a two-phase multiplier to account for the differences from single-phase flow. A summary of the literature reviewed for frictional pressure drop is provided in Table 2.2.

Lockhart and Martinelli (1949) proposed a correlation for the frictional pressure drop of a two-phase mixture for different flow mechanisms. They identified four flow mechanisms for two-phase flow based on the liquid and gas Reynolds numbers:

Table 2.2: Summary of In-Tube Condensation Literature: *ΔP*

Author	Fluids	D_h (mm)	Flow Range	Saturation Conditions	Orientation
Lockhart and Martinelli (1949)	Air-Benzene, Kerosene, Water, Oil	1.49 – 25.83		Adiabatic	Horizontal
Chisholm (1973)	Various fluid mixtures			Adiabatic	Horizontal and Vertical
Friedel (1979)	H_2O, R113, R22, R12, R11, N_2, NH_3, air-water, air-oil, CH_4-water, etc.	5 – 51 3 – 260 1 – 200	32 – 8200 kg m^{-2} s^{-1} 20 – 8410 kg m^{-2} s^{-1} 2 – 10330 kg m^{-2} s^{-1}	20 – 72 bar 0.1 – 212 bar 0.02 – 178 bar	Vertical, downflow Vertical, upflow Horizontal
Beattie and Whalley (1982)	Various fluid mixtures			Adiabatic	Horizontal Vertical, upflow
Barnea (1990)	Various Fluids	> 50		Slug Flow	Vertical, upflow
Klausner *et al.* (1991)	R11	19.1	138 – 401 kg m^{-2} s^{-1}	Adiabatic Flow Boiling	Vertical, upflow Vertical, downflow
Mishima and Hibiki (1996)	Air-water	1 – 4	V:0.09 – 79.3 m s^{-1} L:0.01 – 1.67 m s^{-1}	Adiabatic	Vertical, upflow
Lee and Lee (2001)	Air-Water	0.78 – 6.67	V:0.05 – 18.7 m s^{-1} L:0.03 – 2.39 m s^{-1}	Adiabatic	Horizontal, rectangular
Chen *et al.* (2001)	Air-Water, R410a	1 – 9	50 – 3000 kg m^{-2} s^{-1}	298 K, 278 K	Horizontal
Cavallini *et al.* (2002)	R22, R134a, R125, R32, R236ea, R407c, R410a	8	100 – 750 kg m^{-2} s^{-1}	30 – 50°C	Horizontal
Garimella *et al.* (2005)	R134a	0.5 – 4.91	150 – 750 kg m^{-2} s^{-1}	1396 kPa	Horizontal
Liu *et al.* (2005)	Air-water/ethanol/oil	0.9 – 3		Adiabatic	
Zhang *et al.* (2010)	Air-water/ethanol/oil, N_2-water/R113, R12, R22, R134a, R404a, ammonia	0.07 – 6.25		Adiabatic Flow Boiling	Horizontal Vertical, upflow
Dalkilic *et al.* (2010)	R600a R134a	4 8.1	75 – 115 kg m^{-2} s^{-1} 300 – 400 kg m^{-2} s^{-1}	30 – 43°C 40 – 50°C	Horizontal Vertical, downflow
Kim and Mudawar (2012)	Air/CO_2/N_2-water, N_2-ethanol, R12, R22, R134a, R236ea, R245fa, R404a, R410a, R407c, propane, methane, ammonia, CO_2, water	0.07 – 6.22	4.0 - 8528 kg m^{-2} s^{-1}	$0.0052 < P_r < 0.91$	Horizontal Vertical, upflow
Lips and Meyer (2012)	R134a	8.38	200 - 600 kg m^{-2} s^{-1}	40°C	Horizontal Inclined/ Vertical – upflow and downflow

turbulent-turbulent, laminar-turbulent, turbulent-laminar, and laminar-laminar. Although the data considered were for adiabatic conditions, they suggest that the correlation is applicable for phase change processes as well. Data from four studies in the literature were correlated using the Martinelli parameter defined as the ratio of the pressure drop assuming liquid flow to the pressure drop assuming vapor flow:

$$X^2 = \frac{(dP/dz)_l}{(dP/dz)_v} \tag{2.1}$$

This parameter was used to determine a two-phase multiplier that correlates the two-phase and single-phase pressure drops:

$$\phi_l^2 = \frac{(dP/dz)_f}{(dP/dz)_l} \tag{2.2}$$

Lockhart and Martinelli presented empirical curves to represent their data graphically; however, they did not present an equation that could be used for design calculations. Chisholm (1967) expanded on their analysis and proposed an expression for the liquid two-phase multiplier of Lockhart and Martinelli (1949):

$$\phi_l^2 = 1 + \frac{C}{X} + \frac{1}{X^2} \tag{2.3}$$

where the Chisholm parameter C depends on the liquid-vapor flow mechanisms as defined by Lockhart and Martinelli. Re = 2000 represents the transition boundary between turbulent and laminar flow for each phase. The single-phase liquid pressure gradient is given by:

$$\left(\frac{dP}{dz}\right)_l = \frac{1}{2} f_l \frac{((1-x)G)^2}{\rho_l D} \tag{2.4}$$

16

Chisholm (1973) also studied the frictional pressure gradient of two-phase flows during evaporation. He proposed a new expression for a two-phase multiplier (ϕ_{lo}^2) defined as the ratio of the two-phase pressure drop to the liquid-only pressure drop. Liquid-only refers to the treatment of the entirety of the flow in the channel as liquid at the same mass flux as the two-phase flow. A parameter Γ, analogous to the Martinelli parameter for liquid-only and vapor-only pressure gradients, was introduced. The two-phase multiplier takes the form:

$$\phi_{lo}^2 = 1 + (\Gamma^2 - 1)\left(Bx^{(2-n)/2}(1-x)^{(2-n)/2} + x^{2-n} \right) \tag{2.5}$$

where B is a function of mass flux and Γ. The exponent n is the power to which the Reynolds number is raised in the Blasius friction factor equation.

Friedel (1979) compiled a data bank of over 25,000 fictional pressure drop measurements to develop a more widely applicable correlation. The data included horizontal, vertical upflow and vertical downflow orientations. The tube orientation was distinguished because of the significant difference between upward and downward flow in slip behavior and momentum exchange in the phases. The fluids considered mostly consisted of water, R12, air-water and air-oil, although other synthetic refrigerants, ammonia, methane-water and other single and two-component fluids were present in the data bank. The tube geometry was primarily circular but some data for rectangular and annular tubes were also included. It was determined through statistical regression that the most significant parameters affecting frictional pressure drop were mass flow rate, quality, hydraulic diameter, length, gravity, and fluid properties. Only about one third of the data were used in the model development, but the remainder were used to evaluate the model results. For vertical downward flow, both single- and two-component mixture

17

studies were included. A two-phase multiplier for the liquid-only pressure drop was proposed for horizontal and vertical upward flow, and a different correlation was proposed for vertical downward flow. The vertical downward flow multiplier takes the following form:

$$\phi_{lo}^2 = C_{F1} + \frac{48.6C_{F2}}{\text{Fr}^{0.03}\text{We}^{0.12}} \tag{2.6}$$

where C_{F1} and C_{F2} are functions of the quality, property ratios of the liquid and vapor phases, and liquid- and vapor-only friction factor. The Weber number and Froude number are also included in the correlation. The most significant difference between the downflow correlation and the horizontal and upflow correlations is the larger coefficient on the C_{F2} term, indicating a larger pressure drop than in identical conditions for other orientations. This is mainly due to greater void fraction and smaller slip ratio for this orientation.

Beattie and Whalley (1982) developed a simple two-phase pressure drop correlation that implicitly accounts for flow regimes rather than explicitly specifying transition criteria. They note that especially in the annular and bubbly regimes, the homogeneous model is valid for the void fraction. They propose calculating a two-phase friction factor based on the Colebrook-White equation (Colebrook, 1939). The homogeneous two-phase density is used. The two-phase viscosity is a combination of expressions for bubble flow and annular flow:

$$\mu = \mu_l(1+\alpha_{\text{homogeneous}})(1+2.5\alpha_{\text{homogeneous}}) + \mu_v\alpha_{\text{homogeneous}} \tag{2.7}$$

These properties are used to calculate a two-phase Reynolds number. Because turbulent effects are seen in two-phase flows at very low Reynolds number, they recommend

applying the friction factor equation for all Reynolds numbers rather than only those in the turbulent regime. The proposed model was compared with a data bank for adiabatic horizontal and vertical upward flows. The model predicted the data as well as other more complicated correlations.

Barnea (1990) examined the assumptions used to calculate two-phase pressure drop in vertical slug flow. She assessed the validity of a common simplification in slug flow modeling: the assumption that the Taylor bubble is cylindrical in shape with a flat nose rather than a curved nose. This investigation was primarily analytical and focused on vertical upward air-water flow in large tubes ($D > 50$ mm). In this geometry, it was noted that the liquid film around the upward flowing Taylor bubble changes direction and behaves as a downward falling film. Five methods of calculating the pressure drop in slug flow were compared. The pressure drop was overpredicted if the Taylor bubble was modeled using the simplifying assumption of a flat nose rather than the more physically accurate curved nose shape. It was seen that the liquid holdup is independent of the bubble shape, the bubble length, and the liquid slug length. Therefore the slug geometry is not needed to determine the hydrostatic pressure drop.

Klausner *et al.* (1991) experimentally investigated the two-phase frictional pressure drop and void fraction for R11 in adiabatic and flow boiling conditions. They conducted experiments using vertical 19.1 mm diameter tubes in both the upward and downward flow directions. The mass flux range in these experiments was 138 to 401 kg m^{-2} s^{-1}. The pressure drop and volume fraction in the test section was measured using a liquid balancing column. This method enabled more accurate measurements of the gravitational component of the pressure drop as well as the volume fraction. Their

experimental data along with other data from the literature were used to develop correlations for the void fraction and frictional pressure drop in vertical tubes. A "characteristic shear stress" defined, based only on the frictional pressure gradient, rather than the interfacial shear stress, based on the total pressure gradient, was used to develop the correlation to avoid negative values of the shear stress in cases where gravitational head exceeds frictional losses.In downflow conditions, capillary waves were observed in the annular liquid film. These were not present for the upward flow orientation. Because of a strong correlation between the "characteristic friction factor," defined using the "characteristic shear stress" described above, and the Weber number defined by the film thickness, it was concluded that the capillary waves have a significant influence on frictional pressure drop in vertical downward flow. It was also noted that due to the greater stability of downward flow in the annular regime, there was less breakup of the liquid film leading to smaller pressure drops than for upward flow. Although the focus of the present study is on condensation rather than adiabatic or boiling flow, this study provides insights into the differences between upward and downward two-phase flow orientations.

Mishima and Hibiki (1996) developed a model for the frictional pressure drop in vertical upward flow of air-water mixtures in capillary tubes ($1 - 4$ mm diameter). Because of the significance of the internal diameter to the calculation, the diameter measurement was determined by examining the pressure drop of single-phase laminar flow through the tube. The friction factor for Hagen-Poiseuille flow is given by $f = 64 / \text{Re}$. This relationship was used to iteratively obtain the internal diameter of the tube with $\pm$ 2% uncertainty. The pressure drop model was based on the Lockhart-

Martinelli method (Lockhart and Martinelli, 1949) with the two-phase multiplier following Chisholm (1967), Eq. (2.3). Their model presents a modification to the Chisholm parameter to account for changes in diameter:

$$C = 21\left(1 - e^{-0.319D}\right) \tag{2.8}$$

where D is the tube diameter in millimeters.

Lee and Lee (2001) developed a correlation for the two-phase frictional pressure drop in horizontal rectangular channels with hydraulic diameter $0.78 < D_h < 6.67$ mm. Experiments were conducted using a 20 mm wide test section with the channel height varying between 0.4 mm and 4 mm. The water and air superficial velocities ranged from 0.03 to 2.39 m s^{-1} and from 0.05 to 18.7 m s^{-1}, respectively. The experimental facility was validated by comparing the single phase friction factor for air to laminar and turbulent flow models. The two-phase pressure drop model was developed following the method of Lockhart and Martinelli (1949). The Chisholm parameter C showed poor agreement with the Lockhart and Martinelli model, especially for the laminar-laminar regime and the smallest channel size, in which the flow pattern is mostly plug or slug flow. As in Lockhart and Martinelli's model, the flow was classified into four regimes, but the value of C was modified to account for surface tension, channel size, and flow rate. Their model was able to predict their data to within $\pm10\%$ as well as predict the data from other horizontal and vertical studies to within $\pm20\%$.

Chen *et al.* (2001) examined the applicability of the homogeneous and Friedel (1979) models for two-phase pressure drop to small tubes. They noted that many of the major empirical correlations were developed for tube diameters greater than 10 mm and therefore may not be suitable predictors for tubes in the 1 to 9 mm diameter range. An

21

experimental study was performed to measure the frictional pressure drop of two-phase R410A and air-water mixtures in round horizontal tubes. For the R410A experiments, the diameter was varied from 1 to 7 mm, while the mass flux was varied from 50 to 600 kg m^{-2} s^{-1}. For the air-water experiments, the diameter ranged from 3 to 9 mm, while the mass flux was between 50 and 3000 kg m^{-2} s^{-1}. It was observed that the homogeneous model predicted the data the best. Both models still significantly overpredicted the data in the air-water experiments and underpredicted the data for R410A. Modifications to both correlations using the Bond number and Weber number were proposed to better account for surface tension effects at small tube diameters. The modified correlations were used to predict their experimental data as well as the data from other studies in the literature. The mean deviation from the data was improved from 53.7% to 30.9% using a modification to the homogeneous model, and from 218.0% to 19.8% using a modification to the Friedel correlation.

Cavallini *et al.* (2001, 2002) investigated heat transfer and pressure drop during condensation of seven synthetic refrigerants. The working fluids investigated included pure HCFCs and HFCs as well as azeotropic and zeotropic mixtures. Models were developed from a data bank of 600 data points for condensation in 8 mm diameter horizontal tubes. In the data bank, the saturation temperature ranged from 30°C to 70°C, and the mass flux ranged from 100 to 750 kg m^{-2} s^{-1}. The models were also compared to 1778 data points for HCFC and HFC refrigerants as well as 386 data points for CFC refrigerants. The data were grouped into flow regimes based on the dimensionless vapor velocity ($j_v^* = xG / [gD\rho_v(\rho_l - \rho_v)]^{0.5}$) and the turbulent-turbulent Martinelli parameter (X_{tt}). Based on flow regime transition criteria from the literature (Breber *et al.*, 1980; Sardesai

et al., 1981; Tandon *et al.*, 1982; 1985; Dobson and Chato, 1998), flows with dimensionless vapor velocity > 2.5 were assigned to the annular flow regime. Below this value, wavy-stratified flow and slug flow were observed with a transition at $X_{tt} = 1.6$. The pressure drop model was developed using the Friedel (1979) two-phase multiplier. It was observed that heat transfer correlations that use the Friedel pressure drop correlation such as Kosky and Staub (1971) failed to adequately predict the data in the annular regime. They note that the Friedel correlation was developed to cover all flow regimes and therefore may not be best suited for the annular regime specifically. For the annular regime, a regression analysis was performed on the data set to adjust the coefficients for the Friedel horizontal pressure drop correlation. The resulting equation predicted the data with an average deviation of -7% and an average absolute deviation of 14%. Cavallini *et al.* (2009) proposed a similar model to account for factors such as entrainment, surface roughness and smaller diameters.

Garimella *et al.* (2005) studied horizontal condensation of R134a for tube diameters ranging from 0.5 to 4.9 mm at a saturation pressure of 1396 kPa (52.3°C). An experimentally validated multiple flow regime pressure drop model was developed from these data and previous studies. Previous work by Coleman and Garimella (2000b) on flow regime identification was used to assign appropriate flow regimes to the pressure drop data. Distinct models were developed for intermittent/wavy flow and annular/mist/dispersed flow based on previous work by Garimella *et al.* (2002), Garimella *et al.* (2003), and Garimella (2003). The intermittent flow model included the contributions of the liquid slug, the film-slug interface and the slug-to-bubble transitions. A slug frequency model was developed for this regime. The annular model was

developed by relating the measured interfacial shear stress to the corresponding single-phase friction factor. The data were grouped based on liquid-phase laminar ($Re_l < 2100$) and turbulent ($Re_l > 3400$) flow. Linear interpolation was used to determine the pressure drop in the transition region. Surface tension effects were accounted for by including the non-dimensional parameter ψ, as defined by Lee and Lee (2001), in the expression for the interfacial friction factor. The model predicted 82% of the experimental data to within $\pm 20\%$. It also showed the decrease in two-phase pressure drop towards the single-phase gas value at high quality ($x \gtrsim 0.9$).

Liu *et al.* (2005) observed that the Lockhart-Martinelli and homogeneous pressure drop models did not accurately describe their data at low liquid flow rates. They proposed a flow regime dependent model based on a two-phase dimensionless pressure factor similar to the Fanning friction factor in single-phase flow. They determined that when the ratio of the gas-to-liquid superficial velocities was greater than 0.5, the homogeneous model could be used to calculate frictional pressure drop. Below this transition criterion, they proposed a correlation for the pressure factor that was dependent on the slip ratio and modified Reynolds number of the flow based on the two-phase mixture velocity and fluid properties.

Zhang *et al.* (2010) modified the Mishima and Hibiki (1996) correlations for frictional pressure drop and void fraction in minichannels. They noted that the Lockhart and Martinelli (1949) forms of determining frictional pressure drop were generally good predictors of the data. They expressed concerns that the dimensional nature of the Mishima and Hibiki correlations would cause difficulty in scaling the physical phenomena for two-phase flow. Therefore, nondimensional parameters were sought to

replace the hydraulic diameter in the previous correlations. Using an artificial neural network and a database of 2201 data points from 13 studies, the Laplace constant, also known as the confinement number or the Suratman number ($Su = [\rho_v \sigma D_h]/\mu_v^2$), was identified as the best nondimensional substitute for the hydraulic diameter. One advantage of the Laplace constant is that it scales with the wavelength of Rayleigh-Taylor instabilities that influence transitions between flow regimes. The database consisted of measurements of adiabatic flow of pure and mixed fluids as well as flow boiling in horizontal and vertical upward flow. The channel hydraulic diameters considered ranged from 0.07 to 6.25 mm. The majority of the data was in the laminar-laminar region according to the flow divisions defined by Lockhart and Martinelli ($Re_l <$ 2000, $Re_v < 2000$). They noted that the Reynolds number may be a more significant parameter when predicting pressure drop in the turbulent-turbulent regime. The resulting correlation predicted the data with a mean deviation of 17.9% for adiabatic two-phase mixtures and 21.7% for adiabatic two-phase flow of pure fluids.

Dalkilic *et al.* (2010) measured the frictional pressure drop during condensation of R600a (isobutane) and R134a. The tests with R600a were in horizontal circular tubes with a 4 mm diameter and mass flux ranging from 75 – 115 kg m^{-2} s^{-1}. The tests with R134a were in vertical downward circular tubes with a diameter of 8.1 mm and mass flux ranging from 300 to 400 kg m^{-2} s^{-1}. All the experiments in this study were performed in the annular flow regime; therefore, the quality range for R600a was 0.45 – 0.9 while for R134a, it was 0.7 – 0.95. The measured frictional pressure drop was compared with correlations in the literature. It was observed that the Cavallini *et al.* (2002) and Chen *et al.* (2001) correlations predicted the vertical downward pressure drop in the R134a tests

the best. Of these two, only the Chen correlation was also able to predict the R600a data. It was noted that the pressure drop during annular flow was independent of tube orientation.

Kim and Mudawar (2012) compiled a database of 7115 frictional pressure drop data points from 36 different sources to develop a universal correlation for frictional pressure drop applicable to many different fluids, geometries and flow conditions. They note that a fundamental difference in two-phase flow patterns between boiling flows and adiabatic or condensing flows is the presence of entrained droplets in annular flow. Therefore, their database consisted of only adiabatic and condensing two-phase conditions, because the annular regime is usually dominant in mini- and microchannels. The diameters considered ranged from 0.0695 to 6.22 mm, and the mass flux range considered was 4.0 to 8528 kg m^{-2} s^{-1}. The majority of the data is for horizontal channels; however, one study (135 data points) with vertical upward flow was also included. They compared many common correlations with their database and noted that only a few were able to adequately predict the full body of data. Therefore a new model was presented as a modification to the Lockhart and Martinelli (1949) correlation. Because shear and surface tension effects are stronger than gravitational effects for mini- and microchannels, an expression for *C* was determined using dimensionless groups such as the Reynolds number, Suratman number, and density ratio. The resulting model showed good agreement with the data, having an average absolute deviation of 23.3% over the entire database. However, they note the need for mechanistic theoretical models in the future.

Lips and Meyer (2012) experimentally investigated the frictional pressure drop and void fraction of condensing R134a in inclined tubes with an 8.38 mm diameter.

Experiments were performed for mass flux ranging from 200 to 600 kg m^{-2} s^{-1} and saturation temperature 40°C. They note several significant differences in the pressure drop between horizontal, downward and upward flow. The pressure drop in the test section after being corrected for static head terms in the pressure tap lines was seen to increase with inclination angle during upward flow and decrease with inclination angle in downward flow due to the contribution of the gravitational pressure term. One of the main challenges in determining the frictional pressure drop in the vertical orientations was that knowledge of the void fraction is required to compute the gravitational term. Thus, the selection of an appropriate void fraction model is critical to obtaining accurate frictional pressure drop measurements in the vertical orientation. While they found that several pressure drop and void fraction correlations were able to predict the vertical upward data, there was less agreement for the downward orientation. The Friedel (1979) correlation with the Chisholm (1973) void fraction model predicted the data well for larger pressure drop measurements (high mass flux, high quality), but none of the correlations were satisfactory in predicting the results over the entire measurement range. By observing the apparent gravitational pressure drop and void fraction (the difference between vertical and horizontal measurements), it was noted that for downward flow, the apparent void fraction was highly sensitive to the inclination angle. This indicates that the apparent void fraction is not a good estimate of the actual void fraction in downward flow. This is partly due to differences in flow patterns in inclined tubes based on the orientation. They cite the need for more studies on the void fraction in downward flow.

Two-phase pressure drop has been studied extensively in horizontal larger diameter tubes under adiabatic conditions. Most of the two-phase pressure drop models

27

are based on a semi-empirical two-phase multiplier approach, however multi-regime models may be more beneficial because they account for the effects of different flow mechanisms. Many condensation studies of synthetic refrigerants are documented in the literature; however, very little work has been done to measure and model the pressure drop of condensing hydrocarbons in small channels and vertical downward flow. There are several experimental challenges in determining the frictional pressure drop for vertical flows such as accurately accounting for the void fraction in the static head terms. At small diameters, many of the classical correlations are not applicable because surface tension effects are more prominent. There is a need to extend the data bank in the literature to include more hydrocarbon flows, because the properties of these fluids are different from those of air-water mixtures and synthetic refrigerants.

2.3.   Heat Transfer

A review of the relevant literature on heat transfer during condensation is presented here. Most studies have focused on determining the heat transfer coefficient for refrigerant flows in large diameter channels oriented horizontally. Relatively few studies have considered vertical downward condensation mechanisms. The heat transfer models in the literature are commonly based on one or more of the following approaches: gravity-driven flow models, two-phase multiplier models, and boundary layer shear-driven annular flow models. A summary of the relevant literature on condensation heat transfer is ptovided in Table 2.3.

Soliman *et al.* (1968) developed a correlation to predict the condensation heat transfer coefficient in annular flow based on the wall shear stress. Beginning with the

Table 2.3: Summary of in-Tube Condensation Literature: *h*

Author	Fluids	D_h (mm)	Flow Range	Saturation Conditions	Orientation
Soliman *et al.* (1968)	R22, R113, ethanol, methanol, toluene, trichloroethlyene	7.44 – 11.66	$6 < u_v < 305$ m s^{-1}		Horizontal Vertical, downflow
Traviss *et al.* (1973)	R12, R22	8	161 – 1533 kg m^{-2} s^{-1}	25 – 58°C	Horizontal
Shah (1979)	R11, R12, R22, R113, water, methanol, benzene, trichloroethylene, ethanol	7.4 – 40	8 to 1600 kg m^{-2} s^{-1}	21 - 310°C (0.0019 < P_r < 0.44)	Horizontal Vertical
Breber *et al.* (1980)	R11, R12, R113, steam, n-pentane	4.8 – 50.8	17.63 – 1600.3 kg m^{-2} s^{-1}		Horizontal
Moser *et al.* (1998)	R11, R12, R22, R113, R125, R134a, R410a	3.14 – 20	87 – 1532 kg m^{-2} s^{-1}	21 – 79°C	Horizontal
Cavallini *et al.* (2002)	R22, R134a, R125, R32, R236ea, R407c, R410a	8	100 – 750 kg m^{-2} s^{-1}	30 – 50°C	Horizontal
Wang *et al.* (2002)	R134a	1.46	150 - 750 kg m^{-2} s^{-1}	61 – 66°C	Horizontal
Shin and Kim (2004)	R134a	0.691	100 – 600 kg m^{-2} s^{-1}	40°C	Horizontal
Lee *et al.* (2006b, a)	R22, propylene, propane, isobutane	8 – 10.92	50 - 300 kg m^{-2} s^{-1}	35 – 45°C	Horizontal
Bandhauer *et al.* (2006)	R134a	0.5 – 1.5	150 – 750 kg m^{-2} s^{-1}		Horizontal
Wen *et al.* (2006)	R134a, R290 (propane), R600 (butane), R600/R290 (50/50 wt.%)	2.46	205 – 510 kg m^{-2} s^{-1}		Serpentine, downward
Fernando *et al.* (2008)	Propane	1.42	19 – 53 kg m^{-2} s^{-1}	30 – 50°C	Vertical, downflow
Park *et al.* (2008)	R22, propylene, propane, DME, isobutene	8.8	100 – 300 kg m^{-2} s^{-1}	40°C	Horizontal
Shah (2009)	Water, R134a, R404a, R410a, isobutane, propane, benzene, methanol, ethanol, toluene, etc.	2 – 49	4 – 820 kg m^{-2} s^{-1}	$P_r = 0.0008 - 0.905$	Horizontal Vertical, upflow Vertical, downflow
Dalkilic *et al.* (2011)	R134a	8.1	260 – 515 kg m^{-2} s^{-1}	40, 50°C	Vertical, downflow
Derby *et al.* (2012)	R134a	1	75 – 450 kg m^{-2} s^{-1}	35, 45°C	Horizontal

Carpenter and Colburn (1951) heat transfer model, the friction, momentum and gravity components of the shear stress were evaluated and modified to better describe the physical mechanisms of condensation. Due to vapor shear, they state that the annular film transitions from laminar to turbulent at lower Reynolds number ($Re_l \approx 240$) than in bulk single-phase flow; therefore, the liquid-vapor interface was modeled based on turbulent-turbulent conditions. The frictional component of the shear stress was related to the frictional pressure drop and was determined using the method of Lockhart and Martinelli (1949). The momentum component of the shear stress was determined based on the momentum change in the vapor core due to the change in quality during condensation. The Zivi (1964) void fraction model was used for this analysis. The final component of the shear stress was due to gravity and was based on the Zivi void fraction and Froude number. This term goes to zero for horizontal flows. It was noted that the friction term dominates at high to moderate quality. However, for low qualities, the gravity term is significant due to a thicker liquid film. For increasing density ratio (ρ_l / ρ_v), the effects of momentum become more important. It was also noted that for vertical upward flows, the liquid film begins flowing in the opposite direction at the point where the shear stress tends to zero. This causes pressure and flow fluctuations to propagate, and these conditions are outside the range of applicability of this model. The model was compared with data sets from the literature for fluids with Prandtl numbers ranging from 1 to 10 and vapor velocity ranging from 6 to 305 m s^{-1}. Data for horizontal and vertical downward condensation were considered. The data were correlated with respect to the liquid Prandtl number and the shear stress to determine a best fit as shown in Eq. (2.9).

$$\frac{h\mu_l}{k_l \rho_l^{1/2}} = 0.036 \, \mathrm{Pr}_l^{0.65} \, \tau_{\mathrm{wall}}^{1/2}$$

(2.9)

30

Soliman (1986) extended this correlation to include the mist flow regime. The mist-annular transition was determined to occur for modified Weber number between 20 and 30. In the mist flow regime, higher heat transfer coefficients are expected because the liquid film thickness is decreased by entrainment in the vapor core. (None of the data in the present study were in the mist flow regime based on this criterion).

Traviss *et al.* (1973) studied the condensation of synthetic refrigerants R12 and R22 in horizontal tubes. The goal of the research was to develop a semi-analytical correlation for condensation heat transfer coefficient applicable for the practical range of refrigeration condensers. Experiments were conducted in 8 mm diameter tubes for mass flux ranging from 161 to 1533 kg m^{-2} s^{-1} and saturation temperatures from 25 to 58°C. The experimental facility consisted of a 4.4 m long test section that was instrumented with thermocouples and differential pressure measurements at 0.737 m intervals. A sight glass was also included to observe the flow pattern at the exit of the test section. The primary focus of this study was on annular flow characteristics. The heat transfer-momentum analogy was applied to the heat transfer during annular flow, and the von Kármán universal velocity profile (von Kármán, 1930) was used to describe the liquid film. The heat transfer coefficient was related to the frictional pressure drop via the wall shear stress and was integrated over the liquid film thickness. The correlation developed by them can be expressed in two terms as shown in Eq. (2.10): one a function of liquid Reynolds number and Prandtl number, the other a function of quality and the property ratio $(\rho_v / \rho_l)(\mu_l / \mu_v)^{0.2}$ contained in the turbulent-turbulent Martinelli parameter formula.

$$\mathrm{Nu} = \frac{\mathrm{Pr_l}\,\mathrm{Re_l^{0.9}}}{T^+} F\left(X_{tt}\right)$$
$$F\left(X_{tt}\right) = 0.15\left(X_{tt}^{-1} + 2.85 X_{tt}^{-0.476}\right)$$

(2.10)

The dimensionless temperature, T^+, is determined from the von Kármán universal velocity profile. Although the eddy diffusivity ratio was taken to be unity for the development of this correlation, it was observed that increasing this value to 1.4 increased heat transfer coefficient predictions by 10%. Although the correlation was only validated for horizontal condensation, it is noted that its applicability should extend to inclined tubes as well. It was observed that for turbulent-turbulent Martinelli parameter greater than 0.155 (said to be in the mist/dispersed regime), the correlation under predicted the data due to liquid entrainment in the vapor core. A correction factor improved the model predictions for this region. For low quality data points in the slug flow regime ($x < 0.10$), the model showed less agreement as well. However, a linear interpolation with a single-phase correlation improved the agreement.

Shah (1979) sought to develop a general correlation for condensation heat transfer coefficient that was applicable to a wide range of fluids and flow conditions. An empirical model was proposed by correlating 21 data sets including 474 data points. The data included horizontal and vertical condensation measurements in tube diameters ranging from 7.4 to 40 mm, saturation temperatures ranging from 21 to 310°C ($0.0019 < P_r < 0.44$), and mass flux ranging from 8 to 1600 kg m^{-2} s^{-1}. A two-phase modifier approach was used to adjust single-phase heat transfer coefficients (calculated using the Dittus-Boelter equation) to two-phase flow in any flow regime. The multiplier is a function of quality and reduced pressure as shown in Eq. (2.11).

$$h = h_{lo}\left((1-x)^{0.8} + \frac{3.8x^{0.76}(1-x)^{0.04}}{P_r^{0.38}} \right) \qquad (2.11)$$

The use of the Dittus-Boelter equation for the single-phase heat transfer component was applied for $Re_{lo} > 350$. The local heat transfer coefficient correlation is proposed and integrated over tube length to yield the average heat transfer coefficient. It is noted that although vapor quality does not always vary linearly with condenser length, the error in assuming a linear variation is negligible for $\Delta x < 20\%$ and small for $\Delta x < 40\%$. Therefore, in these cases, an arithmetic mean quality can be applied in the local heat transfer correlation without significant loss in accuracy. The model predicted the data with a 17% average absolute deviation. At high qualities, entrance effects and liquid entrainment in the vapor core were cited as possible reasons for the experimental values being larger than the model predictions. It is also noted that less accuracy is expected as saturation conditions approach the critical pressure.

Breber *et al.* (1980) developed a correlation for horizontal in-tube condensation heat transfer coefficient based on the applicable flow regimes. They compared data from ten different studies with the flow regime map from Taitel and Dukler (1976). The data included tubes with internal diameter between 4.8 mm and 50.8 mm and mass flux between 17.6 and 1600.3 kg m^{-2} s^{-1}. The fluids considered were R11, R12, R113, steam and n-pentane. They found good agreement in general with the Taitel and Dukler flow map, especially in the annular regime. The slug flow and intermittent flow data showed the largest discrepancies. The data for the small diameter (4.8 mm) tubes also showed poor agreement because surface tension effects were not considered. They observed a transition region rather than an abrupt change between annular and wavy flow. Using the Martinelli parameter and the Wallis dimensionless gas velocity as coordinate axes, they suggest simplified criteria for selecting the form of the heat transfer coefficient based on

flow regime. For gravity dominated flow (wavy and stratified flow), a modification to the Nusselt (1916) correlation for falling film heat transfer is presented as shown in Eq. (2.12). For shear-dominated flow (annular and bubble flow), the convective heat transfer is found using the ratio of two-phase pressure to liquid drop as defined by Lockhart and Martinelli (1949) and Chisholm (1967). This method was also applied to intermittent flow with the admission that it is an approximation.

$$h_{cg} = F_g \left(\frac{k_l^3 \rho_l (\rho_l - \rho_v) g i_{fg}}{4 \mu_l (T_{sat} - T_{wall}) D} \right)^{1/4}$$ (2.12)

Moser *et al.* (1998) developed a heat transfer coefficient correlation based on the equivalent Reynolds number model. The rationale behind this method is to define an all-liquid flow with a heat transfer coefficient equivalent to the value in two-phase flow under the same conditions. A modification was proposed to the Akers *et al.* (1959) correlation based on the heat-momentum analogy. They cited deficiencies in the previous model including the assumption that the ratio of the vapor to liquid friction factor was unity and that the driving temperature difference was between the bulk fluid and the wall rather than the liquid film and the wall. In their model, the equivalent Reynolds number was defined based on the all liquid flow representing the same wall shear stress as the two-phase flow. The Friedel (1979) correlation for horizontal flows was used to estimate the frictional pressure drop in the heat-momentum analogy formulation of the equivalent Reynolds number. The equivalent Reynolds number is defined as,

$$\text{Re}_{eq} = \phi_{lo}^{8/7} \, \text{Re}_{lo}$$ (2.13)

where the two-phase multiplier is defined by Friedel (1979). The Petukhov (1970) correlation for single-phase heat transfer was then applied using the equivalent Reynolds

number. A correction factor was also defined to account for the differences between the film and bulk temperatures in the flow. The resulting expression is provided in Eq. (2.14).

$$\mathrm{Nu} = \frac{0.0994^{C_1} \, \mathrm{Re}_l^{C_2} \, \mathrm{Re}_{eq}^{1+0.875C_1} \, \mathrm{Pr}_l^{0.815}}{\left(1.58\ln(\mathrm{Re}_{eq}) - 3.28\right)\left(2.58\ln(\mathrm{Re}_{eq}) + 13.7\,\mathrm{Pr}_l^{2/3} - 19.1\right)} \tag{2.14}$$

where $C_1 = 0.126 \, \mathrm{Pr}_l^{-0.448}$ and $C_2 = -0.113\mathrm{Pr}_l^{-0.563}$. The predictions of the model were compared with data sets from the literature for local and average heat transfer coefficients for a variety of synthetic refrigerants. The conditions in this database included tube diameters from 3.14 to 20 mm, mass flux ranging from 87 to 1532 kg m^{-2} s^{-1}, and saturation temperature ranging from 21 to 79°C. The model was found to predict the data better than the Traviss *et al.* (1973) and Shah (1979) models, with an average absolute deviation of 13.64%. It was observed that the model under predicted the data more often than over predicting it. Uncertainty in the two-phase pressure drop, liquid entrainment in the vapor core and stratification of the flow were cited as possible causes of the under prediction. They note that the model is sensitive to the predictive ability of the two-phase pressure drop correlation. They also note that this study extends the range of applicability of the Shah (1979) correlation to diameters as small as 3.14 mm.

Cavallini *et al.* (2001, 2002) performed an experimental study of condensing halogenated refrigerants in 8 mm diameter tubes. The results of this study and data from Tang (1997), Dobson and Chato (1998), and Zhang (1998) were used to develop a multi-regime heat transfer model on the basis of 600 measurements spanning tube diameters of 3.1 to 8.8 mm, saturation temperatures from 30°C to 70°C and mass flux from 100 to 750 kg m^{-2} s^{-1}. The fluids considered in the development of this model included several high pressure synthetic refrigerants such as R410a. The data were classified into flow regimes

based on the dimensionless vapor velocity and the turbulent-turbulent Martinelli parameter. It was observed that in the annular regime, the heat transfer coefficient was dependent on the mass flux, quality and saturation temperature. However in the stratified regime, the temperature difference between the condensing fluid and the wall proved to be significant. In the annular regime, the model was based on that of Kosky and Staub (1971) relating the interfacial shear stress and the pressure gradient to the heat transfer coefficient. For stratified flow, the heat transfer was modeled as the sum of two components. Heat transfer through the thin film at the top of the tube was modeled as a gravity dominated process similar to the Nusselt (1916) falling film analysis. At the bottom of the tube, heat transfer through the thicker liquid film was determined based on the Dittus-Boelter equation and the liquid pool angle, defined using the Zivi (1964) void fraction. The heat transfer coefficient in the stratified regime was determined as the linear interpolation between purely stratified flow and annular flow at the transition boundary. (The present study addresses vertical condensation; therefore, the stratified regime is not observed.) For slug flow, an empirical correlation that predicted abrupt transitions to stratified flow was developed. Therefore, the heat transfer coefficient for slug flow was computed as a linear interpolation between the single phase and stratified values. The model predicted the data with an average deviation of -2.2% and an average absolute deviation of 13.0%.

Wang *et al.* (2002) conducted an experimental study of condensation in minitubes and developed a correlation from their results based on the flow regimes and transitions between annular and stratified flow. The experimental facility consisted of an air-cooled multi-tube test section. The bulk air temperature was measured using an array of

thermocouples. In-tube condensation and flow visualization experiments were performed for 1.46 mm hydraulic diameter channels over a mass flux range of 150 to 750 kg m^{-2} s^{-1}. Models were developed for condensation in annular and stratified flow. These models were then combined based on the proportion of each phase present along the length of the tube. The correlations in the literature with which they compared their data did not capture the trends of their data well, suggesting that these correlations do not account for all the physical mechanisms governing flows for these conditions.

Shin and Kim (2004) report a novel method of measuring heat transfer for R134a condensing in microchannels at low heat duty and mass flow rate. They conducted experiments in a single 0.691 mm diameter tube with mass flux ranging from 100 to 600 kg m^{-2} s^{-1}. The test section consisted of a single copper tube and single fin positioned in an air duct with the fin parallel to the air flow. An identical single tube and fin construction contained a resistance heater rather than refrigerant. The small heat duty in the test section was measured using an approach similar to a thermal anemometer. Identically spaced thermocouples on the fins were monitored, and when the temperature readings matched within 0.5°C, the test section heat duty could be determined from the electric power dissipation. They report the ability to measure heat duties as low as 0.75 W. The Shah (1979) and Akers *et al.* (1959) correlations did not predict the data well.

Lee *et al.* (2006b, a) performed experiments on condensing hydrocarbons to compare the heat transfer and pressure drop with corresponding values for R22. The hydrocarbons investigated in this study included R1270 (propylene), R290 (propane) and R600a (isobutane). The test facility was constructed in the form of a typical vapor compression cycle consisting of a compressor, a condenser, an expansion valve, and an

evaporator. For the condensation experiments, the test section consisted of a 6.23 m long horizontal double-pipe condenser with a U-bend in the middle. In these studies, three different inner tube diameters were included, ranging from 9.52 to 10.92 mm. The test section was divided into 8 subsections, each 675 mm long. The local heat transfer coefficient was determined for each subsection from temperature and pressure measurements of the fluids and tube walls at the inlet and outlet of each subsection. The heat duty in each subsection was determined from the temperature rise of the water in the outer tube. The average heat transfer coefficient over the entire test section was also determined. It was observed that the hydrocarbon refrigerants had higher heat transfer coefficients than R22 by at least 31%, most probably due to the difference in thermophysical properties between refrigerants and hydrocarbons. The increase was greater for smaller diameter tubes. At high quality ($x > 0.4$), it was observed that propane had a lower heat transfer coefficient than R1270 or R600a. No uncertainties are reported for these data. The data were found to agree within $\pm$20% with the predictions of the Shah (1979), Traviss *et al.* (1973), and Cavallini and Zecchin (1974) correlations. While this study provides insights on hydrocarbon condensation, the tube sizes considered are much larger then the diameter of interest to the present study and may not be directly applicable.

Bandhauer *et al.* (2006) developed an experimentally validated model for microchannel condensation heat transfer. Experiments were conducted to measure the local heat transfer coefficient during condensation of R134a in circular channels with diameter ranging from 0.5 to 1.5 mm and mass flux ranging from 150 to 750 kg m^{-2} s^{-1}. The small quality changes and related small heat duty in the test section were measured

with low uncertainty using the thermal amplification technique developed by Garimella and Bandhauer (2001). A secondary low flow rate coupling fluid loop was added to the test section to measure the heat duty with low uncertainty while still allowing the condensation heat transfer resistance to be dominant relative to the high flow rate primary coupling fluid loop. Using this approach, the test section heat duty was determined to within a maximum uncertainty of ±10%, while the heat transfer coefficient was typically measured to within ±20% uncertainty. The heat transfer coefficient was observed to increase by 10% to 40% as the diameter was reduced. The data were compared with a number of correlations in the literature. These models were grouped into gravity driven correlations, two-phase multiplier correlations, homogeneous flow models and boundary layer annular flow models. The gravity driven models did not predict the data well because they were developed for wavy and stratified flow, which were inapplicable to most of their data based on the criteria of Coleman and Garimella (2000b, 2003). Among the two-phase multiplier models, Moser *et al.* (1998) predicted the data well, with an average absolute deviation of 14%. Although the Traviss *et al.* (1973) correlation showed the largest average absolute deviation of the annular flow boundary layer models (38%), their approach along with that of Moser *et al.* (1998) formed the basis of the model proposed in this study. The interfacial shear stress was determined from the frictional pressure drop model of Garimella *et al.* (2005) for annular flow. The dimensionless temperature, T^{+}, was determined using a method similar to that of Traviss *et al.* (1973) by integrating over the film thickness for a two-region, rather than a 3 region velocity profile. The basic form of the heat transfer model can be expressed as in Eq. (2.15).

$$h = \frac{\rho_{l} c_{p,l} u_{\tau}}{T^{+}}$$
(2.15)

The model predicted the data well, with an average absolute deviation of 10%. It was noted that the steeper slope of the heat transfer coefficient data for high quality ranges could be due to liquid entrainment effects in the vapor core. It was also noted that more explicit analysis for heat transfer in intermittent and mist flow could be used to refine the model.

Fernando *et al.* (2008) studied a shell-and-tube condenser with propane as the working fluid. The 36 tubes in the heat exchanger were constructed from extruded aluminum with six rectangular channels in each. The hydraulic diameter of the channels was 1.42 mm. The individual channels were rectangular, with a semicircular channel at either side of each multiport tube. The shell side of the heat exchanger contained water as the coupling fluid. The local condensation heat transfer coefficient and length of desuperheating, condensing and subcooling sections of the heat exchanger were measured. Propane entered the condenser as a superheated vapor and exited as a subcooled liquid. Water temperature measurements were taken at 13 points along the length of the condenser and were used to determine the transitions between single- and two-phase flow as well as the local heat transfer coefficient of the vapor, condensing, and liquid regions. Due to the number of channels, the mass flux was low, ranging from 19 to 53 kg m^{-2} s^{-1}. Three saturation temperatures were considered: 30, 40 and 50°C. The results were compared with model predictions from the literature. Poor agreement was found with most correlations in the literature. For the condensing region, the results were predicted best by a modification to the Nusselt (1916) correlation for laminar film condensation. The deviations from this model were possibly due to surface tension effects in the rectangular channels. For low mass flux as considered in their study, the

vertical downward condensation heat transfer mechanism was concluded to be gravity-dominated. The mass flux range considered in the present study is slightly larger (75 – 125 kg m^{-2} s^{-1}); therefore, shear and surface tension forces are expected to begin to be more important.

Park *et al.* (2008) conducted horizontal condensation experiments for 5 fluids including R22, propylene, propane, dimethyl ether, and isobutane. The test section was a copper tube with 8.8 mm inner diameter and an outer tube with a 2 mm annular gap through which cooling water flowed. The test section heat duty was determined using an array of 4 thermocouples soldered to the test section wall. The inlet quality was controlled by an electric pre-heater that is inserted in the hydrocarbon flow stream. Local heat transfer coefficient and pressure drop was measured for quality increments less than 12%. Experiments were conducted for a saturation temperature of 40°C and mass flux ranging from 100 to 300 kg m^{-2} s^{-1}. The condensation heat transfer coefficient of propane was determined to be significantly greater than R22. This result is explained by comparing the fluid properties in a ratio proportional to the heat transfer coefficient, defined as $\Phi = (c_{p,l} / \mu_l)^{0.4} k_l^{0.6}$ (Jung *et al.*, 1989). The value of this property ratio is 3.83 for propane and 2.11 for R22.

Shah (2009) modified his previous correlation (1979) to reflect a wider range of data including more fluids, mass flux, and reduced pressure. While Propane is included in the data set, it is only for horizontal condensation. For vertical condensation, the tube diameter ranged from 7.4 mm to 47.5 mm. For data with hydrocarbon refrigerants, the tube diameters were 11.6 mm and 18.5 mm. The hydrocarbons used for the vertical correlation were methanol, ethanol, toluene and benzene. Modifications to the previous

correlation included a correction factor based on liquid and vapor viscosity as well as reduced pressure. Three flow regimes were also added to the vertical model based on the dimensionless vapor velocity. In what he terms the "laminar regime," the heat transfer coefficient is calculated using the Nusselt equation for laminar film condensation as shown in Eq. (2.16).

$$h_{Nu} = 1.32 \, Re_l^{-1/3} \left[\frac{\rho_l (\rho_l - \rho_v) g k_l^3}{\mu_l^2} \right]^{1/3} \tag{2.16}$$

In the "turbulent regime," the modified Shah correlation is used as shown in Eq. (2.17).

$$h_l = h_{lo} \left(\frac{\mu_f}{14 \mu_g} \right)^{0.0058 + 0.557 p_r} \left[(1-x)^{0.8} + \frac{3.8 x^{0.76} (1-x)^{0.04}}{p_r^{0.38}} \right] \tag{2.17}$$

In the "transition regime," the heat transfer coefficient is the sum of these two methods. For horizontal tubes, there was good agreement between this correlation and other well validated correlations, although Shah also states that it is also applicable for vertical condensation.

Dalkilic and Wongwises (2010b) examined vertical downward condensation of R134a in 8.1 mm channels. Heat transfer coefficient and frictional pressure drop measurements were taken for vertical downward condensation of R134a in 8.1 mm diameter channels at saturation temperatures of 40 and 50°C. The mass flux range of the experiments was 260 to 515 kg m^{-2} s^{-1}. A general model for heat transfer coefficient in annular flow was developed based on Kosky and Staub (1971) and the von Kármán universal velocity profile. A compilation of 35 void fraction and 13 frictional pressure drop models was presented, and the heat transfer coefficient was calculated using each combination of these models in the general correlation. The pairs that predicted the data

within ±30% were said to constitute successful models. It was observed that 29 of the 35 void fraction models and 11 of the 13 pressure drop models met this criterion. Based on this analysis, the Chen *et al.* (2001) pressure drop model and the Armand (1946) void fraction model were recommended.

Dalkilic *et al.* (2011) proposed a new model from this data set that uses the measured frictional pressure drop as an input. The Paliwoda (1989) correlation for frictional pressure drop was adapted to develop a model that uses experimental pressure drop measurements to determine the heat transfer coefficient. They observed that the data were predicted within ±15% under these conditions. They conclude that the results of these studies indicate that annular condensation correlations are independent of orientation because models developed for horizontal condensation also predicted the data well for vertical condensation.

Derby *et al.* (2012) describe condensation experiments with R134a in channels of various shapes, each with a hydraulic diameter of 1 mm. The purpose of their study was to measure the heat transfer coefficient in condensing flow in square, triangular and semi-circular channels. After describing several methods of determining the heat transfer coefficient, a test section was designed to contain an array of thermocouples in a copper block. The test section heat duty was determined from the temperature gradient in the block. The experimental facility consisted of a pre-heater, test section and post-condenser. A throttle valve was positioned between the pre-heater and test section to control two-phase instabilities. The heat transfer coefficient increased with mass flux and quality. There was not a significant difference in performance at the two saturation temperatures 35°C and 45°C. No significant difference was noticed between channel

shapes either. The Shah (1979) correlation predicted their data the best (20% - 30% average absolute deviation).

More heat transfer studies of hydrocarbon condensation have been performed than pressure drop and flow regime studies. However, generally applicable correlations that predict hydrocarbon flows well are still not available. Studies of vertical downward condensation are still uncommon. Most of the studies of propane in the literature are for either a larger diameter or larger mass fluxes than those of interest in the present study.

2.4. Summary

Extensive research has been performed on two-phase flows in conventional channels, and the gaps in the literature relating to smaller tubes are beginning to be filled. However most flow regime, frictional pressure drop and heat transfer studies consider horizontal or vertical upward flow. Relatively few studies have been performed for vertical downward condensation. The available vertical downward studies are mostly for larger diameters than those considered in the present study. Many of these studies are of conventional tubes with diameters of $25 - 50$ mm diameter although some studies on 8 mm diameter tubes are also available. However, few studies consider the effects of decreasing diameter on vertical downward condensation. Because of differences in the flow mechanisms for vertical upward and vertical downward condensation, studies on minichannel flows in an upward orientation may not be applicable to downward flow.

Hydrocarbon condensation also presents some differences to traditional synthetic refrigerants such as HCFCs and HFCs. As noted in Chapter 1, although propane has a saturation pressure and thermal conductivity comparable to synthetic refrigerants, the

density is much lower, which affects the fluid flow and heat transfer performance. More research is needed on the condensation mechanisms of hydrocarbons. Due to deficiencies in the literature relating to vertical downward condensation of hydrocarbons in small tubes, this study is proposed using the experimental approach and methods described in subsequent chapters.

CHAPTER 3: EXPERIMENTAL APPROACH

The experimental approach used for the condensation measurements conducted in this study is described in this chapter. Heat transfer and pressure drop characteristics of propane condensing in a 1.93 mm vertical round channel are investigated. The local heat transfer coefficient and frictional pressure drop are determined for the conditions summarized in Table 3.1. Experiments are conducted for mass flux ranging from 75 to 150 $\text{kg m}^{-2} \text{s}^{-1}$, at saturation temperatures of 47°C and 74°C, and nominal quality increments of 0.25.

3.1. Experimental Facility

A schematic of the test facility is shown in Figure 3.1. It is designed to measure the local heat transfer coefficient and pressure drop in vertical condensing flow through a

Table 3.1: Test Matrix

Fluid: Propane, ID = 1.93 mm, vertically downward flow			
Mass Flux $\text{kg m}^{-2} \text{s}^{-1}$	**Saturation Temperature** °C	**Saturation Pressure** kPa	**Quality**
75	47	1604	
75	74	2796	
100	47	1604	0.25 – 0.00
100	74	2796	0.50 – 0.25 0.75 – 0.50
125	47	1604	1.00 – 0.75
125	74	2796	
150	47	1604	

single 1.93 mm round channel, with particular attention to ensuring the accurate measurement of the low heat duties at these conditions of interest. The approach was developed based on previous work on flow visualization (Coleman and Garimella, 2000a, 2003), and condensation pressure drop and heat transfer coefficient studies (Garimella *et al.*, 2002; Garimella *et al.*, 2003; Mitra and Garimella, 2003; Bandhauer *et al.*, 2006).

Subcooled liquid propane [6] is pumped through an evaporator that uses hot water as the heating fluid, which is in turn electrically heated, and exits as a superheated vapor [1]. The propane flows through the air-coupled pre-condenser in which it is partially condensed to the desired quality [2,3]. Propane enters the test section, which is a water-coupled tube-in-tube heat exchanger, in which the pressure drop and heat transfer during condensation are measured. The propane exits the test section [4,5] and flows through the air-coupled post-condenser in which it is fully condensed. It exits the post-condenser in a subcooled liquid state [6]. A photograph of the facility is shown in Figure 3.2.

The four major sections of the propane loop, the evaporator, the pre-condenser, the test section and the post-condenser, each with an associated coupling loop, are descibed in detail here. Subcooled propane [6] is pumped through a shell-and-tube heat exchanger (Exergy, Series 35, 00256-02) that serves as an evaporator, which is heated by a hot water loop to achieve a superheated state [1]. Propane is circulated in the loop using a magnetic gear pump (Micropump, GAH Series) rated for a maximum operating pressure of 345 bar (5000 psi) and a maximum differential pressure of 5.2 bar (75 psi). A 0 to 30 V regulated DC power supply (Electro Industries, DIGI 35A) is used to power a 500 – 6000 rpm DC drive for the pump. The propane flow rate is controlled by adjusting inline ball valves and by varying the pump speed. A Coriolis mass flow meter
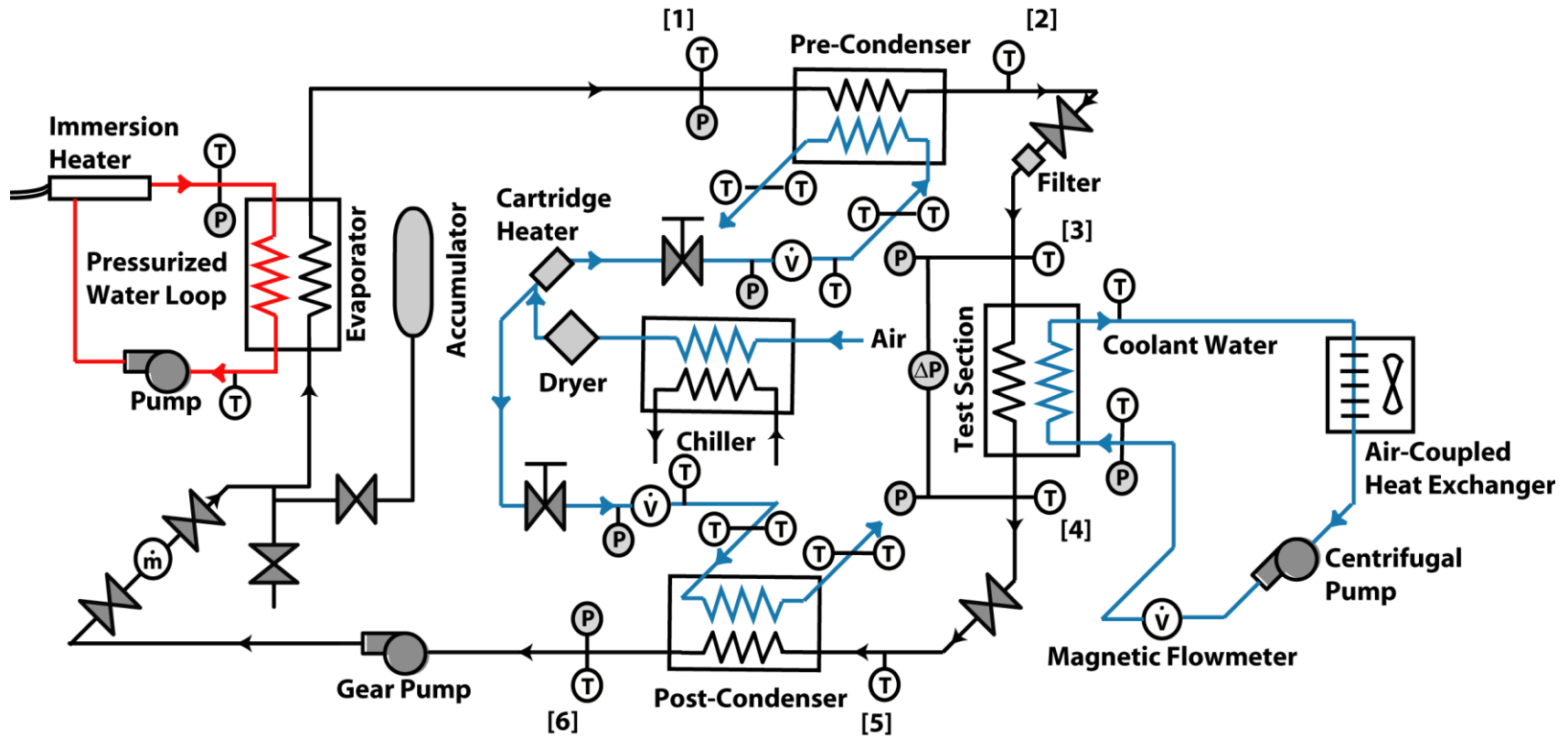
Figure 3.1: Experimental Facility Schematic
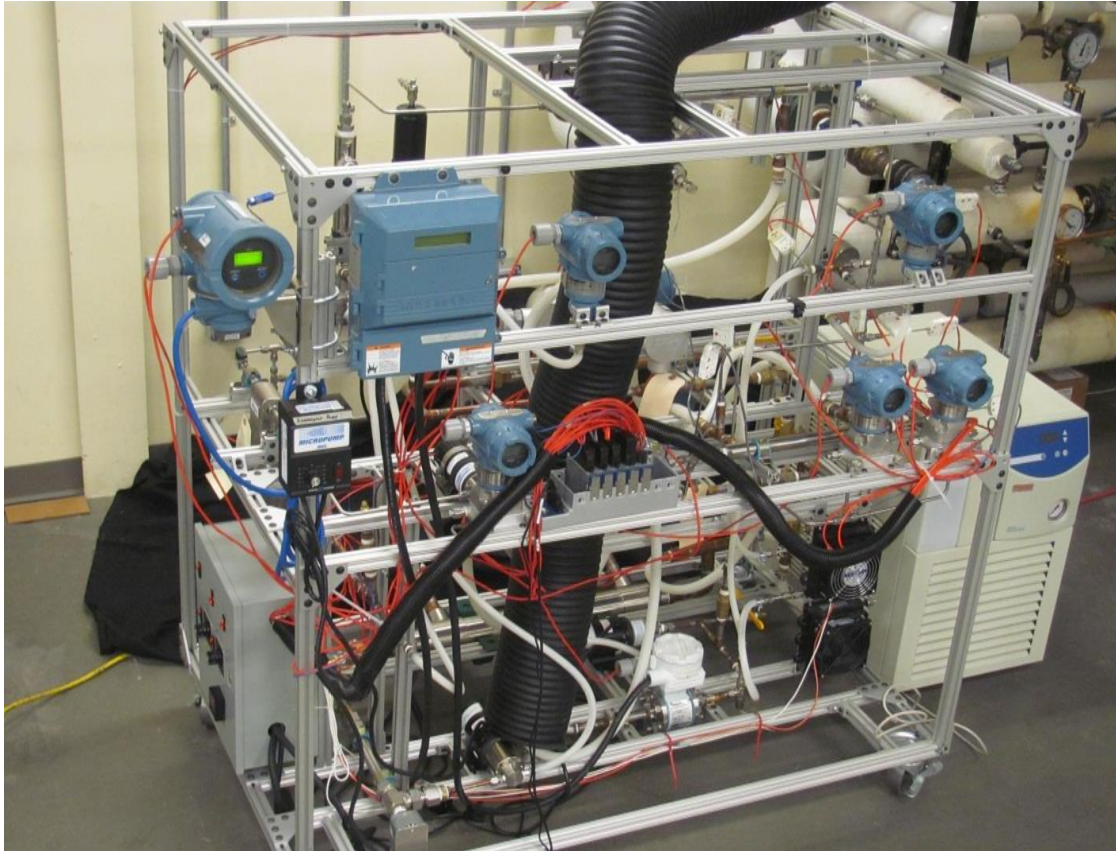
Figure 3.2: Experimental Facility Photograph

(Micromotion, CMFS010, uncertainty: $\pm\,5.6\times10^{-7}$ kg s^{-1}) is installed between the pump and the evaporator to measure the mass flow rate of the liquid propane. A piston hydraulic accumulator (Parker, 276 bar, 0.5 L) connected to a nitrogen tank is used to control the propane loop system pressure. A schematic of the evaporator loop is provided in Figure 3.3.

To achieve set point temperatures in the evaporator higher than 100°C with distilled water as the coupling fluid, the loop is pressurized to 300 – 600 kPa. The water is circulated in counter-flow to the evaporating propane using a gear pump (Micropump, GB Series) with a variable control AC drive. An electric immersion heater (Watlow, Firerod, 500 W) with a 177 mm heated length and 15.9 mm diameter is used to control
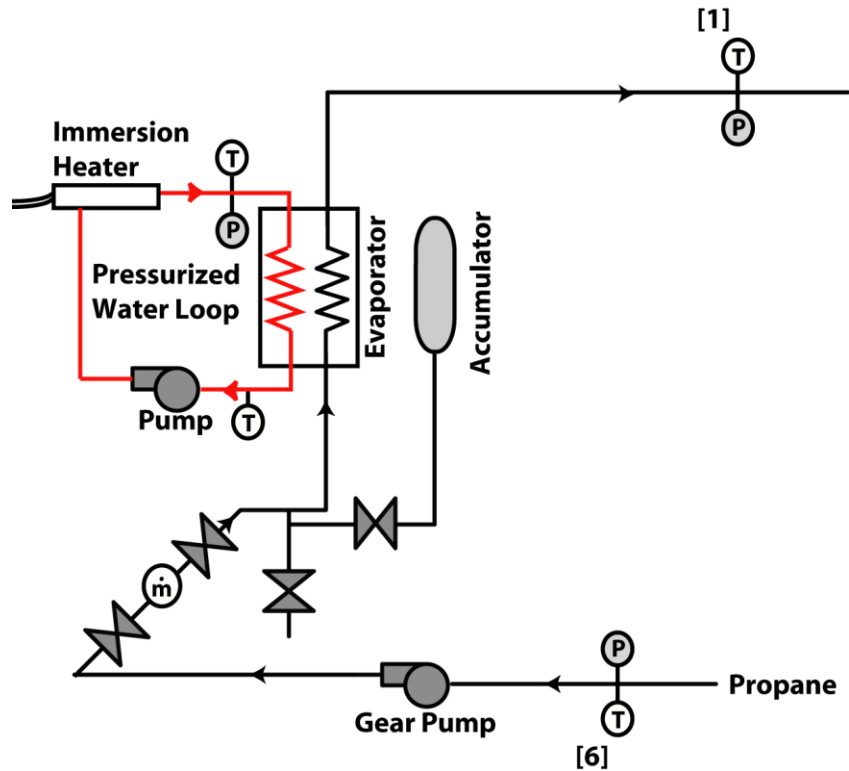
Figure 3.3: Evaporator Loop Schematic

the temperature in the water loop. When mounted in a female run tee (Swagelok, SS-1610-3-12TFT), the heated region is entirely contained in a straight tube section. The inner diameter of the enclosing stainless steel tube is 23.6 mm. The immersion heater is controlled by an Omega controller (CN77523) based on the temperature measurement at the inlet of the evaporator heat exchanger. Water temperature measurements are taken using thermocouples at the inlet and outlet of the heat exchanger. A pressure measurement is taken at the heat exchanger shell inlet to verify that the water is in liquid phase at the inlet of the heat exchanger. An accumulator is installed in the evaporator loop on the heating water side to control the loop pressure and allow for fluid expansion during operation.

The pre-condenser uses compressed air to cool and condense the superheated propane to the desired test section inlet quality. The measured conditions at the

superheated state [1], the heat duty of the pre-condenser, and the measured pressure at the test section inlet [3] are used to determine the thermodynamic state at the inlet to the test section. A schematic of the pre-condenser and coupling loop is provided in Figure 3.4.

A large temperature rise is desired in the coupling fluid to reduce uncertainties in the heat duty calculations. The flow rates necessary to achieve a sufficient temperature rise with water as the coupling fluid are restrictively low (< 0.05 L min^{-1} water); therefore, air was chosen as the coupling fluid. A tube-in-tube heat exchanger of reasonable length required an unacceptably large pressure drop in the air (~6000 kPa). Increasing the annulus size to reduce pressure drop necessitates increased air flow rates to compensate for the reduced heat transfer coefficient, resulting in a decrease in the air temperature rise. Balancing these parameters proved difficult to accomplish in a tube-in-tube heat exchanger; therefore, a shell-and-tube heat exchanger (Exergy Series 23, 00540-05) is installed in counter-flow. The specifications for the pre-condenser heat
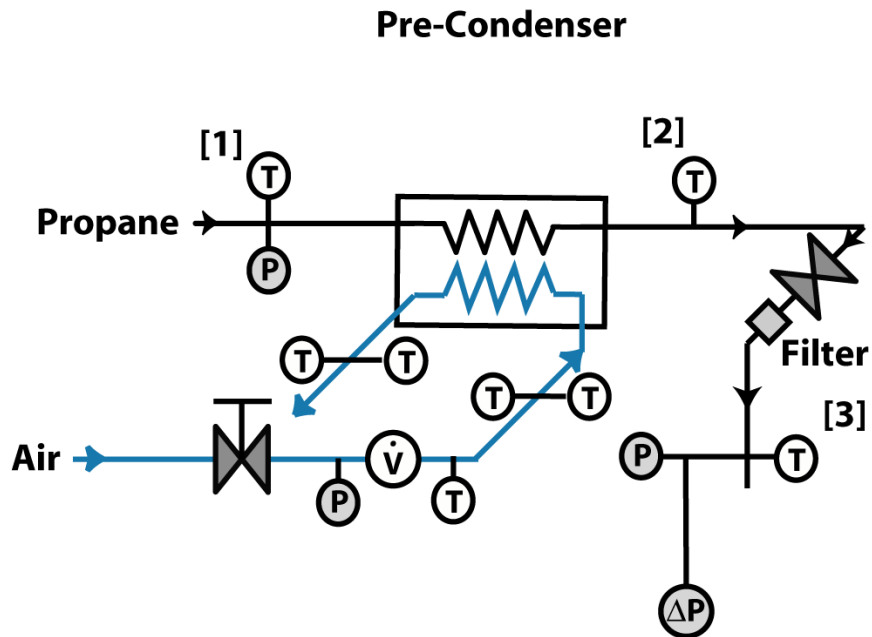
Pre-Condenser

Figure 3.4: Pre-Condenser Schematic

exchanger are shown in Table 3.2.

A schematic of the pre-conditioning loop for the compressed air used in the pre- and post-condensers is provided in Figure 3.5. Ambient air is compressed (Compressor: Quincy, QT-5) and flows through a 25 SCFM dryer (Aurora, HTD0025) dedicated to the compressor to remove moisture from the air. A large shell-and-tube heat exchanger (Exergy Series 73, 00677-3) is used to control the air temperature. A 50/50 ethylene glycol-water mixture is cooled and pumped through the shell side of the heat exchanger by a chiller (Thermo Fisher Scientific, Merlin M75) to cool the air. Downstream of the large heat exchanger, the air passes through a dryer (SPX Hankison, HPR10) dedicated to the facility to remove any water condensate from the cooled moist air. This line splits to deliver cooled air to the pre- and post-condensers. For some tests, it was necessary to heat

Table 3.2: Pre- and Post-Condenser Key Dimensions

Pre- and Post-Condenser Exergy LLC: Shell-and Tube, Series 23, 00540-5		
Length	L_{pre}	275 mm
Shell Outer Diameter	$D_{shell,out}$	25.4 mm
Shell Inner Diameter	$D_{shell,in}$	22.9 mm
Tube Outer Diameter	$D_{tube,out}$	3.82 mm
Tube Inner Diameter	$D_{tube,in}$	3.18 mm
Number of Tubes	N_T	19
Number of Baffles	N_B	14
Tube Pitch	P_T	4.58 mm
Heat Transfer Area	A_{HT}	0.06 m^2
Intermediate Length to Test Section	Pre: $L_{2\text{-to-}3}$ Post: $L_{4\text{-to-}5}$	462 mm 349 mm
Length between measurement and HX	Pre: $L_{1\text{-to-pre}}$ Post: $L_{post\text{-to-}6}$	65 mm 67 mm
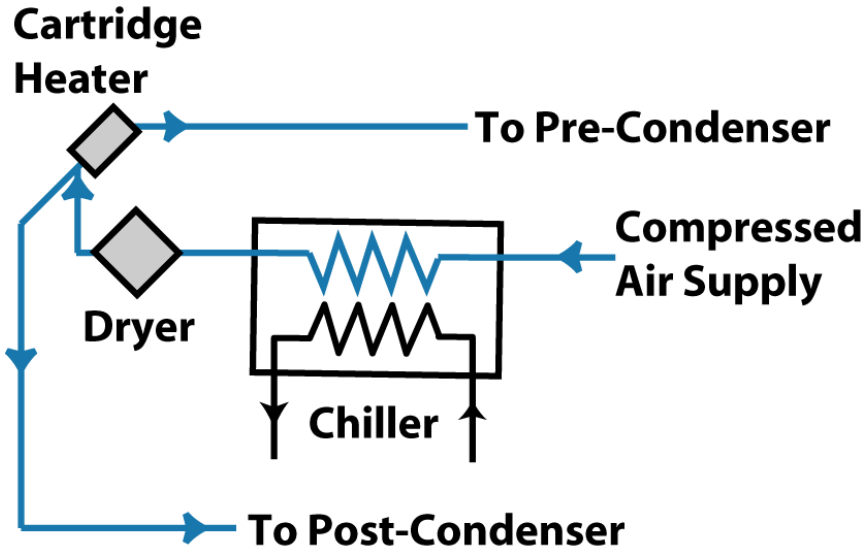
Figure 3.5: Schematic showing the compressed air cooling loop

the air in the pre-condenser to obtain the necessary temperature difference between the air and the condensing propane. Electric cartridge heaters (Watlow, Firerod, 80 W and 500 W), coupled to a variable AC voltage controller, are used to control the air inlet temperature in the pre-condenser for these cases.

The air flow rate to each condenser is controlled by a needle valve, and the flow rate is measured using a gas turbine volume flow meter (Flow Technology, FT-12). Absolute pressure is measured downstream of the needle valve, and a type T thermocouple is located downstream of the flow meter to determine the air density at the flow meter. The density is used to calculate the air mass flow rate from the measured volumetric flow rate. Air temperature measurements are taken using RTDs at the inlet and outlet of the condensers. To ensure accurate bulk air temperature measurements, copper mesh mixing sections are installed upstream of each measurement location. Thermocouples are also installed parallel to the flow stream to provide redundant temperature measurements, which are then averaged. The air exiting the condensers is

exhausted. A schematic showing the air temperature measurement configuration is shown in Figure 3.6.

The test section consists of a vertically oriented tube-in-tube heat exchanger. A schematic of the test section is presented in Figure 3.7. To increase the surface area and enhance the heat transfer on the water-side of the test section, a longitudinally finned test section was manufactured by direct metal laser sintering. The inner test section tube, containing propane, is made of aluminum with an inner diameter of 1.93 mm and an outer diameter of 2.97 mm. The outer tube is made of stainless steel with an inner diameter of 5.35 mm and an outer diameter of 6.35 mm. A photograph of the test section is shown in Figure 3.8. Temperature and absolute pressure measurements are taken upstream and downstream of the test section to set the state of the propane, and a differential pressure measurement is taken across the test section. The pressure drop length between the two measurement points is 262 mm, while the heat transfer length,
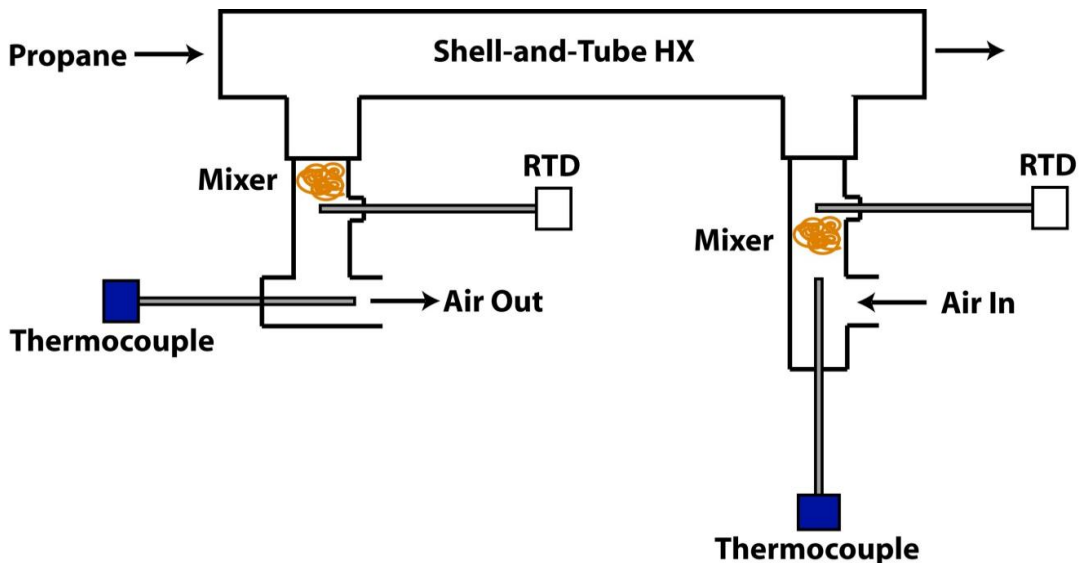
Figure 3.6: Schematic showing the air temperature measurements in the pre- and post-condensers
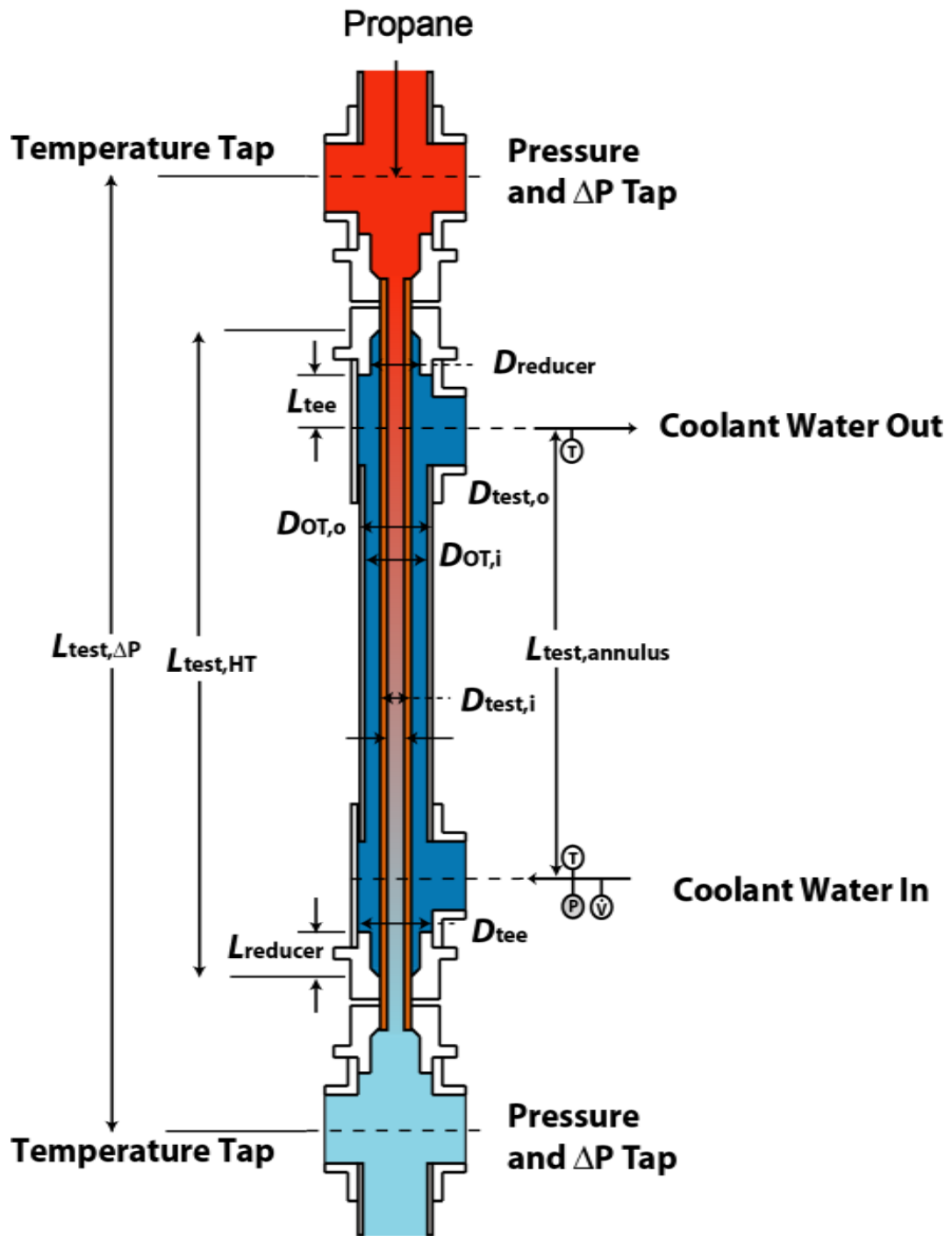
Figure 3.7: Test section schematic
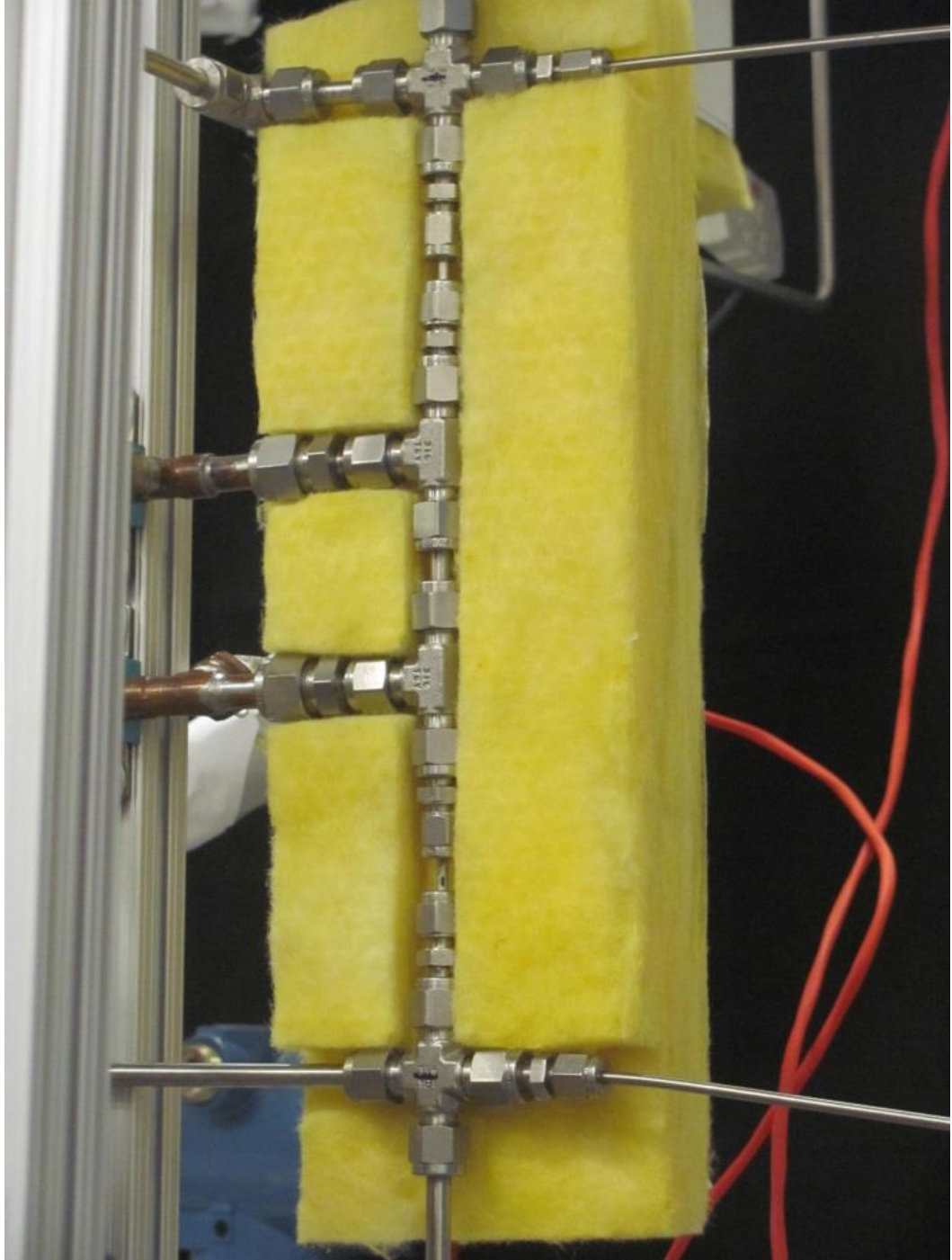
Figure 3.8: Test section photograph

including the annulus and fittings, is 135.10 mm. Detailed dimensions of the finned test section are provided in Table 3.3. A cross sectional schematic of the finned tube and outer shell is shown in Figure 3.9, and photographs of the finned tube are shown in Figure 3.10. The tube consists of 12 equally spaced longitudinal fins that span the length of the test section annulus. Each fin is 0.46 mm wide and 0.84 mm high, and the overall length of the finned tube is 191 mm.

Table 3.3: Test Section Dimensions

Dimension	Variable Name	Length (mm)
Length of Annulus	$L_{annulus}$	58.46
Heat Transfer Length	$L_{test,HT}$	135.10
Total Length	$L_{test,total}$	262
Length of Inner Tube	$L_{test,\Delta P}$	191
Length of reducer	$L_{reducer}$	26.66
Length of Tee	$L_{tee,top}$ $L_{tee,bottom}$	11.41 11.91
Noncondensing Entrance Length	$L_{test,in}$	100
Noncondensing Exit Length	$L_{test,out}$	104
Outer tube, outer diameter	$D_{OT,o}$	6.45
Outer tube, inner diameter	$D_{OT,i}$	5.35
Inner tube, outer diameter	$D_{test,o}$	2.97
Inner tube, inner diameter	$D_{test,i}$	1.93
Swagelok Tee-Fitting, inner diameter	D_{tee}	6.50
Swagelok Reducer-Fitting, inner diameter	$D_{reducer}$	4.40
Fin Width	W_{fin}	0.46
Fin Height	H_{fin}	0.84
Overall Diameter with Fins		4.64
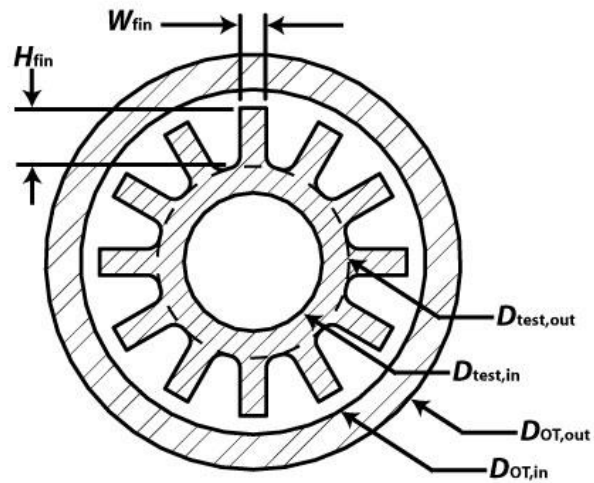
Figure 3.9: Cross sectional schematic of the finned tube test section
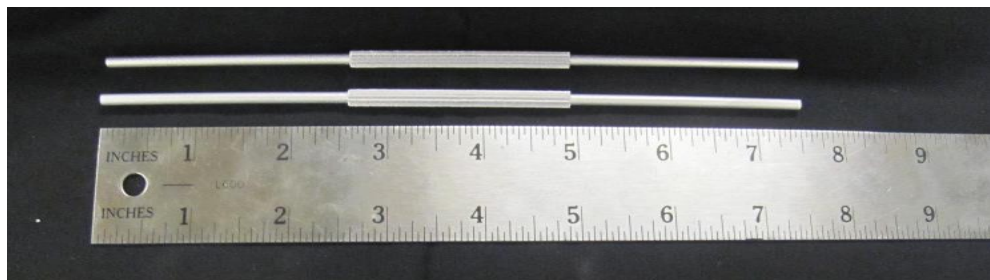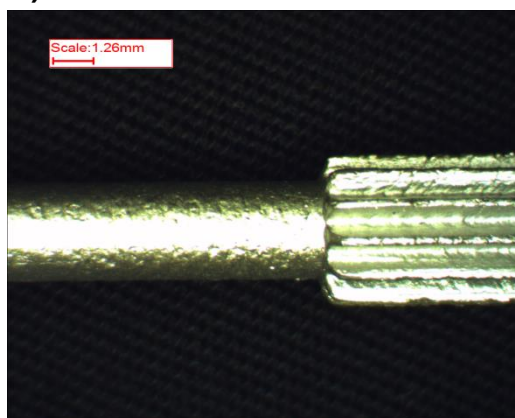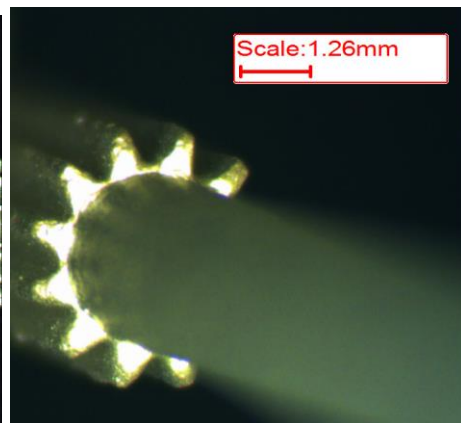
Figure 3.10: Photographs of the DMLS finned test section tube: a) Full horizontal view of two finned tube units with a ruler for scale; b) Comparison of finned and smooth portion of the tube under the microscope; c) Zoomed photograph of the longitudinal fins

The test section is coupled to a closed distilled water loop that is circulated by a centrifugal pump (AMT, 3680-975-97). A schematic of this loop is provided in Figure 3.11. To maintain the desired LMTD in the test section, the temperature of the water loop is controlled using a cross-flow, air-coupled heat exchanger (Lytron, 4105G1SB) and an electric fan (Shengkwei, SK109AP-11-1). A magnetic volumetric flow meter (Rosemount, 8711) is used to measure the water flow rate within this loop. Water temperature measurements are taken at the inlet and outlet of the test section heat exchanger using RTDs. The water loop pressure is measured using an absolute pressure transducer at the inlet of the test section heat exchanger. To measure the condensation heat transfer coefficient of the propane with low uncertainty, it is desirable that the dominant thermal resistance be on the propane side; therefore, the water coupling fluid loop is operated at a high flow rate. However, increasing the water flow rate decreases the temperature rise in the water across the test section, thus increasing the uncertainty of the heat duty calculation.
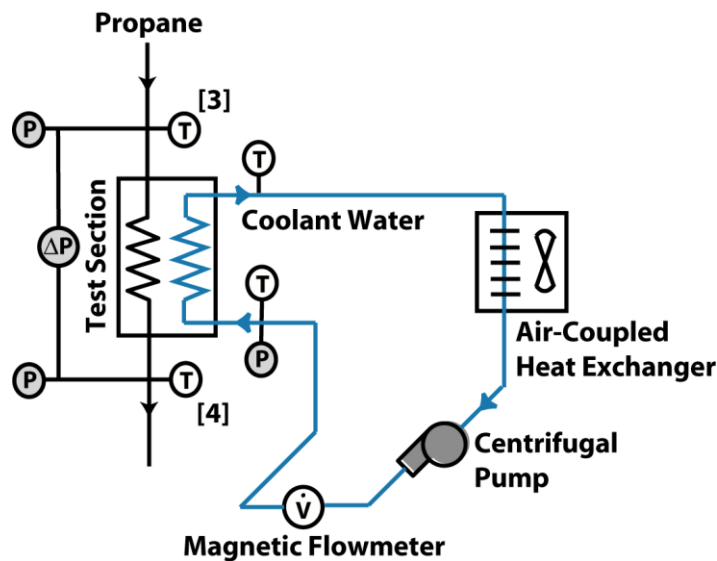
Figure 3.11: Schematic of the test section and coupling loop

The thermal amplification technique developed by Garimella and Bandhauer (2001), has been implemented in larger scale condensation studies in the Sustainable Thermal Systems Laboratory. This technique adds a low flow rate secondary coupling loop to the test section to balance these conflicting requirements of low uncertainty in the heat duty and heat transfer measurement. Using this technique, the primary loop flows at high velocity to decrease the uncertainty related to the thermal resistances, and the secondary loop flows at low velocity to achieve a larger temperature rise. The heat duty is obtained from an energy balance calculation while accounting for the temperature rise in the secondary loop as well as the ambient losses and pump heat addition in the primary loop. The advantages of the thermal amplification technique are mitigated in the present study by the heat duties in the test section, which are of a similar magnitude as the pump heat addition and ambient losses. Due to the low heat duties in the test section compared to pump heat addition and ambient losses in the primary loop, the thermal amplification technique cannot be implemented here. Thus, the heat duty in the test section in the present study is determined from the inlet and exit enthalpy as calculated from an energy balance on the pre- and post-condensers.

The propane exits the test section as a liquid-vapor mixture [4] and is then cooled to a subcooled liquid state [6] in the post-condenser, consisting of a counter-flow shell-and-tube heat exchanger (Exergy Series 23, 00540-5) with cooled compressed air on the shell-side. A schematic of the post-condenser and coupling loop is provided in Figure 3.12. The state is obtained from a combination of pressure and temperature measurements and further validated by a sight glass at the outlet of the post-condenser. Specifications for the post-condenser are shown in Table 3.2 and are identical to those of the pre-
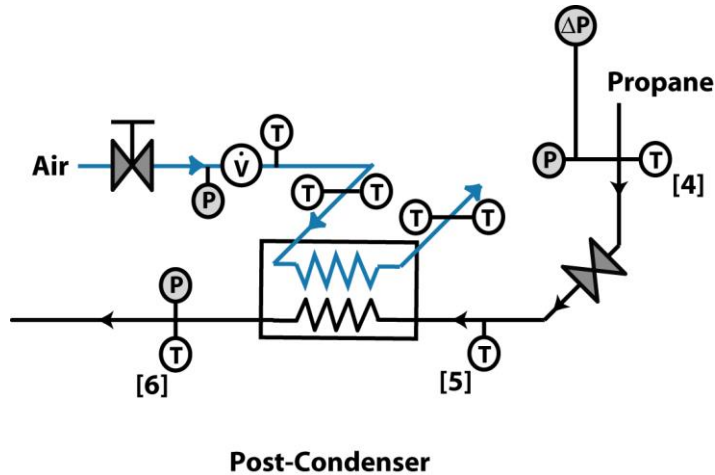
Post-Condenser

Figure 3.12: Schematic of the post-condenser and coupling loop

condenser. The compressed air flowing through the post-condenser is from the same source as that of the pre-condenser; therefore, flow rate adjustments to one heat exchanger inversely affect the flow rate to the other heat exchanger. Absolute pressure measurements are taken at the post-condenser outlet on the propane side and upstream of the gas turbine volume flow meters on the air side. Temperature measurements are taken using RTDs at the inlet and outlet of the post-condenser on the propane side to determine the state of the propane. RTDs and type T thermocouples are positioned upstream and downstream of the post-condenser on the air side in a configuration similar to that used for the pre-condenser. A type T thermocouple is placed directly downstream of the air turbine flow meter to ensure an accurate density (and thus mass flow rate) calculation. The liquid propane enthalpy at the exit of the post-condenser is determined from the measured pressure and temperature. The heat duty in the post-condenser is calculated from the air flow rate and the temperature rise across the heat exchanger. The post-condenser inlet propane enthalpy and thus, the test section exit enthalpy and quality are determined from the post-condenser heat duty.

For the propane loop, 6.35 mm (1/4 in) stainless steel seamless tubing is used to connect all of the system components. The wall thickness of the tubing is 0.889 mm (0.035 in) allowing for a maximum pressure of 35 MPa (5100 psig) (Swagelok, 2011). Propane flows through the tubing between a series of four heat exchangers that control its thermodynamic state. A total of 26 temperature measurements (12 Resistance Temperature Detectors [RTDs] and 14 Type T thermocouples), nine pressure measurements (one differential and eight absolute pressure transmitters), and four flow meters are used to monitor the system and provide data necessary to determine the heat transfer coefficient and pressure drop in the test section tube. The RTDs are placed at positions which benefit more from higher accuracy measurements, and the thermocouples are used in all other positions. The RTDs and thermocouples were calibrated using a calibration bath (Hart Scientific, Model 7340). The 4 − 20 mA analog output of the pressure transducers was scaled for the Data Acquisition System (DAQ) reading using the HART communicator device (Model 275). Specifications of the key pieces of equipment needed for facility operation are provided in Table 3.4 and specifications of each measurement device are shown in Table 3.5.
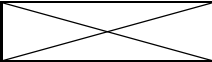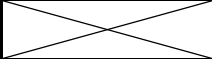
Three major electrical lines are installed to power and monitor the system: 120 VAC, 240 VAC, and 24 VDC. The 120 VAC line powers the AC/DC transformer used for the 24 V DC supply, the thermal controller, the DAQ, the evaporator and test section loop pumps, the fan and the small cartridge heater. The DC line powers most of the instrumentation including the pressure transmitters and the turbine and mass flow meters, as well as the solid state relay. The large immersion heater is connected though the solid state relay to 240 VAC.

The facility is designed for safe operation with hydrocarbons. All instrumentation is rated for explosive environments. The sides of the facility are enclosed with protective plastic curtains that extend to the floor. The main electrical components including the electrical box and pump controls are housed outside the plastic curtains to ensure that they are separated from the propane lines. A continuous exhaust (large, black flexible hose in Figure 3.2) is installed at the low point of the facility because if a leak occurred in the system, the propane (with a density, $\rho = 1.8$ kg m^{-3}) being denser than the surrounding air (with a density, $\rho = 1.2$ kg m^{-3}) would be exhausted from the bottom. The lab area is also instrumented with multiple flammable gas sensors that continuously measure levels of flammable gases in the lab. If flammable gas is detected, the sensors display a local alarm and alert the Environmental Health and Safety Department at the Institute.

Table 3.4: Major Loop Components and Specifications

Equipment	Manufacturer	Model Number	Serial Number	Fluid
Magnetic Gear Pump DC Drive Hub for GAH pump	Micropump	GAH-V21.CFS.A DC306A L15990	1945643	Propane
Magnetic Gear Pump AC Drive	Micropump	GB.P35.PVS.A DP-415A.A	1944885	Water
Centrifugal Pump	AMT	3680-975-97	0905	Water
NESLAB Merlin M75 Recirculating Chiller	Thermo Fisher Scientific	264216042000	010023401120324	50/50 Ethylene Glycol-Water
Firerod Immersion Heater, 500 W	Watlow	L6EX12B		Water
Firerod Cartridge Heater, 80 W, 500 W	Watlow	G1J66 G2A95		Air
Micromega Controller	Omega	CN77523	1340038	
Regulated DC Power Supply	Electro Industries	DIGI 35A		
Air Compressor	Quincy	QT-5		Air
Building Compressed Air Dryer	Aurora	HTC0025		Air
Facility Compressed Air Dryer	SPX Hankison	HPR10	H010A1150307636	Air
Shell and Tube Heat Exchanger	Exergy	00540-05 00540-05 00256-02 00677-03	39027 3900 15205 25547	Propane/Air Propane/Air Propane/Water Air/E-G
Fin and Tube Cross Flow Heat Exchanger and Fan	Lytron / Shengkwei	4105G1SB SK109AP-11-1	761306-02 0844	Water/Air
Hydraulic Piston Accumulator	Parker	ACP05AA050E1KTC	597726-03	Propane/N_2

Table 3.5: Instrument Specifications and Measurement Uncertainties

Instrument	Manufacturer	Model Number	Serial Number	Range	Uncertainty	Fluid
Pressure						
Absolute Pressure Transducer	Rosemount	3051CA4A22A1AB4E5M5	2327260 2327259 2327258 2327261	0 to 4000 psia	±0.065% of span	Propane
Differential Pressure Transducer	Rosemount	3051CD2A22A1AB4E5M5	2327378	-250 to 250 in. H_2O	±0.065% of span	Propane
Absolute Pressure Transducer	Rosemount	3051TA4A2B21AE5M5	1019350 1294374 1019354	0 to 4000 psia	±0.065% of span	Air Air Water
Absolute Pressure Transducer	Rosemount	3051TA5A2B21AE5M5	0921023	0 to 10,000 psia	±0.075% of span	Water
Flow Rate						
Elite Coriolis Mass Flow Sensor and Transmitter	Micromotion	CMFS010M324N2A2E2ZZ 1700R12ABAEZZZ	14186702 3150976		$\pm 5.6 \times 10^{-7}$ kg s^{-1}	Propane
Magnetic Flow Sensor and Transmitter	Rosemount	8711A5A30FR1E5G1 8712CT12M4	0164646 3150976		±0.25% of reading	Water
Turbine Flow Meter and Linear Link Transmitter	Flow Technology	FT-12NEXA-GEA-5 LN-5-C-MA-9	120518M12896 120518M12895 120503E12484 120503E12483	1.25 to 25 ACFM 0.35 to 5 ACFM	±0.30% of reading	Air
Temperature						
RTD	Omega	PR-13-2-100-1/8-6-E			±0.20 °C	Propane, Air, Water
Thermocouple	Omega	TMQSS-062G-6			±0.50 °C	Air, Water

3.2. Experimental Procedures

After construction of the experimental facility was completed, each loop was thoroughly leak tested. The propane loop was pressurized with nitrogen gas up to 2900 kPa and the pressure monitored for a nominal 12 hours, with appropriate adjustments for temperature changes. After pressurizing the system, leaks were detected using a bubble test. In this method, a soapy water mixture is applied to each connection so that any leak present produces bubbles. The loop was also filled with vapor R134a and R404a and a refrigerant leak detector (Yellow Jacket, 69365) was used at all fittings and joints to locate leaks. This process was repeated until all leaks were eliminated from the system. Similar methods were used for the coupling fluid loops to detect and fix leaks.

The propane loop was evacuated using a 7 CFM vacuum pump (J.B. Industries, DV-200N), and a vacuum gauge (Thermal Engineering Co, 14571) was used to measure the pressure. The loop was evacuated to a pressure of 200-300 microns and left evacuated without the vacuum pump to monitor any air ingress over time. The loop was charged with approximately 0.7 kg R134a for shakedown testing and approximately 0.27 kg propane for data collection. The evaporator and test section coupling loops were also evacuated and charged with distilled water.

Before starting up the system, the chiller was turned on and allowed to approach its set point. The propane loop pump was set at a flow rate above the eventual operating set point (around $G = 150$ kg m^{-2} s^{-1}) because the system response time is faster for higher mass fluxes. After a two-phase condition was established, the propane flow rate was adjusted to within ± 1 kg m^{-2} s^{-1} of the desired set point. The evaporator pump was set to about 50 – 70% speed (approximately 4500 – 6300 RPM) and the evaporator loop

temperature control was set in increasing temperature increments of 10°C until the desired set point was attained. The system pressure was monitored and adjusted using the accumulator to maintain operation at a saturation condition within ± 1°C of the desired saturation temperature. The compressed air line was opened and the heater for the pre-condenser was set to about 20 W for the 47°C condition and 250 W for the 74°C condition. The test section coupling loop water pump was turned on. The cross-flow heat exchanger fan was turned on for the 47°C saturation condition and off for the 74°C saturation condition. Using the approach specified above, it typically took 1 to 2 hours for the system to reach steady state in which none of the temperature or pressure readings in the system showed an increase or decrease in the span of 5 minutes.

The saturation temperature and mass flux were fixed for each experimental data set, while the pre- and post-condenser air flow rates were adjusted to vary the inlet quality at the test section. Data were collected starting at low quality points and increasing up to the higher quality points. During operation, data were recorded over a 30 s interval (89 readings) to determine the operating point of the system and assess whether it was at steady state. When the desired point was reached, data were recorded over a 300 s interval (899 readings). The measurements were averaged over this time period and the average values were used to analyze the data as described in Chapter 4. The sampling rate of the data acquisition system was 3 Hz.

After completing data collection, the system was shut down following a procedure similar to that employed for system start-up. First, the heater in the evaporator loop was turned off. The propane flow rate was increased to allow a faster response time. The chiller set point was reduced, and the compressed air flow rates were adjusted so that

there was equal flow through the pre- and post-condensers. The system was allowed to cool and eventually reached a subcooled liquid condition. When the propane temperature at the test section reached the water temperature of the coupling fluid, the water pump was turned off. When all temperatures in the system were sufficiently low, the pumps and chiller were shut off and the compressed air lines were closed.

3.3. System Validation

A series of validation and shakedown tests were performed to ensure that the system was operating properly and yielding accurate measurements. Initially, these tests were conducted using R134a as the working fluid to avoid the flammability concerns during validation. Much of the validation focused on the energy balances in these components, because the accuracy of the pre- and post-condenser measurements is critical to the heat transfer measurements. A summary of the experiments performed to validate the system is presented in Table 3.6.

Table 3.6: Summary of Validation Tests Performed

Validation Test	State	Fluid	Comparison
Pressure Drop	Single Phase	R134a	Churchill (1977b)
Pre- and Post-Condenser Energy Balance	Full Condensation	R134a	Air side and working fluid side heat duty
	Single Phase	R134a Propane	
Nusselt Number	Single Phase	Propane	Churchill (1977a)
Entire Loop Energy Balance	Two-Phase	R134a	Heat inputs and outputs in loop

3.3.1. <u>Single-Phase and Validation Testing Data Analysis</u>

During the condensation experiments, the thermodynamic states at the outlet of the pre-condenser and the inlet to the post-condenser cannot be directly measured. Thus, the heat duty can only be calcualted from the air-side. To ensure accurate calculation of air-side heat duty, validation tests were conducted with full condensation and single-phase cooling of the working fluid (i.e., the heat duty could be deterimed from air and working fluid energy balances). The calculations presented in this section are similar to those for the in-tube condensation tests presented in Chapter 4. Unless specified otherwise below, the same methods were used for the validation testing as for the condensation experiment data reduction.

Single-Phase Frictional Pressure Drop

In this section, the single-phase frictional pressure drop is calculated for a representative data point (Validation, Run 41). For this point, the working fluid is R134a. The R134a validation experiments were performed using a smooth test section with internal diameter 2.15 mm. During operation with propane, the smooth test section was replaced by the finned test section. The refrigerant mass flow rate is 1.518×10^{-3} kg s^{-1}. The refrigerant mass flux through the test section is calculated using Eq. (3.1).

$$G_{\mathrm{ref}} = \frac{\dot{m}_{\mathrm{ref}}}{\pi D_{\mathrm{test,in}}^{2}/4} = 418.0 \text{ kg m}^{-2} \text{ s}^{-1} \tag{3.1}$$

The refrigerant temperature at the inlet of test section ($T_{\mathrm{ref,3}}$) is 30.49°C and the refrigerant temperature at the outlet ($T_{\mathrm{ref,4}}$) is 28.74°C. The refrigerant pressures at the inlet and outlet are 2413.4 kPa and 2418.6 kPa, respectively.

The measured pressure drop across the inlet and outlet pressure taps in the test section is due to frictional, expansion, contraction and static contributions as shown in Eq. (3.2). For a schematic of the test section differential pressure measurement, see Figure 3.13.

$$\Delta P_{\text{measured}} = \Delta P_{\text{frictional}} + \Delta P_{\text{contraction}} - \Delta P_{\text{expansion}} - \Delta P_{\text{static,test}} + \Delta P_{\text{static,line}} \qquad (3.2)$$

The single phase contraction pressure drop was calculated for the three area reductions described for the in-tube condensation experiments. The area ratios were calculated as in Eq. (3.3) to be 0.839, 0.295 and 0.805 for the contractions from the cross
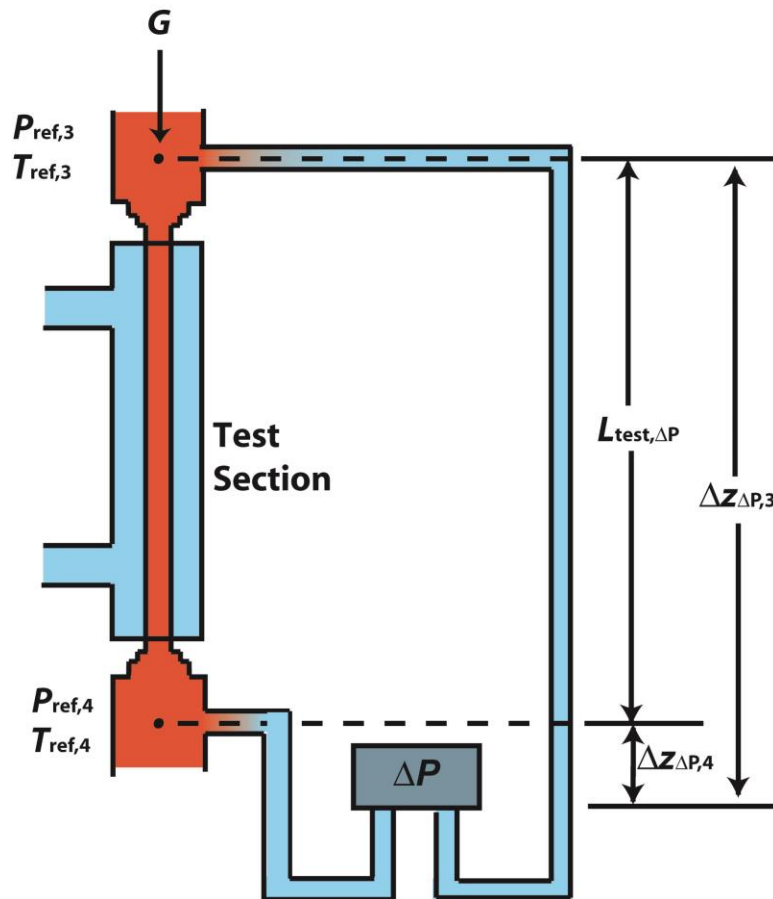
Figure 3.13: Schematic showing the configuration of the test section differential pressure measurements

to the reducer, the reducer to the intermediate contraction, and the contraction to the test section, respectively.

$$A_{\text{ratio,test,1}} = D_{\text{reducer}}^2 / D_{\text{cross}}^2 = (0.00442 \text{ m})^2 / (0.00483 \text{ m})^2 = 0.839$$
$$A_{\text{ratio,test,2}} = D_{\text{contraction}}^2 / D_{\text{reducer}}^2 = (0.00240 \text{ m})^2 / (0.00442 \text{ m})^2 = 0.295 \quad (3.3)$$
$$A_{\text{ratio,test,3}} = D_{\text{test,in}}^2 / D_{\text{contraction}}^2 = (0.00193 \text{ m})^2 / (0.00240 \text{ m})^2 = 0.647$$

For each region, the R134a mass flux is adjusted accordingly:

$$G_{\text{ref}} = 418.0 \text{ kg m}^{-2} \text{ s}^{-1}$$
$$G_{\text{ref,contraction}} = G_{\text{ref}} A_{\text{ratio,test,3}} = 335.5 \text{ kg m}^{-2} \text{ s}^{-1} \quad (3.4)$$
$$G_{\text{ref,reducer}} = G_{\text{ref}} A_{\text{ratio,test,3}} A_{\text{ratio,test,2}} = 98.9 \text{ kg m}^{-2} \text{ s}^{-1}$$

The contraction pressure drop from the line to the test section is given by Hewitt *et al.* (1994) in Eq. (3.5) and consists of reversible and irreversible losses.

$$\Delta P_{\text{contraction}} = \frac{G^2}{2\rho_{\text{ref,3}}} \left(\underbrace{1 - A_{\text{ratio}}^2}_{\text{reversible}} + \underbrace{\left(\frac{1}{C_{\text{C}}} - 1 \right)^2}_{\text{irreversible}} \right) \quad (3.5)$$

The density of R134a at the test section inlet (30.49°C, 2413.4 kPa) is 1196 kg m^{-3}. The coefficient of contraction is given by Geiger and Rohrer (1966) in Eq. (3.6). For the contractions under consideration, the coefficient is 0.8152, 0.6481, and 0.7916 respectively.

$$C_{\text{C}} = 1 - \frac{1 - A_{\text{ratio}}}{2.08 \cdot (1 - A_{\text{ratio}}) + 0.5371} \quad (3.6)$$

Therefore, as defined in Eq. (3.5), the total contraction pressure drop is:

$$\begin{aligned} \Delta P_{\text{contraction}} &= \Delta P_{\text{contraction,1}} + \Delta P_{\text{contraction,2}} + \Delta P_{\text{contraction,3}} \\ &= 1.42 \text{ Pa} + 56.81 \text{ Pa} + 31.06 \text{ Pa} \\ &= 89.29 \text{ Pa} \end{aligned} \quad (3.7)$$

The single-phase expansion pressure drop also consists of reversible and irreversible losses as shown in Eq. (3.8).

$$\Delta P_{\text{expansion}} = \frac{G^2}{2\rho_{\text{ref},4}} \left(\underbrace{\left(1 - A_{\text{ratio}}^2\right)}_{\text{reversible}} - \underbrace{\left(1 - A_{\text{ratio}}\right)^2}_{\text{irreversible}} \right)$$

(3.8)

The density of R134a at the test section outlet (28.74°C, 2418.6 kPa) is 1203 kg m^{-3}. The individual and total expansion pressure drop terms are then:

$$
\begin{aligned}
\Delta P_{\text{expansion}} &= \Delta P_{\text{expansion},1} + \Delta P_{\text{expansion},2} + \Delta P_{\text{expansion},3} \\
&= 1.10 \text{ Pa} + 19.45 \text{ Pa} + 23.02 \text{ Pa} \\
&= 43.57 \text{ Pa}
\end{aligned}
$$

(3.9)

The static head in the test section is calculated from Eq. (3.10),

$$\Delta P_{\text{static,test}} = \rho_{\text{ref,test}} g L_{\text{test,total}} = 3035 \text{ Pa}$$

(3.10)

where the density (1200 kg m^{-3}) is calculated at the average R134a temperature and pressure in the test section (29.60°C, 2416.7 kPa) and the pressure drop length is 258 mm. The static head in the pressure tap lines is calculated similarly. Assuming a constant density (1222 kg m^{-3}) in both lines based on the ambient temperature and test section average pressure (23.64°C, 2416.7 kPa), the equation for the static head reduces to Eq. (3.11).

$$\Delta P_{\text{static,line}} = \rho_{\text{ref,line}} g L_{\text{test,total}} = 3092 \text{ Pa}$$

(3.11)

The measured differential pressure across the test section is 372.2 Pa. The frictional pressure drop is determined from Eq. (3.2) to be 269.8 Pa.

$$
\begin{aligned}
\Delta P_{\text{frictional}} &= \Delta P_{\text{measured}} - \Delta P_{\text{contraction}} + \Delta P_{\text{expansion}} + \Delta P_{\text{static,test}} - \Delta P_{\text{static,line}} \\
&= 372.2 \text{ Pa} - 89.29 \text{ Pa} + 45.57 \text{ Pa} + 3035 \text{ Pa} - 3092 \text{ Pa} \\
&= 269.8 \text{ Pa}
\end{aligned}
$$

It can be seen that for single phase fluid at lower temperature, the net contribution of static head terms ($-$ 57 Pa) is on the same order as the loss terms, although individually, the static head is an order of magnitude greater than the measured differential pressure.

To validate the system, the measured single-phase frictional pressure drop is compared with the value predicted by the Churchill (1977b) correlation. The Reynolds number of the flow for the representative data point is 4728 ($\mu_{\text{ref,test}} = 1.90 \times 10^{-4}$ kg m^{-1} s^{-1}). The Darcy friction factor for single phase liquid R134a is calculated to be 0.039 from Eq. (3.12). The roughness of the smooth tube is 0.0015 mm (Munson *et al.*, 2006).

$$f = 8\left[\left(\frac{8}{\text{Re}}\right)^{12} + \frac{1}{(B+C)^{1.5}}\right]^{1/12}$$

$$\text{where } B = \left(2.457\ln\frac{1}{(7/\text{Re})^{0.9} + 0.27(e/D_{\text{test,in}})}\right)^{16} \text{ and} \qquad (3.12)$$

$$C = \left(\frac{37530}{\text{Re}}\right)^{16}$$

The predicted frictional pressure drop is then,

$$\Delta P_{\text{test,f,Churchill}} = f_{\text{test}}\frac{L_{\text{test},\Delta P}}{D_{\text{test,in}}}\frac{G_{\text{ref}}^2}{2\rho_{\text{ref,test}}} = 271.1 \text{ Pa} \qquad (3.13)$$

The pressure drop length is 203.1 mm, the diameter is 2.15 mm, and the density is 1200 kg m^{-3}. Thus, the measured value differs from the predicted value by 0.5%. For the entire validation data set spanning laminar, transition, and turbulent flows, the absolute deviation between measured and predicted pressure drop values ranges from 0% to 58% (13% average). Comparison between these values was used to determine the validity of the facility measurements and data reduction.

Pre- and Post-Condenser Energy Balance Validation

The energy balance in the pre- and post-condensers was validated by comparing the heat duty as computed from the enthalpy change in the propane line and the air line. This analysis is described here for a representative data point (Validation Propane, Run 42). For this test, the working fluid is propane at single-phase operating conditions. The propane mass flow rate is 7.779×10^{-4} kg s^{-1}, and the mass flux is 265.9 kg m^{-2} s^{-1} as calculated using Eq. (3.1). For the propane validation tests, the finned test section was used; therefore, the internal diameter by which the mass flux is defined is 1.93 mm.

The pressure and temperature at the inlet of the pre-condenser [1] are 2637.9 kPa and 60.83°C, respectively. At this point, the propane is subcooled by 10.17°C. Therefore the enthalpy of the propane at the inlet of the pre-condenser is 369.7 kJ kg^{-1}. The second enthalpy value is taken from measurement point [3] at the entrance to the test section rather than at point [2] at the exit of the pre-condenser in which there is no pressure measurement. (See Figure 3.4 for the position of the pressure and temperature measurements). The propane enthalpy at the inlet of the test section using the elevation adjusted pressure (see Chapter 4) is then: $i_{propane,3} = f(2640.6 \text{ kPa}, 23.17°C) = 258.5$ kJ kg^{-1}. The intermediate losses between the pre-condenser and the test section as well as the losses from the pressure tap lines at the inlet of the test section are calculated as in Chapter 4 to be -0.06 W and -0.02 W respectively (heat gained from the environment). The heat duty on the propane-side is then:

$$\begin{aligned}
\dot{Q}_{\text{pre,propane}} &= \dot{m}_{\text{propane}}\left(i_{\text{propane,1}} - i_{\text{propane,3}}\right) - \dot{Q}_{23,\text{loss}} - \dot{Q}_{\text{test,line,in,loss}} \\
&= (7.779 \times 10^{-4}\ \text{kg s}^{-1})(369.7\ \text{kJ kg}^{-1} - 258.5\ \text{kJ kg}^{-1}) \\
&\quad -(-0.06\ \text{W}) - (-0.02\ \text{W}) \\
&= 85.14 \pm 0.66\ \text{W}
\end{aligned} \tag{3.14}$$

The heat duty on the air side is caluclated from the temperature rise of the air adjusted for ambient losses. The pre-condenser air inlet temperatures are 14.55°C (RTD) and 14.25°C (thermocouple) for an average inlet temperature of 14.40°C. The pre-condenser air inlet enthalpy is calculated at the measured pressure (133.11 ± 2.07 kPa), average inlet temperature, and humidity ratio (ω = 0.00152) to be 291.1 kJ kg^{-1}. The measured air temperatures at the pre-condenser outlet are 37.22°C (RTD) and 36.94°C (thermocouple) for an average outlet temperature of 37.08°C. The differences in the temperature measurements using RTDs and thermocouples ($\Delta T_{\text{air,pre,in}}$ = 0.30°C, $\Delta T_{\text{air,pre,out}}$ = 0.28°C) are much less than the overall temperature rise in the air (15.06°C). The pre-condenser outlet enthalpy is calculated at ambient pressure (93 kPa) to be 314.1 kJ kg^{-1}. The air volumetric flow rate through the pre-condenser is 139.7 ± 0.4 L min^{-1}. The density of air at the flow meter is 1.619 kg m^{-3} calculated at 13.18°C, 133.11 kPa and ω = 0.00152. Therefore, the air mass flow rate through the pre-condenser is $\dot{m}_{\text{air,pre}} = \dot{V}_{\text{air,pre}}\rho_{\text{air,pre,flow}} = 3.768 \times 10^{-3}$ kg s^{-1}. The ambient heat loss between propane measurement [1] (see Figure 3.4) and the pre-condenser is 0.14 W. The heat loss from the air side of the pre-condenser is 0.01 W, therefore the net ambient loss is 0.15 ± 0.04 W. The heat duty in the pre-condenser on the air-side is then,

$$\begin{aligned}
\dot{Q}_{\text{pre,air}} &= \dot{m}_{\text{air,pre}}\left(i_{\text{air,pre,out}} - i_{\text{air,pre,in}}\right) + \dot{Q}_{\text{1-to-pre,loss}} + \dot{Q}_{\text{pre,loss}} \\
&= (3.768 \times 10^{-3}\ \text{kg s}^{-1})(314.1\ \text{kJ kg}^{-1} - 291.1\ \text{kJ kg}^{-1}) + 0.14\ \text{W} + 0.01\ \text{W} \\
&= 86.65 \pm 2.03\ \text{W}
\end{aligned} \tag{3.15}$$

There is a 1.8% difference in the heat duty measurement between the two methods. These values are within the experimental uncertainty of the air-side heat duty. These values were compared for all the single phase tests using propane and R134a as well as for full condensation across the pre-condenser using R134a. For the single-phase propane validation tests, the heat duty difference in the pre-condenser ranged from 1.3% to 2.8% (average 2.0%).

The energy balance in the post-condenser is validated similarly. In the previous representative data point, the post-condenser air temperature rise is only 3.6°C; therefore, another representative point is chosen to demonstrate the post-condenser validation under conditions that allow a clearer illustration of the analysis (Validation Propane, Run 19). For this data point, the propane mass flow rate is 9.255×10^{-4} kg s^{-1}, which yields a mass flux of 316.3 kg m^{-2} s^{-1}. The propane enthalpy at the outlet of the test section is: $i_{propane,4} = f(2672.4 \text{ kPa}, 39.76°C) = 305.9$ kJ kg^{-1}. The losses from the pressure tap lines at the outlet of the test section and the intermediate losses between the test section and post-condenser are calculated as in Chapter 4 to be 0.29 W and 0.21 W, respectively. The outlet enthalpy at 2675.5 kPa and 21.01°C is calculated to be 254.7 kJ kg^{-1}. Therefore, the heat duty in the post-condenser on the propane side is 46.87 ± 0.72 W.

$$
\begin{aligned}
\dot{Q}_{post,propane} &= \dot{m}_{propane}(i_{propane,4} - i_{propane,6}) - \dot{Q}_{test,line,out,loss} - \dot{Q}_{45,loss} \\
&= (9.255 \times 10^{-4} \text{ kg s}^{-1})(305.9 \text{ kJ kg}^{-1} - 254.7 \text{ kJ kg}^{-1}) \\
&\quad - 0.29 \text{ W} - 0.21 \text{ W} \\
&= 46.87 \pm 0.72 \text{ W}
\end{aligned}
\tag{3.16}
$$

The heat duty on the air side is calcuated using Eq. (3.17). The air volumetric flow rate is 141.1 ± 0.4 L min^{-1}. The air density at the flow meter is $\rho_{air,post} = f(128.96 \text{ kPa}, 15.01°C, \omega = 0.00152) = 1.558$ kg m^{-3}. Therefore, the air mass flow rate is

3.663×10^{-3} kg s^{-1}. The inlet air temperatures are 16.65°C (RTD) and 16.30°C (thermocouple), resulting in an average value of 16.48°C. The outlet air temperatures are 29.30°C (RTD) and 29.04°C (thermocouple) resulting in an average value of 29.17°C. The corresponding inlet air enthalpy is 293.2 kJ kg^{-1}, while the outlet air enthalpy is 306.1 kJ kg^{-1}. The ambient heat gain is 0.24 W in the post-condenser, and 0.03 W between the heat exchanger and the outlet measurement location for a net heat gain from the environment of 0.27 ± 0.07 W. The air-side heat duty in the post-condenser is given by,

$$
\begin{aligned}
\dot{Q}_{\text{post,air}} &= \dot{m}_{\text{air,post}} \left(i_{\text{air,post,out}} - i_{\text{air,post,in}} \right) + \dot{Q}_{\text{post,loss}} + \dot{Q}_{\text{post-to-6,loss}} \\
&= (3.663 \times 10^{-3} \text{ kg s}^{-1})(306.1 \text{ kJ kg}^{-1} - 293.2 \text{ kJ kg}^{-1}) \\
&\quad + (-0.24 \text{ W}) + (-0.03 \text{ W}) \\
&= 46.90 \pm 1.62 \text{ W}
\end{aligned}
\tag{3.17}
$$

The difference between measurements is 0.03 W (0.1% of the propane-side heat duty). For the single-phase propane validation experiments, the heat duty difference ranged from 0.0% to 1.4% (average 0.6%).

Single-Phase Heat Transfer Coefficient Validation

This section presents calculations for the single phase heat transfer coefficient for the representative data point discussed above to illustrate the post-condenser energy balance during shakedown testing (Propane Validation, Run 19). As mentioned above, the propane mass flow rate is 9.255×10^{-4} kg s^{-1}, which yields a mass flux of 316.3 kg m^{-2} s^{-1}. The elevation adjusted pressures and temperatures are 2677.3 kPa and 27.15°C at the test section inlet, and 2672.4 kPa and 39.76°C at the test section outlet for an average of 2674.8 kPa and 33.46°C. The viscosity in the test section at the average

conditions is 9.206×10^{-5} kg m^{-1} s^{-1}. This results in a Reynolds number of 6632, implying that the flow is in the transition region.

It should be noted that the test conditions for this point were selected to validate the pre- and post-condensers at higher heat duties more representative of the two-phase test conditions; therefore, the propane undergoes heating rather than cooling in the test section. The propane enthalpy at the inlet of the test section is 269.4 kJ kg^{-1}, while it is 305.9 kJ kg^{-1} at the outlet. The test section heat duty and LMTD are calculated using Eq. (3.18) and (3.19), respectively.

$$\dot{Q}_{\text{test}} = \dot{m}_{\text{propane}}(i_{\text{ref,3}} - i_{\text{ref,4}}) \tag{3.18}$$

$$\Delta T_{\text{LM,test}} = \frac{(T_{\text{propane,3}} - T_{\text{water,test,out}}) - (T_{\text{propane,4}} - T_{\text{water,test,in}})}{\ln \dfrac{T_{\text{propane,3}} - T_{\text{water,test,out}}}{T_{\text{propane,4}} - T_{\text{water,test,in}}}} \tag{3.19}$$

The test section heat duty is -32.24 W and the LMTD is -19.69 K (the negative values indicate heating of the fluid). From these two values, the conductance of the test section can be calculated to be: $UA_{\text{test}} = \dot{Q}_{\text{test}} / \Delta T_{\text{LM,test}} = 1.64$ W K^{-1}. The propane thermal resistance is then calcualted to be 0.542 K W^{-1} from a resistance network analysis, as shown in Eq. (3.20). The wall and water-side thermal resistances are calculated to be 0.0022 K W^{-1} and 0.066 K W^{-1}, respectively. (See Chapter 4 for a more detailed discussion of this method.)

$$R_{\text{test,propane}} = \frac{1}{UA_{\text{test}}} - R_{\text{test,wall}} - R_{\text{test,water}} \tag{3.20}$$

The propane-side heat transfer coefficient is calculated to be 2251 W m^{-2} K^{-1} and the Nusselt number is 47.41 ± 2.07, using Eq. (3.21) and (3.22).

$$h_{\text{test,propane}} = \frac{1}{R_{\text{test,propane}} \pi D_{\text{test,in}} L_{\text{test,HT}}} \tag{3.21}$$

$$\text{Nu}_{\text{propane,test}} = \frac{h_{\text{test,propane}} D_{\text{test,in}}}{k_{\text{propane,test}}} \tag{3.22}$$

This value is compared to the Nusselt number predicted by Churchill (1977a; 1977b) as in Eq. (3.12) and (3.23), respectively. The roughness of the DMLS finned test section is 0.015 mm. The predicted Nusselt number is 46.62. The measured value deviates from the predicted value by 0.79 (1.7% of the predicted value) and is within the range of experimental uncertainty. The absolute difference between the measured and predicted Nusselt number values for the single-phase propane validation experiments ranges from 0.2% to 15.9% (average 5.8%).

$$\text{Nu} = \left(4.364^{10} + \left(\frac{e^{\frac{2200-\text{Re}}{365}}}{4.364^2} + \frac{1}{\left(6.3 + \frac{0.079 \left(\frac{f}{8} \right)^{0.5} \text{Re}\,\text{Pr}}{\left(1 + \text{Pr}^{0.8} \right)^{5/6}} \right)^2} \right)^{-5} \right)^{1/10} \tag{3.23}$$

3.3.2. <u>Single-Phase Validation Testing Results</u>

The results of the pressure drop validation tests are shown in Figure 3.14. For all the single-phase pressure drop validation experiments, the absolute deviation between measured and predicted values ranges from 0% to 58% with an average absolute deviation of 13%. The data are grouped into laminar, transition and turbulent flow. Good

agreement is observed for the transition region (2,300 < Re < 10,000). The absolute deviation between measured and predicted values ranges from 0% to 22%, with an average of 5%. The average uncertainty of the data in this region is 16.9% of the measured value. The laminar data (Re < 2,300) show poor agreement; this is due to the small magnitude of the measured values (16 to 79 Pa), for which the frictional pressure drop constitutes only a small fraction of the total measured pressure drop (24% to 51%, average 41%); here the average experimental uncertainty is 67% of the deduced frictional pressure drop values. For these data,the absolute deviation ranges from 23% to 58% with an average absolute deviation of 45%. For these small pressure drops, the contributions
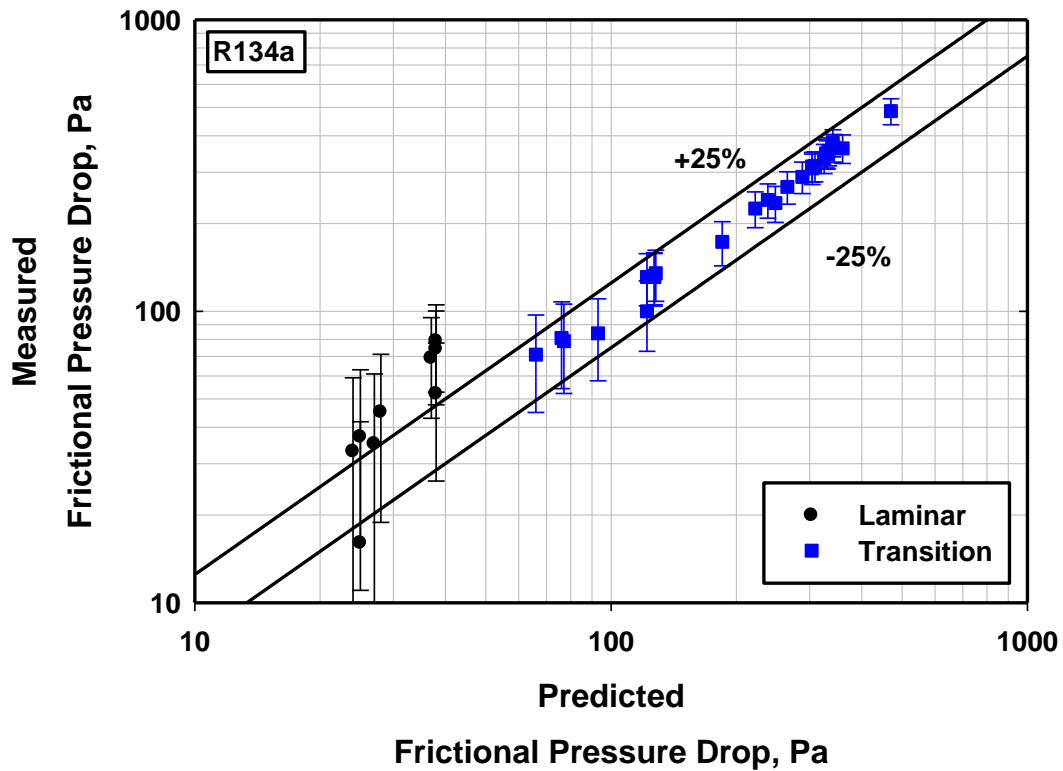
Figure 3.14: Frictional pressure drop validation results using R134a

of the minor losses and static terms are much greater relative to the measured value, which leads to greater uncertainty. The range of pressure drop measurements in the transition region ($71 < \Delta P < 486$ Pa) is more representative of the experimental operating conditions because two-phase pressure drops are larger than those for single-phase flow. Therefore, due to the accuracies observed from these measurements, it was determined that the system can adequately measure the frictional pressure drop in the two-phase experiments of interest in the present study.

Heat duty measurements from the air side and working fluid properties were compared for the pre- and post-condenser. The system was operated so that the fluid was in single phase at the inlet and outlet of the heat exchanger so that the working fluid state point could be calculated directly from pressure and temperature measurements. Several cases of full condensation across each heat exchanger using R134a as the working fluid were measured to demonstrate operation at heat duties that were comparable to the expected two-phase requirements. For the propane validation tests, single-phase heat duty measurements were also taken to complement the R134a validation results. The results for the R134a tests are shown in Figure 3.15, while the propane validation results are shown in Figure 3.16. The data are summarized in Table 3.7. For the single-phase R134a tests, the average difference between the heat duty measured on the refrigerant side and the coolant side of the pre-condenser is 1.5%, with a range of 0.0% to 5.0%. For the post-condenser, the corresponding average is 2.0%, with a range of 0.1% to 7.0%. Under full condensation in each heat exchanger with R134a, the average difference for the pre-condenser is 2.8%, with a range of 0.0% to 11.0%. For the post-condenser, the corresponding average is 4.6%, with a range of 2.4% to 6.0%. For all the R134a data, the
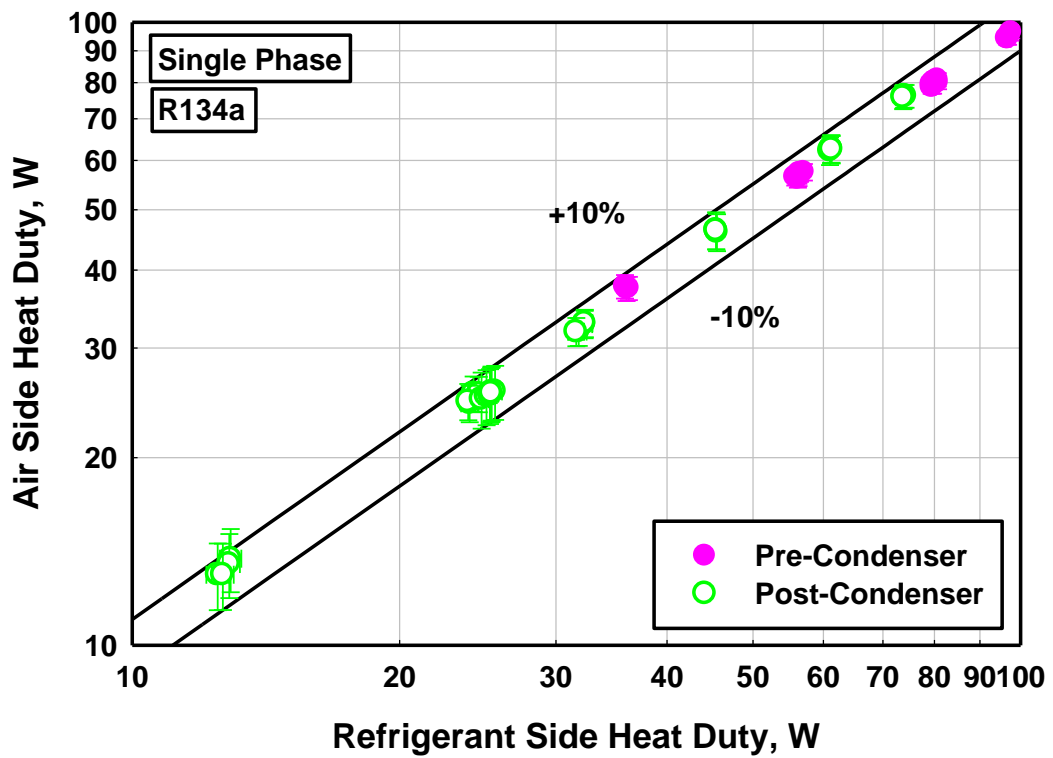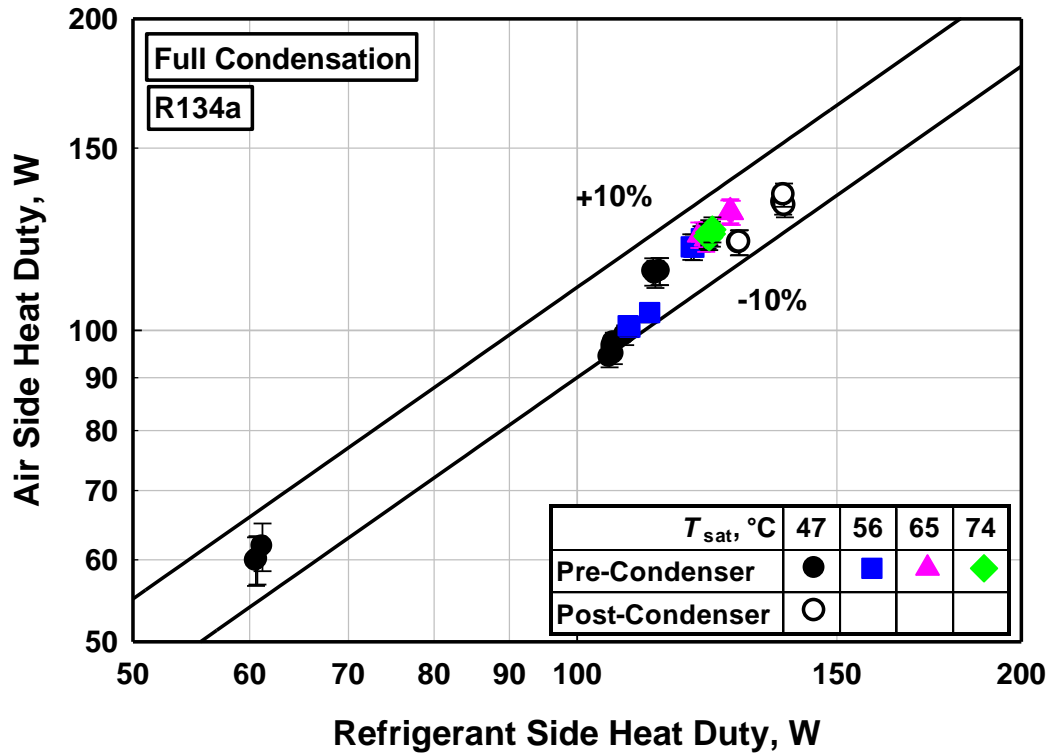
Figure 3.15: Energy balance validation testing results for full condensation and single-phase conditions using R134a
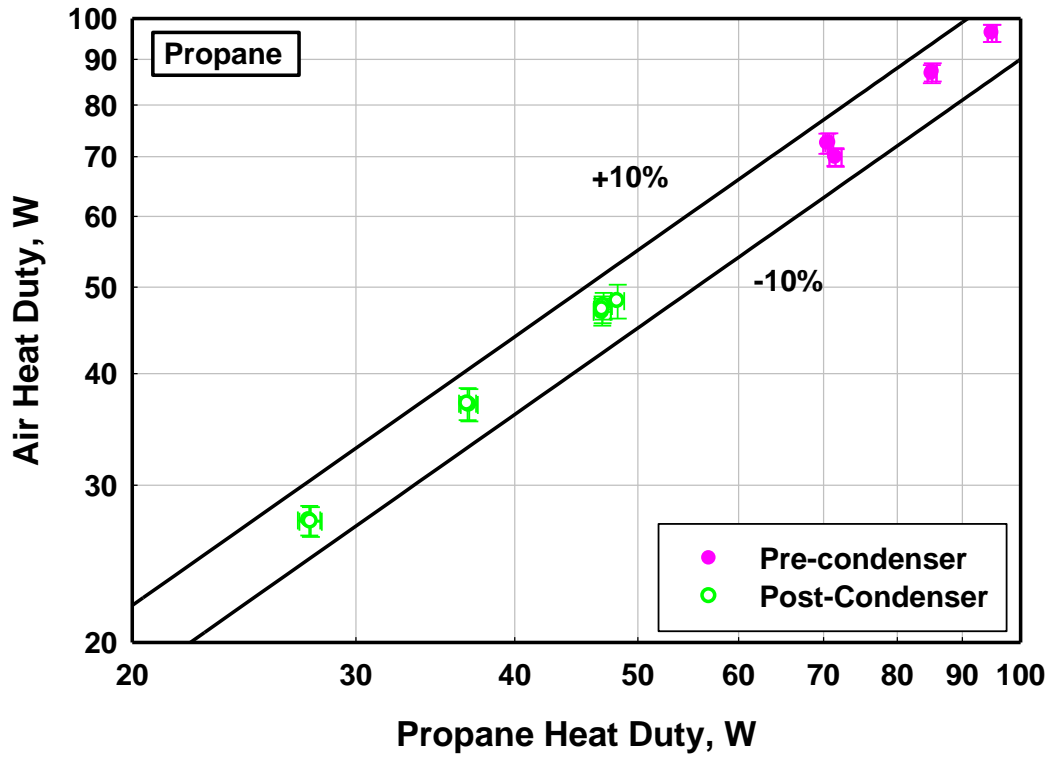
Figure 3.16: Single phase validation testing results using propane

Table 3.7: Energy balance validation summary

Heat Exchanger	Test Condition	R134a Heat Duty Difference, %			Propane Heat Duty Difference, %		
		Minimum	Maximum	Average	Minimum	Maximum	Average
Pre-Condenser	All Data	0.0	11.0	2.2	1.3	2.8	2.0
	Full Condensation	0.0	11.0	2.8			
	Single Phase	0.0	5.0	1.5	1.3	2.8	2.0
Post-Condenser	All Data	0.1	7.0	2.4	0.0	1.4	0.6
	Full Condensation	2.4	6.0	4.6			
	Single Phase	0.1	7.0	2.0	0.0	1.4	0.6

average difference between the measured heat duties on the refrigerant and coolant sides is 2.2%, with a range of 0.0% to 11.0%. For the post-condenser, the corresponding average is 2.4%, with a range of 0.1% to 7.0%. The full condensation experiments were performed at four saturation conditions (T_{sat} = 47, 56, 65, and 74°C). It was observed that the energy balance agreement was similar, regardless of the saturation condition or heat duty. Due to the limitations on the heater and heat exchanger capacities, full condensation in the post-condenser was only measured at the 47°C saturation temperature condition.

The single-phase propane tests showed an air-to-propane heat duty difference ranging from 1.3% to 2.8% in the pre-condenser (2.0% average deviation) and from 0.0% to 1.4% in the post-condenser (0.6% average deviation). These data are in agreement with the trends observed in the R134a validation experiments. During two-phase experiments, the heat duty in the pre-condenser ranged from 16 W to 137 W and between 22 W and 94 W in the post-condenser.The difference between the heat duty measurements on the propane and coolant sides is independent of the magnitudes of the heat duties measured.

In addition to the R134a and propane heat duty validation experiments, the single-phase heat transfer coefficient of propane was measured and compared with the predictions of the Churchill (1977a) correlation. It should be noted that the propane is undergoing heating rather than cooling for these single-phase experiments so as to measure higher heat duty conditions in the pre-condenser, which are more representative of the conditions in the two-phase experiments, for the energy balance validation experiments, which were conducted simultaneously. The results are summarized in Figure 3.17. The difference between the measured Nusselt number and the predicted

value ranges from 0.2% to 15.9%, with an average absolute deviation of 5.8% for Reynolds number from 2983 to 6633, which spans the transition and turbulent regimes. The agreement between the measured and predicted values is better in the fully turbulent regime and as the Reynolds number increases. The average absolute deviation for Re > 5000 is 4.8%. The flow rates for these tests were higher than the test conditions in the condensing experiments so that a reasonable heat duty (12.1 W to 32.4 W) could be obtained for single-phase operation in the test section. For the single-phase propane tests, the measured heat transfer coefficients compare favorably with the predicted values.

An overall loop energy balance was performed for two-phase operation with R134a showing 1.5% error on average. Figure 3.18 shows a graphical depiction of the
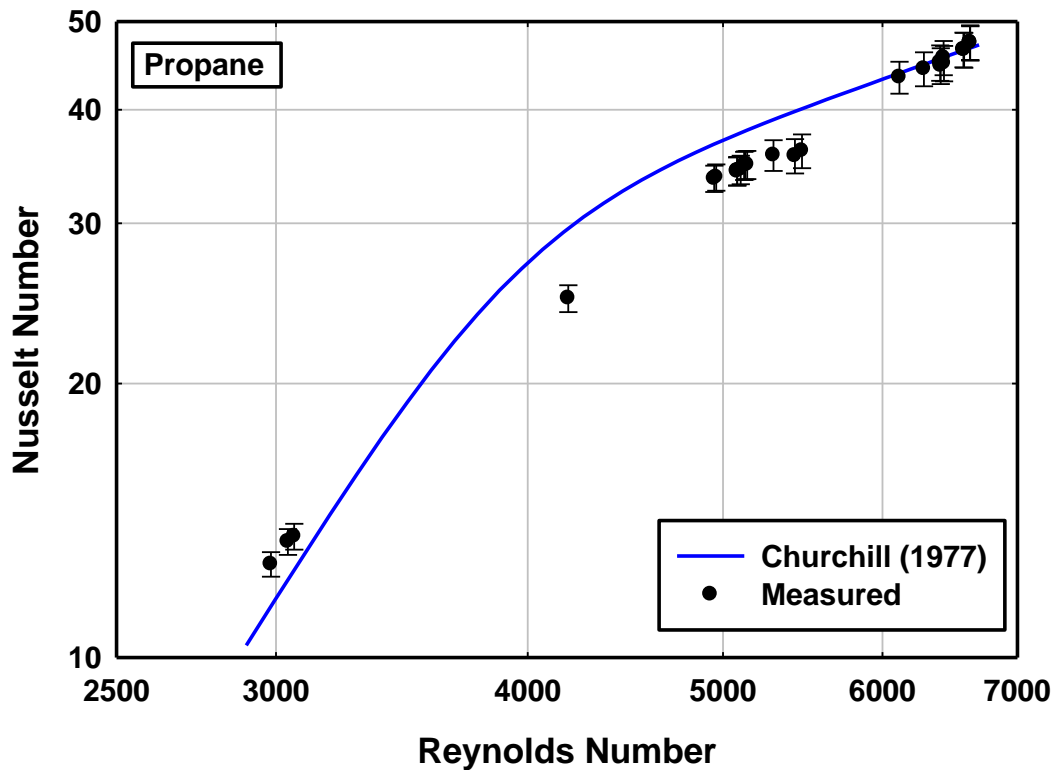
Figure 3.17: Single-phase heat transfer coefficient validation testing using propane, showing measured values and predicted curves

loop energy balance, tracing the heat inputs and outputs for a representative data point. The graph uses the subcooled liquid propane at the outlet of the post-condenser as a reference point. The test section coupling loop was not running during this measurement; therefore, the heat loss in the test section was solely due to conduction and free convection of the water in the annulus. The heat output of the system is greater than the heat input by 1.5% on average, suggesting that the heat losses are overestimated by a small amount. However during two-phase heat transfer experimentation, the overall energy balance was not a reliable measure of the system performance due to large uncertainty in the test section water heat duty measurement.

From these test results, it was determined that the system is functioning adequately and can yield acceptable measurements in the two-phase experiments. Those results are described in the following chapters.
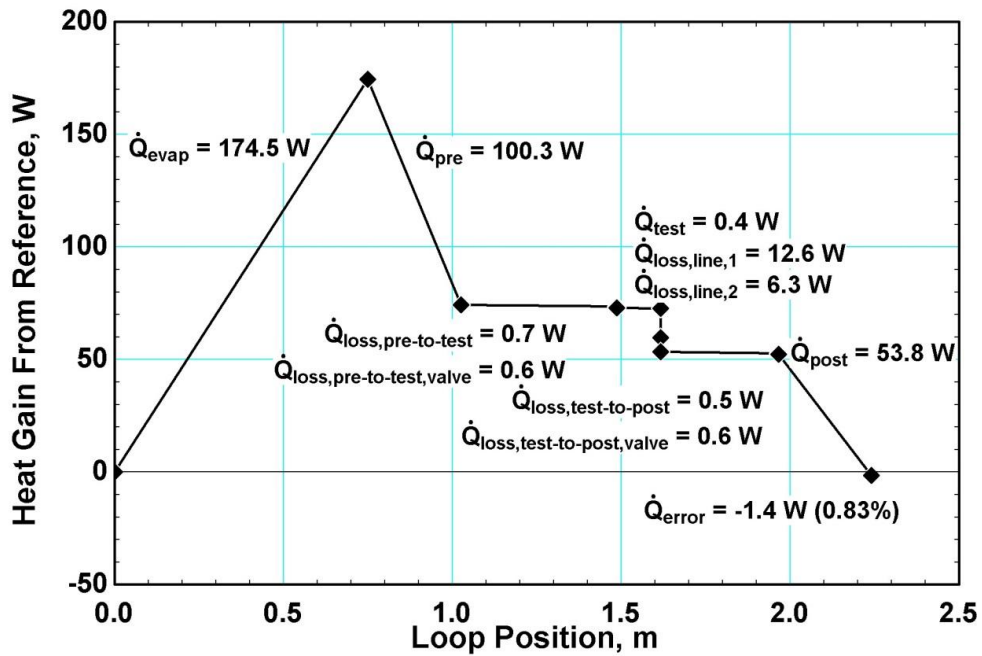
Figure 3.18: Graphical depiction of facility loop energy balance with the subcooled liquid R134a as the reference state

CHAPTER 4: DATA ANALYSIS

This chapter describes the data reduction methods and calculation of uncertainties related to the condensation heat transfer coefficient and frictional pressure drop. A sample calculation is presented for a representative data point to assist the discussion. The thermodynamic states and properties of water, air and propane are evaluated using Engineering Equation Solver (EES) software (Klein, 2011) along with the property database in REFPROP 9.0 (Lemmon *et al.*, 2010). The uncertainty propagation analysis in EES is based on the methods in Taylor and Kuyatt (1994). A detailed explanation of the method of uncertainty propagation is provided in Appendix A, and a more detailed exposition of the sample data point analysis is provided in Appendix C.

The data reduction procedure is illustrated using a representative data point (Run 7): 47.03°C saturation temperature, 100.2 kg m^{-2} s^{-1} mass flux and quality change from 0.72 to 0.46. The measured temperature and pressure values with uncertainties along with the associated saturation temperature of the propane are presented in Table 4.1. The temperature, pressure and flow rate measurements for the coupling fluids are shown in Table 4.2. From Eq. (4.1), the mass flux through the test section is calculated to be 100.2 ± 0.19 kg m^{-2} s^{-1}, where the mass flow rate is $\dot{m}_{\text{propane}} = 2.932 \times 10^{-4}$ $\pm\, 5.6 \times 10^{-7}$ kg s^{-1} and the inner diameter of the test section ($D_{\text{test,in}}$) is 1.93 mm.

$$G_{\text{propane}} = \frac{\dot{m}_{\text{propane}}}{\pi D_{\text{test,in}}^2 / 4} \tag{4.1}$$

Table 4.1: Propane Measurements, $\dot{m}_{propane} = 2.932 \times 10^{-4}$ kg s^{-1}

		Temperature		Pressure		Saturation Temperature	
		°C		kPa		°C	
Pre-Condenser	Inlet	$T_{propane,1}$	82.91 ± 0.20	$P_{propane,1}$	1615.7 ± 1.95	$T_{sat,1}$	47.32
	Outlet	$T_{propane,2}$	47.31 ± 0.20				
Test Section	Inlet	$T_{propane,3}$	47.01 ± 0.20	$P_{propane,3}$	1607.1 ± 1.95	$T_{sat,3}$	47.08
	Outlet	$T_{propane,4}$	46.52 ± 0.20	$P_{propane,4}$	1604.0 ± 1.95	$T_{sat,4}$	46.98
Post-Condenser	Inlet	$T_{propane,5}$	46.75 ± 0.20				
	Outlet	$T_{propane,6}$	28.33 ± 0.20	$P_{propane,6}$	1604.1 ± 1.95	$T_{sat,6}$	47.00

Table 4.2: Coupling Fluid Measurements

		Temperature		Pressure		Volumetric Flow Rate	
		°C		kPa		L min^{-1}	
Pre-Condenser (air)	Flow Meter	$T_{air,pre,flow}$	31.23 ± 1.00	$P_{air,pre}$	119.40 ± 2.07	$\dot{V}_{air,pre}$	118.1 ± 0.4
	Inlet	$T_{air,pre,in,1}$	31.52 ± 0.20				
		$T_{air,pre,in,2}$	31.27 ± 0.50				
	Outlet	$T_{air,pre,out,1}$	48.36 ± 0.20				
		$T_{air,pre,out,2}$	48.32 ± 0.50				
Test Section (water)	Inlet	$T_{water,test,in}$	36.80 ± 0.20	$P_{water,test}$	236.23 ± 2.07	$\dot{V}_{water,test}$	2.398
	Outlet	$T_{water,test,out}$	36.98 ± 0.20				
Post-Condenser (air)	Flow Meter	$T_{air,post,flow}$	17.65 ± 1.00	$P_{air,post}$	154.03 ± 2.07	$\dot{V}_{air,post}$	165.9 ± 0.5
	Inlet	$T_{air,post,in,1}$	18.93 ± 0.20				
		$T_{air,post,in,2}$	18.63 ± 0.50				
	Outlet	$T_{air,post,out,1}$	29.32 ± 0.20				
		$T_{air,post,out,2}$	29.17 ± 0.50				
Evaporator (water)	Inlet	$T_{water,evap,in}$	97.19 ± 1.00	$P_{water,evap}$	172.25 ± 5.17		
	Outlet	$T_{water,evap,out}$	96.37 ± 1.00				

4.1. Calculation of Condensation Heat Duty and Average Quality

The heat duties in the pre- and post-condensers are used to calculate the condensation heat duty and inlet and outlet qualities of the condensing propane in the test section.

Figure 4.1 shows a schematic of the pre-condenser with the air coupling loop and the associated heat duty and ambient losses. The air inlet and outlet temperatures are taken to be the average of the RTD ($T_{air,pre,in/out,1}$) and thermocouple ($T_{air,pre,in/out,2}$) measurements in order to obtain a more accurate bulk air temperature. In the pre-condenser, the average air inlet temperature is $31.39 \pm 0.27°C$, while the outlet temperature is $48.34 \pm 0.27°C$. The air temperature rise across the pre-condenser is therefore $16.94°C$. The humidity ratio (ω) of the compressed air is assumed to be 0.00152
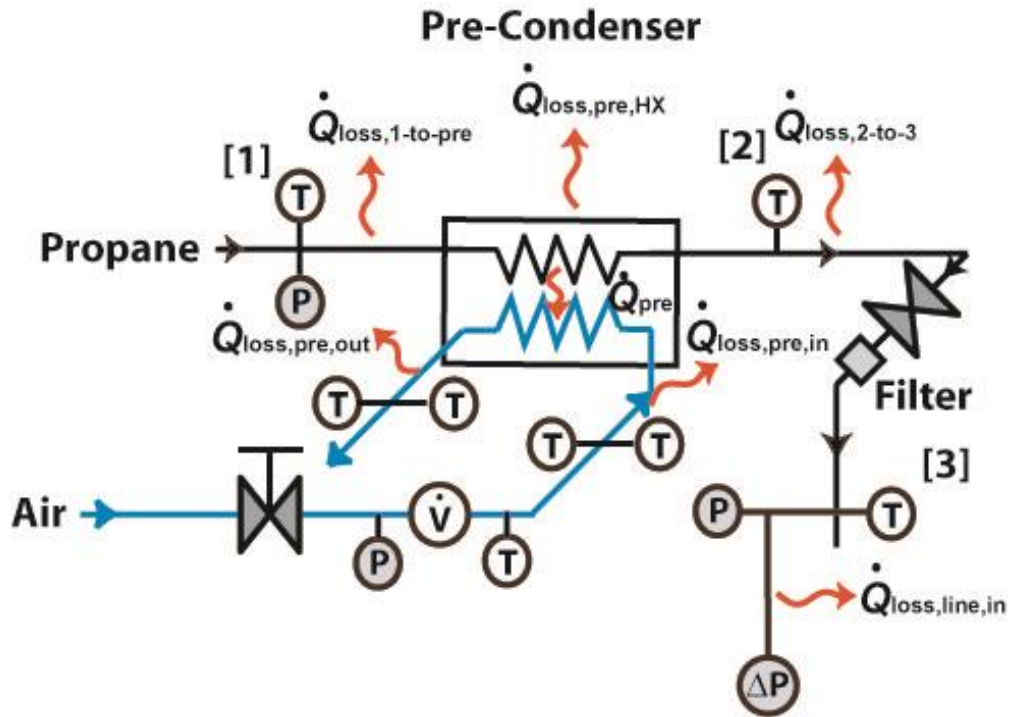
Figure 4.1: Schematic showing the pre-condenser, its coupling loop and heat losses

based on the analysis in Appendix B. The pre-condenser air inlet enthalpy is calculated as a function of the measured pressure (119.40 ± 2.07 kPa), average inlet temperature, and humidity ratio to be 308.3 kJ kg^{-1}. The pre-condenser outlet enthalpy is calculated to be 325.4 kJ kg^{-1} at the outlet pressure, which is assumed to be equal to the measured pressure in the exhaust duct (93 kPa). The volumetric flow rate of air through the pre-condenser is 118.1 ± 0.4 L min^{-1}. The density of air at the flow meter at 31.23°C, 119.40 kPa and ω = 0.00152 is 1.365 kg m^{-3}. Therefore, the air mass flow rate through the pre-condenser is $\dot{m}_{air,pre} = \dot{V}_{air,pre}\rho_{air,pre} = 2.686 \times 10^{-3}$ kg s^{-1}. Detailed calculations for the heat losses to the ambient are described below. The ambient heat loss in the line between propane state [1] and the pre-condenser inlet is 0.21 W, while the heat loss from the pre-condenser is 0.45 W, for a total ambient loss of 0.66 ± 0.17 W. An uncertainty of ±25% was assigned to all ambient loss terms. The heat duty in the pre-condenser is calculated from an energy balance on the air side, as shown in Eq. (4.2). The uncertainty in the pre-condenser heat duty is 2.9%.

$$\begin{aligned}
\dot{Q}_{pre} &= \dot{m}_{air,pre}\left(i_{air,pre,out} - i_{air,pre,in}\right) + \dot{Q}_{1\text{-to-pre,loss}} + \dot{Q}_{pre,loss} \\
&= (2.686 \times 10^{-3}\text{ kg s}^{-1})(325.4\text{ kJ kg}^{-1} - 308.3\text{ kJ kg}^{-1}) + 0.21\text{ W} + 0.45\text{ W} \quad (4.2) \\
&= 46.71 \pm 1.33\text{ W}
\end{aligned}$$

The pre-condenser inlet propane enthalpy is calculated from the pressure and temperature at state point 1: 1615.7 kPa, 82.91°C. With a saturation temperature of 47.33°C, the propane is superheated by 35.58°C. The propane enthalpy is then, $i_{propane,1} = f(P_{propane,1}, T_{propane,1}) = 700.8$ kJ kg^{-1}. The outlet enthalpy is calculated from an energy balance on the propane side as shown in Eq. (4.3).

$$i_{\text{propane},2} = i_{\text{propane},1} - \frac{\dot{Q}_{\text{pre}}}{\dot{m}_{\text{propane}}}$$

$$= 700.8\,\text{kJ kg}^{-1} - \frac{46.71\,\text{W}}{0.0002932\,\text{kg s}^{-1}} = 541.5\,\text{kJ kg}^{-1}$$

(4.3)

The ambient heat loss between the pre-condenser and the test section is determined for three sections: the straight tube sections, the valve and the filter. The losses from the tube represent the majority of the total loss because of the much greater surface area. The heat loss terms for the tube, the valve, and the filter are 0.41 W, 0.07 W, and 0.03 W, respectively. The ambient loss from the test section inlet pressure tap line is also taken into account at this point. As is shown in Section 4.1.1 , this loss is 0.38 W for a total heat loss of 0.89 ± 0.22 W between the pre-condenser and the test section. A further energy balance calculation is conducted to determine the test section inlet enthalpy:

$$i_{\text{propane},3} = i_{\text{propane},2} - \frac{\dot{Q}_{\text{loss,2-to-3}}}{\dot{m}_{\text{propane}}}$$

$$= 541.5\,\text{kJ kg}^{-1} - \frac{0.89\,\text{W}}{0.0002932\,\text{kg s}^{-1}} = 538.5\,\text{kJ kg}^{-1}$$

(4.4)

The measured pressure of the propane at the inlet of the test section is adjusted to account for the elevation difference between the pressure tap and the transducer. Figure 4.2 shows a schematic of the pressure tap lines with the position of the pressure transducers and thermocouples relative to the test section inlet and outlet taps. For the test section inlet, the pressure transducer is positioned 202 mm above the pressure tap. The fluid in the upper portion is assumed to be saturated vapor. The adjusted pressure is obtained iteratively from the following set of equations:
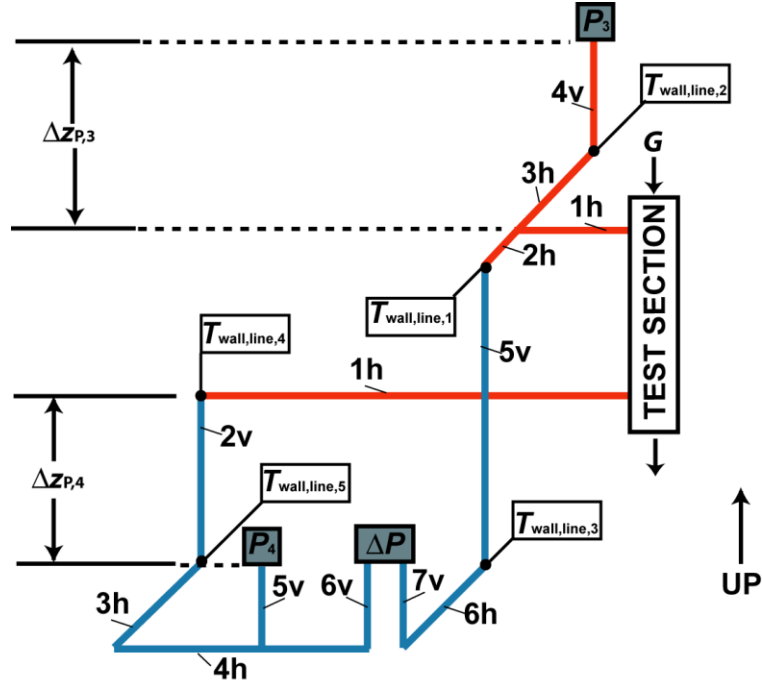
Figure 4.2: Schematic showing pressure tap lines, position of wall temperature measurements, and segment labels

$$\rho_{\text{propane,v,3}} = f\left(P_{\text{propane,3,adj.}}, x = 1\right)$$

$$P_{\text{propane,3,adj.}} = P_{\text{propane,3}} + \rho_{\text{propane,v,3}} g \Delta z_{P_3}$$

(4.5)

where g is the acceleration due to gravity (9.81 m s^{-2}), $P_{\text{propane,3}}$ is the measured pressure at the test section inlet (1607.1 kPa), $\rho_{\text{propane,v,3}}$ is the density of the propane at saturated vapor conditions, and Δz_{P_3} is the elevation difference between the pressure tap and the transducer. Based on these calculations, the density of the saturated vapor phase propane is 35.95 kg m^{-3} and the adjusted pressure is 1607.2 kPa. Since the fluid in this vertical line is saturated vapor, the difference between the adjusted and measured pressure is small. The test section inlet quality is then: $x_3 = f(i_{\text{propane,3}}, P_{\text{propane,3,adj.}}) = 0.72 \pm 0.02$ which is an uncertainty of 2.2% of the calculated value.

The outlet quality in the test section is calculated using a similar energy balance analysis on the post-condenser. Figure 4.3 shows a schematic of the post-condenser with the coupling loop and the associated heat duty and ambient losses. In the post-condenser, the average air inlet temperature is $18.78 \pm 0.27°C$, while the outlet temperature is $29.24 \pm 0.27°C$. The air temperature rise in the post-condenser is $10.46°C$. The post-condenser air inlet enthalpy is calculated at the measured pressure (154.03 ± 2.07 kPa), average inlet temperature, and humidity ratio to be 295.5 kJ kg^{-1}. The post-condenser outlet enthalpy is calculated at the exhaust pressure (93 kPa) to be 306.2 kJ kg^{-1}. The volumetric flow rate through the post-condenser is 165.9 ± 0.5 L min^{-1}. The density of air at the flow meter at $17.65°C$, 154.03 kPa and $\omega = 0.00152$ is 1.844 kg m^{-3}. The mass flow rate of air through the pre-condenser is $\dot{m}_{air,post} = \dot{V}_{air,post} \rho_{air,post} = 5.099 \times 10^{-3}$ kg s^{-1}. Because the average air
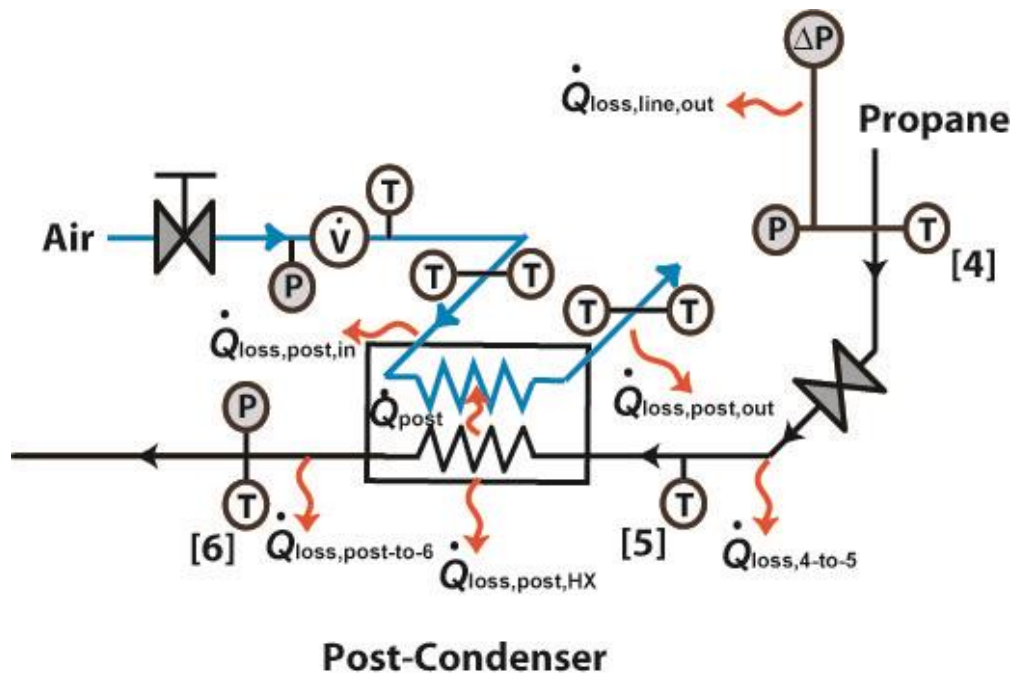
Figure 4.3: Schematic showing the post-condenser, its coupling loop and heat losses

temperature in the post-condenser (24.01°C) is lower than the ambient temperature (30.71°C), there is a heat gain from the environment of 0.30 W. The ambient heat loss between the post-condenser and the propane temperature and pressure measurements at point [6] downstream is 0.01 W for a net heat gain from the environment of 0.31 ± 0.08 W. The heat duty is calculated in Eq. (4.6).

$$
\begin{aligned}
\dot{Q}_{\text{post}} &= \dot{m}_{\text{air,post}} \left(i_{\text{air,post,out}} - i_{\text{air,post,in}} \right) + \dot{Q}_{\text{post,loss}} + \dot{Q}_{\text{post-to-6,loss}} \\
&= (5.099 \times 10^{-3} \text{ kg s}^{-1})(306.2 \text{ kJ kg}^{-1} - 295.5 \text{ kJ kg}^{-1}) \\
&\quad + (-0.30 \text{ W}) + (-0.01 \text{ W}) \\
&= 54.18 \pm 2.12 \text{ W}
\end{aligned}
\tag{4.6}
$$

The uncertainty in the post-condenser heat duty is 4.3%.

The propane enthalpy at the outlet of the post-condenser is calculated from the pressure and temperature at measurement point [6]: 1604.1 kPa, 28.33°C. For a saturation temperature of 47.00°C, the propane is subcooled by 18.67°C. The propane enthalpy is then, $i_{\text{propane,6}} = f(P_{\text{propane,6}}, T_{\text{propane,6}}) = 274.2$ kJ kg^{-1}. The post-condenser inlet enthalpy is calculated from an energy balance on the propane side as shown in Eq. (4.7).

$$
\begin{aligned}
i_{\text{propane,5}} &= i_{\text{propane,6}} + \frac{\dot{Q}_{\text{post}}}{\dot{m}_{\text{propane}}} \\
&= 274.2 \text{ kJ kg}^{-1} + \frac{54.18 \text{ W}}{0.0002932 \text{ kg s}^{-1}} = 459.0 \text{ kJ kg}^{-1}
\end{aligned}
\tag{4.7}
$$

The ambient heat loss between the post-condenser and the test section is determined for two sections: the straight tube sections (0.30 W) and the valve (0.07 W). The ambient loss from the test section outlet pressure tap line is 0.34 W for a total heat loss of 0.71 ± 0.18 W between the pre-condenser and the test section. The test section outlet enthalpy is calculated in a manner similar to what was used for the pre-condenser:

$$i_{\text{propane,4}} = i_{\text{propane,3}} + \frac{\dot{Q}_{\text{loss,4-to-5}}}{\dot{m}_{\text{propane}}}$$

$$= 459.0 \text{ kJ kg}^{-1} + \frac{0.71\,\text{W}}{0.0002932\,\text{kg s}^{-1}} = 461.4\,\text{kJ kg}^{-1}$$

(4.8)

The measured pressure of the propane at the outlet of the test section is also adjusted for elevation. The test section outlet pressure transducer is positioned 83 mm below the pressure tap. The density of the fluid in the pressure tap line is determined based on the measured wall temperatures at these points of the line. The wall temperature at the top of the line ($T_{\text{wall,line,4}}$) is 32.45°C, while at the bottom of the line ($T_{\text{wall,line,5}}$), it is 31.67°C. The ambient heat loss calculation for this tube segment is descibed in more detail in the next section of this chapter and uses the average of these two wall temperature values (32.06°C). The heat loss in this segment (0.02 W) and the fluid temperature, which was also 32.06°C, are obtained iteratively from the measured wall temperature. The small heat loss in this segment leads to a calculated temperature difference of only 0.0003°C across the tube wall. The adjusted pressure is obtained iteratively as before from the following set of equations:

$$\rho_{\text{propane,line,out}} = f\left(P_{\text{propane,4,adj.}}, T = 32.06°C\right)$$

$$P_{\text{propane,4,adj.}} = P_{\text{propane,4}} - \rho_{\text{propane,line,out}}\, g\, \Delta z_{P_4}$$

(4.9)

The measured pressure at the test section outlet ($P_{\text{propane,4}}$) is 1604.0 kPa. With a density of 482.7 kg m^{-3}, the adjusted pressure is 1603.6 kPa. The test section outlet quality is then: $x_4 = f(i_{\text{propane,4}}, P_{\text{propane,4,adj.}}) = 0.46 \pm 0.02$ which is an uncertainty of 5.4% of the calculated value. The quality change across the test section is thus 0.26, and the average quality in the test section is 0.59 ± 0.01 (2.5% uncertainty), as shown in Eq. (4.10).

$$\Delta x_{\text{test}} = x_3 - x_4$$

(4.10)

The heat duty in the test section is calculated in Eq. (4.11) using the inlet and outlet enthalpies found previously.

$$
\begin{aligned}
\dot{Q}_{test} &= \dot{m}_{propane}(i_{ref,3} - i_{ref,4}) \\
&= (2.932 \times 10^{-4} \text{ kg s}^{-1})(538.5 \text{ kJ kg}^{-1} - 461.4 \text{ kJ kg}^{-1}) \\
&= 22.61 \pm 2.54 \text{ W}
\end{aligned}
\tag{4.11}
$$

The uncertainty in the test section heat duty is 11.2%. Over the entire data set, the uncertainty in the test section heat duty ranges from 7.7% to 25.4%.

4.1.1. __Ambient Heat Losses__

As shown in Figure 4.1 and Figure 4.3, ambient heat losses are calculated for the region between measurement location [1] and the pre-condenser, the pre-condenser shell, the pre-condenser air inlet and outlet lines, the intermediate region between the pre-condenser and the test section, the test section water jacket, the pressure tap lines, the intermediate region between the test section and the post-condenser, the post-condenser shell, the post-condenser air inlet and outlet lines, and the intermediate region between the post-condenser and measurement location [6]. For each of these ambient loss calculations, a resistance network approach is used, accounting for natural convection and radiation between the surface of the insulation and the ambient. Figure 4.4 shows a representative resistance network for heat transfer from the fluid to ambient ($T_{amb} = 30.71°C$). The thermal pathway consists of convection from the fluid stream to the tube wall, conduction through the tube wall, the wrap insulation ($k_{ins,wrap} = 0.043 \text{ W m}^{-1} \text{ K}^{-1}$), and the tube insulation ($k_{ins} = 0.019 \text{ W m}^{-1} \text{ K}^{-1}$), and natural convection and radiation to the environment. For larger tube diameter segments
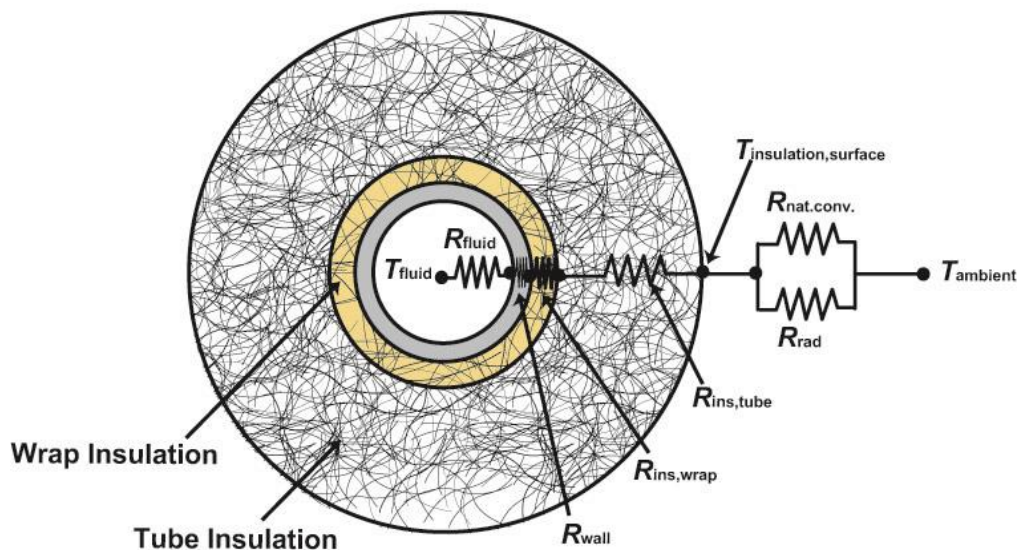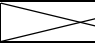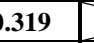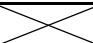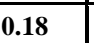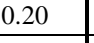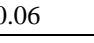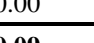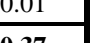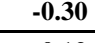
Figure 4.4: Schematic showing the resistance network for ambient loss calculations

(> 25 mm) the tube insulation directly contacts the tube wall without any layer of wrap insulation.

Table 4.3 provides a summary of all the ambient heat loss terms in the system along with the associated surface areas and fluid temperatures. Most of the regions of heat loss to the environment are subdivided into constituent components and segments to better model the amount of heat transfer for changing geometry, conditions and orientation of the component. The heat loss term for the region is the sum of its component heat losses. The surface area displayed is based on the outer diameter of the insulation (87 mm or 73.4 mm) and the length of each segment.

The method for calculating the ambient losses is descibed here in detail for one segment, followed by any variations to the method required for other geometries. The

Table 4.3: Ambient Losses, T_{amb} = 30.71°C

	Surface Area	Orientation	T_{fluid}	Radiation Heat Loss	Free Convection Heat Loss	Total Heat Loss
	m²		°C	W	W	W
1 to Pre	**0.018**	**Horizontal**	**82.91**	**0.15**	**0.06**	**0.21**
Pre-Condenser	**0.159**			**0.34**	**0.11**	**0.45**
Air Inlet	0.042	Vertical	31.39	0.01	0.00	0.01
Shell	0.075	Horizontal	39.87	0.18	0.05	0.23
Air Outlet	0.042	Vertical	48.34	0.15	0.06	0.21
Pre to Test	**0.127**			**0.38**	**0.12**	**0.51**
Line	0.108	Horizontal	47.16	0.31	0.09	0.41
Valve	0.014	Horizontal	47.16	0.05	0.02	0.07
Filter	0.005	Horizontal	47.16	0.02	0.01	0.03
Inlet Pressure Tap	**0.319**			**0.29**	**0.08**	**0.38**
Segment 1	0.015	Horizontal	47.01	0.05	0.02	0.07
Segment 2	0.016	Horizontal	39.29	0.03	0.01	0.04
Segment 3	0.100	Horizontal	34.67	0.09	0.02	0.12
Segment 4	0.003	Vertical	30.06	-0.01	0.00	-0.01
Segment 5	0.106	Vertical	35.32	0.12	0.03	0.14
Segment 6	0.053	Horizontal	31.35	0.01	0.00	0.01
Segment 7	0.026	Vertical	31.35	0.00	0.00	0.01
Test Section	**0.142**			**0.18**	**0.04**	**0.23**
Water Inlet	0.071	Horizontal	36.80	0.09	0.02	0.11
HX	0.030	Vertical	36.89	0.04	0.01	0.06
Water Outlet	0.041	Horizontal	36.98	0.05	0.01	0.06
Outlet Pressure Tap	**0.300**			**0.28**	**0.06**	**0.34**
Segment 1	0.056	Horizontal	46.52	0.20	0.06	0.26
Segment 2	0.053	Vertical	32.06	0.02	0.00	0.02
Segment 3	0.068	Horizontal	31.67	0.02	0.00	0.02
Segment 4	0.071	Horizontal	31.67	0.02	0.00	0.02
Segment 5	0.026	Vertical	31.67	0.01	0.00	0.01
Segment 6	0.026	Vertical	31.67	0.01	0.00	0.01
Test to Post	**0.096**			**0.28**	**0.09**	**0.37**
Line	0.082	Horizontal	46.64	0.23	0.07	0.30
Valve	0.014	Horizontal	46.64	0.05	0.02	0.07
Post-Condenser	**0.145**			**-0.23**	**-0.06**	**-0.30**
Air Inlet	0.035	Horizontal	18.78	-0.09	-0.03	-0.12
Shell	0.075	Horizontal	24.01	-0.13	-0.03	-0.17
Air Outlet	0.035	Horizontal	29.24	-0.01	0.00	-0.01
Post-to-6	**0.018**	**Horizontal**	**28.33**	**-0.01**	**0.00**	**-0.01**

region between the pressure and temperature tap upstream of the pre-condenser and the heat exchanger is 65 mm long. The propane flow in this portion of the loop is superheated vapor; therefore, the propane thermal resistance is determined assuming single-phase forced convection. The local Reynolds number for the propane is calculated as follows:

$$\text{Re}_{\text{1-to-pre,propane}} = \frac{G_{\text{propane}} D_{\text{line,in}}}{\mu_{\text{propane,pre,in}}} = \frac{(100.2 \text{ kg m}^{-2} \text{ s}^{-1})(0.00457 \text{ m})}{1.01 \times 10^{-5} \text{ kg m}^{-1} \text{ s}^{-1}} = 8094 \qquad (4.12)$$

where the inner diameter of the propane tubing in the main loop is 4.57 mm and the viscosity of the propane vapor is 1.01×10^{-5} kg m^{-1} s^{-1}. Using Eq. (3.12), the Churchill (1977b) friction factor correlation, the Darcy friction factor for single phase propane vapor is calculated to be 0.033.

$$f = 8\left(\left(\frac{8}{\text{Re}}\right)^{12} + \frac{1}{\left(B+C\right)^{1.5}}\right)^{1/12}$$

$$\text{where } B = \left(2.457 \ln \frac{1}{(7/\text{Re})^{0.9} + 0.27(e/D_{\text{line,in}})}\right)^{16} \text{ and} \qquad (4.13)$$

$$C = \left(\frac{37530}{\text{Re}}\right)^{16}$$

where $e = 0.0015$ mm is the roughness of the tube (Munson *et al.*, 2006). The friction factor is then used in the Churchill (1977a) correlation for the Nusselt number, given by Eq. (3.23).

$$\mathrm{Nu} = \left(4.364^{10} + \left(\frac{e^{\frac{2200-\mathrm{Re}}{365}}}{4.364^2} + \frac{1}{\left(6.3 + \frac{0.079\left(\frac{f}{8}\right)^{0.5} \mathrm{Re}\,\mathrm{Pr}}{\left(1+\mathrm{Pr}^{0.8}\right)^{5/6}} \right)^2} \right)^{-5} \right)^{1/10} \tag{4.14}$$

where the Prandtl number is 0.835. For turbulent flow through the tube, the Nusselt number is 26.82. The heat transfer coefficient for the propane is then $h_{\mathrm{propane,1\text{-}to\text{-}pre}} = 157.2$ W m^{-2} K^{-1} for a propane vapor conductivity of 0.027 W m^{-1} K^{-1}. The fluid stream resistance is calculated from Eq. (4.15) to be 6.814 K W^{-1}.

$$\begin{aligned}
R_{\mathrm{1\text{-}to\text{-}pre,propane}} &= \frac{1}{h_{\mathrm{1\text{-}to\text{-}pre,propane}}\pi D_{\mathrm{line,in}}L_{\mathrm{1\text{-}to\text{-}pre}}} \\
&= \frac{1}{(157.2 \text{ W m}^{-2}\text{ K}^{-1})\pi(0.00457 \text{ m})(0.065 \text{ m})} = 6.81 \text{ K W}^{-1}
\end{aligned} \tag{4.15}$$

The conduction resistance through the tube wall is calculated using Eq. (4.16). The thermal conductivity of the stainless steel wall is evaluated at the outer wall temperature, which is obtained iteratively (81.49°C): $k_{\mathrm{SS316}} = 14.4$ W m^{-1} K^{-1}.

$$\begin{aligned}
R_{\mathrm{1\text{-}to\text{-}pre,wall}} &= \frac{\ln(D_{\mathrm{line,out}}/D_{\mathrm{line,in}})}{2\pi k_{\mathrm{SS316}}L_{\mathrm{1\text{-}to\text{-}pre}}} \\
&= \frac{\ln(0.00635 \text{ m}/0.00457 \text{ m})}{2\pi(14.4 \text{ W m}^{-1}\text{ K}^{-1})(0.065 \text{ m})} = 0.0559 \text{ K W}^{-1}
\end{aligned} \tag{4.16}$$

The conduction resistance through the insulation layers is calculated in a similar manner. The outer diameter of the rigid tube insulation is 87 mm, while the inner diameter is 25 mm. The thermal conductivity of the tube insulation is 0.019 W m^{-1} K^{-1}. The wrap insulation fills the gap between the stainless steel tube outer diameter and the

tube insulation inner diameter. The density of the wrap insulation is less than that of the tube insulation, and the thermal conductivity is 0.043 W m^{-1} K^{-1}. Therefore the insulation conduction resistance is calculated by considering two conductive resistances in series, as shown in Eq. (4.17) and (4.18).

$$
\begin{aligned}
R_{\text{1-to-pre,insulation,wrap}} &= \frac{\ln(D_{\text{insulation,tube,in}} / D_{\text{line,out}})}{2\pi k_{\text{insulation,wrap}} L_{\text{1-to-pre}}} \\
&= \frac{\ln(0.025 \text{ m} / 0.00635 \text{ m})}{2\pi(0.043 \text{ W m}^{-1} \text{ K}^{-1})(0.065 \text{ m})} = 77.67 \text{ K W}^{-1}
\end{aligned}
\tag{4.17}
$$

$$
\begin{aligned}
R_{\text{1-to-pre,insulation,tube}} &= \frac{\ln(D_{\text{insulation,tube,out}} / D_{\text{insulation,tube,in}})}{2\pi k_{\text{insulation,tube}} L_{\text{1-to-pre}}} \\
&= \frac{\ln(0.087 \text{ m} / 0.025 \text{ m})}{2\pi(0.019 \text{ W m}^{-1} \text{ K}^{-1})(0.065 \text{ m})} = 160.7 \text{ K W}^{-1}
\end{aligned}
\tag{4.18}
$$

Heat is transferred to the envionment ($T_{\text{amb}} = 30.71°C = 303.86$ K) via two modes – radiation and natural convection. The surface temperature of the insulation is determined to be 32.17°C (305.32 K), by iteration. All air properties are calculated at the film temperature ($T_{\text{film}} = 31.44°C = 304.59$ K) defined as the average between the insulation surface temperature and the ambient temperature. The radiation heat transfer coefficient is found using Eq. (4.19):

$$
\begin{aligned}
h_{\text{1-to-pre,rad}} &= \epsilon\sigma\left(T_{\text{1-to-pre,insulation,surface}}^2 + T_{\text{amb}}^2\right)\left(T_{\text{1-to-pre,insulation,surface}} + T_{\text{amb}}\right) \\
&= 5.77 \text{ W m}^{-2} \text{ K}^{-1}
\end{aligned}
\tag{4.19}
$$

where the emissivity of the All Service Jacket (ASJ) tape (Venture Tape 1540CW) is $\epsilon = 0.9$ and $\sigma = 5.67 \times 10^{-8}$ W m^{-2} K^{-4} is the Stefan-Boltzmann constant. For a surface area of 0.018 m^2, the radiation thermal resistance is,

$$R_{\text{1-to-pre,rad}} = \frac{1}{\pi D_{\text{insulation,tube,out}} L_{\text{1-to-pre}} h_{\text{1-to-pre,rad}}}$$

$$= \frac{1}{\pi (0.087 \text{ m})(0.065 \text{ m})(5.77 \text{ W m}^{-2} \text{ K}^{-1})} = 9.76 \text{ K W}^{-1} \tag{4.20}$$

The heat lost due to radiation is then calculated using Eq. (4.21).

$$\dot{Q}_{\text{1-to-pre,loss,rad}} = \frac{T_{\text{amb}} - T_{\text{1-to-pre,insulation,surface}}}{R_{\text{1-to-pre,rad}}} = 0.15 \text{ W} \tag{4.21}$$

The natural convection heat transfer coefficient is determimned using correlations by Churchill and Chu (1975b, a) for a horizontal cylinder or a modified vertical flat plate. Because this segment is a horizontal cylinder, the Rayleigh number is calculated with the insulation outer diameter as the characteristic length according to Eq. (4.22),

$$\text{Ra}_D = \frac{\rho_{\text{air,film}} g \beta_{\text{air,film}} |T_{\text{insulation,surface}} - T_{\text{amb}}| D_{\text{insulation,tube,out}}^3}{\mu_{\text{air,film}} \alpha_{\text{air,film}}} \tag{4.22}$$

where the air properties at the film temperature are $\rho_{\text{air,1-to-pre}}$ = 1.16 kg m^{-3}, $\beta_{\text{air,1-to-pre}}$ = 0.0033 K^{-1}, $\mu_{\text{air,1-to-pre}}$ = 1.88 $\times$ 10^{-5} kg m^{-3}, and $\alpha_{\text{air,1-to-pre}}$ = 2.26$\times$ 10^{-5} m^2 s^{-1}. The Rayleigh number for this segment is 84,136. With this Ra, for a horizontal cylinder, the natural convection Nusselt number is calculated to be 7.14 according to Eq. (4.23).

$$\text{Nu}_{\text{nat.conv.}} = \left(0.60 + \frac{0.387 \text{Ra}^{1/6}}{\left(1 + \left(\frac{0.559}{\text{Pr}} \right)^{9/16} \right)^{8/27}} \right)^2 \tag{4.23}$$

The Prandtl number of air at the film temperature is 0.719 and the thermal conductivity is 0.026 W m^{-1} K^{-1}. Therefore, the natural convection heat transfer coefficient is 2.25 W m^{-2} K^{-1}.

$$h_{nat.conv.,1-to-pre} = \frac{Nu_{nat.conv.,1-to-pre} \cdot k_{air,1-to-pre}}{D_{insulation,tube,out}} = 2.25 \text{ W m}^{-2} \text{ K}^{-1} \qquad (4.24)$$

The thermal resistance and the heat loss are calculated as with the radiation term described above. The natural convection thermal resistance is 24.98 K W^{-1}, and the heat loss due to natural convection is 0.06 W. All of these terms are combined and Eq. (4.25) and (4.26) are solved simultaneously to deterimne the heat loss (0.21 W) and insulation surface temperature (32.17°C), which was used above to obtain the required temperature difference. It can be seen that radiation contributes more to the ambient heat loss than natural convection.

$$\dot{Q}_{1-to-pre,loss} = \frac{T_{propane,1} - T_{1-to-pre,insulation,surface}}{R_{1-to-pre,ref} + R_{1-to-pre,wall} + R_{1-to-pre,insulation,wrap} + R_{1-to-pre,insulation,tube}} \qquad (4.25)$$

$$\dot{Q}_{1-to-pre,loss} = \left(T_{1-to-pre,insulation,surface} - T_{amb}\right)\left(\frac{1}{R_{1-to-pre,rad}} + \frac{1}{R_{1-to-pre,nat.conv.}}\right) \qquad (4.26)$$

The ambient losses in the other components of the loop are calculated in much the same way, with appropriate modifications made for the respective geometries. The ambient loss from the pre-condenser excludes the wrap insulation resistance because the outer diameter of the shell-and-tube heat exchanger is 25.4 mm. Figure 4.5 shows a schematic of the shell-and-tube heat exchanger highlighting the baffle and tube geometries. The fluid convective resistance is calculated from the heat transfer coefficient of air in the shell of the heat exchanger. The heat transfer coefficient is determined based on the methods described in Janna (1993). The specifications for the pre-condenser heat exchanger are shown in Table 3.2. The clearance between adjacent tubes and the baffle spacing are determined from these parameters:
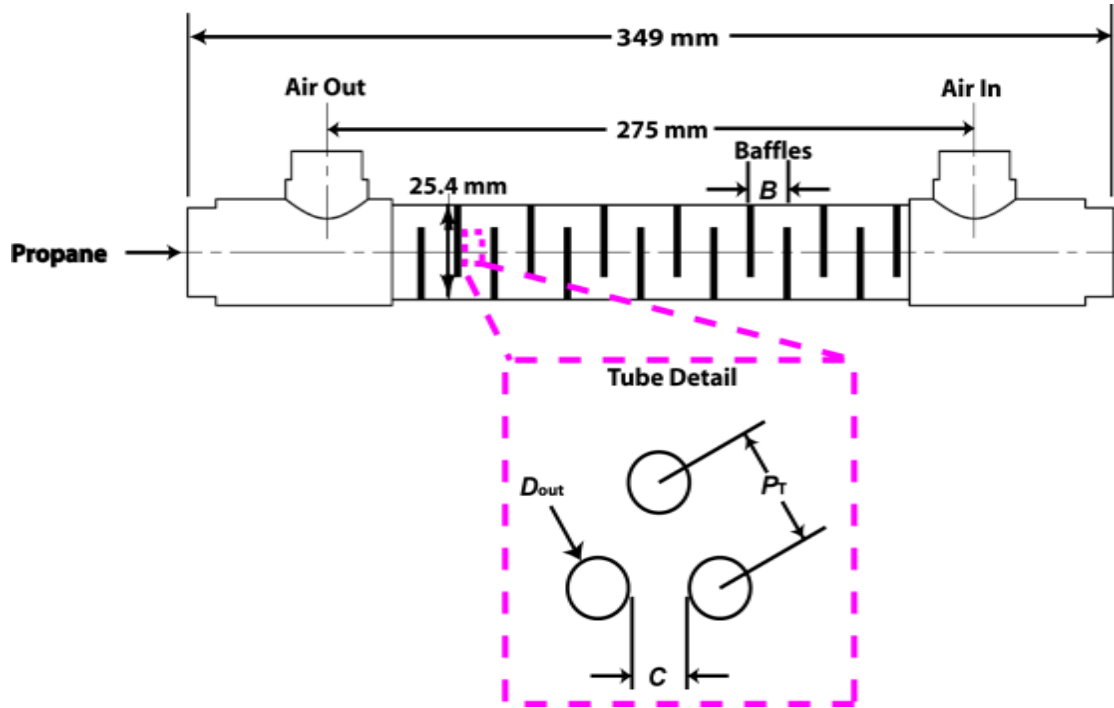
Figure 4.5: Schematic showing the baffle and tube configurations for the shell-and-tube heat exchangers used for the pre- and post-condensers

$$C_{\text{pre}} = p_{\text{t,pre}} - D_{\text{pre,tube,o}} = 0.76 \text{ mm}$$
$$B_{\text{pre}} = L_{\text{pre}} / N_{\text{b,pre}} = 19.6 \text{ mm}$$

$$(4.27)$$

where the tube pitch is 4.58 mm, the tube outer diameter is 3.82 mm, the length is 0.275 m, and the number of baffles is 14.

With an internal shell diameter of 22.9 mm, tube clearance of 0.76 mm, baffle spacing of 19.6 mm, and tube pitch of 4.58 mm, the characteristic area of the shell is calculated using Eq. (4.28) to be 74.6 mm^2.

$$A_{\text{pre,s}} = \frac{D_{\text{pre,shell,in}} C_{\text{pre}} B_{\text{pre}}}{p_{\text{t,pre}}} = 74.6 \text{ mm}^2 \qquad (4.28)$$

For a triangular pitch layout, the equivalent diameter is given by Eq. (4.29). For a tube pitch of 4.58 mm and outer diameter of 3.82 mm, the equivelent diameter is calculated to be 2.2 mm.

$$D_{\text{pre,e}} = \frac{3.44\,p_{\text{t,pre}}^{2}}{\pi D_{\text{pre,tube,o}}} - D_{\text{pre,tube,o}} = 2.2 \text{ mm} \tag{4.29}$$

These values along with the air flow rate (0.0027 kg s^{-1}) are used to calculate the Reynolds number as shown in Eq. (4.30).

$$\text{Re}_{\text{pre,shell}} = \frac{\dot{m}_{\text{air,pre}} D_{\text{pre,e}}}{\mu_{\text{air}} A_{\text{pre,s}}} = 4111 \tag{4.30}$$

The viscosity of air at the pre-condenser average temperature (39.87°C), pressure of 119.40 kPa, and humidity ratio 0.00152 is 1.92×10^{-5} kg m^{-1} s^{-1}. The air Prandtl number at these conditions is 0.715. From Janna (1993), Eq. (4.31), the resulting Nusselt number is 31.29.

$$\text{Nu}_{\text{pre,shell}} = 0.36\,\text{Re}_{\text{pre,shell}}^{0.55}\,\text{Pr}_{\text{pre,shell}}^{1/3} \tag{4.31}$$

The heat transfer coefficient is then calculated with Eq. (4.32) to be 386.5 W m^{-2} K^{-1}.

$$h_{\text{pre,shell}} = \frac{\text{Nu}_{\text{pre,shell}} k_{\text{air}}}{D_{\text{pre,e}}} = \frac{(31.29)(0.027 \text{ W m}^{-1}\text{ K}^{-1})}{0.0022 \text{ m}} = 386.5 \text{ W m}^{-2}\text{ K}^{-1} \tag{4.32}$$

This value is used to calculate the fluid convective resistance for the pre-condenser:

$$\begin{aligned} R_{\text{pre,shell}} &= \frac{1}{h_{\text{pre,shell}} \pi D_{\text{pre,shell,in}} L_{\text{pre}}} \\ &= \frac{1}{(386.5 \text{ W m}^{-2}\text{ K}^{-1})\pi(0.0229 \text{ m})(0.275 \text{ m})} = 0.13 \text{ K W}^{-1} \end{aligned} \tag{4.33}$$

The same method is used to calculate the post-condenser ambient losses. The total heat loss in the pre- and post-condensers is the sum of the heat loss from the heat exchanger shell and the copper inlet and outlet lines between the heat exchanger and the temperature measurement locations.

The heat losses in the intermediate regions between the pre- and post-condensers are calculated similarly. Because the propane state is two-phase in these regions, the fluid convective resistance is small and therefore neglected. The ambient loss resistance network begins at the tube wall and assumes the average temperature of the propane as being approximately equal to the inside wall temperature. For the valve wall resistance, the hydraulic diameter (19 mm for the valve) is used to calcualte the wall conduction resistance. All other resistance terms are calcualted as described above.

The last component category that differs in ambient loss calculation method is the natural convection around the vertical tubes. As a representative case, the downward vertical segment in the test section inlet pressure tap line ("5v") is shown here. See Figure 4.2 for a schematic showing the location of each of the pressure tap line segments. According to Sparrow and Gregg (1956), natural convection from a vertical cylinder is similar to that of a vertical flat plate. Therfore the Rayleigh number is calculated with the insulation tube length as the characteristic length according to Eq. (4.34),

$$\mathrm{Ra}_{L} = \frac{\rho_{\mathrm{air,film}}\, g\, \beta_{\mathrm{air,film}} \left| T_{\mathrm{insulation,surface}} - T_{\mathrm{amb}} \right| L^{3}}{\mu_{\mathrm{air,film}} \alpha_{\mathrm{air,film}}} \qquad (4.34)$$

For this segment, the air properties at the film temperature (30.80°C) are $\rho_{\mathrm{air,line,in,5v}} = 1.16$ kg m^{-3}, $\beta_{\mathrm{air,line,in,5v}} = 0.0033$ K^{-1}, $\mu_{\mathrm{air,line,in,5v}} = 1.88 \times 10^{-5}$ kg m^{-3}, and $\alpha_{\mathrm{air,line,in,5v}} = 2.25 \times 10^{-5}$ m^{2} s^{-1}. The segment length of 457 mm yields a Rayleigh number

of 1,372,390. For a vertical flat plate, the natural convection Nusselt number is 18.05 according to Churchill and Chu (1975b), Eq. (4.35).

$$\mathrm{Nu}_{\text{nat.conv.,plate}} = \left(0.825 + \frac{0.387\mathrm{Ra}_L^{1/6}}{\left(1 + \left(\frac{0.492}{\mathrm{Pr}} \right)^{9/16} \right)^{8/27}} \right)^2 \qquad (4.35)$$

The Prandtl number of air at the film temperature is 0.719 and the thermal conductivity is 0.026 W m^{-1} K^{-1}. Based on criteria by Sparrow and Gregg (1956), the flat plate Nusselt number is modified for a cylinder according to Eq. (4.36),

$$\mathrm{Nu}_{\text{nat.conv.,vertical,cylinder}} = \begin{cases} \mathrm{Nu}_{\text{nat.conv.,plate}} & \text{if } \dfrac{D}{L} > \dfrac{35}{\mathrm{Gr}_L^{0.25}} \\[2ex] \mathrm{Nu}_{\text{nat.conv.,plate}} \dfrac{\zeta}{\ln(1+\zeta)} & \text{if } \dfrac{D}{L} \leq \dfrac{35}{\mathrm{Gr}_L^{0.25}} \end{cases} \qquad (4.36)$$

where Gr$_L$ = Ra$_L$ / Pr = 1,908,483 is the Grashof number and the parameter ζ is defined as:

$$\zeta = \frac{1.8}{\mathrm{Nu}_{\text{nat.conv.,plate}}} \frac{L}{D} \qquad (4.37)$$

For this segment, the outer diameter of the insulation is 73.7 mm, therefore $D/L = 0.161 < 0.942$. Thus, the flat plate Nusselt number is modified using $\zeta = 0.619$ to be 23.19. The natural convection heat transfer coefficient is then 1.38 W m^{-2} K^{-1}, based on the applicable tube length of 457 mm.

$$h_{\text{nat.conv.,line,in,5v}} = \frac{\mathrm{Nu}_{\text{nat.conv.,line,in,5v}} \cdot k_{\text{air,line,in,5v}}}{L_{\text{line,in,5v}}} = 1.38 \text{ W m}^{-2} \text{ K}^{-1} \qquad (4.38)$$

For this segment and the other pressure tap line segments, the outer wall temperature is measured and the fluid temperature is unknown. Therefore, the internal fluid temperature is obtained iteratively along with the other ambient loss heat transfer quanities by adding the following equation:

$$\dot{Q}_{loss} = \frac{T_{ref} - T_{wall,out}}{R_{wall}} \quad (4.39)$$

In the pressure tap line segments with stationary fluid, for simplicity, it is assumed that the inner wall temperature is equal to the fluid temperature.

Anologous methods are used to determine the ambient losses from each segment in the faciltiy loop. The parameters that vary are length of segment, size of insulation, horizontal or vertical orientation, known temperature, and fluid flow conditions (single phase, two-phase, or static). The detailed results for each segment are summarized in Table 4.3.

4.2. Test Section Heat Transfer Coefficient

The heat transfer coefficient is determined using the *UA*-LMTD method. The LMTD in the test section is calculated using Eq. (3.19). For the representative data point, the measured inlet and outlet propane temperatures are 47.01 ± 0.20°C and 46.52 ± 0.20°C, respectively. The measured water inlet and outlet temperatures are 36.80 ± 0.20°C and 36.98 ± 0.20°C, respectively. Therefore, the LMTD in the test section is 9.87 K.

$$\Delta T_{\text{LM,test}} = \frac{(T_{\text{propane,3}} - T_{\text{water,test,out}}) - (T_{\text{propane,4}} - T_{\text{water,test,in}})}{\ln \dfrac{T_{\text{propane,3}} - T_{\text{water,test,out}}}{T_{\text{propane,4}} - T_{\text{water,test,in}}}}$$

$$= \frac{(47.01°C - 36.98°C) - (46.52°C - 36.80°C)}{\ln \dfrac{47.01°C - 36.98°C}{46.52°C - 36.80°C}} \qquad (4.40)$$

$$= 9.87 \pm 0.20 \text{ K}$$

The average measured propane temperature (46.77°C) in the test section is also compared to the calcualted average saturation temperature (47.03°C) based on the pressure (1605.4 kPa) in the test section. The difference is defined as $\Delta T_{\text{p}} = T_{\text{propane,test,avg}} - T_{\text{sat,testavg}} = -0.27°C$. Over the range of data collected in this study, this difference varies from -0.08°C to -0.49°C (-0.23°C average).

From the calcualted LMTD and condensation heat duty (22.61 W), the conductance of the test section for the representative point is 2.29 W K^{-1}, as shown in Eq. (4.41).

$$UA_{\text{test}} = \frac{\dot{Q}_{\text{test}}}{\Delta T_{\text{LM,test}}} = 2.29 \text{ W K}^{-1} \qquad (4.41)$$

With the *UA* known, it is possible to deduce the condensation heat transfer coefficient through a thermal resistance analysis. The thermal resistance network used for the test section is shown in Figure 4.6. The propane-side resistance is obtained from the *UA*, the wall resistance, and the water-side resistance as shown in Eq. (3.20).

$$R_{\text{test,propane}} = \frac{1}{UA_{\text{test}}} - R_{\text{test,wall}} - R_{\text{test,water}} \qquad (4.42)$$
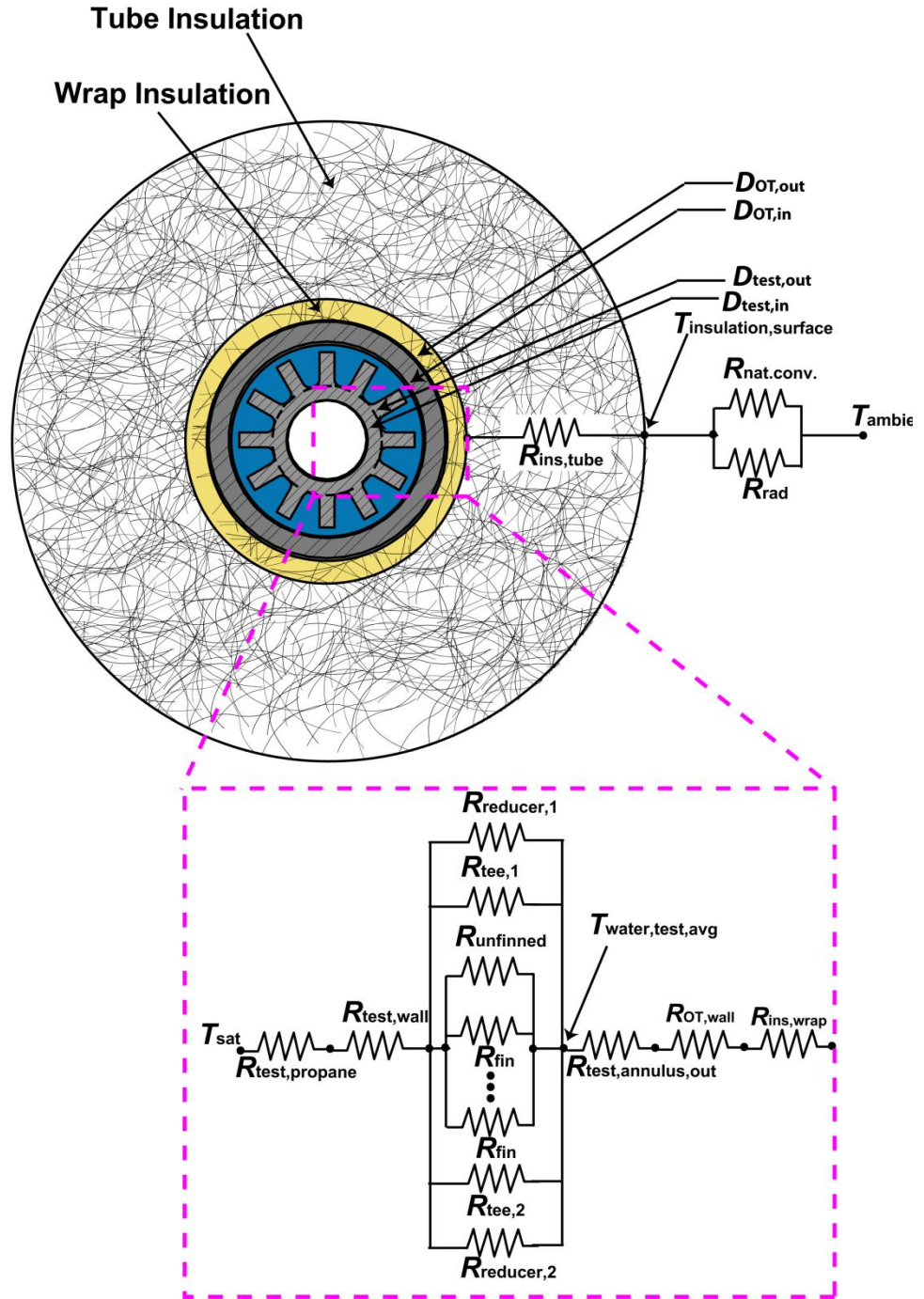
Figure 4.6: Schematic showing the resistance network in the longitudinally finned test section

The test section wall resistance is 0.0021 K W^{-1}, as shown in Eq. (4.43). The heat transfer

length ($L_{\text{test,HT}}$) is 135.1 mm and the inner and outer diameters of the test section are 1.93

mm and 2.97 mm, respectively. The thermal conductivity of aluminum at the average

fluid temperature in the test section (46.77°C) is 237.0 W m^{-1} K^{-1}.

$$R_{\text{test,wall}} = \frac{\ln(D_{\text{test,out}} / D_{\text{test,in}})}{2\pi k_{\text{Al}} L_{\text{test,HT}}} = 2.1 \times 10^{-3} \text{ K W}^{-1} \tag{4.43}$$

The equivalent convective resistance for the water side, shown in Eq. (4.44),

accounts for the parallel resistance due to forced convection through the annulus and

natural convection in the Swagelok fittings at either end of the test section as can be seen

in Figure 4.7. It is important to include the thermal resistance terms for the end caps of
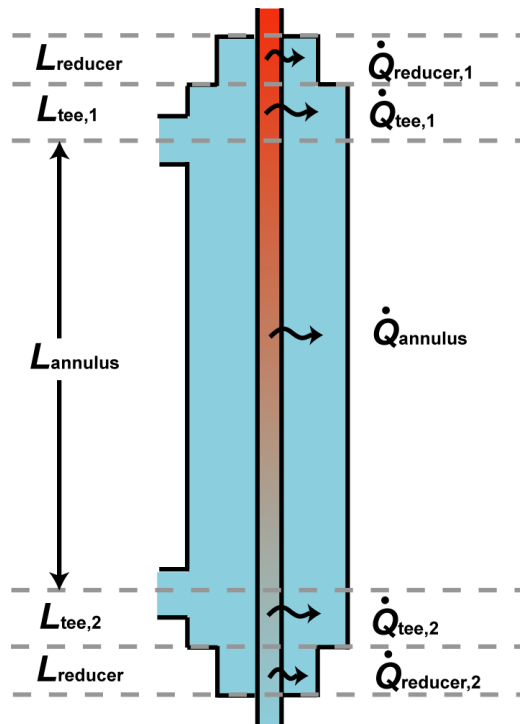
Figure 4.7: Schematic showing the heat duty components in the test section

the tube-in-tube heat exchanger so that the water-side thermal resistance in the test section is not overestimated.

$$\frac{1}{R_{test,water}} = \frac{1}{R_{test,annulus}} + \frac{1}{R_{test,tee,1}} + \frac{1}{R_{test,tee,2}} + 2\left(\frac{1}{R_{test,reducer}}\right) \qquad (4.44)$$

It is desireable for the water flow rate through the annulus to be as high as possible to decrease the thermal resistance on the water-side. A low water-side resistance relative to the condensing propane resistance is desireable because it improves the accuracy of the deduced propane heat transfer coefficients. However, at such high flow rates, the temperature difference in the water is small, yielding high uncertainty in heat duty measurements taken directly from the water side. The change in water temperature across the test section from an inlet temperature of 36.80°C and flow rate of 2.398 L min^{-1} is 0.18°C, which is less than the uncertainty of the individual RTD measurements. Thus, the condensation heat duty must be determined from energy balances on the pre- and post-condenser, as discussed above. To further decrease the coolant thermal resistance, a test section with external longitudinal fins is used. Figure 4.8 shows a schematic of the finned tube with key dimensions such as the fin height and width.

The thermal resistance in the annulus is determined using the Taborek (1997) correlation for the heat transfer coefficient in longitudinally finned annuli. The flow area of the finned annulus is calculated from Eq. (4.45),

$$\begin{aligned} A_{flow} &= \frac{\pi}{4}\left(D_{OT,in}^2 - D_{test,out}^2\right) - N_{fins}H_{fin}W_{fin} \\ &= 10.99 \text{ mm}^2 \end{aligned} \qquad (4.45)$$

where $N_{\text{fins}} = 12$ is the number of fins, and H_{hin} and W_{fin} are the height (0.84 mm) and width (0.46 mm) of each fin. The wetted perimeter includes the inner and outer tube profiles as described in Eq. (4.46).

$$P_{\text{wetted}} = \pi\left(D_{\text{OT,in}} + D_{\text{test,out}}\right) + 2N_{\text{fins}}H_{\text{fin}}$$
$$= 46.18 \text{ mm} \tag{4.46}$$

From these two values, the hydraulic diameter of the annulus is $D_{\text{annulus,h}} = 4A_{\text{flow}} / P_{\text{wetted}}$ = 0.95 mm.

For the fin analysis, an adiabatic tip is assumed. Therefore the surface area of a single fin, the tube base, and the total surface area are determined to be:

$$A_{\text{fin}} = 2L_{\text{annulus}}H_{\text{fin}} = 97.63 \text{ mm}^2 \tag{4.47}$$

$$A_{\text{base}} = \left(\pi D_{\text{test,out}} - N_{\text{fins}}W_{\text{fin}}\right)L_{\text{annulus}} = 226.3 \text{ mm}^2 \tag{4.48}$$

$$A_{\text{surface}} = A_{\text{base}} + N_{\text{fins}}A_{\text{fin}} = 1398 \text{ mm}^2 \tag{4.49}$$

The volmetric flow rate of the water coupling fluid in the test section is 2.398 L min^{-1}. The density of water at the average temperature of 36.89°C, 993.4 kg m^{-3},
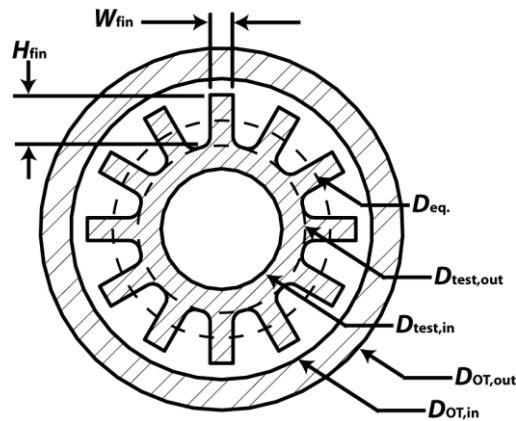
Figure 4.8: Schematic showing a cross section of the longitudinally finned test section with key dimensions

yields a water mass flow rate of 0.040 kg s^{-1}:

$$\dot{m}_{\text{water,test}} = \dot{V}_{\text{water,test}} \rho_{\text{water,test}}$$
$$= (2.398 \text{ L min}^{-1})(993.4 \text{ kg m}^{-3}) = 0.040 \text{ kg s}^{-1} \tag{4.50}$$

The Reynolds number of the water flow is therefore 4964. For this geometry, Taborek classifies any flow with Re < 15,000 as "transition flow" and provides an expression for the Nusselt number as a combination of the corresponding expressions for laminar and turbulent flow:

$$\text{Nu}_{\text{test,annulus}} = \left(\text{Nu}_{\text{L}}^{z} + \text{Nu}_{\text{x}}^{z} \right)^{1/z} \phi_{\text{liq}} \tag{4.51}$$

where the exponent z is defined as in Eq. (4.52):

$$z = \max \left[1.2, \ 0.1 \text{Re}_{\text{test,annulus}}^{0.4} \right] = 3.01 \tag{4.52}$$

The parameter ϕ_{liq} is defined by the ratio of the bulk viscosity of the water to the viscosity at the tube wall. The viscosity at the tube wall is calculated at the temperature of the outer surface of the inner tube.

$$\phi_{\text{liq}} = \left(\frac{\mu_{\text{water,test}}}{\mu_{\text{water,wall}}} \right)^{0.14}$$
$$= \left(\frac{6.93 \times 10^{-4} \text{ kg m}^{-1} \text{ s}^{-1}}{6.82 \times 10^{-4} \text{ kg m}^{-1} \text{ s}^{-1}} \right)^{0.14} = 1.002 \tag{4.53}$$

The laminar term of the Nusselt number is calculated using a leading coefficient $\text{Nu}_{\infty} = 4.12$ and an expression similar to the heat transfer from a flat plate:

$$\text{Nu}_{\text{L}} = \left((\text{Nu}_{\infty})^{3} + \text{Nu}_{\text{L,a}}^{3} \right)^{1/3} = 15.23 \tag{4.54}$$

114

$$Nu_{L,a} = 2.1 \left(Re_{test,annulus} \, Pr_{water,test} \, \frac{D_{annulus,h}}{L_{test,annulus}} \right)^{1/3} \tag{4.55}$$

$$= 15.13$$

Here, the water Prandtl number is 4.62. The turbulent term is a modification of the turbulent heat transfer in a smooth annulus at $Re_{T15} = 15,000$ as shown in Eq. (4.56),

$$Nu_x = \frac{(f_{T15}/8) \, Re_{T15} \, Pr_{water,test}}{1.07 + 12.7(f_{T15}/8)^{0.5}(Pr_{water,test}^{2/3} - 1)} \, \phi_{liq} \left(0.86 r_{test}^* \right) \left(\frac{Re_{test,annulus}}{15,000} \right)^{1.25} \tag{4.56}$$

$$= 5.19$$

The Darcy friction factor is given by:

$$f_{T15} = \left(0.79 \ln \left(Re_{T15} \right) - 1.64 \right)^{-2} = 0.028 \tag{4.57}$$

The radius ratio r_{test}^* is defined as the ratio of the equivalent outer diameter of the finned tube (3.82 mm) to the inner diameter of the outside tube (5.35 mm). The equivalent finned tube diameter is defined as the outer diameter of an inner tube that presents a blockage to the flow area in the annulus that is equivalent to the blockage presented by the finned tube (See Figure 4.8). This yields a radius ratio of 0.71. The laminar and turbulent terms are combined as in Eq. (4.51) to yield an annulus Nusselt number of 15.46.

The heat transfer coefficient in the annulus is calculated using Eq. (4.58) to be 10,165 W m^{-2} K^{-1},

$$h_{test,annulus} = \frac{Nu_{test,annulus} k_{water,test}}{D_{test,h}} = 10165 \text{ W m}^{-2} \text{ K}^{-1} \tag{4.58}$$

where the thermal conductivity of the water at these operating conditions is 0.626 W m^{-1} K^{-1} and the annulus hydraulic diameter is 0.95 mm. The water-side heat

transfer coefficient (10,165 W m^{-2} K^{-1}) is representative of the 47°C saturation conditions, in which the mean value (± standard deviation) is 10,167 ± 19 W m^{-2} K^{-1}.

The fin parameter for a straight rectangular fin with adiabatic tip is 434.2 m^{-1}, resulting in a fin efficiency of 0.958 as shown in Eq. (4.59) and (4.60).

$$m_{\text{fin}} = \sqrt{\frac{2h_{\text{test,annulus}}}{k_{\text{Al}}W_{\text{fin}}}} \tag{4.59}$$

$$\eta_{\text{fin}} = \frac{\tanh\left(m_{\text{fin}}H_{\text{fin}}\right)}{m_{\text{fin}}H_{\text{fin}}} \tag{4.60}$$

With these values, the thermal resistance of a single fin is 1.05 K W^{-1}, while the thermal resistance of the unfinned portion of the tube is 0.43 K W^{-1}, as shown in Eq. (4.61) and (4.62).

$$R_{\text{fin}} = \frac{1}{\eta_{\text{fin}}h_{\text{test,annulus}}A_{\text{fin}}} \tag{4.61}$$

$$R_{\text{unfinned}} = \frac{1}{h_{\text{test,annulus}}A_{\text{base}}} \tag{4.62}$$

The total thermal resistance in the annulus is therefore:

$$R_{\text{test,annulus}} = \left(\frac{1}{R_{\text{unfinned}}} + \frac{N_{\text{fins}}}{R_{\text{fin}}}\right)^{-1} = 0.073 \text{ K W}^{-1} \tag{4.63}$$

The thermal resistances in the Swagelok tee fittings and reducers are shown in Eq. (4.64) and (4.65). These expressions provide an estimate of the natural convection occuring in these relatively stagnant flow regions at either end of the annulus using an effective thermal conductivity as descibed by Incropera and DeWitt (2007). A similar

approach was taken by Andresen (2006) and Bandhauer *et al.* (2006) to account for these types of stagnant regions.

$$R_{\text{test,tee}} = \frac{\ln\left(D_{\text{tee}} / D_{\text{test,out}}\right)}{2\pi k_{\text{eff,test,tee}} L_{\text{tee}}} \tag{4.64}$$

$$R_{\text{test,reducer}} = \frac{\ln\left(D_{\text{reducer}} / D_{\text{test,out}}\right)}{2\pi k_{\text{eff,test,reducer}} L_{\text{reducer}}} \tag{4.65}$$

The test section dimensions are provided in Table 3.3. The effective conductivity is obtained from the geometry and a modified Rayleigh number. The modified Rayleigh numbers for the tee and reducer are estimated using Eqs. (4.66) and (4.67).

$$\text{Ra}^*_{\text{tee}} = \frac{\left[\ln\left(D_{\text{tee}} / D_{\text{test,out}}\right)\right]^4}{\left(D_{\text{test,out}}^{-3/5} + D_{\text{tee}}^{-3/5}\right)} \frac{\rho_{\text{water,test}} g \beta_{\text{water,test}} \left(T_{\text{wall,out}} - T_{\text{water,test,avg}}\right)}{\mu_{\text{water,test}} \alpha_{\text{water,test}}} = 46.27 \tag{4.66}$$

$$\begin{aligned}\text{Ra}^*_{\text{reducer}} &= \frac{\left[\ln\left(D_{\text{reducer}} / D_{\text{test,out}}\right)\right]^4}{\left(D_{\text{test,out}}^{-3/5} + D_{\text{tee}}^{-3/5}\right)} \frac{\rho_{\text{water,test}} g \beta_{\text{water,test}} \left(T_{\text{wall,out}} - T_{\text{water,test,avg}}\right)}{\mu_{\text{water,test}} \alpha_{\text{water,test}}} \\ &= 1.90\end{aligned} \tag{4.67}$$

where $g = 9.81$ m s^{-2} is the acceleration due to gravity. The difference between the modified Rayleigh number values is mostly due to the different inner diameter of the tee (6.50 mm) and the reducer fittings (4.40 mm). The average water temperature in the test section is 36.89°C. At 36.89°C and 236.23 kPa, the thermal diffusivity of water is 1.51×10^{-7} m^2 s^{-1}, while the thermal expansion coefficient of water is 3.62×10^{-4} K^{-1}. The outer wall surface temperature is found iteratively by accounting for the condensing propane resistance and test section wall resistance as shown in Eq. (4.68). With a test section heat duty of 22.61 W, average condensing temperature of 46.77°C, and

condensation and wall resistances of 0.365 K W^{-1} and 0.0021 K W^{-1}, respectively, the outer test section wall temperature is calculated to be 38.47°C.

$$T_{test,wall,out} = T_{ref,test,avg} - \frac{\dot{Q}_{test}}{R_{test,ref} + R_{test,wall}}$$
$$= 46.77°C - \frac{22.61 \text{ W}}{0.365 \text{ K W}^{-1} + 0.0021 \text{ K W}^{-1}} = 38.47°C \qquad (4.68)$$

Expressions to calculate the effective thermal conductivities for the tee and reducer are provided by Irvine and Hartnett (1975). For Ra* ≤ 100, natural convection is suppressed and the effective thermal conductivity is equal to the thermal conductivity of the fluid. For Ra* > 100, the effective thermal conductivity is calculated using Eq. (4.69). For the tee fitting, the modified Rayleigh number is greater than 100 in 26% of the data points.

$$\frac{k_{eff}}{k_{water}} = 0.386 \left(\frac{Pr}{0.861 + Pr} \right)^{0.25} \left(Ra^{*} \right)^{0.25} \qquad (4.69)$$

As mentioned previously, the thermal conductivity of the water is 0.626 W m^{-1} K^{-1}. Therefore, the effective thermal conductivities for this data point for both the tee and the reducer are 0.626 W m^{-1} K^{-1}. Thus the thermal resistances in the tee are 17.45 K W^{-1} at the top (propane inlet) and 16.71 K W^{-1} at the bottom (propane outlet). The thermal resistance of the reducers are both 3.79 K W^{-1} because the lengths of both reducers are the same. The thermal conductances ($1/R$) of the end sections are significantly smaller than that of the annulus. The values of the tee thermal conductance (0.57 and 0.60 W K^{-1}) are 0.4% of the value of the annulus thermal conductance (13.71 W K^{-1}), and the values of the reducer thermal conductance (0.26 W K^{-1}) are 1.9% that of the annulus (13.71 W K^{-1}). Therefore, most of the energy is transported in the annulus region, and the end areas are relatively inactive.

The heat duty in the test section is the sum of the contributions from the annulus, the tees and the reducers as shown in Figure 4.7. The heat duties in the tee and reducer are determined for both the test section inlet and outlet using Eq. (4.70).

$$\dot{Q}_{test,fitting,j} = \frac{T_{test,wall,out} - T_{water,test,j}}{R_{test,fitting,j}} \tag{4.70}$$

where the subscript "fitting" designates the tee or reducer and the index j designates the test section inlet or outlet. The heat duties from the tee fittings are 0.09 W at the test section propane-side inlet, and 0.10 W at the outlet. The heat duties from the reducers are 0.39 W at the inlet, and 0.44 W at the outlet. In total, the end region heat duty terms are 1.02 W or 4.5% of the total test section heat duty of 22.61 W. While this is a small percentage of the total heat duty, it is important to include in the calculation to avoid overestimation of the water resistance, leading to a higher calculated condensation heat transfer coefficient value.

The equivalent convective resistance on the water side is calculated to be 0.070 K W^{-1} using Eq. (4.44).

$$\frac{1}{R_{test,water}} = \frac{1}{R_{test,tee,1}} + \frac{1}{R_{test,annulus}} + \frac{1}{R_{test,tee,2}} + 2\left(\frac{1}{R_{test,reducer}}\right)$$

$$= \frac{1}{17.45 \text{ K W}^{-1}} + \frac{1}{0.073 \text{ K W}^{-1}} + \frac{1}{16.71 \text{ K W}^{-1}} + 2\left(\frac{1}{3.79 \text{ K W}^{-1}}\right)$$

$$R_{test,water} = 0.070 \text{ K W}^{-1}$$

The thermal resistance of the condensing propane is calculated from the test section conductance, wall resistance and water-side convective resistance based on Eq. (4.71).

$$R_{\text{test,propane}} = \frac{1}{UA_{\text{test}}} - R_{\text{test,wall}} - R_{\text{test,water}}$$

$$= \frac{1}{2.29 \text{ W K}^{-1}} - 0.0021 \text{ K W}^{-1} - 0.070 \text{ K W}^{-1} = 0.365 \text{ K W}^{-1}$$

(4.71)

The resistance ratio, i.e. the ratio of the resistance presented by the condensing side to resistances of the wall and the water side, is calculated using Eq. (4.72). A larger resistance ratio is desirable, because it indicates that the condensation resistance is dominant, reducing uncertianty in the calculated value. In this study, it is observed that for resistance ratio greater than about 1.8, the coupling fluid resistance contributes to less than 50% of the total uncertainty in the heat transfer coefficient.

$$R_{\text{ratio,test}} = \frac{R_{\text{test,propane}}}{R_{\text{test,wall}} + R_{\text{test,water}}}$$

$$= \frac{0.365 \text{ K W}^{-1}}{0.0021 \text{ K W}^{-1} + 0.070 \text{ K W}^{-1}} = 5.08$$

(4.72)

In the data from the present study, the resistance ratio ranges from 2.67 to 15.28 with an average of 6.32.

The ratio of propane resistance to the wall resistance is shown in Eq. (4.73). The test section tube material was chosen with a high thermal conductivity to ensure that the wall resistance contributed minimally to the heat transfer coefficient calculations. The wall resistance ratio is 170.3, which confirms that the conduction resistance in the wall is minimal.

$$R_{\text{ratio,test,wall}} = \frac{R_{\text{test,propane}}}{R_{\text{test,wall}}}$$

$$= \frac{0.365 \text{ K W}^{-1}}{0.0021 \text{ K W}^{-1}} = 170.3$$

(4.73)

Finally, the condensing propane heat transfer coefficient is calculated using Eq. (3.21) to be 3346 with a 13.6% uncertainty. The heat transfer length is 135.1 mm, which includes both the annulus and end cap regions.

$$
\begin{aligned}
h_{\text{test,propane}} &= \frac{1}{R_{\text{test,propane}}\pi D_{\text{test,in}} L_{\text{test,HT}}} \\
&= \frac{1}{(0.365 \text{ K W}^{-1})\pi(0.00193 \text{ m})(0.1351 \text{ m})} = 3346 \pm 457 \text{ W m}^{-2} \text{ K}^{-1}
\end{aligned}
\tag{4.74}
$$

The coupling fluid resistance contributes 33% of the heat transfer coefficient uncertainty, while the LMTD measurement contributes 3% of the uncertainty. The major portion of the uncertainty (84%) is from the heat duty measurements based on the previously described energy balances. The post-condenser air thermocouple measurements each contribute about 25% to the uncertainty. The pre- and post-condenser air pressure measurements contributed about 9.9% and 8.7%, respectively, to the uncertainty. The post-condenser temperature measurements contribute more to the uncertainty than the pre-condenser measurements due to the higher heat duty of the post-condenser for this data point.

The Nusselt number for the condensing propane is calculated from the heat transfer coefficient using the thermal conductivity of saturated liquid propane (0.084 W m^{-1} K^{-1}).

$$
\text{Nu}_{\text{propane,test}} = \frac{h_{\text{test,propane}} D_{\text{test,in}}}{k_{\text{propane,test,l}}} = 77.0 \pm 10.5
\tag{4.75}
$$

4.3. Test Section Pressure Drop

The frictional pressure drop of the condensing propane is determined from the measured differential pressure in the test section along with the minor losses and static head terms. Figure 4.9 shows a schematic of the test section and the differential pressure measurement positioning. The differential pressure in the test section between the two pressure taps is 1.680 ± 0.0035 kPa. This measured value is due to a combination of frictional pressure drop, contraction and expansion losses in the transition between the main loop and the test section, deceleration of the condensing fluid, and two static head terms due to the vertical orientation of the test section as shown in Eq. (4.76):

$$\Delta P_{\text{measured}} = \Delta P_{\text{frictional}} + \Delta P_{\text{contraction}} - \Delta P_{\text{expansion}} \\ - \left| \Delta P_{\text{deceleration}} \right| - \Delta P_{\text{static,test}} + \Delta P_{\text{static,line}} \tag{4.76}$$

The contraction pressure drop from the line to the test section is given by Hewitt *et al.* (1994) in Eq. (4.77).

$$\Delta P_{\text{contraction}} = \frac{G^2}{2\rho_{\text{propane,l,3}}} \left(\underbrace{1 - A_{\text{ratio}}^2}_{\text{reversible}} + \underbrace{\left(\frac{1}{C_{\text{C}}} - 1 \right)^2}_{\text{irreversible}} \right) \psi_H \tag{4.77}$$

The liquid density of propane at the test section inlet is 454.5 kg m^{-3}. Three distinct contractions were identified between the cross fitting with the pressure tap and the test section tube: the cross to the reducer, the reducer to the intermediate contraction, and the contraction to the test section. The area ratio is defined in Eq. (4.78) for each of these regions.

$$A_{\text{ratio,test.1}} = D_{\text{reducer}}^{2} / D_{\text{cross}}^{2} = (0.00442 \text{ m})^{2} / (0.00483 \text{ m})^{2} = 0.839$$

$$A_{\text{ratio,test,2}} = D_{\text{contraction}}^{2} / D_{\text{reducer}}^{2} = (0.00240 \text{ m})^{2} / (0.00442 \text{ m})^{2} = 0.295 \qquad (4.78)$$

$$A_{\text{ratio,test,3}} = D_{\text{test,in}}^{2} / D_{\text{contraction}}^{2} = (0.00193 \text{ m})^{2} / (0.00240 \text{ m})^{2} = 0.647$$

For each region, the propane mass flux is adjusted accordingly:

$$G_{\text{propane}} = 100.2 \text{ kg m}^{-2} \text{ s}^{-1}$$

$$G_{\text{propane,contraction}} = G_{\text{propane}} A_{\text{ratio,test,3}} = 64.8 \text{ kg m}^{-2} \text{ s}^{-1} \qquad (4.79)$$

$$G_{\text{propane,reducer}} = G_{\text{propane}} A_{\text{ratio,test,3}} A_{\text{ratio,test,2}} = 19.1 \text{ kg m}^{-2} \text{ s}^{-1}$$

The coefficient of contraction is given by Chisholm (1983) in Eq. (4.80). For regions 1, 2, and 3, the coefficients are 0.7958, 0.6508, and 0.7247, respectively.
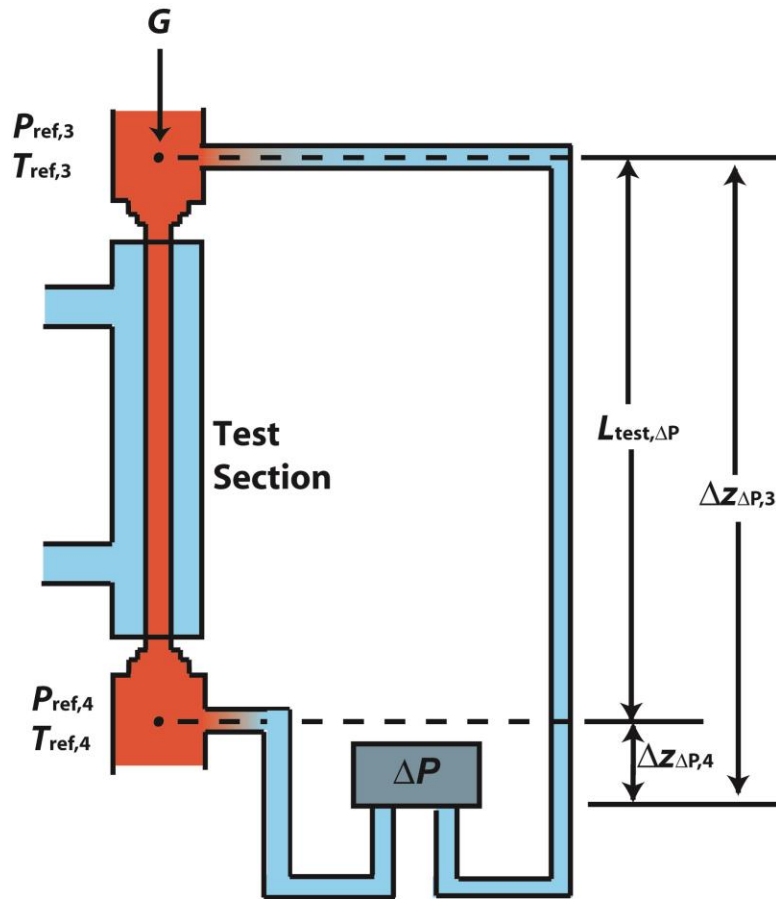
Figure 4.9: Schematic showing the configuration of the test section differential pressure measurements

$$C_C = \cfrac{1}{0.639\left(1 - A_{\text{ratio,test}}\right)^{1/2} + 1} \qquad (4.80)$$

Hewitt *et al.* (1994) recommend the homogeneous flow multiplier for the contraction pressure drop calculation as shown in Eq. (4.81). This value is the same for each contraction and is calculated from the test section inlet quality and density ratio.

$$\begin{aligned}
\psi_{\text{H}} &= 1 + \left(\frac{\rho_{\text{propane,l,3}}}{\rho_{\text{propane,v,3}}} - 1\right)x_3 \\
&= 1 + \left(\frac{454.5\ \text{kg m}^{-3}}{35.95\ \text{kg m}^{-3}} - 1\right)(0.72) = 9.40
\end{aligned} \qquad (4.81)$$

Therefore, as defined in Eq. (4.77), the total contraction pressure drop is:

$$\begin{aligned}
\Delta P_{\text{contraction}} &= \Delta P_{\text{contraction,1}} + \Delta P_{\text{contraction,2}} + \Delta P_{\text{contraction,3}} \\
&= 1.37\ \text{Pa} + 52.18\ \text{Pa} + 75.44\ \text{Pa} \\
&= 129.00 \pm 32.25\ \text{Pa}
\end{aligned} \qquad (4.82)$$

A $\pm 25\%$ uncertainty is assigned to these minor loss terms.

The expansion pressure drop from the test section to the line is given by Hewitt *et al.* (1994), as shown in Eq. (4.83). The expansion pressure drop consists of a reversible pressure recovery due to a change of kinetic energy along with an irreversible loss due to friction. As with the contraction pressure drop, the expansion losses are calculated for three distinct flow area regions.

$$\Delta P_{\text{expansion}} = \frac{G^2}{2\rho_{\text{propane,l,4}}}\left(\underbrace{\left(1 - A_{\text{ratio}}^2\right)}_{\text{reversible}} - \underbrace{\left(1 - A_{\text{ratio}}\right)^2}_{\text{irreversible}}\right)\psi_S \qquad (4.83)$$

The liquid density of the propane at the outlet of the test section is 454.7 kg m^{-3}, while the mass flux and area ratio values are the same as for the contraction terms.

The separated flow multiplier as defined in Eq. (4.84) is recommended for expansion pressure drop terms. The test section outlet quality is 0.46 and the parameter $B = 0.25$ is given by Chisholm (1983).

$$
\begin{aligned}
\psi_S &= 1 + \left(\frac{\rho_{\text{propane},l,4}}{\rho_{\text{propane},v,4}} - 1 \right) \left[Bx_4 (1 - x_4) + x_4^2 \right] \\
&= 1 + \left(\frac{454.7 \text{ kg m}^{-3}}{35.86 \text{ kg m}^{-3}} - 1 \right) \left[0.25(0.46)(1 - 0.46) + 0.46^2 \right] = 4.18
\end{aligned}
\tag{4.84}
$$

Therefore, the total expansion pressure drop, as defined in Eq. (4.83), is:

$$
\begin{aligned}
\Delta P_{\text{expansion}} &= \Delta P_{\text{expansion},1} + \Delta P_{\text{expansion},2} + \Delta P_{\text{expansion},3} \\
&= 0.45 \text{ Pa} + 8.02 \text{ Pa} + 21.07 \text{ Pa} \\
&= 29.54 \pm 7.39 \text{ Pa}
\end{aligned}
\tag{4.85}
$$

The expansion pressure drop represents an overall pressure recovery. Therefore, the difference in the contraction and expansion losses represents the net pressure drop due to "end effects": $\Delta P_{\text{endeffects}} = \Delta P_{\text{contraction}} - \Delta P_{\text{expansion}} = 99.44$ Pa.

The propane also experiences a pressure recovery due to decreasing velocities during condensation. The deceleration pressure drop can be derived from an axial momentum balance as shown in Carey (2008).

$$
\left| \Delta P_{\text{deceleration}} \right| =
\left|
\begin{aligned}
& \left\| G_{\text{propane}}^2 \left(\frac{x^2}{\rho_{\text{propane},v,4}\alpha} + \frac{(1-x)^2}{\rho_{\text{propane},l,4}(1-\alpha)} \right) \right\|_{\substack{\alpha = \alpha_{\text{test,out}} \\ x = x_4}} \\
& - \left| G_{\text{propane}}^2 \left(\frac{x^2}{\rho_{\text{propane},v,3}\alpha} + \frac{(1-x)^2}{\rho_{\text{propane},l,3}(1-\alpha)} \right) \right|_{\substack{\alpha = \alpha_{\text{test,in}} \\ x = x_3}}
\end{aligned}
\right|
\tag{4.86}
$$

$$
= 83.39 \pm 20.85 \text{ Pa}
$$

The void fraction, α, is a function of quality and propane liquid and vapor densities and dynamic viscosities. The void fraction is calculated from the Winkler *et al.* (2012)

correlation. This void fraction model is developed for condensing R134a in minichannels ($2 < D_\mathrm{h} < 4.91$ mm) in the intermittent regime and is defined in Eq. (4.87). Although the void fraction model by Mishima and Hibiki (1996) also worked well in the data reduction and modeling, the Winkler *et al.* correlation is chosen because it is developed for condensation of refrigerants that are more similar in thermophysical properties to hydrocarbons than air-water or steam two-phase flow studies.

$$\alpha_{\substack{\mathrm{Winkler,} \\ 2012}} = \frac{\alpha_\mathrm{homogeneous}}{1.153 + 0.071\ \mathrm{m\ s^{-1}} \big/ j} \tag{4.87}$$

In this correlation, j is the total volumetric flux defined as the sum of the vapor and liquid phase superficial velocity terms, Eq. (4.88), and the homogeneous void fraction model is defined in Eq. (4.89).

$$j = \frac{Gx}{\rho_\mathrm{v}} + \frac{G(1-x)}{\rho_\mathrm{l}} \tag{4.88}$$

$$\alpha_\mathrm{homogeneous} = \left(1 + \left(\frac{1-x}{x}\right)\left(\frac{\rho_\mathrm{v}}{\rho_\mathrm{l}}\right)\right)^{-1} \tag{4.89}$$

The void fractions at the test section inlet and outlet are 0.76 and 0.82, respectively. Thus, the magnitude of the deceleration pressure drop is 83.39 ± 20.85 Pa, with a $\pm 25\%$ assigned uncertainty.

Because of the vertical orientation of the test section, the static head of the two-phase fluid is a significant quantity. The differential equation describing the hydrostatic pressure with respect to elevation, z, is shown in Eq. (4.90). The void fraction is calculated from Eq. (4.87).

$$\left.\frac{dP}{dz}\right|_g = g\left(\alpha\rho_v + (1-\alpha)\rho_l\right) \tag{4.90}$$

To determine the two-phase static head, the test section is subdivided into three segments: entrance, condensing, and exit regions. The entrance and exit segments span the length between the pressure tap and the annulus and are assumed to be adiabatic for the purpose of this analysis. The void fraction is therefore constant over the entrance and exit lengths (100 mm and 104 mm respectively). The static head in the entrance and exit segments is therefore calculated in Eq. (4.91) using the void fraction and density at the inlet and outlet of the test section.

$$
\begin{aligned}
\Delta P_{\text{static,test,in}} &= g\left(\alpha_{\text{test,in}}\rho_{\text{propane,v,3}} + (1-\alpha_{\text{test,in}})\rho_{\text{propane,l,3}}\right)L_{\text{test,entrance}} \\
\Delta P_{\text{static,test,out}} &= g\left(\alpha_{\text{test,out}}\rho_{\text{propane,v,4}} + (1-\alpha_{\text{test,out}})\rho_{\text{propane,l,4}}\right)L_{\text{test,exit}}
\end{aligned}
\tag{4.91}
$$

The static head in the entrance and exit segments is 110.2 ± 84.0 Pa and 139.2 ± 81.2 Pa respectively. A $\pm25\%$ uncertainty in the void fraction model, $\pm3\%$ uncertainty in the density, and ±1 mm uncertainty in the length measurements are used in estimating the uncertainties of these static head terms. The uncertainty propagation calculations are described in detail in Appendix A.

Because the void fraction varies over the condensing length of the test section, the static head is approximated by a summation of the two-phase static head over 15 segments of equal length $\Delta z = L_{\text{test,annulus}} / 15 = 3.90$ mm. The density is held constant at the average saturation pressure of the test section (1605.4 kPa): $\rho_{\text{propane,test,l}} = 454.6$ kg m^{-3} and $\rho_{\text{propane,test,v}} = 35.90$ kg m^{-3}.

$$\Delta P_{\text{static,test,HX}} = \int_0^{L_{\text{test,annulus}}} g\left(\alpha \rho_{\text{propane,test,v}} + (1-\alpha)\rho_{\text{propane,test,l}}\right) dz$$

$$\approx \sum_{i=1}^{15} g\left(\alpha_i \rho_{\text{propane,test,v}} + (1-\alpha_i)\rho_{\text{propane,test,l}}\right)\Delta z = 70.6 \pm 49.1 \text{ Pa} \tag{4.92}$$

Over the length of the condensing region (58.46 mm), the void fraction changes as a function of quality, which is a function of position. To determine the shape of the function $x(z)$ during condensation, for simplicity the heat transfer is approximated using the Shah (1979) equation for heat transfer coefficient during condensation. The results of a simple segmented model showed a quadratic regression equation between quality and position is the best fit with $R^2 = 1$ (Figure 4.10). With the curve shape determined, the test section quality at each segment is approximated by quadratic interpolation between the test section inlet and outlet quality. Eq. (4.93) shows the general form for quadratic interpolation.

$$x(z) = a_0 - a_1 z + a_2 z^2 \tag{4.93}$$

From the boundary conditions, $x(0) = x_3$ and $x(L_{\text{test,annulus}}) = x_4$, the coefficients a_0 and a_1 are determined. Therefore, the quality of a given segment is defined as:
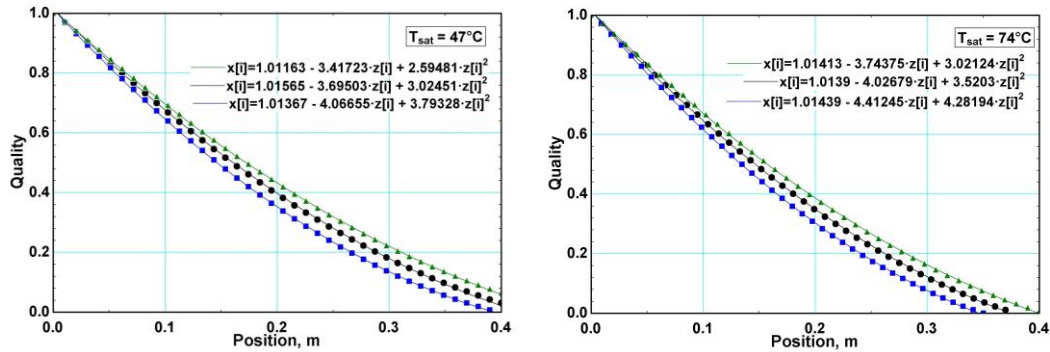
Figure 4.10: Quality change as a function of position during condensation

$$x_i = x_3 - \left(a_2 L_{\text{test,annulus}} + \Delta x / L_{\text{test,annulus}} \right) z_i + a_2 z_i^{\,2} \qquad (4.94)$$

To perform the quadratic interpolation, one more condition is necessary to define the coefficient of the quadratic term, a_2. The concavity of the approximated quadratic curve is small, especially for the length scale of the test section (58.46 mm) compared to that of the approximated model (400 mm). Therefore, it was determined to be sufficient to approximate the a_2 coefficient by a linear regression of the coefficients of the quadratic term of the regression curve with the mass flux and saturation temperature for the six nominal conditions presented ($G = 75$, 100, 125 kg m^{-2} s^{-1}, $T_{\text{sat}} = 47$, $74°$C). This results in the following expression for a_2:

$$a_2 = 4.7785 - 0.02459 G_{\text{ref}} + 0.01741 T_{\text{sat}} \qquad (4.95)$$

The total two-phase static head in the test section is therefore the sum of the static head in the entrance, condensing region, and exit of the test section:

$$\begin{aligned}
\Delta P_{\text{static,test}} &= \Delta P_{\text{static,test,in}} + \Delta P_{\text{static,test,HX}} + \Delta P_{\text{static,test,out}} \\
&= 110.2 \text{ Pa} + 70.51 \text{ Pa} + 139.2 \text{ Pa} = 319.9 \pm 126.7 \text{ Pa}
\end{aligned} \qquad (4.96)$$

One more static head term is required to correct for the elevation differences between the differential pressure transducer and the pressure taps.

$$\begin{aligned}
\Delta P_{\text{static,line}} &= \rho_{\text{propane,line,in,down}} \, g \Delta z_{\Delta P_3} - \rho_{\text{propane,line,out}} \, g \Delta z_{\Delta P_4} \\
&= 1230 \pm 50.1 \text{ Pa}
\end{aligned} \qquad (4.97)$$

Based on wall surface temperatures of the pressure tap lines, it is determined that the fluid in the vertical columns is subcooled liquid. The density of the liquid propane in the inlet pressure tap line is determined based on the measured wall temperatures at the top ($T_{\text{wall,line,1}} = 39.29°$C) and bottom ($T_{\text{wall,line,3}} = 31.35°$C) of the line. See Figure 4.2 for the position of the wall temperature measurements in relation to the pressure tap and the

differential pressure transducer. The ambient heat loss calculation for this tube segment is descibed in more detail in Section 4.1.1 and uses the average wall temperature between these measurements (35.32°C). The heat loss in this segment (0.14 W) is used to determine the fluid temperature, which is also 35.32°C. The small heat loss in this segment leads to a calculated temperature difference of only 0.001°C across the tube wall. Therefore the density in the inlet pressure tap line at 35.32°C and the adjusted pressure 1607.2 kPa is 477.0 kg m^{-3}. As determined before in Eq. (4.9), the density in the outlet pressure tap line is 482.7 kg m^{-3}. The inlet pressure tap is elevated 347 mm above the transducer, while the outlet pressure tap is elevated 83 mm above the transducer.

The frictional pressure drop is then calculated by rearranging the terms in Eq. (4.76):

$$
\begin{aligned}
\Delta P_{\text{frictional}} &= \Delta P_{\text{measured}} - \Delta P_{\text{contraction}} + \Delta P_{\text{expansion}} \\
&\quad + \left| \Delta P_{\text{deceleration}} \right| + \Delta P_{\text{static,test}} - \Delta P_{\text{static,line}} \\
&= 1680 \text{ Pa} - 129.00 \text{ Pa} + 29.54 \text{ Pa} + 83.39 \text{ Pa} + 319.9 \text{ Pa} - 1230 \text{ Pa} \\
&= 0.753 \pm 0.142 \text{ kPa}
\end{aligned}
\tag{4.98}
$$

The frictional pressure gradient is calculated by dividing the frictional pressure drop by the length of the test section tube (191 mm). The uncertainty of the frictional pressure gradient is 19% of the calculated value.

$$
\left. \frac{dP}{dz} \right|_{\text{frictional}} = \frac{\Delta P_{\text{frictional}}}{L_{\text{test},\Delta P}} = \frac{0.753 \text{ kPa}}{0.191 \text{ m}} = 3.944 \pm 0.743 \text{ kPa m}^{-1}
\tag{4.99}
$$

CHAPTER 5: RESULTS AND MODEL DEVELOPMENT

This chapter presents the results from the experiments and analyses described in the previous chapters to obtain the frictional pressure drop and heat transfer coefficient during condensation of propane in the 1.93 mm diameter vertical tube under consideration in the present study. The data are compared with applicable models from the literature, and where possible, new correlations are proposed to predict these condensation phenomena.

5.1. Results

The frictional pressure drop and heat transfer coefficient were measured over the test matrix, shown inTable 5.1, which covers two saturation temperatures, 47°C and 74°C (0.37 and 0.66 reduced pressures), four mass fluxes, 75, 100, 125 and 150 kg m^{-2} s^{-1}, and

Table 5.1: Test Matrix

Fluid: Propane, ID = 1.93 mm, vertically downward flow			
Mass Flux kg m^{-2} s^{-1}	**Saturation Temperature** °C	**Saturation Pressure** kPa	**Quality**
75	47	1604	0.25 – 0.00 0.50 – 0.25 0.75 – 0.50 1.00 – 0.75
75	74	2796	
100	47	1604	
100	74	2796	
125	47	1604	
125	74	2796	
150	47	1604	

four quality increments at each saturation condition. The operating parameters were maintained within a tight tolerance of the nominal test matrix condtions. The average absolute deviation from the nominal mass flux is 0.4%, while the average absolute deviation from the nominal saturation temperature is 0.55°C (1.0%).

The range of mass fluxes and qualities obtained in the experiments is depicted graphically in Figure 5.1. Over the entire data set, inlet and outlet quality data from 0.99 to 0.03 are shown. The quality changes for any data point are greater near the saturated vapor condition due to the larger heat transfer coefficients at high quality than at low quality; therefore, while average quality increments of 25% are attempted, there is necessarily some overlap in the quality ranges at these conditions. For the 74°C saturation conditions, the quality range overlap is partially due to the smaller latent heat at higher saturation conditions (291.8 kJ kg^{-1} at 47°C and 214.4 kJ kg^{-1} at 74°C), leading to a larger quality change for a similar heat duty in the test section. The quality change for each data point is depicted graphically in Figure 5.2. For the 47°C saturation condition, the average quality change is 0.24, while for the 74°C saturation condition, the average quality change is 0.47. The average quality change for all data obtained in the present study is 0.33.

The vapor and liquid Reynolds numbers are defined as the Reynolds number if each phase were to flow alone through the channel.

$$\text{Re}_v = \frac{GxD}{\mu_v}, \quad \text{Re}_l = \frac{G(1-x)D}{\mu_l} \tag{5.1}$$
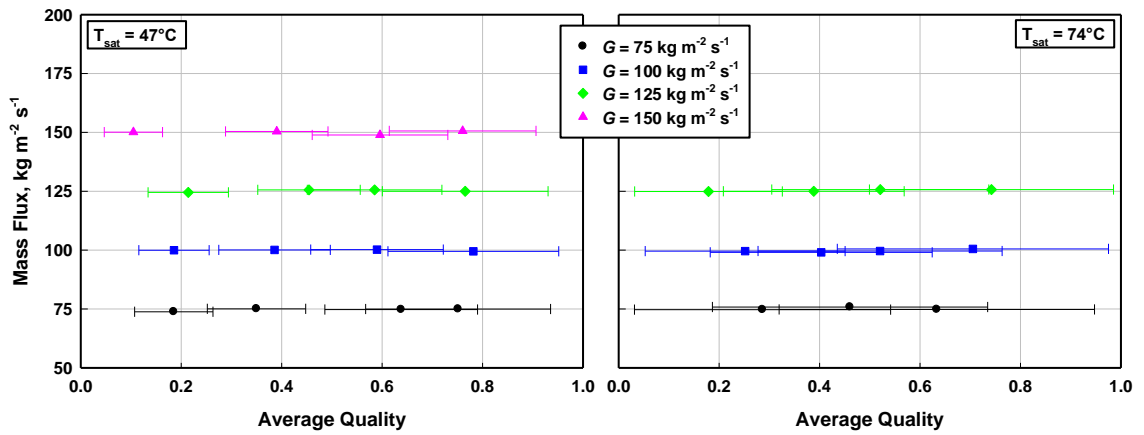
Figure 5.1: Quality and mass fluxes obtained in the present study
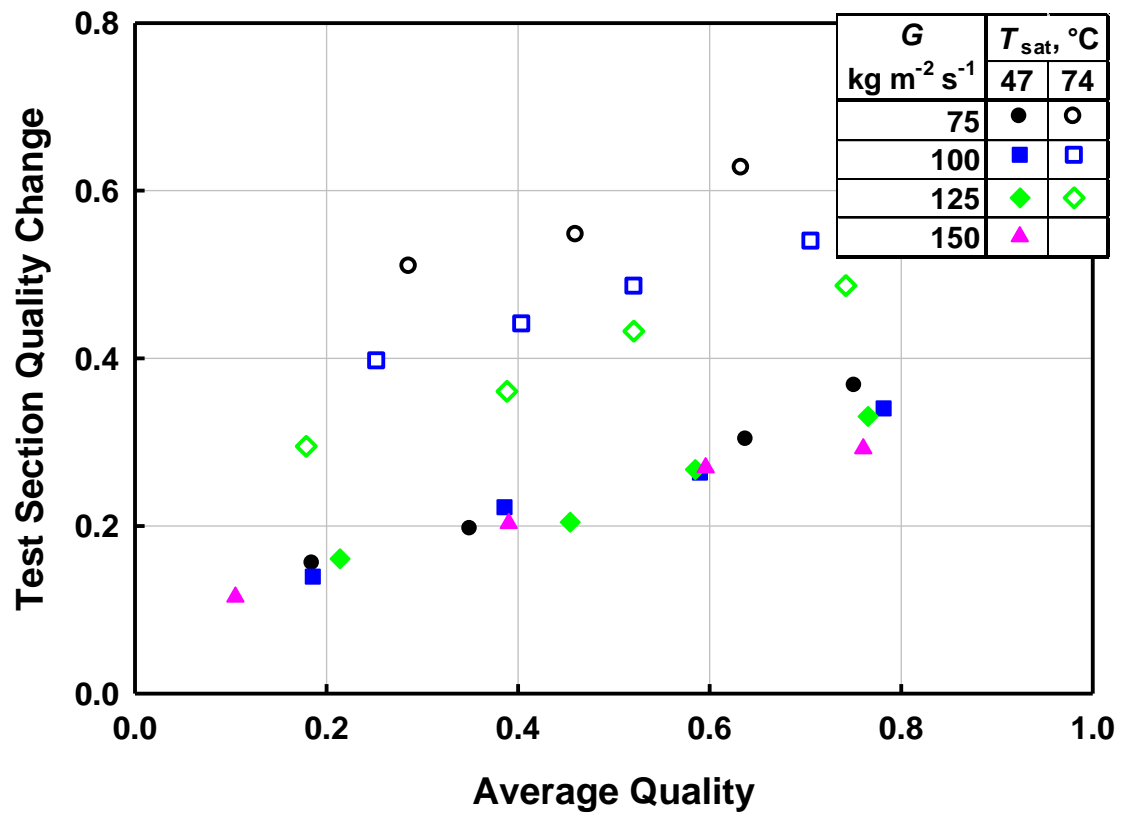
Figure 5.2: Quality change in the test section for all data from the present study

Figure 5.3 shows the vapor and liquid Reynolds numbers for all the test conditions. The vapor Reynolds number ranges from 2845 to 23,886, while the liquid Reynolds number ranges from 475 to 3,731. It should be noted that the vapor phase is turbulent (Re > 10,000) for almost half of the experimental conditions, with some of the data, especially the low quality points in the transition region. The liquid phase is in the laminar regime (Re < 2300) for most of the data range. As with the vapor Reynolds number, some of the low quality data points show liquid flow in the transition region. However, as described in Chapter 2 (Soliman *et al.*, 1968), for annular flows, the liquid film may become turbulent at Reynolds numbers as low as 240. Therefore, more of the data may have turbulent liquid flows than the above grouping suggests.

5.1.1. <u>Pressure Drop</u>

The frictional pressure drop is determined from the measured pressure drop accounting for the minor losses due to expansion and contraction, the deceleration of the condensing fluid, and the static head due to the two-phase fluid in the test section and single-phase liquid in the differential pressure tap lines. A graphical depiction of the individual contributions of each pressure drop term to the overall measured and frictional values is provided in Figure 5.4. For each saturation temperature case, the data points are presented in order of increasing mass flux and quality. Each mass flux data set is grouped by the vertical lines on the plot from 75 to 150 kg m^{-2} s^{-1}. The relative contribution of each of these terms is summarized in Table 5.2. Overall, the frictional pressure drop contributes an average of 46.5% to the total measured pressure drop. With the exception of the static head in the pressure tap lines, which is practically constant, the frictional
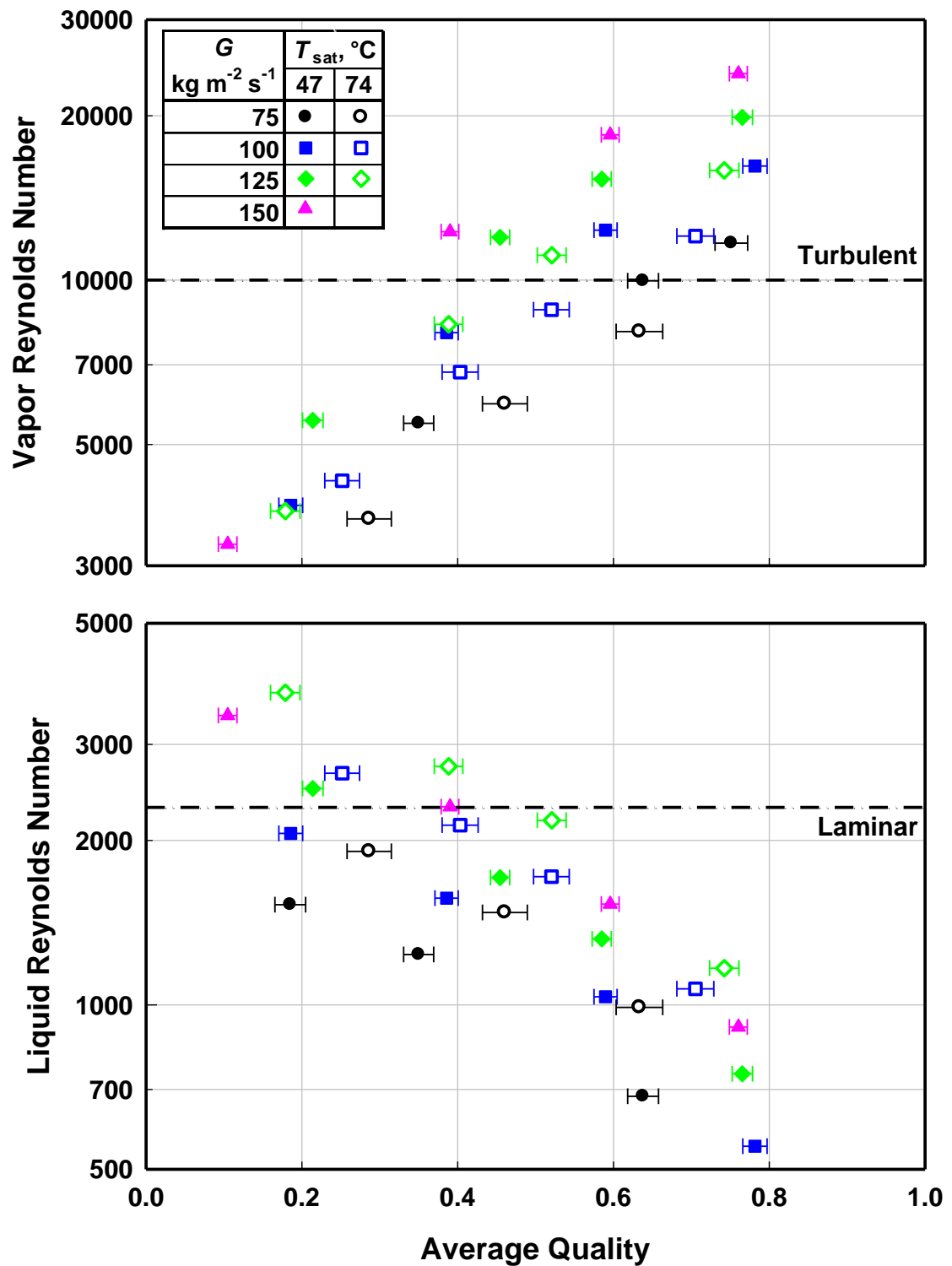
Figure 5.3: Liquid and vapor Reynolds numbers for the data obtained in the present study
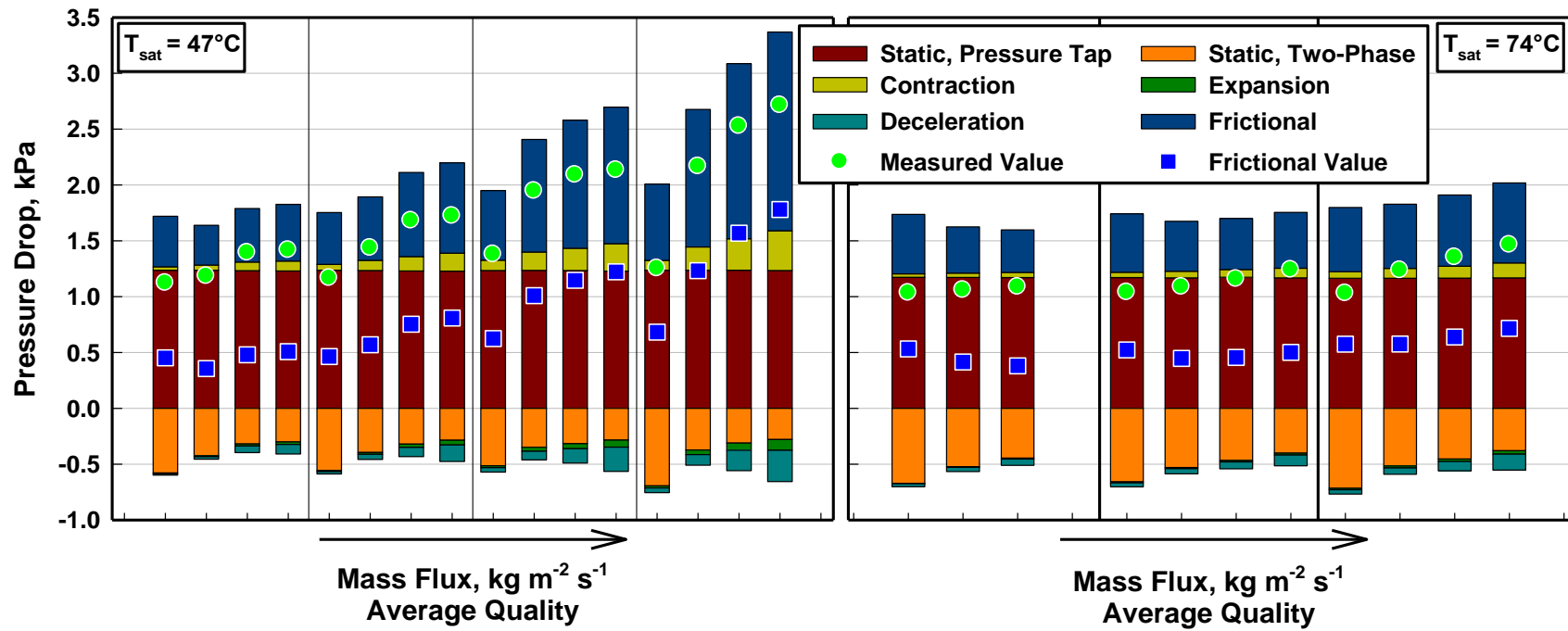
Figure 5.4: Contributions to the pressure drop measurements

Table 5.2: Relative Pressure Drop Contributions and Uncertainties

Saturation Temperature	$\dfrac{\Delta P_{\text{frictional}}}{\Delta P_{\text{measured}}}$	$\dfrac{\Delta P_{\text{deceleration}}}{\Delta P_{\text{measured}}}$	$\dfrac{\Delta P_{\text{endeffects}}}{\Delta P_{\text{measured}}}$	$\dfrac{\Delta P_{\text{static, two-phase}}}{\Delta P_{\text{measured}}}$	$\dfrac{\Delta P_{\text{static, pressure-taps}}}{\Delta P_{\text{measured}}}$	$\dfrac{U_{dP_f/dz}}{dP_f/dz}$
°C	%	%	%	%	%	%
47	47.5	5.0	6.0	26.3	77.9	18.9
74	45.0	5.1	4.6	46.4	101.9	18.6
Average	46.5	5.1	5.4	34.5	87.7	18.8

term has the greatest contribution. At the high saturation temperature condition, the two-phase static head term has a slightly larger contribution (46.4%) than the frictional term (45.0%). By contrast, for the low saturation temperature, the two-phase head contributes 26.3% compared to the frictional contribution of 47.5%. Although the frictional component is not the dominant term, the uncertainty of the high saturation temperature conditions is slightly lower than that of the low saturation temperature condition. The slight difference is due to the smaller difference in saturated liquid and saturated vapor density ($\rho_l - \rho_v = 418.8$ kg m^{-3} at 47°C and 321.25 kg m^{-3} at 74°C), which is an important term in the calculation of the uncertainty of the static head terms (see Appendix A for a more detailed discussion). For all the pressure drop data obtained in the present study, 85% of the data have an uncertainty within ±25%, while 30% of the data have an uncertainty within ±15%. The deceleration (5.1%) and minor losses (5.4%) contribute minimally to the pressure drop value.

The pressure drops are shown in Figure 5.5. At the 47°C saturation condition, the frictional pressure drop clearly increases with increasing mass flux and quality for all but the lowest quality points. At low quality, low mass flux, and high saturation temperature, the resolution of the pressure drop data is lower and a decrease in frictional pressure drop

with increasing quality is observed. For these cases, the decrease in the two-phase static head in the test section was greater than the increase in measured overall pressure drop. The accuracy of these frictional pressure drops is lower due to the two-phase static head, which is the greatest contributor to these pressure drop measurements, having large uncertainties.

Figure 5.6 shows the frictional pressure gradient data grouped by mass flux so that the trends with saturation temperature can be observed. For the high saturation temperature case, the frictional pressure drop values are lower due to a reduction in the interfacial shear stress between vapor and liquid. The liquid-vapor density ratio and viscosity ratio decrease for increasing saturation pressure from 12.67 to 5.16 and from 8.30 to 4.79, respectively. The increased density of the vapor phase at a given mass flux results in reduced vapor velocity, which in turn contributes to a decrease in the interfacial shear between the vapor and liquid phases. The increase in vapor viscosity reduces the vapor-phase Reynolds number, which similarly reduces the interfacial shear between the two phases. Table 5.3 summarizes some of the key properties and property ratios for propane.

Although the trend of the frictional pressure drop with respect to quality is difficult to determine for the higher saturation temperature, the pressure drop clearly increases with increasing mass flux. Figure 5.7 shows the monotonically increasing trend in the frictional pressure drop with mass flux.
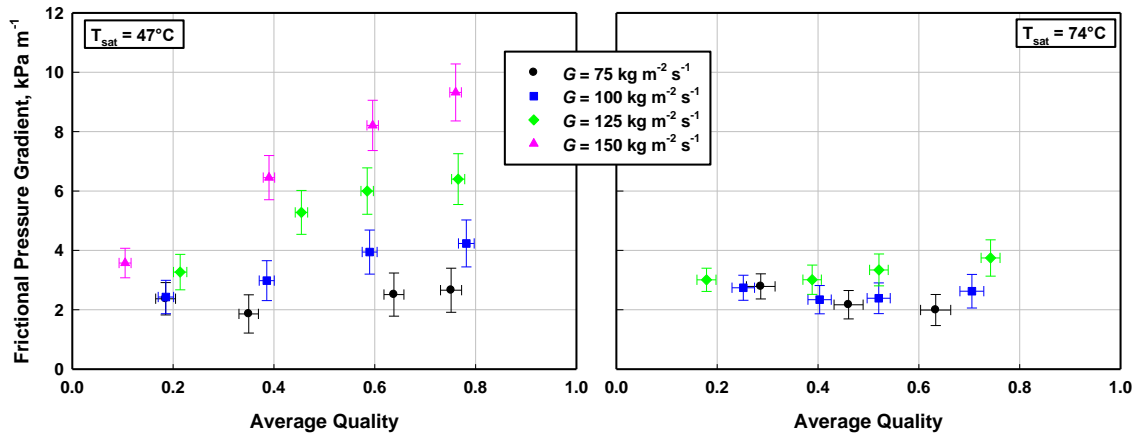
Figure 5.5: Measured frictional pressure drop results: trends with mass flux
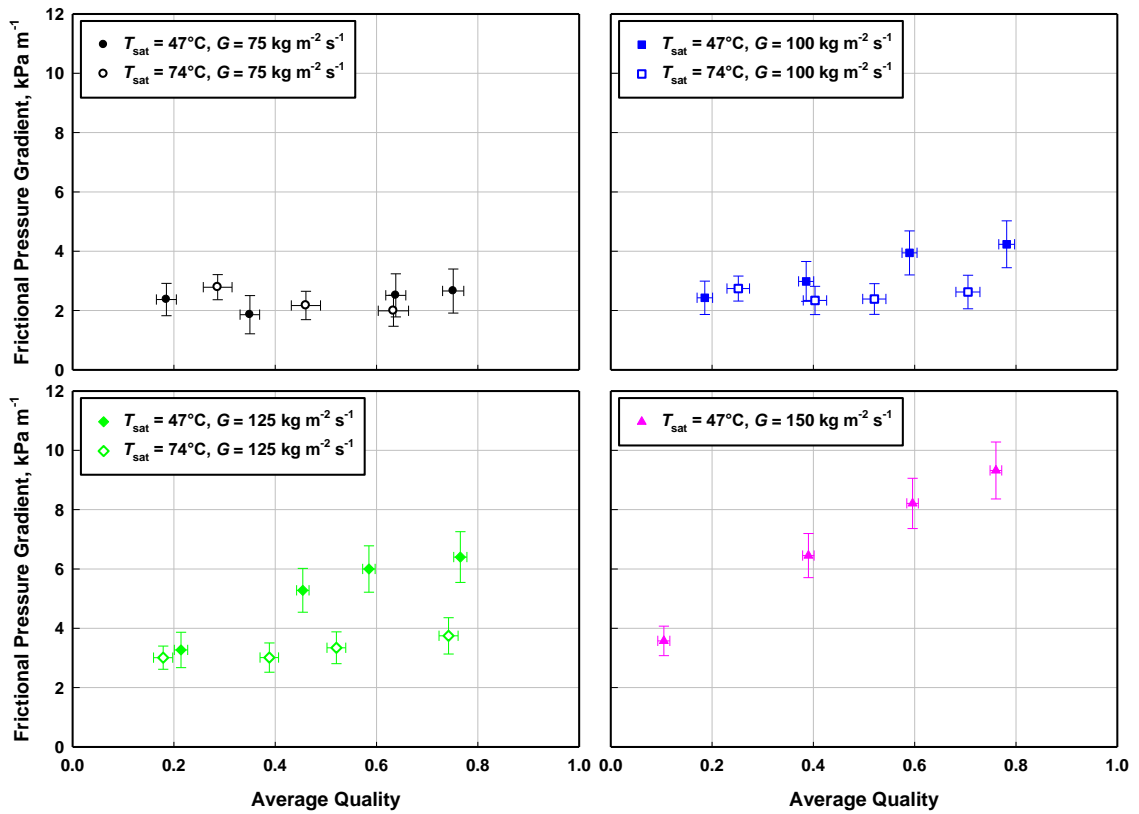
Figure 5.6: Frictional pressure gradient results: trends with saturation temperature

Table 5.3: Propane Property Comparison (Lemmon *et al.*, 2010)

	T (°C)	i_{fg} (kJ kg^{-1})	σ (N m^{-1} × 10^3)	Pr$_l$	ρ (kg m^{-3})			μ (kg m^{-1} s^{-1} × 10^6)			k (W m^{-1} K^{-1} × 10^3)			$c_{p,l}$ (kJ kg^{-1} K^{-1})		
					liquid	vapor	$\dfrac{\text{liquid}}{\text{vapor}}$	liquid	vapor	$\dfrac{\text{liquid}}{\text{vapor}}$	liquid	vapor	$\dfrac{\text{liquid}}{\text{vapor}}$	liquid	vapor	$\dfrac{\text{liquid}}{\text{vapor}}$
Propane	47.0	291.8	4.42	2.77	454.7	35.87	12.67	76.65	9.24	8.30	83.88	22.81	3.68	3.03	2.42	1.25
	74.0	214.4	1.65	2.96	392.4	71.15	5.16	54.00	11.29	4.79	72.64	31.21	2.33	3.98	3.80	1.05
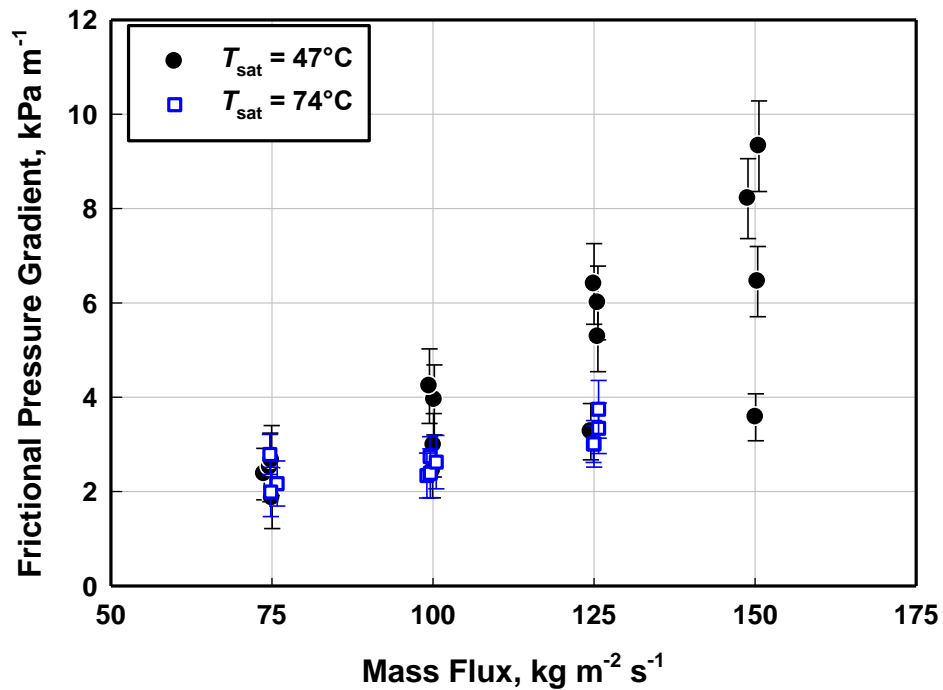
Figure 5.7: Frictional pressure drop results with respect to mass flux

As noted by Lips and Meyer (2012), accurately accounting for the void fraction is critical to obtaining accurate frictional pressure drop data in vertical two-phase flow. Because flow visualization and direct measurement of the void fraction are beyond the scope of this study, multiple void fraction models were considered including Baroczy (1965), Zivi (1964), Chisholm (1973), Mishima and Hibiki (1996), and Winkler *et al.* (2012). Although the Mishima and Hibiki void fraction model was developed for vertical flow in small diameter tubes, the Winkler *et al.* model was ultimately used to analyze the data because it was developed for refrigerant flows that are more similar to hydrocarbons than air-water or steam, and also because the diameter under consideration here is similar to those of Winkler *et al.* (2012).

5.1.2. <u>Heat Transfer Coefficient</u>

The heat transfer coefficient is determined from the test section heat duty, which is directly related to the quality change in the test section as well as the LMTD. The test section heat duty for all measurements is presented in Figure 5.8, while the LMTD is shown in Figure 5.9. It should be noted that the operating conditions were adjusted to maintain an acceptably low quality change while also reducing uncertainty in the measurement of heat duty. The test section heat duties range from 9.8 W to 38.1 W, while the uncertainties range from 7.7% to 25.4% (12.2% average). There is a trade-off between obtaining low uncertainties and finer resolution of the local heat transfer coefficient. At lower heat duties, the uncertainty in the measured heat transfer coefficient is greater; however, at higher heat duties, the quality change is larger, leading to coarser resolution in the local heat transfer coefficient.

Heat transfer coefficients for all test conditions are presented in Figure 5.10. The heat transfer coefficient increases with mass flux and quality. At higher qualities, the liquid film thickness is smaller and experiences a larger degree of vapor shear due to the high velocities, which results in a lower thermal resistance due to the liquid film, which in turn results in larger heat transfer coefficients. For the flow conditions in the present study, no liquid entrainment in the vapor core is expected based on the mist flow regime transition criterion $(20 < We < 30)$ presented by Soliman (1986). This could perhaps be inferred from the uniform increase in heat transfer coefficient at high quality ranges, rather than a sharp increase resulting from extra thinning of the liquid film by entrainment in the vapor core.
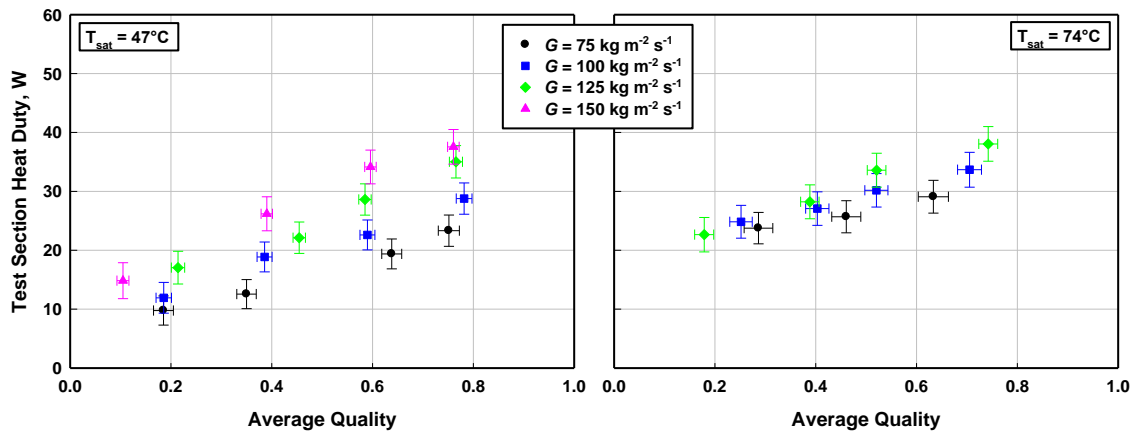
Figure 5.8: Measured test section heat duty
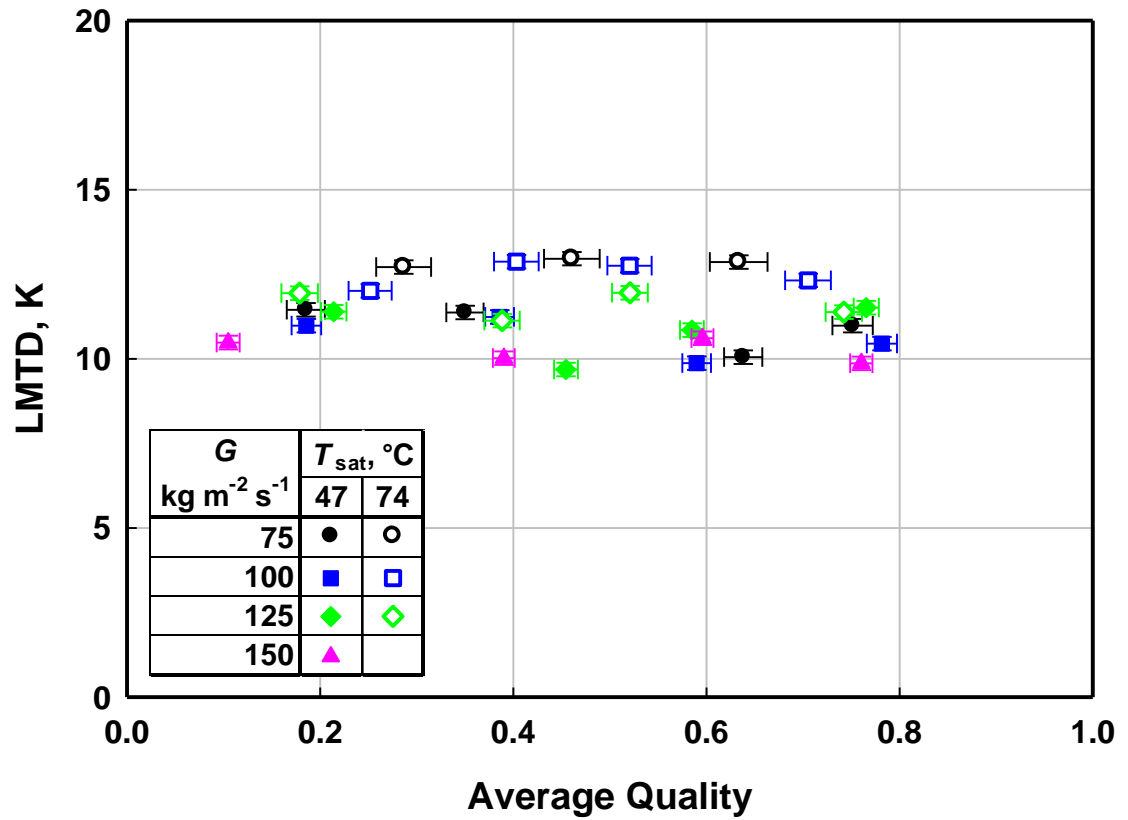
Figure 5.9: Test section log mean temperature difference

143

Figure 5.11 shows the heat transfer coefficient data grouped by mass flux so that the trends with saturation temperature can be observed. In the high quality cases, it was observed that the heat transfer coefficient has little dependence on saturation temperature. However, a more pronounced increase with saturation temperature is seen in the heat transfer coefficient at low qualtiy and mass flux. Although the measured heat transfer coefficient is unexpectedly higher for the higher saturation temperature, the values at 47°C and 74°C are mostly within the range of experimental uncertainty. The difference in heat transfer coefficient between 47°C and 74°C for similar quality ranges from 66 to 1489 W m^{-2} K^{-1} (average 658 W m^{-2} K^{-1}), while the error bands for data at these two saturation conditions span between 648 and 1222 W m^{-2} K^{-1} (average 872 W m^{-2} K^{-1}); therefore, all but three data points at low quality and low mass flux fall within the range of experimental uncertainty of each other. Therefore, definitive conclusions cannot be drawn from these trends. At higher saturation temperatures, the annular film thickness is larger which tends to decrease the heat transfer coefficient at high quality points (likely in the annular regime). However, several factors such as flow regime, void fraction, and trade-offs in fluid property changes could mitigate the expected decrease in heat transfer coefficient at these saturation conditions. At low quality, the flow is likely in the intermittent regime, and while the film thickness around the bubble is comparable to annular flow, the higher conductivity of the liquid slug could counteract the decrease in heat transfer coefficient due to larger film thickness at higher saturation temperatures. For saturation temperature increasing from 47°C to 74°C, the latent heat of vaporization decreases from 291.8 kJ kg^{-1} to 214.4 kJ kg^{-1}, leading to a decrease in heat transfer coefficient. However, the liquid and vapor specific heats increase from 3.03 to
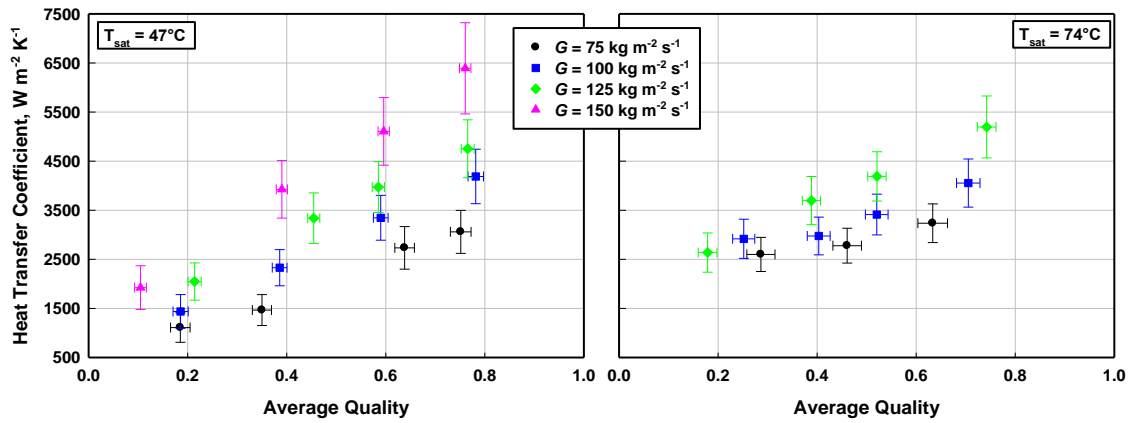
Figure 5.10: Measured heat transfer coefficient: trends with mass flux
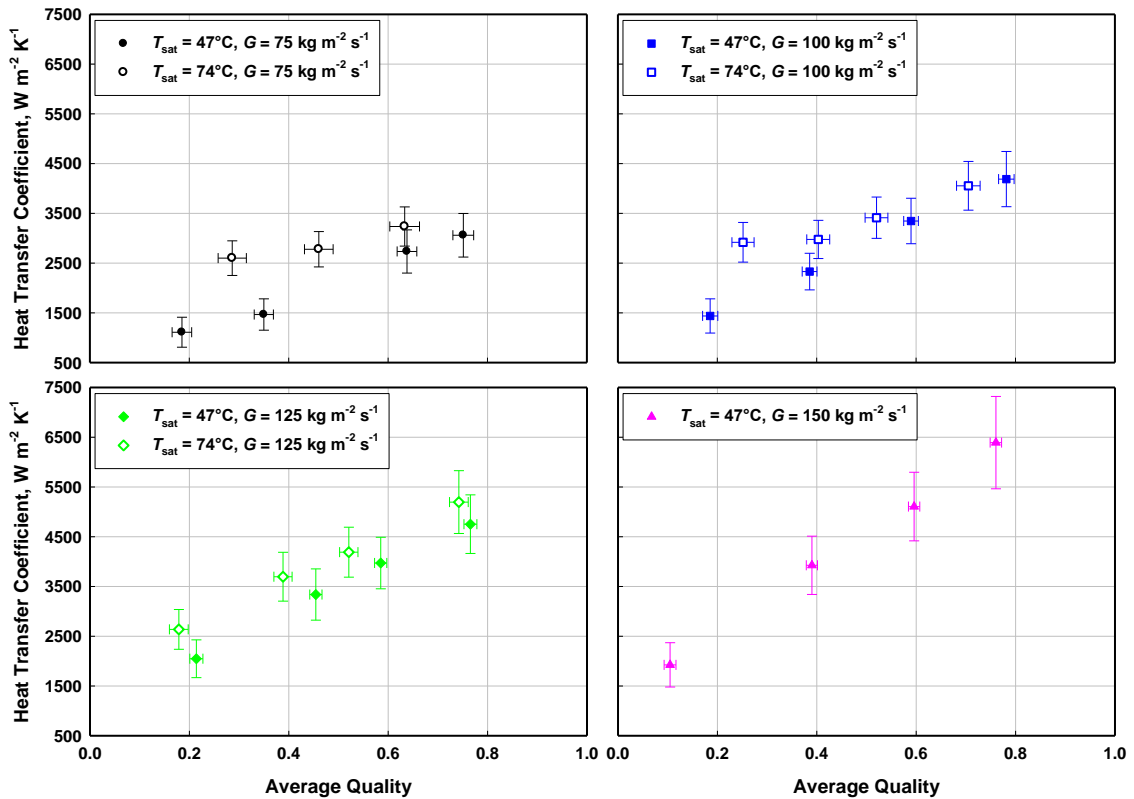
Figure 5.11: Measured heat transfer coefficient: trends with saturation temperature

145

3.98 kJ kg^{-1} K^{-1} and from 2.42 to 3.80 kJ kg^{-1} K^{-1}, respectively, counteracting the effects of the change in latent heat. It should be noted that at the 74°C saturation condition, the liquid-vapor specific heat ratio is close to unity (1.05 compared to 1.25 at 47°C). The vapor-liquid density ratio and viscosity ratio also increase for increasing saturation pressure, as noted above (see Table 5.3), contributing to a decrease in the interfacial shear and thus a decrease in heat transfer coefficient. Competing effects of these property changes may contribute to the observed increase in heat transfer coefficient at higher saturation temperature.

There is a greater quality change in the test section in the high saturation temperature cases as discussed above. For the 74°C data, the quality change ranges from 0.29 to 0.63 compared to a range of 0.12 to 0.37 at the 47°C saturation conditions. Shah (1979) notes that for quality change greater than about 0.20 to 0.40, the arithmetic mean is not the most accurate representation of the average quality. Therefore, the larger quality change in the high saturation temperature data could skew the data towards higher heat transfer coefficients. Over a large change in quality, the void fraction varies appreciably especially at low quality. Thus at the inlet of the test section, the liquid film could be thinner than at the outlet, leading to most of the heat transfer taking place towards the beginning of the test section.

The minumum, maximum, and average quality decrement, resistance ratio, LMTD, and uncertainty in the heat transfer coefficient are shown along with their respective standard deviations in Table 5.4. Overall, the average quality change in the test section is 0.33. At the 74°C saturation condition, the heat losses to the ambient, test section heat duty and the LMTD became more dominant factors influencing the

146

Table 5.4: Quality Change, Resistance Ratio, LMTD and Uncertainty in heat transfer coefficient

Saturation Temperature	47°C			74°C			Average		
	Min	Max	Avg ± STD	Min	Max	Avg ± STD	Min	Max	Avg ± STD
Quality Change	0.12	0.37	0.24 ± 0.08	0.29	0.63	0.47 ± 0.09	0.12	0.63	0.33 ± 0.10
Resistance Ratio	2.67	15.28	6.71 ± 3.59	3.66	7.22	5.75 ± 1.20	2.67	15.28	6.32 ± 2.90
LMTD, [K]	9.7	11.5	10.7 ± 0.63	11.1	13.0	12.3 ± 0.63	9.7	13.0	11.3 ± 1.00
$\dfrac{U_{h_{ref}}}{h_{ref}}$, [%]	12.4	27.1	16.9 ± 4.5	12.0	15.2	12.9 ± 1.0	12.0	27.1	15.3 ± 4.0

uncertainty in the test results. To ensure accurate measurements and low uncertainty, a higher LMTD was maintained and tightly controlled. The necessity of a higher test section heat duty led to a greater quality change. At the low saturation temperature conditions, the resistance ratio was the primary indicator of the reliability of the data. As discussed in Chapter 4, the resistance ratio is defined as the ratio of the refrigerant thermal resistance to the sum of the wall and coupling fluid thermal resistances in the test section:

$$R_{\text{ratio}} = \frac{R_{\text{ref}}}{R_{\text{wall}} + R_{\text{coupling}}} \tag{5.2}$$

The average resistance ratio for the low saturation temperature cases is 6.71, while for the high saturation temperature, it is 5.75. The resistance ratio for all test conditions is shown in Figure 5.12. The resistance ratios decrease with increasing quality mainly due to the larger heat transfer coefficient values and therefore, lower thermal resistance on the propane side. A larger resistance ratio is desirable as it indicates that the coupling fluid resistance is a smaller fraction of the overall measured heat transfer term, U. Thus the uncertainties related to the coupling fluid contribute less to the overall

147
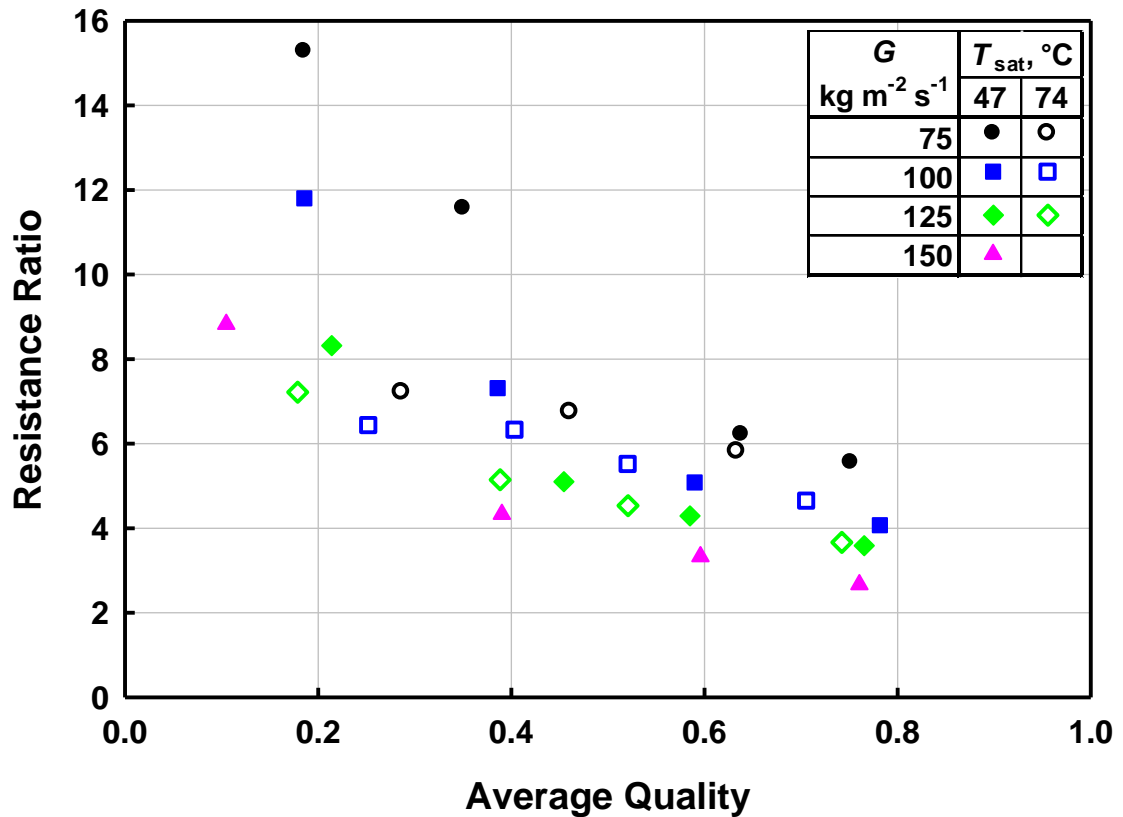
Figure 5.12: Test section resistance ratio

uncertainty of the propane heat transfer coefficient. Figure 5.13 shows the uncertainty in the heat transfer coefficient as well as the relative contribution of the coupling fluid resistance to the overall heat transfer coefficient uncertainty as a function of the resistance ratio. For all the data, the refrigerant heat duty measurements, rather than the coupling fluid, contribute the major fraction of the overall uncertainty.

The experimental uncertainty in the heat transfer coefficient data ranges from 12.0% to 27.1% with an average of 15.3%. The average uncertainty at the low saturation temperature is 16.9%, while it is 12.9% at the high saturation temperature. Overall, 96% of the data have an uncertainty less than ±25%, while 67% of the data have an
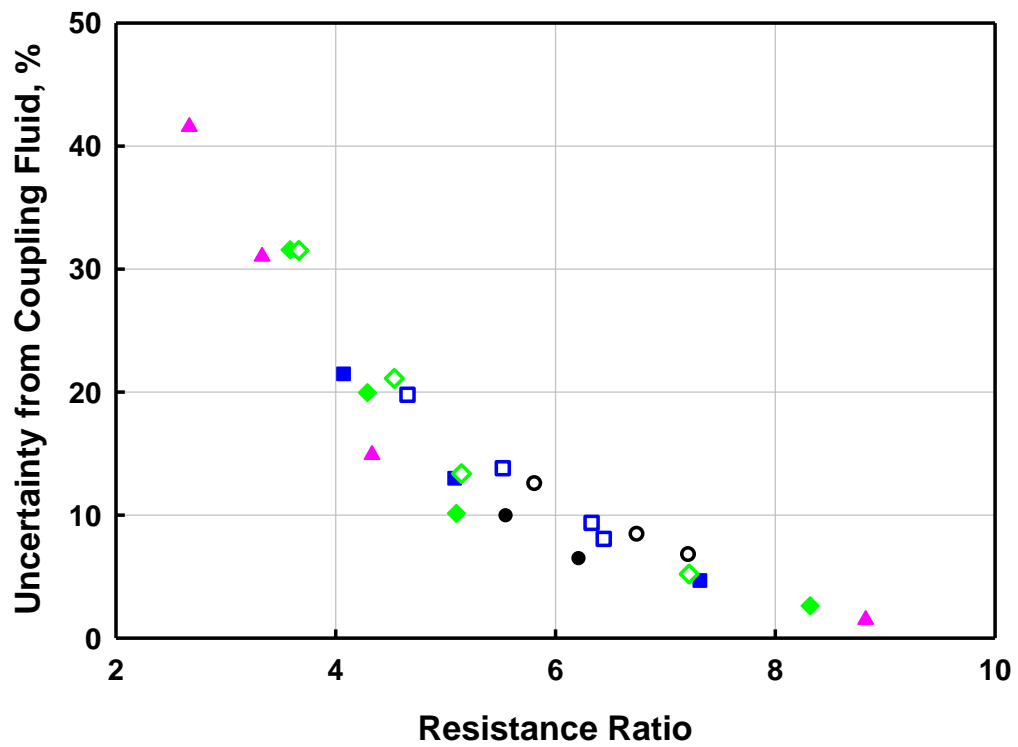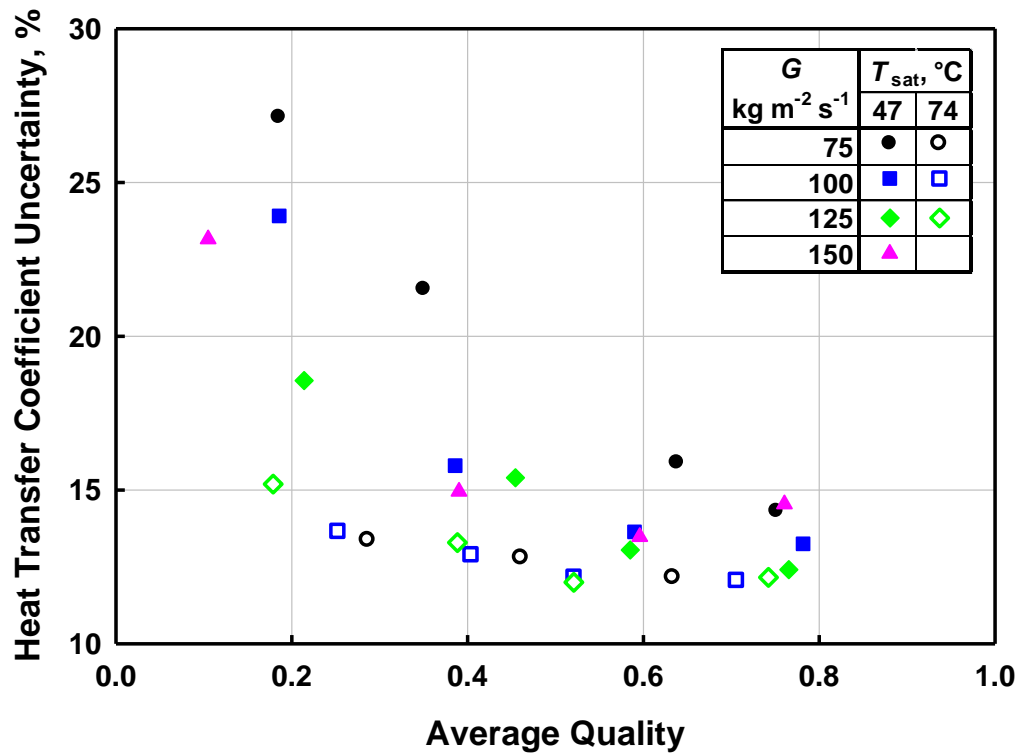
Figure 5.13: Effect of the resistance ratio on the heat transfer coefficient uncertainty

uncertainty less than ±15%. The larger uncertainty at low qualities is due to the low test section heat duty corresponding to the lower quality change associated with these points.

5.2.   Comparison with the Literature

The pressure drop and heat transfer data from the present study are compared with predictions of correlations in the literature here. The ability of each model to predict the data from the present study is evaluated and observations of the merits and deficiencies of each model are discussed. The average deviation (AD) and absolute average deviation (AAD) are used to evaluate agreement between measured and predicted values. These quantities are defined in Eq. (5.3).

$$AD = \frac{1}{n}\sum \frac{x_{\text{literature}} - x_{\text{measured}}}{x_{\text{measured}}} \times 100\%$$

$$AAD = \frac{1}{n}\sum \left| \frac{x_{\text{literature}} - x_{\text{measured}}}{x_{\text{measured}}} \right| \times 100\%$$

(5.3)

The average deviation provides a measure of whether the correlation under-predicts or over-predicts the data. The average absolute deviation is more suitable for assessing the overall agreement of the model with the data and the scatter of the data from the predictions of the correlation under consideration.

5.2.1. <u>Flow Regime Maps</u>

Flow regimes were not observed in the present study. However, an understanding of the most applicable flow regimes for the conditions of the present study can serve as a basis for model dvelopment.

Figure 5.14 shows the data from the present study plotted on the flow regime map of Mishima and Ishii (1984). The transition criteria for this map were developed by relating void fraction conditions corresponding to different flow pattern geometries to the vapor and liquid superficial velocity. The map identifies four distinct flow patterns: bubbly, slug, churn and annular flow. Theis flow map was based on data for air-water and steam-water flows in tube diameters ranging from 10 mm to 25 mm. Mishima and Hibiki (1996) found that this map fit their data well for vertical upward flow of air-water and steam-water mixtures in 1 to 4 mm tube diameters.

It can be seen from this plot that the data from the present study are in the slug
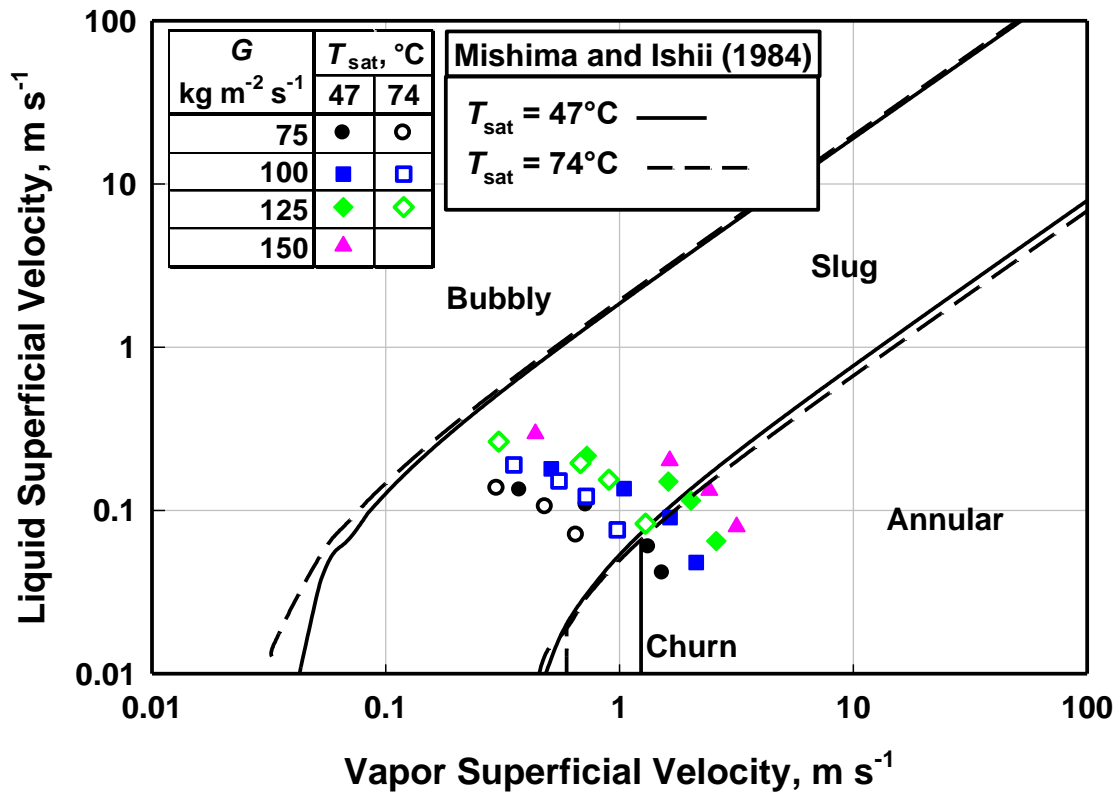
Figure 5.14: Data from the present study plotted on the flow regime map of Mishima and Ishii (1984)

flow and annular flow regimes. At the 47°C saturation temperature condition, half of the data are in the slug regime, while the other half are annular. At the 74°C saturation temperature condition, all of the data are in the slug flow regime. It should be noted that for the higher saturation temperature, the churn flow regime is almost entirely absent from the map.

The flow regime map of Coleman and Garimella (1999); Coleman (2000); Coleman and Garimella (2000c, a, 2003) was developed using experimental observations for hydraulic diameters ranging from 1 to 5 mm for horizontal air-water flows and condensing R134a. The map identifies four major flow regimes with various subcategories for each: intermittent (plug/slug flow), wavy (disperse and discrete), annular, and mist flow. Figure 5.15 shows the data from the present study compared with the flow regime map. Because wavy flow is not relevent to vertical condensation, only the transition line between intermittent and annular/mist flow is considered here. According to this plot, the majority of the data are in the annular flow regime. There are six low quality points that are identified as slug flow. Although this is a horizontal flow map, it is likely to provide predictions applicable to the present study because the hydraulic diameter range studied is similar to the diameter under investigation here and the transition criteria were developed using refrigerant flows, which are more similar in properties to hydrocarbons than air-water flows.

Other maps are available in the literature; however, the maps considered above provide an approximate indication of the flow regimes likely to be applicable here.
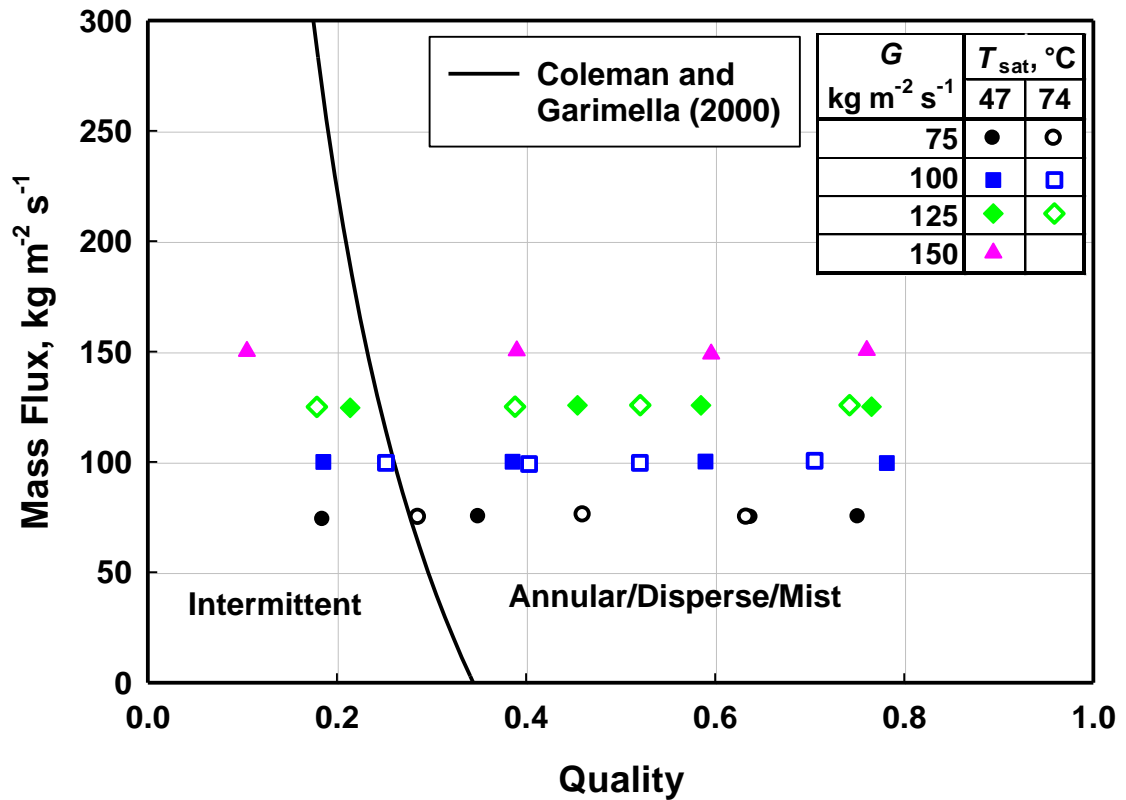
Figure 5.15: Coleman and Garimella (2000) flow regime map for transition from intermittent flow

5.2.2. Pressure Drop

In this section, the frictional pressure gradient data are compared with predictions from nine different correlations in the literature. A graphical summary of the agreement between the measured and predicted values is shown in Figure 5.16 and Figure 5.17.

One of the simpler two-phase frictional pressure drop idealizations is the homogeneous model (Hewitt *et al.*, 1994). This formulation treats the vapor and liquid flows as a single homogeneous fluid. The homogeneous density is defined as in Eq. (5.4),

while the two-phase mixture viscosity is defined according to McAdams *et al.* (1942) as in Eq. (5.5).

$$\rho_{tp} = \left(\frac{x}{\rho_v} + \frac{1-x}{\rho_l} \right)^{-1}$$

(5.4)
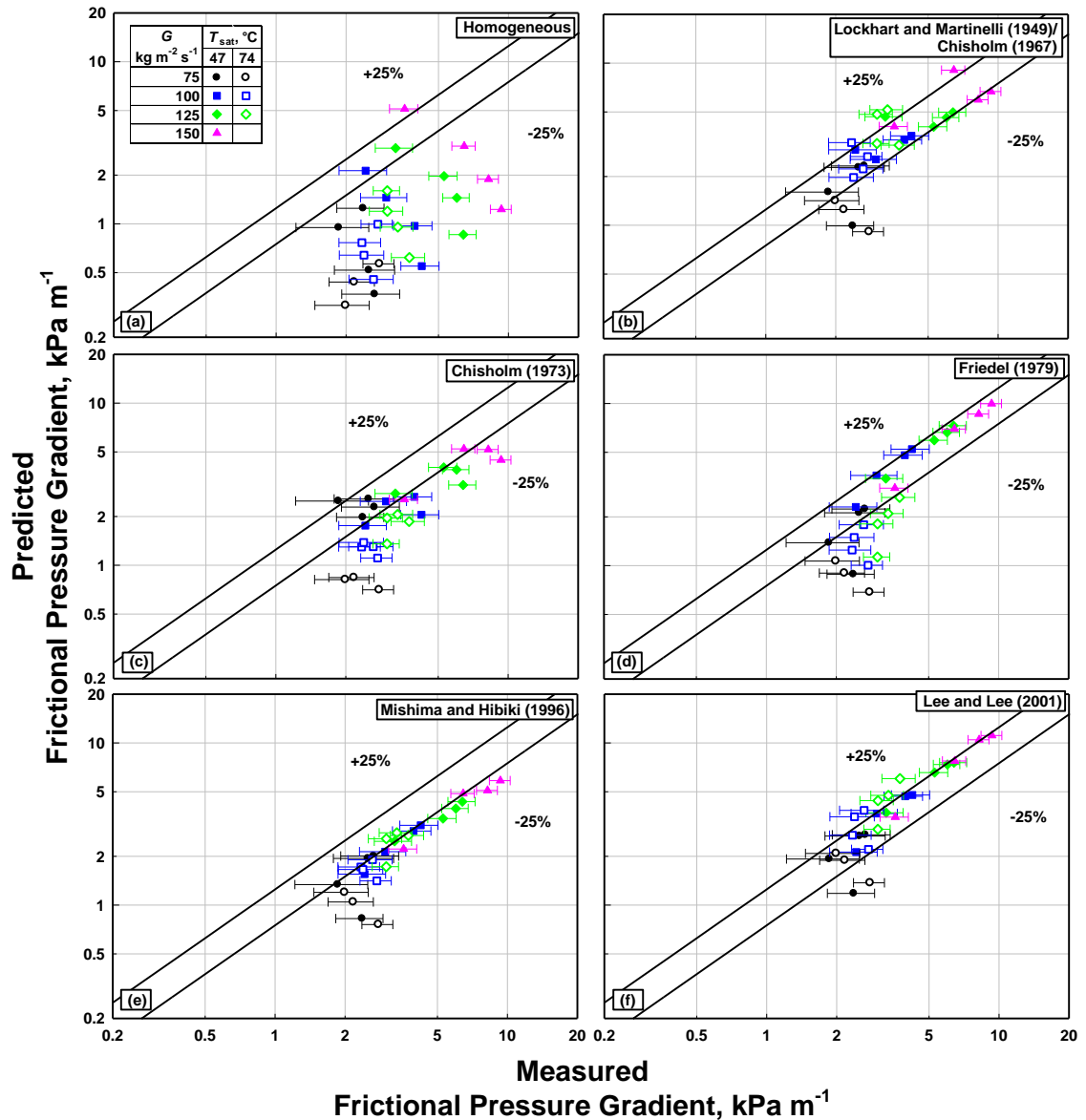
Figure 5.16: Comparison of frictional pressure gradient data with predictions from the literature

$$\mu_{\text{tp}} = \left(\frac{x}{\mu_{\text{v}}} + \frac{1-x}{\mu_{\text{l}}} \right)^{-1} \tag{5.5}$$

The two-phase Reynolds number is given by $\text{Re}_{\text{tp}} = GD / \mu_{\text{tp}}$. The homogeneous Darcy friction factor is calculated according to the Blasius expression: $f_{\text{tp}} = 0.316\text{Re}_{\text{tp}}^{-0.25}$. The frictional pressure gradient is determined by the usual method as shown in Eq. (5.6).

$$\left(\frac{dP}{dz} \right)_{\text{homogeneous}} = \frac{1}{2} f_{\text{tp}} \frac{G^2}{\rho_{\text{tp}} D} \tag{5.6}$$

Hewitt *et al.* (1994) note that the homogeneous model yields a poor representation of pressure drop except at high reduced pressures. The homogenous model strongly under-predicts the data from the present study (Figure 5.16a). The AD is –62.3%, while the AAD is 65.8%. The data are very scattered ($R^2 = 0.06$), and the trends are not captured well.

Lockhart and Martinelli (1949) and Chisholm (1967) present a correlation for determining the frictional pressure drop in adiabatic two-phase flow using a two-phase multiplier and applying this to a single-phase pressure drop model. The approach uses the Martinelli parameter:

$$X = \left(\frac{(dP / dz)_{\text{l}}}{(dP / dz)_{\text{v}}} \right)^{1/2} \tag{5.7}$$

Overall, this correlation slightly under-predicts the data (Figure 5.16b). The AD is -6.6%, while the AAD is 27.1%. Although this is a purely empirical correlation, it predicts the data well. Less agreement is observed for $x < 0.5$ (31.7% AAD) than for the higher quality range (22.0% AAD). This correlation captures the trends of the data fairly well, although $R^2 = 0.62$. As noted above, there was not a significant change in the

measured frictional pressure gradient with quality for the 74°C saturation condition, while the Lockhart-Martinelli correlation predicts that there should be changes in the pressure gradient.

Chisholm (1973) proposed a correlation for the liquid only two-phase multiplier for frictional pressure drop during evaporation. This model generally under-predicts the data (Figure 5.16c). The AD is -35.4%, while the AAD is 38.1%. The deviations may possibily due to the fact that the Baroczy (1966) correlation, from which Chisholm's correlation was developed, is said to underestimate the friction in some conditions.

The Friedel (1979) correlation is a commonly used model for two-phase frictional pressure drop. This model generally under-predicts the data; however, the larger pressure drop (and generally more reliable) data are mostly over-predicted (Figure 5.16d). The AD is -20.1% and the AAD is 29.6%. It captures the trends of the data very well ($R^2 = 0.92$), and there is good agreement compared to the other models considered in the present study. Although this is one of the few correlations that is specifically applicable to vertical downward flow, it was developed for tube diameters between 5 and 51 mm, which is larger than the tube considered in the present study, which may contribute to the observed deviations.

Mishima and Hibiki (1996) developed a modification to the Lockhart-Martinelli method (Lockhart and Martinelli, 1949) for calculating the frictional pressure drop in vertical upward flow of air-water and steam-water mixtures in capillary tubes (1 to 4 mm diameter). This model entirely under-predicts the data (Figure 5.16e). The AD is -34.2%, while the AAD is 34.2%. The predictions are very consistent and capture the trends of the data well ($R^2 = 0.92$). It was developed for similar tube diameters and orientation as the

present study; however, the deviation may be due to the fact that air-water and steam mixtures have very different thermophysical properties than those of condensing hydrocarbons. Differences in the flow regimes observed between vertical upflow and downflow may also contribute to the deviations. The expression for the Chisholm parameter also does not take into account flow regime transitions.

Lee and Lee (2001) also proposed a modified correlation for the Chisholm parameter C in the Lockhart and Martinelli (1949) model, accounting for the effects of surface tension, channel size and flow rate through the use of several dimensionless parameters. This model over-predicts the data, especially at higher mass fluxes (Figure 5.16f). The AD is 12.0%, while the AAD is 23.2%. The model captures the trends of the data well ($R^2 = 0.92$). The deviations from the data may partly be because this correlation was developed for similar hydraulic diameter but for horizontal rectagular channels with adiabatic air-water flow. The parameters that include surface tension effects are also only included in the laminar-laminar regime, while these effects may be relevant in other flow conditions for small tubes. The data from the present study are in the laminar-turbulent and turbulent-turbulent regimes; therefore the predictions of the data do not include the effects of the surface tension.

Chen *et al.* (2001) proposed modifications to the homogeneous and Friedel (1979) expressions for frictional pressure drop by means of a correction factor Ω. The modification to the Friedel (1979) model fully under-predicts the data (Figure 5.17a), unlike the original correlation which over-predicts the data for high mass flux and quality. The absolute agreement is significantly worse than the original correlation. The
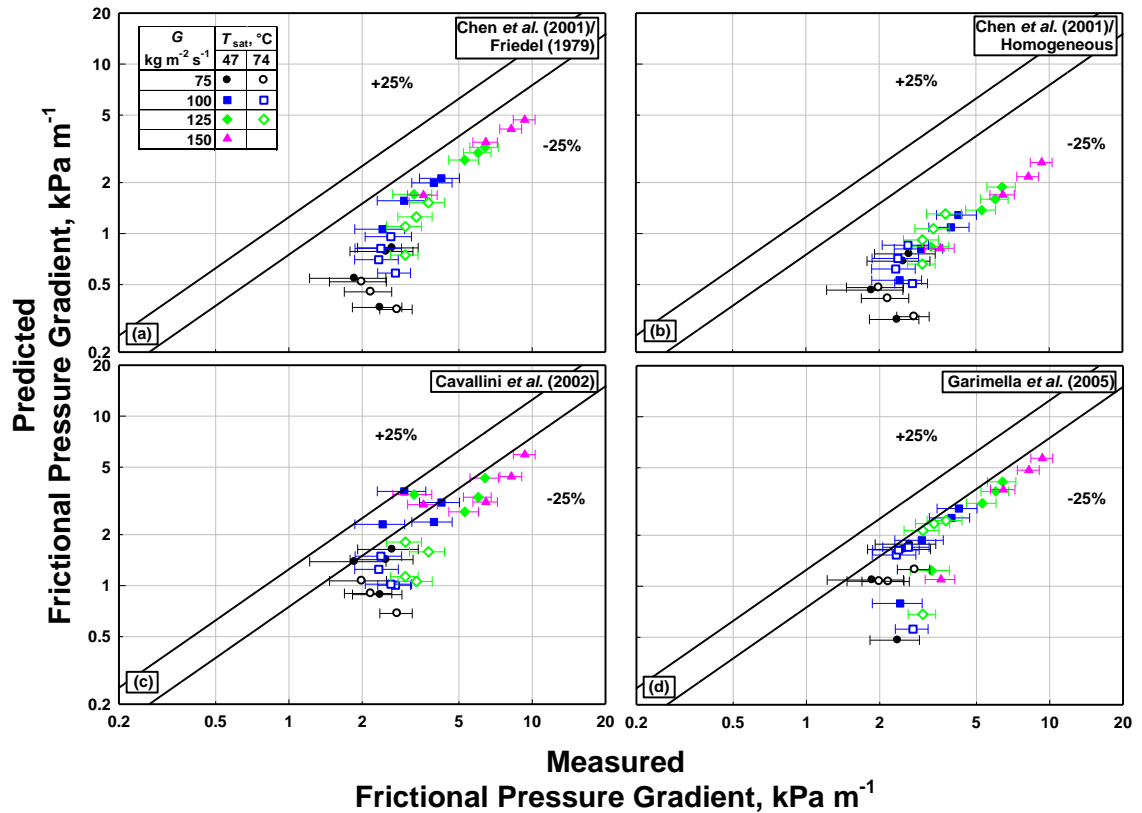
Figure 5.17: Comparison of frictional pressure gradient data with predictions from the literature

AD is -61.8%, while the AAD is 61.8%. The predicted trends are not significantly altered by the modification factor ($R^2 = 0.95$).

The modification to the homogeneous model decreases the performance as well (Figure 5.17b). All the data are under-predicted by this model to a greater degree than the original. The AD is -74.3%, while the AAD is 74.3%. However, the trends of the data are captured more consistently ($R^2 = 0.93$), and there is less scatter when the modification factor is applied to the homogeneous model.

Cavallini *et al.* (2001, 2002) modified the Friedel (1979) two-phase multiplier for the frictional pressure drop in the annular regime. This model generally under-predicts

the data (Figure 5.17c). The predictions are more scattered because the criterion for applying the modified correlation ($j_v^* > 2.5$) is satisfied for only 48% of the data. The rest of the data have the same predictions as the original Friedel correlation. For the entire data set, the AD is -41.1%, while the AAD is 43.0%. For the reduced data set to which the modified correlation is applied, the data is entirely under-predicted (AD is -45.8%, while the AAD is 45.8%). Thus, the modification of Cavallini et al. (2002) does not improve the prediction of the data. This could be in part due to the fact that this correlation was developed for horizontal, rather than vertical, tubes and synthetic refrigerants rather than hydrocarbons.

Garimella et al. (2005) developed an experimentally validated multiple flow regime pressure drop model based on studies of condensing R134a in tubes of diameter ranging from 0.5 to 4.9 mm. This model entirely under-predicts the data (Figure 5.17d), especially at low qualities (54.9% AAD, $x < 0.5$), with an AD of -45.8% and AAD of 45.8%. There is not much scatter in the data, though, and it captures the trends well ($R^2 = 0.88$). Possible factors that contribute to the deviation include formulation for a horizontal orientation and synthetic refrigerant R134a rather than for hydrocarbons. These differences could affect parameters such as slug frequency and velocity as well as interfacial friction factors based on different fluid properties.

A summary of the predictive capability of each of the above models and correlations is presented in Table 5.5 and Figure 5.18. Only the Lee and Lee (2001) model over-predicts the data; all other models under-predict the measured results. While no model adequately predicts these pressure drop results, the Lee and Lee (2001) model shows the best agreement with the data (23.2% AAD). The Lockhart and Martinelli

(1949) model (27.1% AAD) and the Friedel (1979) correlation (29.6%) also show

reasonable levels of agreement.

Table 5.5: Comparison of Pressure Drop Data with the Literature

	Average Deviation (%)	Average Absolute Deviation (%)
Homogeneous	-62.6	65.8
Lockhart and Martinelli (1949) / Chisholm (1967)	-6.6	27.1
Chisholm (1973)	-35.4	38.1
Friedel (1979)	-20.1	29.6
Mishima and Hibiki (1996)	-34.2	34.2
Chen *et al.* (2001): Friedel	-61.8	61.8
Chen *et al.* (2001): homogeneous	-74.3	74.3
Lee and Lee (2001)	12.0	23.2
Cavallini *et al.* (2002)	-41.1	43.0
Garimella *et al.* (2005)	-45.8	45.8
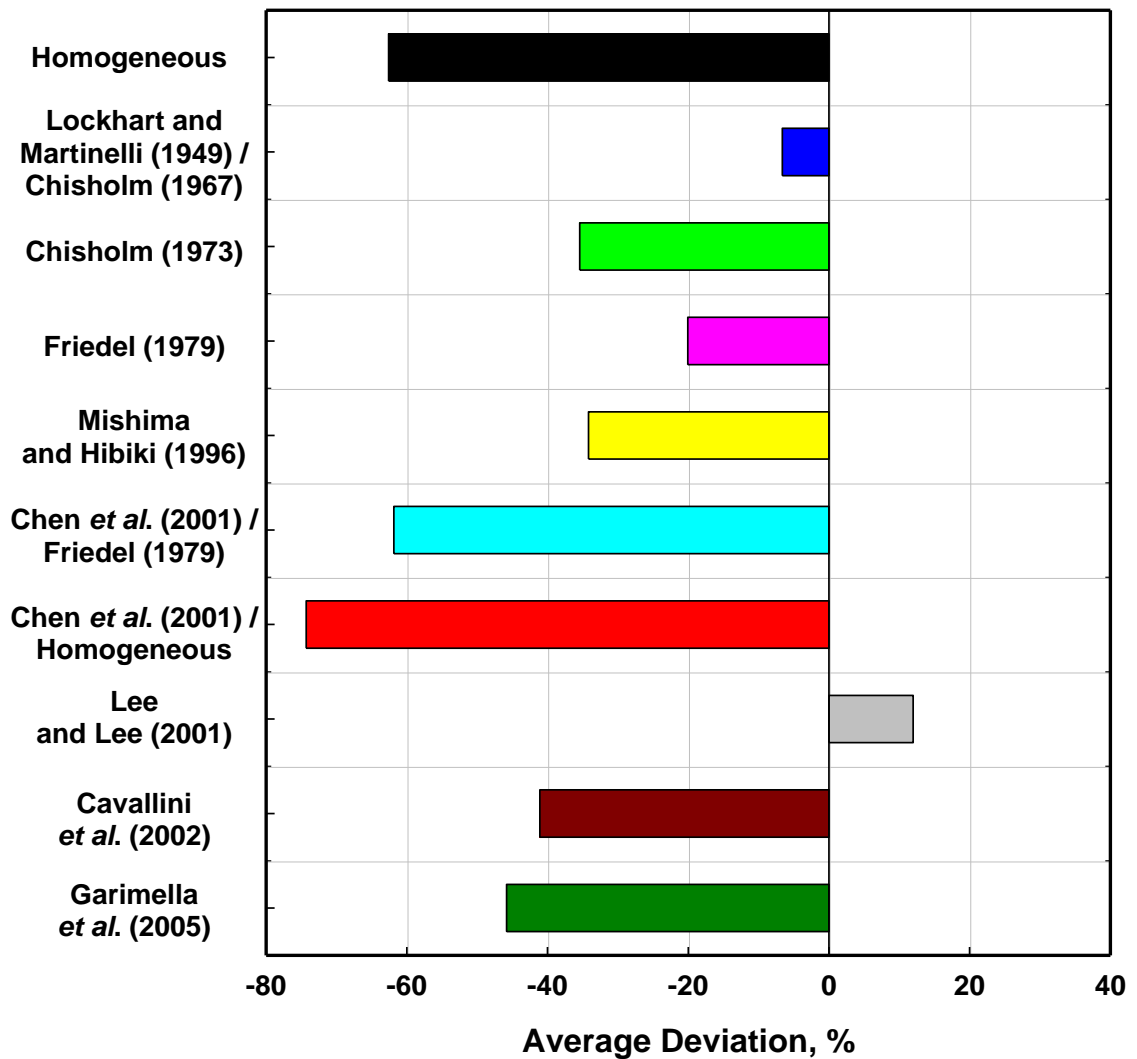
Figure 5.18: Comparison of Pressure Drop Data with the Literature – Average Deviation

5.2.3. <u>Heat Transfer Coefficient</u>

In this section, predictions of several different models for the two-phase heat transfer coefficient were compared with the experimental data. Figure 5.19 and Figure 5.20 show the predicted heat transfer coefficient values plotted against the measured
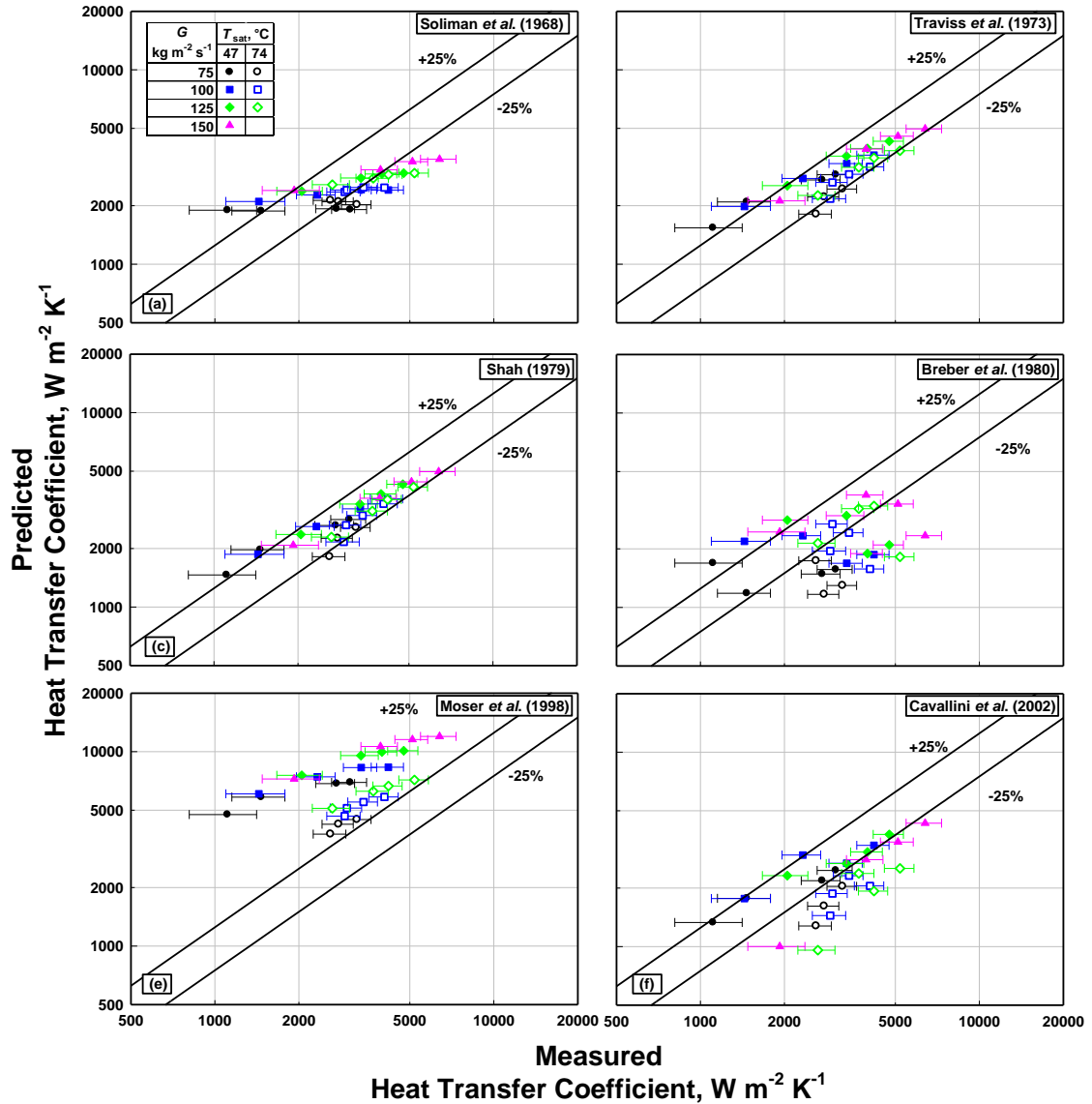
Figure 5.19: Comparison of heat transfer coefficient data with predictions from the literature

values for all of the models considered.

The Soliman *et al.* (1968) correlation predicts the condensation heat transfer coefficient in annular flow based on the wall shear stress. This model under-predicts most of the data (Figure 5.19a). The AD is -15.7%, while the AAD is 29.5%. Although there is little scatter in the predictions, the model does not predict the trends of the data well (R^2 = 0.69). There is less agreement at higher heat transfer coefficient values, which corresponds to greater quality (24.0% AAD for $x < 0.5$, 35.4% AAD for $x > 0.5$). This trend may indicate the the frictional term of the shear stress is underpredicted as this term should dominate at high quality. The correlation was developed for larger diameter channels (7.44 to 11.66 mm) than in the present study, which could lead to an underprediction of the frictional shear component due to smaller pressure gradient values.

The Traviss *et al.* (1973) model is a semi-analytical correlation for the heat transfer coefficient developed for condensation of refrigerants in annular flow. This model slightly under-predicts the data, with an AD of -3.9% and an AAD of 17.2% (Figure 5.19b). The trends in the data are captured well by this model (R^2 = 0.84), because the flow in the present study is expected to be in the annular and intermittent flow regimes that are similar to the conditions for which this correlation was developed. The deviations with the measured data could potentially be because the tube diameter and mass flux are smaller in the present study than those for which the model was developed. Fluid property differences between synthetic refrigerants R12 and R22 and hydrocarbons could also contribute to the deviations.

Shah (1979) developed an empirical correlation for the heat transfer coefficient applicable to a wide range of fluids and flow conditions. Although this is an empirical

correlation, it predicts the data well compared to many of the other models considered (Figure 5.19c). This relative success could be due to the large data bank used in developing the correlation that includes both vertical and horizontal condensation. The model under-predicts the data with an AD of -5.7% and AAD of 15.6%. The deviations from the predicted values could partially be due to the smaller diameter tube considered in the present study. There is low scatter in the predictions and the trends are captured well ($R^2 = 0.84$). The agreement is similar for all operating conditions.

Breber *et al.* (1980) present a method for determining the heat transfer coefficient of condensation in a horizontal tube for shear and gravity dominated flow. For this model, all the data except the low quality points for each mass flux are assigned to the annular regime, and the remaining data points are assigned to the Wavy-Annular transition region. The model under-predicts most of the data with an AD of -24.8% and an AAD of 37.4%. As can be seen in Figure 5.19d, there is a lot of scatter in the predictions of this model and it does not follow the trends of the data well ($R^2 = 0.08$). This is partly due to the stratified and wavy flow regime effects incorporated into the model that are not present in vertical flow. The tube diameters considered in the model formulation (4.8 to 50.8 mm) are also larger than those in the present.

Moser *et al.* (1998) developed a heat transfer coefficient correlation based on the equivalent Reynolds number model. They report that their correlation mostly under-predicts their data. In the present study, it was observed that this correlation was one of the two models considered that over-predicted the measured data (Figure 5.19e). This may be attributed partly to the fact that the frictional pressure drop two-phase multiplier uses the horizontal and vertical upward expression rather than the vertical downward

164

multiplier given by Friedel (1979). The model shows very poor agreement with the data, having an AD and AAD of 137.1%. Because this model showed the worst performance of the studies considered, it was concluded that the equivalent Reynolds number method may not be applicable to the conditions of this study.

Cavallini *et al.* (2001, 2002) developed a multi-regime heat transfer model to predict the heat transfer coefficient in condensing halogenated refrigerants in horizontal tubes. Although the correlation predicts flow for several data from this study to be in the stratified regime due to its development being for horizontal flow that is not applicable to the present study, the correlation is applied in the usual manner here to compare its predictive capabilities.. The data from the present study are under-predicted by this model (Figure 5.19f). The AD is -25.4%, while the AAD is 33.0%. The predictions are more scattered than those of other correlations ($R^2 = 0.55$). Of the 27 data points considered, 13 were assigned to the annular regime, 12 points to the annular-stratified transition regime, and two points to the stratified-slug and slug regimes. The deviations in the predictions are partially due to the different flow regime classifications and their applicability to the actual flow conditions in the present study. The stratified regime is not appropriate to apply to vertical flow, and there is actually worse agreement (55.8% AAD) for the data assigned to this regime than that assigned to the annular regime (31.1% AAD). As noted above in the discussion of pressure drop, the modification to the Friedel (1979) correlation used to predict the pressure drop in the annular flow regime calcualtions under-predicts the pressure drop in the present study; thus, the heat transfer coefficient is under-predicted in the annular regime.

Bandhauer *et al.* (2006) developed an experimentally validated model for microchannel condensation heat transfer of R134a in circular channels with diameter ranging from 0.5 to 1.5 mm and mass flux ranging from 150 to 750 kg m^{-2} s^{-1}. This model under-predicts the data with an AD of -28.4% and an AAD of 29.2% (Figure 5.20a); however, the trends in the data are captured reasonably well ($R^2 = 0.79$). Although differences in the model development parameters, such as smaller diameter, higher mass flux, syntheic refrigerants instead of hydrocarbons, with the present study may contribute to the observed deviations, it seems likely that the pressure drop model used in the shear stress formulation is the more significant factor. It was demonstrated above that the
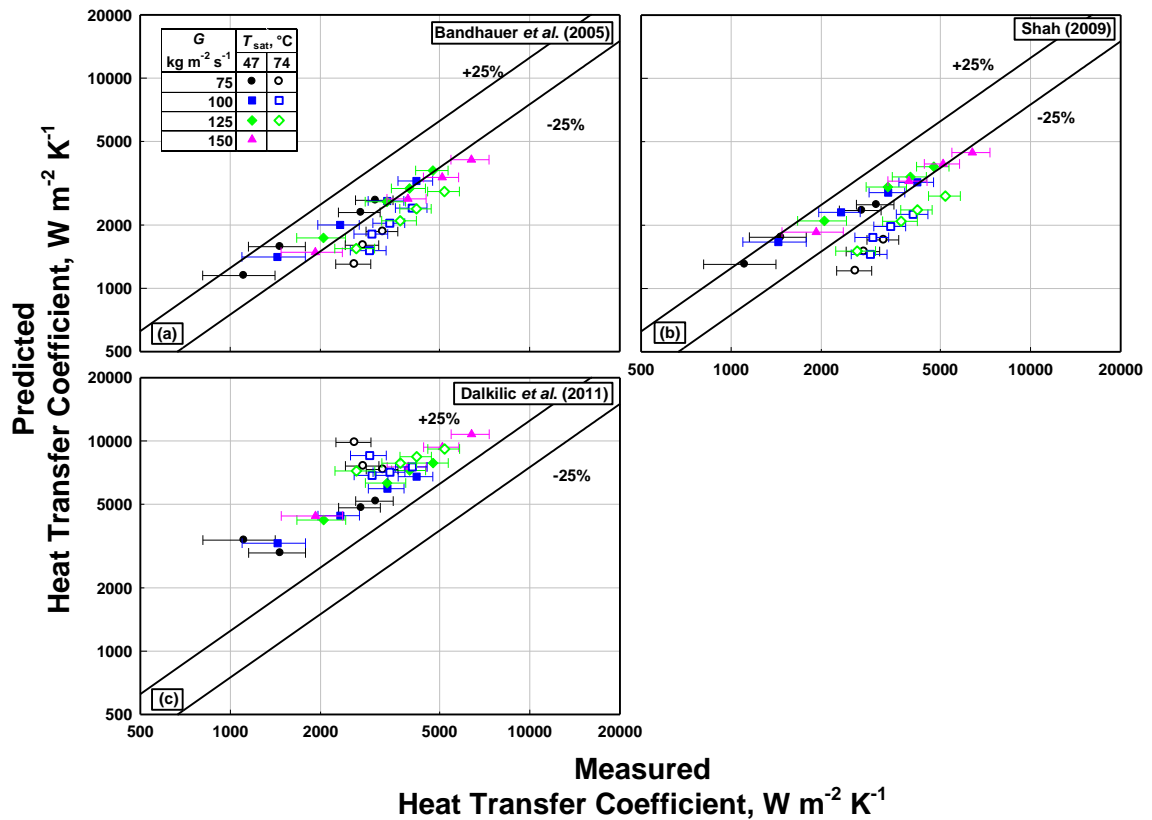
Figure 5.20: Comparison of heat transfer coefficient data with predictions from the literature

pressure drop model of Garimella *et al.* (2005) does not describe the data well, which may explain some of the differences with the heat transfer coefficient data.

Shah (2009) modified his previous correlation (1979) to account for a wider range of data including more fluids, mass fluxes and reduced pressures. While propane is included in the data set, it is only for horizontal condensation. This model showed worse agreement with the data than the original Shah (1979) correlation (Figure 5.20b). The data set falls entirely within Regime I for this correlation. The data were under-predicted with an AD of -23.6% and an AAD of 27.6%. There is also more of a distinct grouping of the data along the lines of reduced pressure. The low saturation temperature data are better predicted (15.3% AAD) than the high saturation temperature data (45.6% AAD). This demonstrates that the added correction factor for reduced pressure fails to improve the predictions. This is an entirely empirical correlation, and the data for hydrocarbons consisted of data on significantly larger tube diameters than that of interest in the present study.

Dalkilic *et al.* (2011) proposed a heat transfer coefficient model that uses the measured frictional pressure drop as an input. Although this correlation was developed for vertical downward condensation, it does not predict the data well (Figure 5.20c). Unlike most of the other correlations considered, it over-predicts the data with an AD and AAD both of 113.9%. The predictions for the lower saturation temperature and higher quality data are closest to the measured values. The AAD for the 47°C saturation temperature data is 94.8% compared to 141.6% for the 74°C data. The AAD for the data at high quality ($x > 0.5$) is 83.0% compared to 142.5% at low quality. It should be noted that this correlation is very sensitive to the pressure drop value used. Without adequate

pressure drop measurements or prediction capabilities, this model is not as useful in predicting the heat transfer coefficient.

Table 5.6 and Figure 5.21 summarize the average deviation and average absolute deviation between each heat transfer coefficient correlation's predictions and the data from the present study. Most of the correlations for heat transfer under-predict the data with the exception of Moser *et al.* (1998) and Dalkilic *et al.* (2011). The Shah (1979) correlation (15.6% AAD) and the Traviss *et al.* (1973) correlation (17.2% AAD) predict the data the best. However, none of the correlations adequately predicts the present data over the entire range of conditions considered here.

Table 5.6: Comparison of Heat Transfer Data with the Literature

	Average Deviation (%)	Average Absolute Deviation (%)
Soliman *et al.* (1968)	-15.7	29.5
Traviss *et al.* (1973)	-3.9	17.2
Shah (1979)	-5.7	15.6
Breber *et al.* (1980)	-24.8	37.4
Moser *et al.* (1998)	137.1	137.1
Cavallini *et al.* (2002)	-25.4	33.0
Bandhauer *et al.* (2006)	-28.4	29.2
Shah (2009)	-23.6	27.6
Dalkilic *et al.* (2011)	113.9	113.9
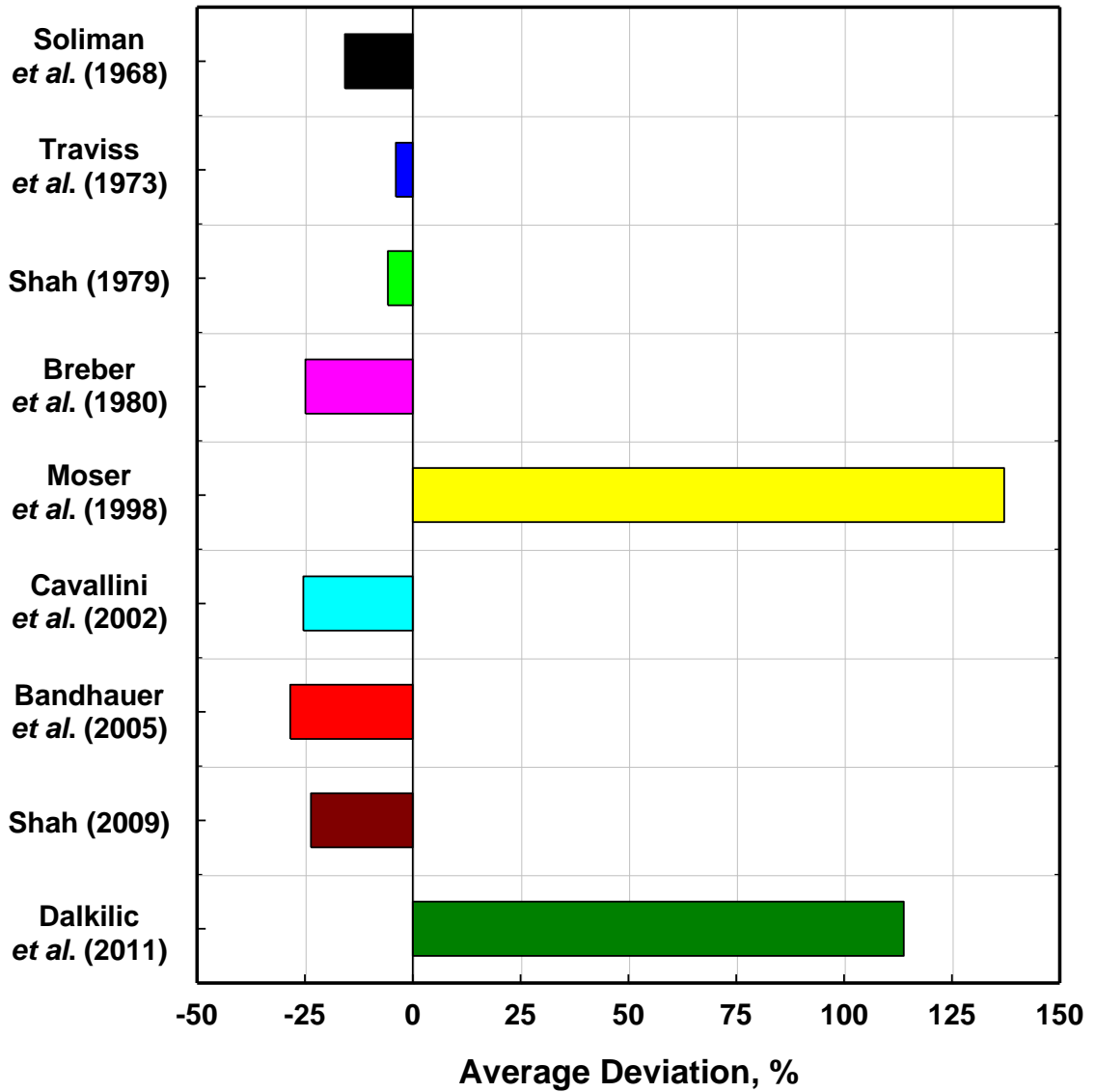
Figure 5.21: Comparison of Heat Transfer Data with the Literature – Average Deviation

5.3.   Model Development

Semi-empirical models were developed for the frictional pressure drop and the heat transfer coefficient during condensation of propane in 1.93 mm diameter channels based on the results of the present study and the analyses discussed above.

5.3.1. <u>Pressure Drop Model</u>

The correlations proposed by Garimella *et al.* (2005) were used as the basis for a new frictional pressure drop correlation applicable to the flow conditions of the present study. Although this correlation does not predict the pressure drop data as well as some of the other models considered, there are several advantages to its use as a starting point for the new correlation. It captures the trends in the current data well, suggesting that the physical basis of the correlation is applicable even though the scaling may need adjustment. It is also a multi-regime correlation with easily applicable flow regime classifications. Although several of the Lockhart-Martinelli based methods predicted the data well, the empirical nature of these correlations make them less desireable to use for the present model. The Mishima and Hibiki (1996) model incorporates hydraulic diameter as the primary parameter; however, the present study only considers one tube diameter, thus discerning the effect of diameter from these results is not possible. Lee and Lee (2001) add a surface tension parameter, but this is incorporated in the Garimella *et al.* (2005) model.

Figure 5.22 and Figure 5.23 show the predictions of the original Garimella *et al.* (2005) model and the data from the current study compared as in the previous section as
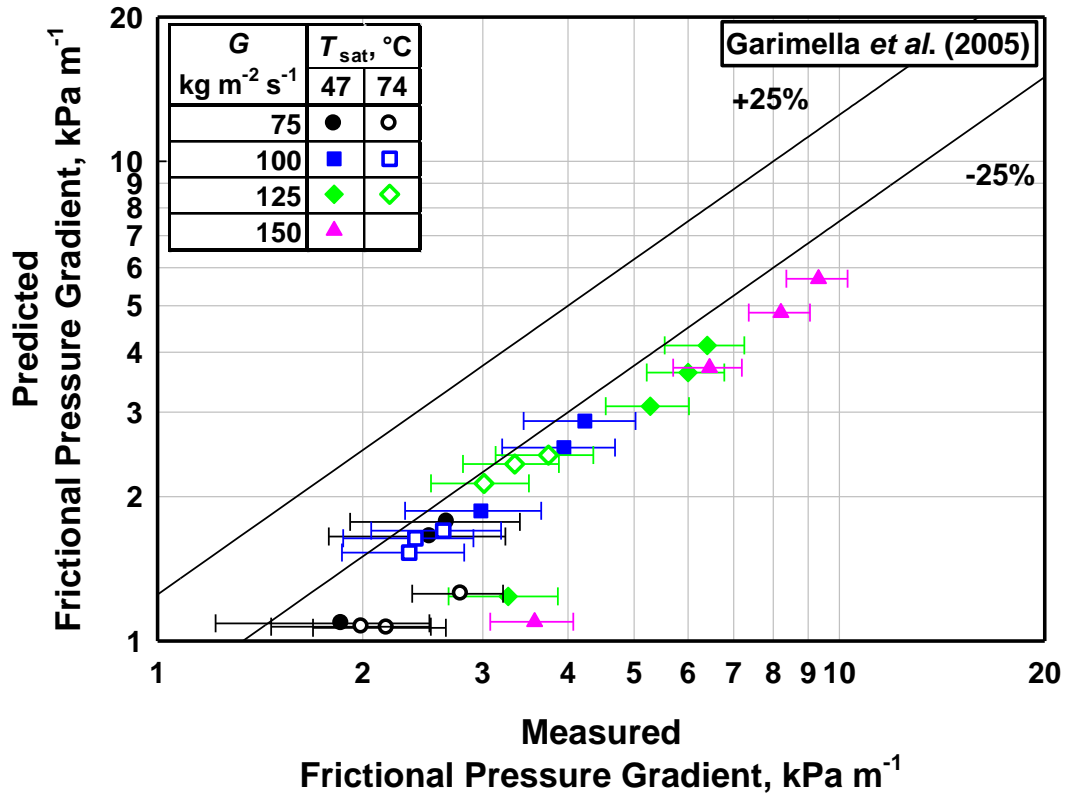
Figure 5.22: Comparison of the current pressure drop data with predictions from Garimella *et al*. (2005)
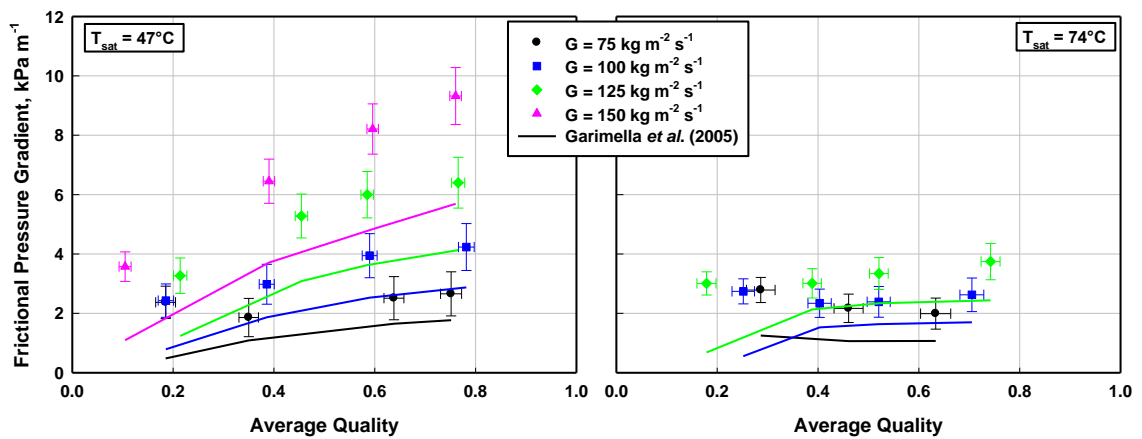
Figure 5.23: Predictions of Garimella *et al*. (2005) correlation overlaid on

well as overlaid as a function of quality and mass flux. At the 74°C saturation temperature, the apparent crossover of the 75 and 100 kg m^{-2} s^{-1} curves is due to the large test section quality change at the lowest quality point at a mass flux of 75 kg m^{-2} s^{-1} ($\Delta x = 0.51$). The void fraction curve is steeper in the quality range of this point; therefore, taking the arithmetic mean of the quality and void fraction is likely to yield an overprediction of both of these parameters at this point. Furthermore, this point is aproximately 1.3 standard deviations above the mean quality change of this data set (0.33 ± 0.14); it is therefore not representative of the majority of the data from this study (78% of the data consists of the quality change within $\pm$ 1 standard deviation from the mean).

As in the previous correlation, the data from this study were grouped into intermittent and annular/disperse/mist flow regimes based on the flow regime map of Coleman and Garimella (2000a, 2003). Figure 5.15 shows the Coleman and Garimella flow map applied to the data from the current study. According to this grouping, six of the 27 data points were in the intermittent regime, while the remaining 21 data points were in the annular regime. There was less agreement with the pressure drop data when the Mishima and Ishii (1984) flow map was used to group the data.

The model for pressure drop in annular flow was developed in terms of the interfacial friction factor and the void fraction.

$$\left(\frac{dP}{dz}\right)_{f,annular} = \frac{1}{2} f_i \frac{(Gx)^2}{\rho_v \alpha^{2.5}} \frac{1}{D} \tag{5.8}$$

The void fraction model of Winkler *et al.* (2012) was used to reduce the data as well as in the model proposed here. Although the Winkler *et al.* void fraction model was developed

for the intermittent regime, it is applied to all the data points in this study. The void fraction is defined in Eq. (5.9),

$$\alpha_{\substack{\text{Winkler,} \\ \text{2012}}} = \frac{\alpha_{\text{homogeneous}}}{1.153 + 0.071 \text{ m s}^{-1}\Big/ j} \tag{5.9}$$

where j is the volumetric flux density defined as the sum of the liquid and gas superficial velocity, Eq. (5.10), and the homogeneous void fraction is defined in Eq. (5.11).

$$j = \frac{Gx}{\rho_v} + \frac{G(1-x)}{\rho_l} \tag{5.10}$$

$$\alpha_{\text{homogeneous}} = \left(1 + \left(\frac{1-x}{x}\right)\left(\frac{\rho_v}{\rho_l}\right)\right)^{-1} \tag{5.11}$$

The following discussion describes the model developed by Garimella $et\ al.$ (2005) and proposes modifications to the correlations to better predict the present data. The ratio of the interfacial to liquid friction factor, as defined by Garimella $et\ al.$ (2005), can be expressed in Eq. (5.12) as a function of the Martinelli parameter, "actual" liquid Reynolds number based on the annular flow area of the liquid phase, and the surface tension parameter, $\psi = j_l \mu_l / \sigma$, introduced by Lee and Lee (2001). The superficial liquid velocity is defined using the Winkler $et\ al.$ void fraction: $j_l = G\ (1-x)\ /\ [\rho_l\ (1-\alpha)]$. The "actual" liquid Reynolds number is defined as: $\text{Re}_l = G\ D\ (1-x)\ /\ [(1+\alpha^{1/2})\ \mu_l]$.

$$\frac{f_i}{f_l} = NX^a \, \text{Re}_l^b \, \psi^c \tag{5.12}$$

The experimental value of the interfacial shear stress was calculated from the measured frictional pressure gradient as in Eq. (5.13).

$$f_{i,\text{measured}} = \frac{2\rho_v \alpha^{2.5} D \left(dP/dz \right)_{f,\text{measured}}}{\left(Gx \right)^2} \tag{5.13}$$

Regression analyses were conducted on the interfacial friction factor to yield:

$$\frac{f_i}{f_l} = 0.0019 X^{0.6} \, \text{Re}_l^{0.930} \, \psi^{-0.121} \tag{5.14}$$

For the intermittent regime, the frictional pressure drop model includes contributions from the film-bubble interface, the liquid slug and the slug film transitions:

$$
\begin{aligned}
\left(\frac{dP}{dz} \right)_{f,\text{intermittent}} &= \left(\frac{dP}{dz} \right)_{\substack{\text{film} \\ \text{bubble}}} \left(\frac{L_{\text{bubble}}}{L_{\text{unit cell}}} \right) \\
&+ \left(\frac{dP}{dz} \right)_{\text{slug}} \left(\frac{L_{\text{slug}}}{L_{\text{unit cell}}} \right) + \Delta P_{\substack{\text{one} \\ \text{transition}}} \left(\frac{N_{\text{unit cells}}}{L} \right)
\end{aligned}
\tag{5.15}
$$

The individual pressure drop terms are calculated as described in Garimella *et al.* (2002). The pressure gradient in the slug is given in Eq. (5.16),

$$\left(\frac{dP}{dz} \right)_{\text{slug}} = -\frac{0.3164}{\text{Re}_{\text{slug}}^{0.25}} \frac{\rho_l u_{\text{slug}}^2}{2D} \tag{5.16}$$

where u_{slug} is defined in the same way as j in Eq. (4.88) and the slug Reynolds number is defined in the usual way using the slug velocity: $\text{Re}_{\text{slug}} = \rho_l u_{\text{slug}} D / \mu_l$. The pressure gradient in the film/bubble region is given in Eq. (5.17).

$$\left(\frac{dP}{dz} \right)_{\substack{\text{film/} \\ \text{bubble}}} = -\frac{0.3164}{\text{Re}_{\text{bubble}}^{0.25}} \frac{\rho_v \left(u_{\text{bubble}} - u_{\text{interface}} \right)^2}{4R_{\text{bubble}}} \tag{5.17}$$

The bubble-to-slug velocity ratio was set at 1.2 as in the Garimella *et al.* model. The bubble radius is taken to be 90% of the tube radius as in the Garimella *et al.* model. The

interface velocity is taken to be twice the film velocity, which is determined by solving the continuity equation:

$$u_{\text{slug}} = u_{\text{bubble}} \left(\frac{R_{\text{bubble}}}{R_{\text{tube}}} \right)^2 + u_{\text{film}} \left(1 - \left(\frac{R_{\text{bubble}}}{R_{\text{tube}}} \right)^2 \right) \tag{5.18}$$

The pressure drop in one transition from the film to the slug is given in Eq. (5.19).

$$\Delta P_{\substack{\text{one} \\ \text{transition}}} = -\rho_1 \left(1 - \left(\frac{R_{\text{bubble}}}{R_{\text{tube}}} \right)^2 \right) \left(u_{\text{slug}} - u_{\text{film}} \right) \left(u_{\text{bubble}} - u_{\text{film}} \right) \tag{5.19}$$

The relative length of the slug region is given in Eq. (5.20),

$$\frac{L_{\text{slug}}}{L_{\text{UC}}} = k \frac{j_1}{j_1 + j_v} \tag{5.20}$$

where j_v and j_1 denote the vapor and liquid superficial velocities and the parameter $k = 0.7228 + 0.4629 \exp(-0.9604D)$ as defined in the previous correlation.

After examining different parameters in this model including k, the slug frequency, related to the number of unit cells per length, was observed to have the greatest effect on the model predictions. Because of the limited data set in the intermittent regime and the absence of flow visualization data, the parameters in this model were not explicitly determined by the experiment. However, a regression fit based on the data was performed to relate the unit cells per length to the slug Reynolds number.

$$D \left(\frac{N_{\text{UC}}}{L} \right) = \omega \frac{D}{U_{\text{bubble}}} = \frac{D}{L_{\text{UC}}} = a \, \text{Re}_{\text{slug}}^{b} \tag{5.21}$$

The number of unit cells per length was determined by rearranging the terms of Eq. (5.15). Although this method introduces more uncertainty in the model, direct measurement of this quantity is beyond the scope of this study. Further work is needed

175
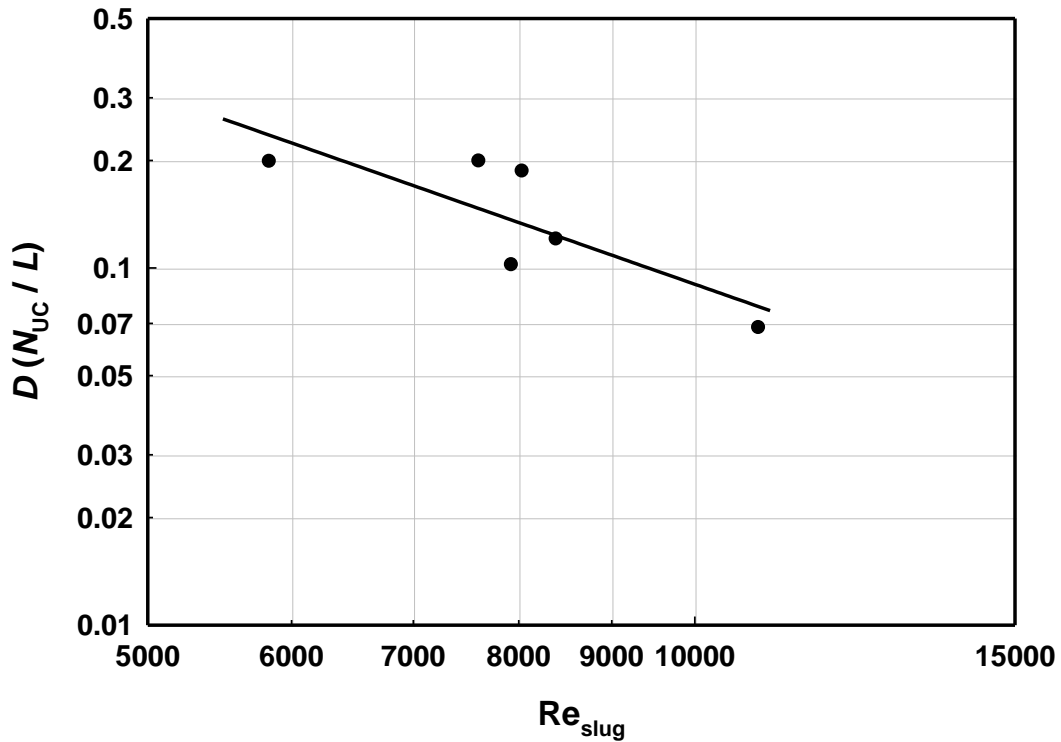
Figure 5.24: Slug frequency vs. slug Reynolds number

with additional data to develop a more robust pressure drop correlation for the intermittent regime. Figure 5.24 shows the results of the regression analysis with a power fit curve overlaid on the plot. The coefficients were determined to be $a = 1.232 \times 10^6$ and $b = -1.784$. The coefficient of determination for the regression curve is $R^2 = 0.65$.

The proposed model for the frictional pressure gradient is summarized in Table 5.7.

Figure 5.25 shows the experimental results for the pressure gradient compared to the model predictions. The proposed model predicts the data with an average deviation of -3.9% and an average absolute deviation of 12.0%. The maximum deviation is 34.1%. The AAD in the annular regime is 9.7%, and in the intermittent regime, it is 19.8%. The

Table 5.7: Frictional Pressure Drop Model Summary

Flow Regime	Equations Garimella *et al.* (2005)
Annular	$$\left(\frac{dP}{dz}\right)_{\text{f,annular}} = \frac{1}{2}f_i\frac{(Gx)^2}{\rho_v\alpha^{2.5}}\frac{1}{D}$$ $$\frac{f_i}{f_l} = 0.0019X^{0.6}\,\text{Re}_l^{0.930}\,\psi^{-0.121}$$
Intermittent	$$\left(\frac{dP}{dz}\right)_{\text{f,intermittent}} = \left(\frac{dP}{dz}\right)_{\substack{\text{film}\\ \text{bubble}}}\left(\frac{L_{\text{bubble}}}{L_{\text{unit cell}}}\right)$$ $$+\left(\frac{dP}{dz}\right)_{\text{slug}}\left(\frac{L_{\text{slug}}}{L_{\text{unit cell}}}\right) + \Delta P_{\substack{\text{one}\\ \text{transition}}}\left(\frac{N_{\text{unit cells}}}{L}\right)$$ $$\left(\frac{dP}{dz}\right)_{\substack{\text{film/}\\ \text{bubble}}} = -\frac{0.3164}{\text{Re}_{\text{bubble}}^{0.25}}\frac{\rho_v\left(u_{\text{bubble}}-u_{\text{interface}}\right)^2}{4R_{\text{bubble}}}$$ $$\left(\frac{dP}{dz}\right)_{\text{slug}} = -\frac{0.3164}{\text{Re}_{\text{slug}}^{0.25}}\frac{\rho_l u_{\text{slug}}^2}{2D}$$ $$\Delta P_{\substack{\text{one}\\ \text{transition}}} = -\rho_l\left(1-\left(\frac{R_{\text{bubble}}}{R_{\text{tube}}}\right)^2\right)\left(u_{\text{slug}}-u_{\text{film}}\right)\left(u_{\text{bubble}}-u_{\text{film}}\right)$$ $$D\left(\frac{N_{UC}}{L}\right) = \omega\frac{D}{U_{\text{bubble}}} = \frac{D}{L_{UC}} = \left(1.232\times10^6\right)\text{Re}_{\text{slug}}^{-1.784}$$

larger error in the intermittent regime is mainly due to the fact that these small pressure drop measurements at low quality could not be resolved with as much accuracy relative to the two-phase static head term. The model predicts 85% of the data to within ± 25% deviation and 56% of the data to within ± 10% deviation.

Figure 5.26 shows the frictional pressure gradient data with the predictions of the present model overlaid. The trends with mass flux and quality correspond well with the data at both saturation conditions, although there is less agreement for the highest mass
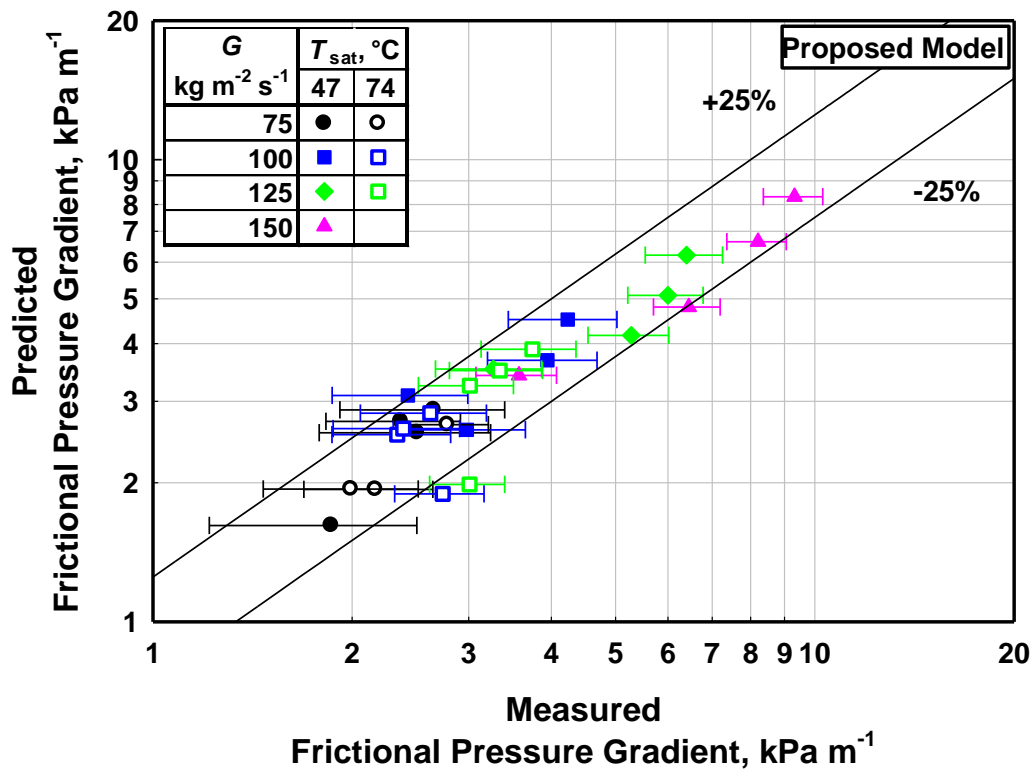
Figure 5.25: Comparison of the pressure drop data with predictions of the present model
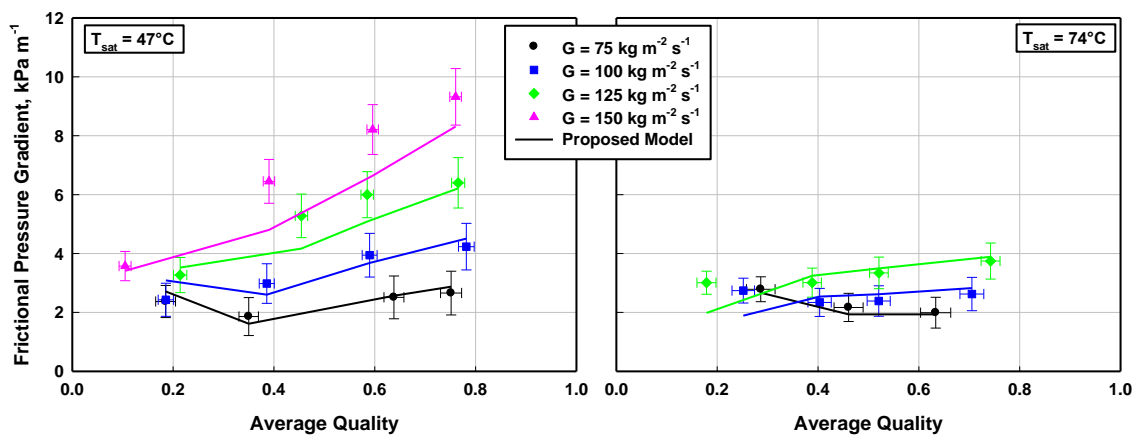
Figure 5.26: Predictions of the present model with the pressure drop data

flux. The deviation in the annular regime is partly due to the fact that the void fraction model is primarily for the intermittent regime. As with the Garimella *et al*. (2005) correlation described above, the crossover in the 74°C, 75 and 100 kg m^{-2} s^{-1} curves is due to the errors associated with void fraction prediction at large quality changes for these data points, and is not a reflection of the overall trend of the frictional pressure gradient.

Figure 5.27 shows an illustration of the trends of the pressure drop model with mass flux. The model represents the trends observed in the data. As expected, the model predicts that the pressure drop increases with increasing mass flux. There is a discontinuity in the curve corresponding to the transition from the intermittent to the annular regime. Because the transition quality decreases for increasing mass flux, there are small regions in which the pressure drop is greater for lower mass flux. The model also shows a decrease in pressure drop as the quality approaches single-phase vapor flow. Figure 5.28 shows the trends of the pressure drop model with respect to saturation temperature. The pressure drop is seen to decrease with increasing saturation temperature. This is due partly to decreasing liquid-to-vapor density and viscosity ratios which lead to reduced interfacial shear between the two phases. The transition between intermittent and annular flow is less abrupt at higher saturation temperature.
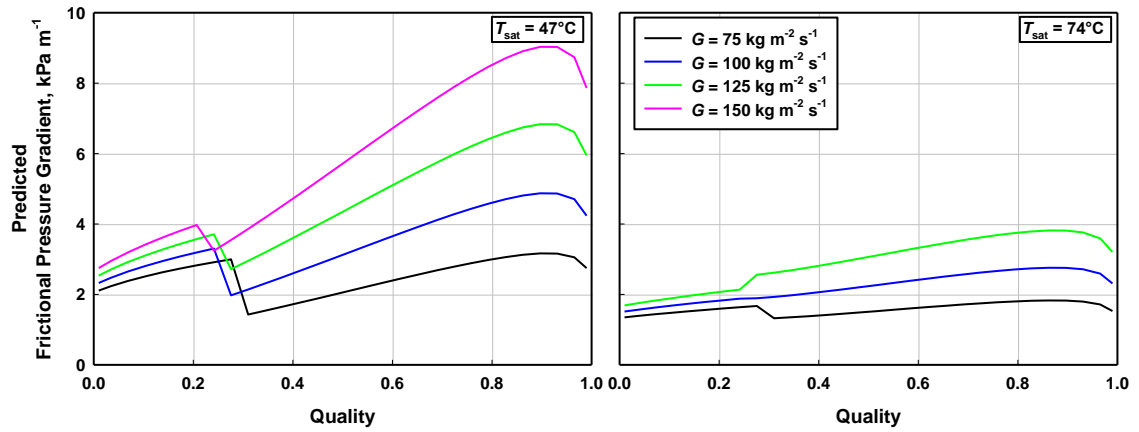
Figure 5.27: Illustration of pressure drop model trends with respect to mass flux, *D* = 1.93 mm
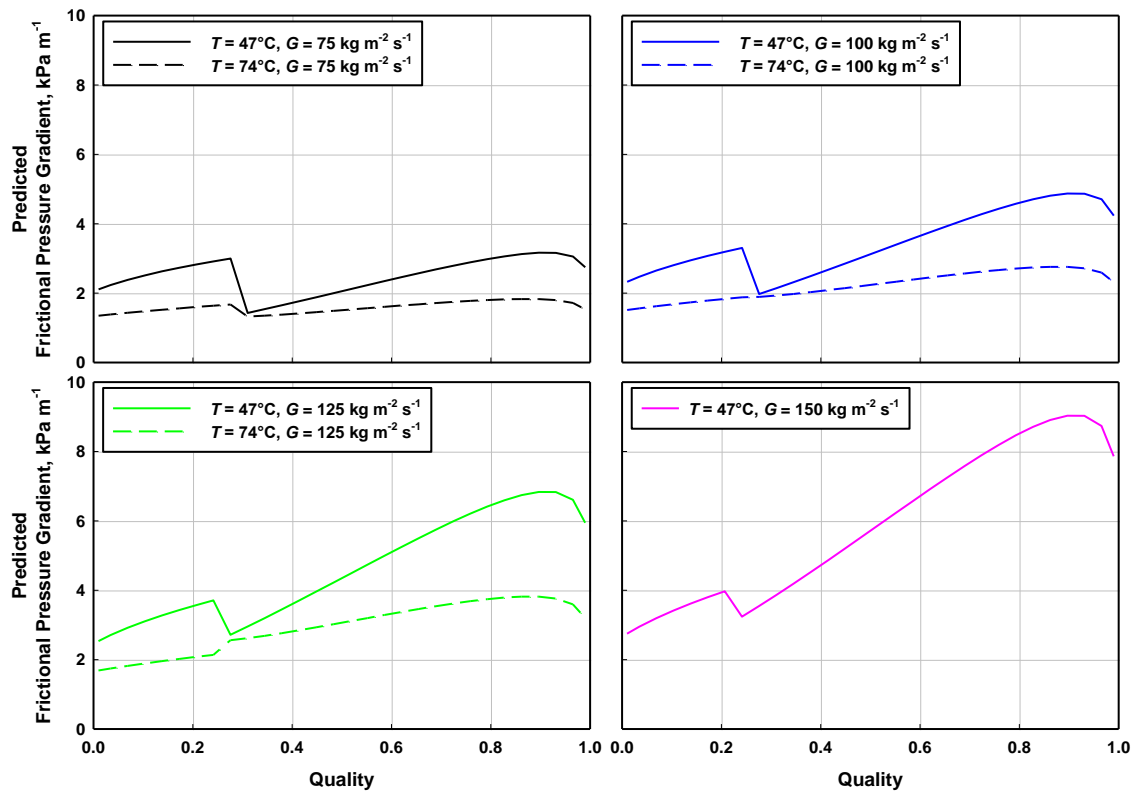
Figure 5.28: Illustration of pressure drop model trends with respect to saturation temperature, *D* = 1.93 mm

5.3.2. <u>Heat Transfer Coefficient</u>

Annular flow is a common flow regime for vertical condensation in small diameter channels. This is also the case in the present study, based on the Coleman and Garimella (2000a, 2003) flow regime map. Therefore, the heat transfer coefficient was modeled for annular flow condensation using the heat transfer-momentum analogy and the Traviss *et al.* (1973) correlation as a basis.

As noted above, the Traviss *et al.* (1973) model is one of the best predictors of the data from the present study. It is also a semi-empirical model that seeks to describe the physical mechanisms of heat transfer occuring during condensation in annular flow. Mechanistic models generally have broader application to conditions not directly simulated in their development; therefore, a model like Traviss *et al*. lends itself well to be a starting point for the model development in the present study. Figure 5.29 and Figure 5.30 show the measured heat transfer coefficient data compared to the predictions of Traviss *et al.* (1973). As can be seen in these plots, the model generally captures the trends of the data but under-predicts the measurements especially at high quality.

To better understand how this correlation can be formulated to describe the conditions of the present study, the heat transfer-momentum analogy is examined. The base form for the Nusselt number is derived following the procedure described in Traviss *et al.* (1973). Figure 5.31 shows a schematic of condensation during annular flow in a vertical tube. The two key quantities considered in the derivation, which may be expressed in analogous forms, are the shear stress in the liquid film, τ, and the heat flux from the liquid film to the wall, q''. The shear stress is a function of the liquid viscosity
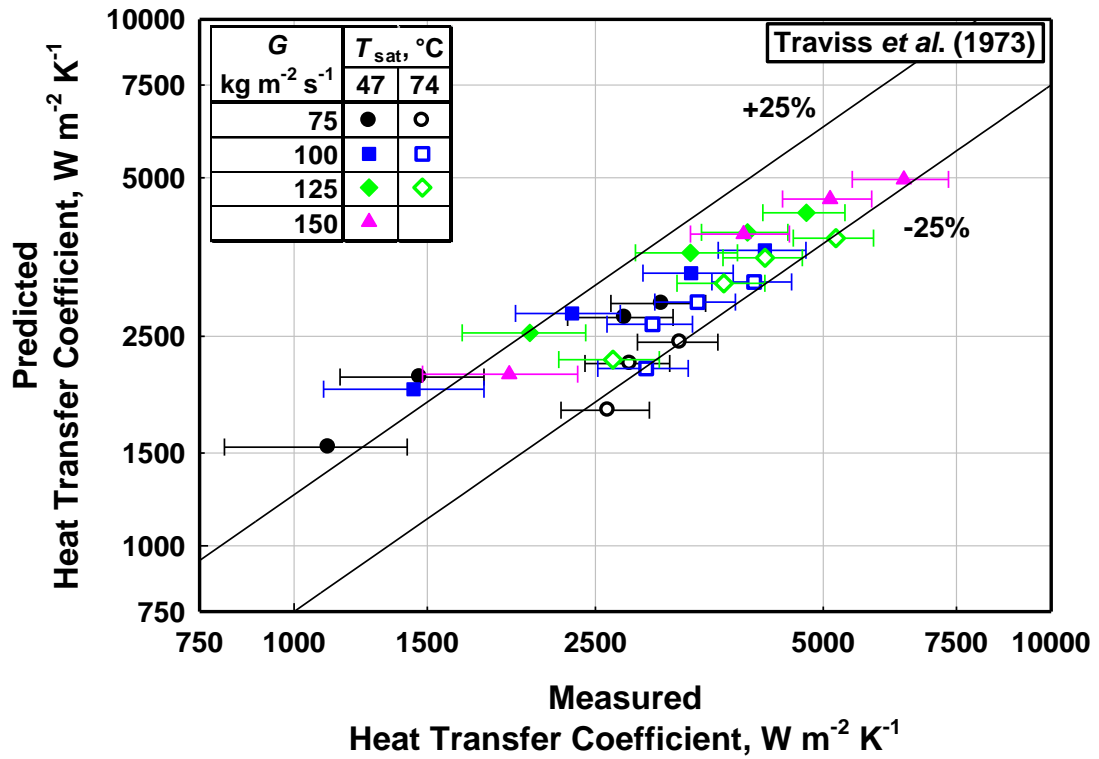
Figure 5.29: Comparison of the heat transfer coefficient data with the predictions of Traviss *et al*. (1973)
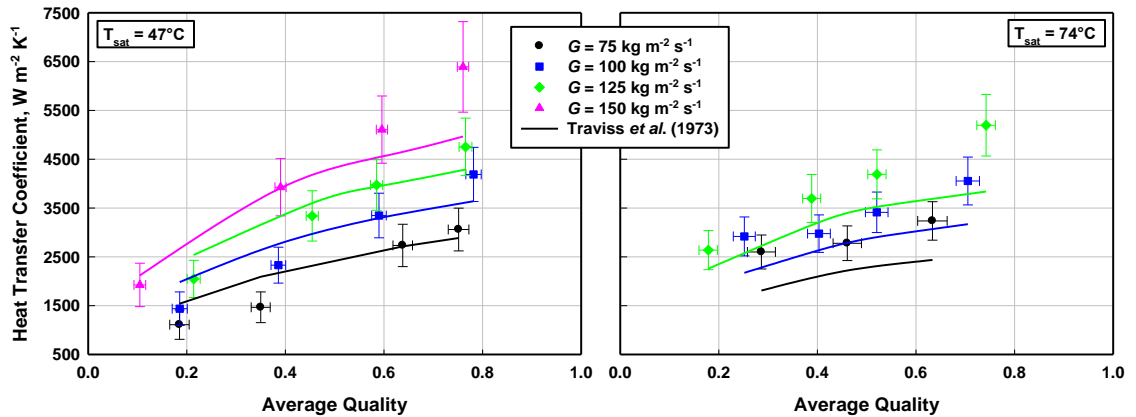
Figure 5.30: Heat transfer coefficient data with the predictions of Traviss *et al*. (1973) overlaid

and velocity gradient as shown in Eq. (5.22), and the heat flux is a function of the liquid conductivity and temperature gradient as shown in Eq. (5.23), where ϵ_m is the eddy viscosity and ϵ_h is the eddy diffusivity, v_l is the liquid kinematic viscosity, and α_l is the thermal diffusivity.

$$\tau = \rho_l \left(v_l + \epsilon_m \right) \frac{dv_z}{dy} \tag{5.22}$$

$$q'' = \rho_l c_{p,l} \left(\alpha_l + \epsilon_h \right) \frac{dT}{dy} \tag{5.23}$$
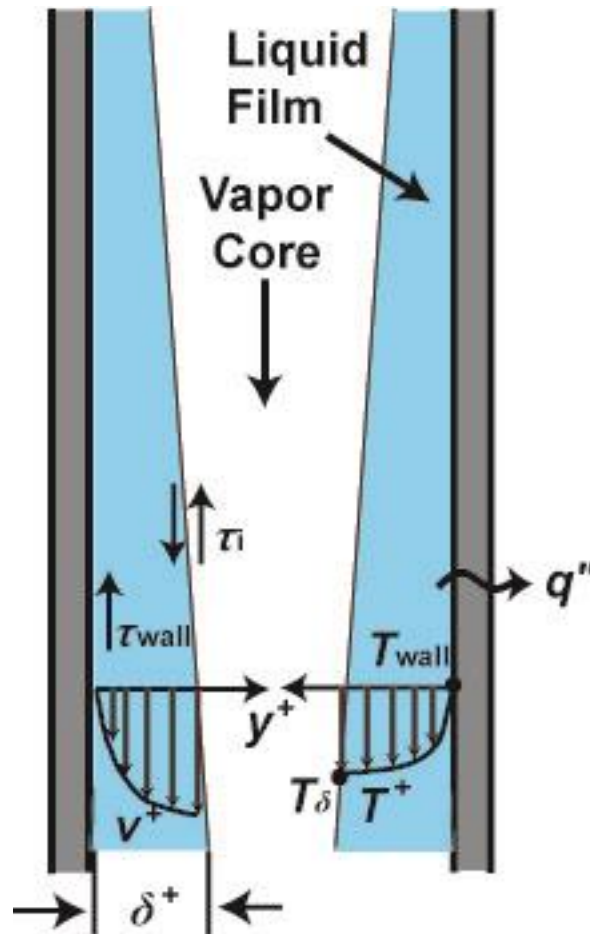
Figure 5.31: Schematic showing momentum and heat transfer mechanisms during annular flow condensation

Assuming that the primary means of heat transfer in annular flow is through the liquid film, the heat transfer coefficient can be expressed as the ratio of the heat flux to the temperature difference across the liquid film: $h = q'' / (T_\delta - T_{\text{wall}})$. The shear stress can be related to the heat flux by means of the ratio of the eddy diffusivity to eddy viscosity, E, which in the present study is assumed to be approximately unity as in Traviss *et al.* (1973). If the velocity gradient is expressed in dimensionless form, and the shear velocity is defined as $u_\tau = (\tau_{\text{wall}} / \rho_1)^{0.5}$, the heat flux expression in Eq. (5.23) can be integrated over the dimensionless film thickness, δ^+, to obtain the heat transfer coefficient:

$$\frac{1}{h} = \frac{T_\delta - T_{\text{wall}}}{q''} = \int_0^{\delta^+} \frac{\nu_1}{\rho_1 c_{\text{p,l}} (\alpha_1 + E\epsilon_{\text{m}}) u_\tau} \, dy^+ \tag{5.24}$$

This expression simplifies to the form:

$$h = \frac{\rho_1 c_{\text{p,l}} (\tau_{\text{wall}} / \rho_1)^{0.5}}{T^+} \tag{5.25}$$

The dimensionless film temperature (T^+) is evaluated using the Von Kármán universal velocity profile given in Eq. (5.26). The turbulent velocity and temperature profiles are shown in the schematic in Figure 5.31.

$$v_z^+ = \begin{cases} y^+ & 0 < y^+ < 5 \\ -3.05 + 5\ln y^+ & 5 < y^+ < 30 \\ 5.5 + 2.5\ln y^+ & 30 < y^+ \end{cases} \tag{5.26}$$

where the dimensionless coordinate is $y^+ = yu_\tau / \nu_1$ and the dimensionless axial velocity is $v_z^+ = v_z / u_\tau$. The wall shear stress is related to the frictional pressure gradient by means of the shear velocity.

$$\left(\frac{dP}{dz} \right)_{\text{f}} = \frac{4\tau_{\text{wall}}}{D} = u_\tau^2 \rho_1 \frac{4}{D} \tag{5.27}$$

The vapor two-phase multiplier given by Soliman *et al.* (1968) is used to calculate the frictional pressure gradient; however, the Martinelli parameter is defined by Eq. (5.7) rather than the turbulent-turbulent formula used in the previous model.

$$\left(\frac{dP}{dz}\right)_f = \frac{1}{2} f_v \frac{(Gx)^2}{\rho_v D} \left(1 + 2.85 X^{0.523}\right)^2 \tag{5.28}$$

Better agreement with the data was found when the vapor friction factor is calculated using the Churchill (1977a) correlation rather than using the Blasius expression. The tube roughness is 0.015 mm for this test section. Combining Eq. (5.25), (5.27) and (5.28) yields a base expression for the Nusselt number.

$$\text{Nu} = \frac{\Pr_l \text{Re}_l}{T^+} F \tag{5.29}$$

where the liquid Reynolds number is defined in Eq. (5.1) and the parameters F and T^+ are defined in Eq. (5.30). The piecewise solution to the integral for T^+ is given in Traviss *et al.* (1973).

$$F = \left(\frac{f_v}{8}\right)^{0.5} \left(\frac{x}{1-x}\right) \left(\frac{\rho_l}{\rho_v}\right)^{0.5} \left(1 + 2.85 X^{0.523}\right)$$

$$T^+ = \begin{cases} 0.707 \Pr_l \text{Re}_l^{0.5} & \text{Re}_l < 50 \\ 5 \Pr_l + 5 \ln\left[1 + \Pr_l\left(0.09636 \text{Re}_l^{0.585} - 1\right)\right] & 50 < \text{Re}_l < 1125 \\ 5 \Pr_l + 5 \ln\left(1 + 5 \Pr_l\right) + 2.5 \ln\left(0.00313 \text{Re}_l^{0.812}\right) & \text{Re}_l > 1125 \end{cases} \tag{5.30}$$

A parametric analysis was performed for different terms in Eq. (5.29) to develop a model that describes the current data. Figure 5.32a shows the influence of F on the
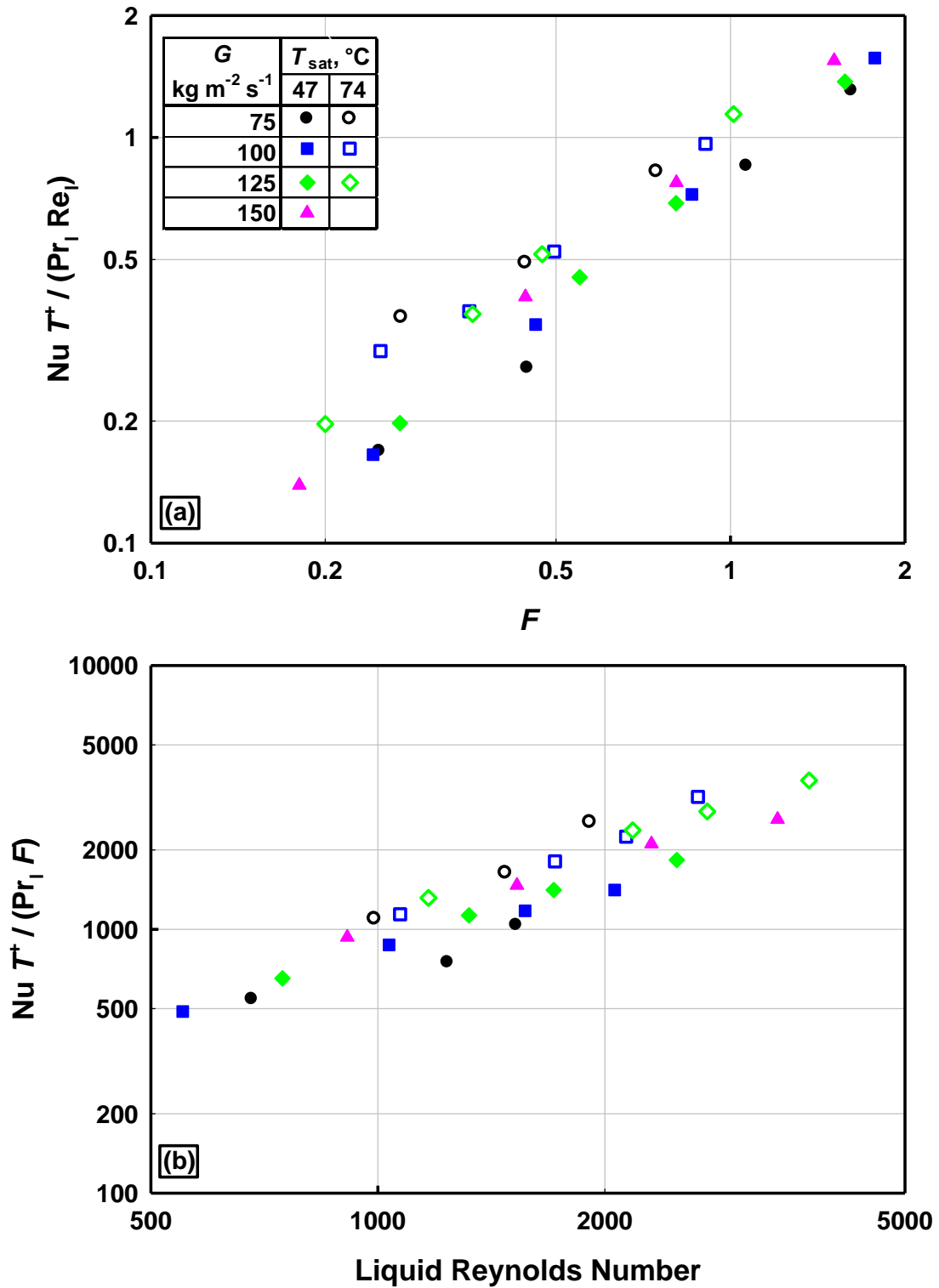
Figure 5.32: Heat transfer coefficient model parametric analysis with respect to F and Re_l

measured Nusselt number. The data have low scatter with respect to this parameter ($r = 0.95$). However, especially at lower values of F, differences can be seen along the lines of saturation temperature. The data are more uniformly distributed with respect to the liquid Reynolds number as can be seen in Figure 5.32b ($r = 0.96$). A regression analysis was performed on the Nusselt number with respect to the Reynolds number and the parameter F to obtain the correlation in Eq. (5.31). The coefficient of determination for the power fit is $R^2 = 0.82$.

$$\mathrm{Nu} = 0.0841 \frac{\mathrm{Pr_l} \, \mathrm{Re_l^{1.349}}}{T^+} F^{1.263} \tag{5.31}$$

Figure 5.33 shows the experimental results compared to the model predictions. This model predicts the data with an average deviation of 1.5% and an average absolute deviation of 13.4%. The maximum absolute deviation between the data and the model is 37.6%. The model predicts 93% of the data to within a $\pm 25\%$ deviation and 37% of the data to within a $\pm 10\%$ deviation.

Figure 5.34 shows the measured heat transfer coefficient data with the predictions of the proposed model overlaid. It can be seen that the model captures the trends of the data over most of the data set. The heat transfer coefficient increases with increasing mass flux and quality. At 47°C saturation temperature, the increasing trend is not as closely followed with mass flux. It is possible that a better approximation of the velocity profile could be applied to bring these values into closer agreement. Also, because the heat transfer coefficient is strongly dependent on shear stress, the evaluation of the two-phase frictional pressure gradient is important to the prediction. While the two-phase modifier proposed by Soliman *et al.* (1968) yields adequate heat transfer results, an
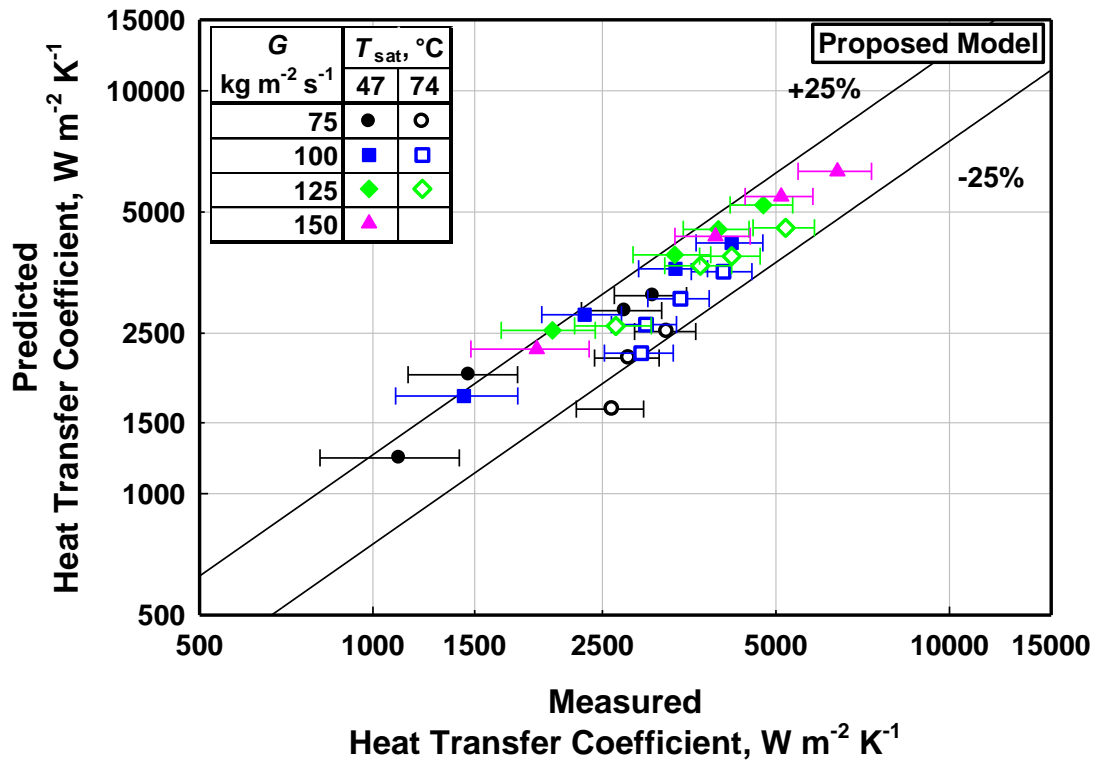
Figure 5.33: Comparison of heat transfer coefficient measurements and model predictions
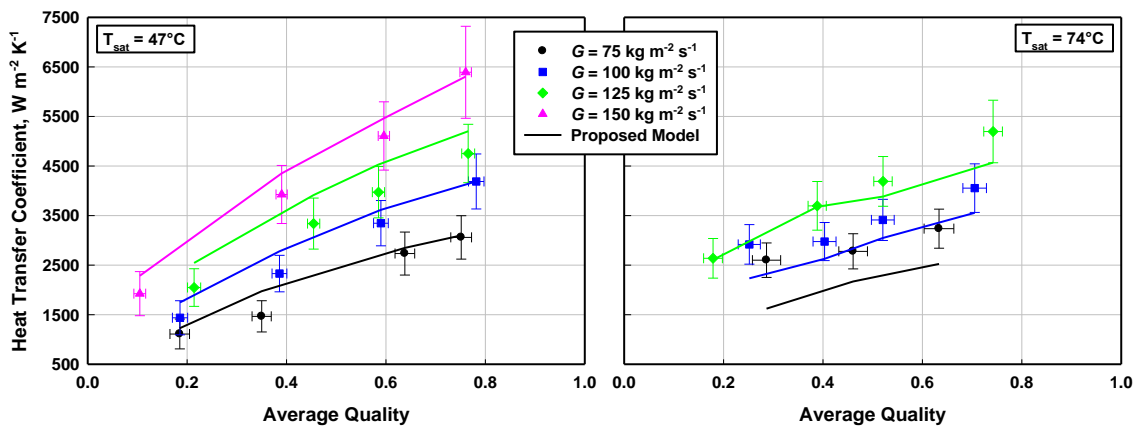
Figure 5.34: Heat transfer coefficient measurements with model predictions overlaid

expression that better approximates the pressure drop would improve the performance of the heat transfer coefficient correlation. The heat transfer coefficient is also under-predicted at the 74°C saturation temperature. This could partly be due to the large quality changes in the measured data points, where the large quality change groups the measured heat transfer coefficients of two possibly distinct quality points in differing regimes, skewing the heat transfer coefficient data higher than the average local quality would suggest. Also, at these low quality points, slug flow is more likely. Because this model is based on annular flow mechanisms, there could be some error at lower quality.

Figure 5.35 illustrates the trends in the heat transfer coefficient model with respect to changing mass flux. It can be seen that the model accurately predicts heat transfer coefficient to increase with increasing mass flux. While the heat transfer coefficient is predicted to monotonically increase with quality for a given mass flux and saturation condition, there is a region of steeper increase at intermediate quality for some of the higher mass flux cases. This region is related to the transition between laminar and turbulent flow of the liquid and vapor friction factors used to compute the Martinelli parameter. Figure 5.36 shows the trends of the heat transfer coefficient model with respect to changing saturation temperature. At higher quality, the heat transfer coefficient decreases with increasing saturation temperature. However, especially at high mass flux, there is a region at low-to-intermediate quality in which the reverse of this trend is predicted. This corresponds with the observations in the data that at lower quality, the heat transfer coefficient increased with increasing saturation temperature, while there was less of a dependence at higher quality. This trend also reflects the shear-based mechanism that was modeled in the proposed correlation. For increasing saturation temperature, the

decrease in liquid-to-vapor density and viscosity ratios and the decrease in latent heat leads to a decrease in shear stress. The effects of this mechanism are more pronounced at higher quality. At high quality, the density ratio is a more significant quantity for the heat transfer coefficient calculation than the Prandtl number. Because the density ratio increases more than the Prandtl number with an increase in saturation temperature, the model predicts a decrease in heat transfer coefficient with respect to saturation temperature at high quality rather than at low quality.

At very high qualities (approximately $x > 0.90$), the model exhibits behavior not seen in the data; however, this trend is due to the model dependence on liquid film thickness, which becomes very thin at higher quality points. At very high qualities, the heat transfer coefficient model shows a sharp increase. The heat transfer coefficient is expected to increase at higher quality because the liquid film is smaller; however, it is possible that this is an artifact of the correlation. As x approaches 1, the $x / (1 - x)$ term in the parameter F approaches infinity. This term dominates the correlation at this quality range. At very low qualities (approximately $x < 0.10$), there is less dependence on changes in mass flux. There is also a discontinuity in the heat transfer coefficient at approximately $x = 0.10$ as quality decreases when vapor Reynolds number transitions to laminar flow from turbulent flow. The development of the correlation assumes a turbulent vapor core, whereas it is unlikely that the vapor core is turbulent at these points. Therefore, the present model may not be applicable in this region. In this region, slug or bubbly flow is expected as well. Therefore, an annular flow based model could exhibit some errors. Further experimental work is needed at very low and high quality ranges to determine whether this model accurately descibes the trends under these conditions.
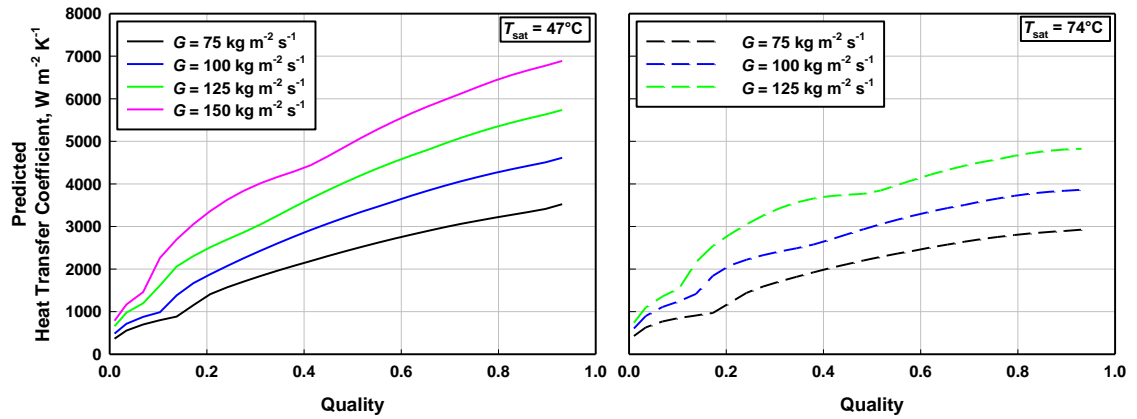
Figure 5.35: Illustration of the heat transfer model trends with respect to mass flux, _D_ = 1.93 mm
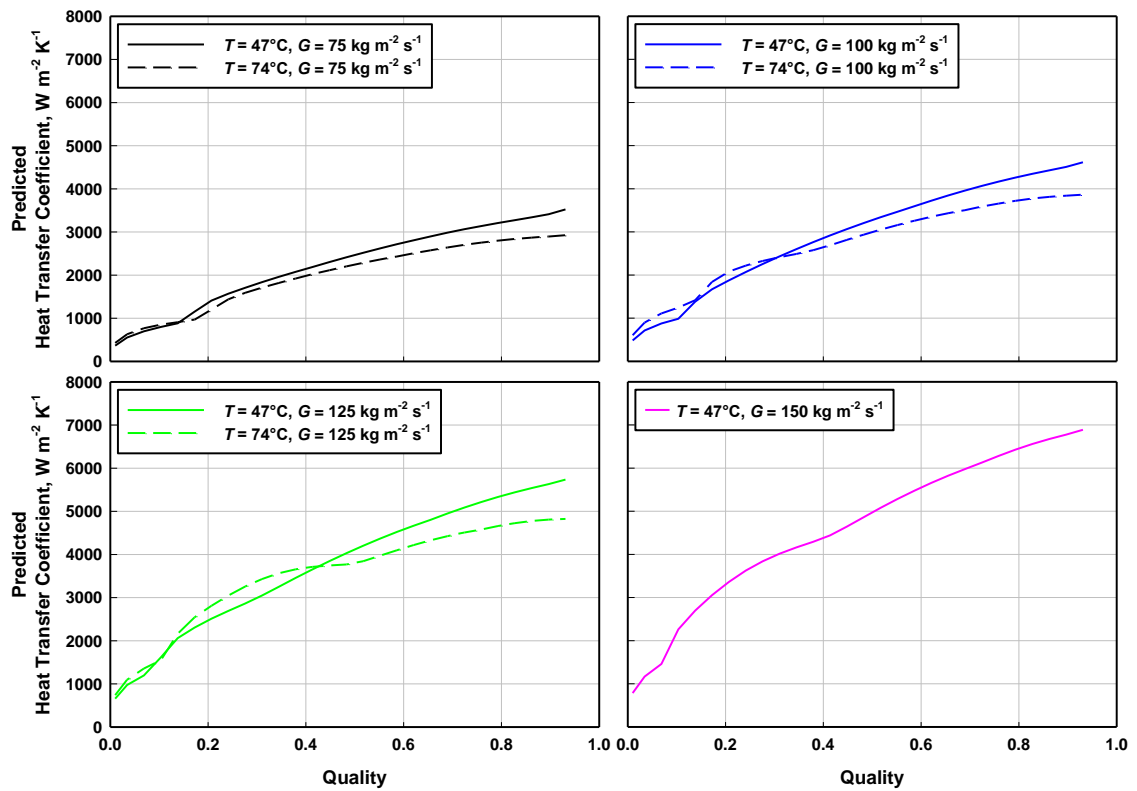
Figure 5.36: Illustration of the heat transfer model trends with respect to saturation temperature, _D_ = 1.93 mm

191

CHAPTER 6: CONCLUSIONS

6.1.   Summary and Conclusions

A study was conducted to determine the heat transfer coefficient and frictional pressure gradient during condensation of propane during condensation in vertical 1.93 mm diameter tubes. Measurements were taken over the entire quality range at approximately $\Delta x \approx 0.25$ increments. Two saturation temperatures were considered: 47°C and 74°C. The mass flux values considered included 75, 100, 125 and 150 kg m^{-2} s^{-1}. It was observed that, in general, the pressure drop increases with increasing mass flux and quality, and decreases with increasing saturation temperature. The heat transfer coefficient data also showed similar trends, although there was a slight negative trend with saturation temperature. The data from this study were used to develop frictional pressure gradient and local heat transfer coefficient correlations.

For the pressure drop model, the data were grouped into intermittent and annular flow regimes based on the transition criteria of Garimella *et al.* (2005) developed from the flow visualization studies of Coleman and Garimella (2000a, 2003). The pressure drop model for the annular flow regime is based on the single-phase vapor pressure gradient, the void fraction, and the interfacial friction factor.

$$\left(\frac{dP}{dz}\right)_{\mathrm{f}} = \frac{1}{2} f_{\mathrm{i}} \frac{(Gx)^2}{\rho_{\mathrm{v}} \alpha^{2.5}} \frac{1}{D} \qquad (6.1)$$

$$\frac{f_{\mathrm{i}}}{f_{\mathrm{l}}} = 0.0019 X^{0.6} \mathrm{Re}_{\mathrm{l,actual}}^{0.930} \psi^{-0.121} \qquad (6.2)$$

The pressure drop model for the intermittent regime includes contributions from the film-bubble interface, the liquid slug, and the slug film transitions:

$$\frac{\Delta P}{L} = \left(\frac{dP}{dx}\right)_{\substack{\text{film} \\ \text{bubble}}} \left(\frac{L_{\text{bubble}}}{L_{\text{unit cell}}}\right) + \left(\frac{dP}{dx}\right)_{\text{slug}} \left(\frac{L_{\text{slug}}}{L_{\text{unit cell}}}\right) + \Delta P_{\text{one transition}} \left(\frac{N_{\text{unit cells}}}{L}\right) \quad (6.3)$$

The individual pressure drop terms were calculated as described in Garimella *et al.* (2005). The slug frequency is predicted using:

$$D\left(\frac{N_{UC}}{L}\right) = \frac{D}{L_{UC}} = \left(1.232 \times 10^6\right) \text{Re}_{\text{slug}}^{-1.784} \quad (6.4)$$

The heat transfer coefficient correlation was developed using the heat transfer-momentum analogy assuming the flow to be annular throughout. The correlation predicts the Nusselt number as a function of Prandtl number, liquid Reynolds number, quality and property ratios, and is applicable for the quality range $0.10 < x < 0.90$.

$$\text{Nu} = 0.0841 \frac{\text{Pr}_1 \text{Re}_1^{1.349}}{T^+} F^{1.263} \quad (6.5)$$

$$F = \left(\frac{f_v}{8}\right)^{0.5} \left(\frac{x}{1-x}\right) \left(\frac{\rho_1}{\rho_v}\right)^{0.5} \left(1 + 2.85 X^{0.523}\right)$$

$$T^+ = \begin{cases} 0.707 \, \text{Pr}_1 \, \text{Re}_1^{0.5} & \text{Re}_1 < 50 \\ 5 \, \text{Pr}_1 + 5 \ln\left[1 + \text{Pr}_1\left(0.09636 \, \text{Re}_1^{0.585} - 1\right)\right] & 50 < \text{Re}_1 < 1125 \\ 5 \, \text{Pr}_1 + 5 \ln\left(1 + 5 \, \text{Pr}_1\right) + 2.5 \ln\left(0.00313 \, \text{Re}_1^{0.812}\right) & \text{Re}_1 > 1125 \end{cases} \quad (6.6)$$

The pressure drop model predicted the data with an average deviation of -3.9% and an average absolute deviation of 12.0%. The heat transfer coefficient model predicted the data with an average deviation of 1.5% and an average absolute deviation of 13.4%. The pressure drop model predicted 85% of the data to within ±25% and 56% of the data

to within ±10%. The heat transfer coefficient model predicted 93% of the data to within ±25% and 37% of the data to within ±10%.

The results of this study will benefit the process industry and other related applications by providing a greater understanding of hydrocarbon condensation for more efficient design of condensers and other phase-change heat exchangers. The refrigeration and HVAC industries will also benefit from the insights of this study as there is more emphasis on efficiently employing low GWP natural refrigerants.

6.2.   Recommendations for Further Study

The present study provides a good basis for the understanding of vertical condensation of hydrocarbons in small diameter channels. While the present study includes 27 distinct data points, a larger database is necessary to develop more broadly applicable models. This includes additional experimental parameters, saturation temperatures, other hydrocarbons, and more tube diameters.

Accurate void fraction predictions are crucial to measuring the frictional pressure drop in vertical tubes. Therefore, a comprehensive study should include flow visualization experiments to map the flow patterns present in vertical downward condensation and quantitatively determine the void fraction.

Accurate heat duty measurements, particularly given the small magnitude of the heat transfer rate for this small diameter tube, proved difficult. A finer resolution in quality measurements should be attempted using alternate methods of measuring the test section heat duty. One possibility is to conduct experiments with several local wall temperature measurements on the surface and/or at varying depths in the wall to measure

the heat duty directly. This method would eliminate the competing factors contributing to the uncertainty that required the quality decrement to be higher in the present study. A finer quality resolution would enable more measurements to be taken for each mass flux and saturation temperature. However, the thermocouple measurement accuracy would have to be substantially higher for such a technique to succeed in measuring local heat transfer coefficients with a high resolution.

The measurement technique for the frictional pressure drop could also be improved to obtain lower uncertainty and better resolution of the data. If the test section is subdivided into smaller length sections and differential pressure measurements are taken at each of these divisions, the relative influence of the two-phase static head could be accounted for more accurately – the large relative magnitude of static head compared to frictional pressure drop affected the frictional pressure drop measurements adversely in the present study..

Overall, this study contributes to the relatively small amount of literature available thus far on vertical downward condensation of hydrocarbons. The correlations developed in this research can be used for design calculations in the applicable ranges.

APPENDIX A:

UNCERTAINTY PROPAGATION

The experimental uncertainty associated with the measurements is determined using the uncertainty propagation analysis capabilities within the Engineering Equation Solver (Klein, 2011) platform. The uncertainty propagation analyses in EES are based on the Taylor and Kuyatt (1994) approach. A sample calculation is presented here to demonstrate the method. The uncertainty of a given quantity is denoted by the variable U. The sample calculation accompanies the analysis for the 47.03°C saturation temperature, 100.2 kg m^{-2} s^{-1} mass flux and 0.72 to 0.46 quality range data point presented in Chapter 4 (Run #7). The uncertainties associated with each measured quanitity are provided in Table 3.5.

A.1. **Uncertainty in Test Section Quality**

The heat duty in the test section is calculated from an energy balance on the pre- and post-condensers resulting in the equation: $\dot{Q}_{\text{test}} = \dot{m}_{\text{propane}} (i_{\text{propane},3} - i_{\text{propane},4})$. A summary of the variables and associated uncertainties that contribute to the uncertainty in the test section heat duty is provided in Table A.1. The uncertainty in the test section heat duty can be expressed as:

$$U_{\dot{Q}_{\text{test}}}^2 = \left(\frac{\partial \dot{Q}_{\text{test}}}{\partial \dot{m}_{\text{propane}}} U_{\dot{m}_{\text{ref}}} \right)^2 + \left(\frac{\partial \dot{Q}_{\text{test}}}{\partial i_{\text{propane},3}} U_{i_{\text{propane},3}} \right)^2 + \left(\frac{\partial \dot{Q}_{\text{test}}}{\partial i_{\text{propane},4}} U_{i_{\text{propane},4}} \right)^2 \qquad \text{(A.1)}$$

The uncertainty in the mass flow rate is $\pm$ 5.6 × 10^{-7} kg s^{-1}. By differentiation, Eq. (A.1) simplifies to:

$$U_{\dot{Q}_{\text{test}}}^2 = \left(\Delta i_{\text{propane,test}} U_{\dot{m}_{\text{propane}}} \right)^2 + \left(\dot{m}_{\text{propane}} U_{i_{\text{propane},3}} \right)^2 + \left(-\dot{m}_{\text{propane}} U_{i_{\text{propane},4}} \right)^2$$

Table A.1: Uncertainty propagation for the test section heat duty. Gray shaded cells denote uncertainty in measured quantities

$\dot{Q}_{test}$ ±2.54 W 11.2%	$i_{propane,3}$ ±4.64 kJ kg^{-1} 0.9%	$\dot{Q}_{pre}$ ±1.33 W 2.9%	$i_{air,pre,in}$ ±0.27 kJ kg^{-1} 0.1%	$T_{air,pre,in}$ $\pm0.27°$C	$T_{air,pre,in,1}$ $\pm0.20°$C
					$T_{air,pre,in,2}$ $\pm0.50°$C
			$i_{air,pre,out}$ ±0.27 kJ kg^{-1} 0.1%	$T_{air,pre,out}$ $\pm0.27°$C	$T_{air,pre,out,1}$ $\pm0.20°$C
					$T_{air,pre,out,2}$ $\pm0.50°$C
			$\dot{m}_{air,pre}$ $\pm4.8\times10^{-5}$ kg s^{-1} 2.0%	$\rho_{air,pre}$ ±0.024 kg m^{-3} 2.0%	$T_{air,pre}$ $\pm0.50°$C
					$P_{air,pre}$ ±2.07 kPa
				$\dot{V}_{air,pre}$: $\pm0.3\%$	
			$\dot{Q}_{pre,losses}$: $\pm25\%$		
	$i_{propane,1}$ ±0.45 kJ kg^{-1} 0.1%	$T_{propane,1}$ $\pm0.2°$C			
	$\dot{Q}_{loss,2-to-3}$: $\pm25\%$				
	$\dot{m}_{ref}$ $\pm5.6\times10^{-7}$ kg s^{-1} 0.2%				
	$\dot{Q}_{loss,4-to-5}$: $\pm25\%$				
	$i_{propane,6}$ ±0.55 kJ kg^{-1} 0.2%	$T_{propane,6}$ $\pm0.2°$C			
$i_{propane,4}$ ±7.27 kJ kg^{-1} 1.6%	$\dot{Q}_{post}$ ±2.12 W 3.9%	$\dot{Q}_{post,losses}$: $\pm25\%$			
		$\dot{m}_{air,post}$ $\pm7.2\times10^{-5}$ kg s^{-1} 1.2%	$\dot{V}_{air,post}$: $\pm0.3\%$		
			$\rho_{air,post}$ ±0.026 kg m^{-3} 1.2%	$T_{air,post}$ $\pm0.50°$C	
				$P_{air,post}$ ±2.07 kPa	
		$i_{air,post,in}$ ±0.27 kJ kg^{-1} 0.1%	$T_{air,post,in}$ $\pm0.27°$C	$T_{air,post,in,1}$ $\pm0.20°$C	
				$T_{air,post,in,2}$ $\pm0.50°$C	
		$i_{air,post,out}$ ±0.27 kJ kg^{-1} 0.1%	$T_{air,post,out}$ $\pm0.27°$C	$T_{air,post,out,1}$ $\pm0.20°$C	
				$T_{air,post,out,2}$ $\pm0.50°$C	

The test section inlet refrigerant enthalpy is given by: $i_{\text{propane},3} = i_{\text{propane},1} - (\dot{Q}_{\text{pre}} + \dot{Q}_{\text{loss,2-to-3}}) / \dot{m}_{\text{propane}}$. Therefore, the uncertainty of the test section

enthalpy can be expressed as follows:

$$U_{i_{\text{propane},3}}^2 = \left(\frac{\partial i_{\text{propane},3}}{\partial i_{\text{propane},1}} U_{i_{\text{propane},1}} \right)^2 + \left(\frac{\partial i_{\text{propane},3}}{\partial \dot{Q}_{\text{pre}}} U_{\dot{Q}_{\text{pre}}} \right)^2 \qquad \text{(A.2)}$$
$$+ \left(\frac{\partial i_{\text{propane},3}}{\partial \dot{Q}_{\text{loss,2-to-3}}} U_{\dot{Q}_{\text{loss,2-to-3}}} \right)^2 + \left(\frac{\partial i_{\text{propane},3}}{\partial \dot{m}_{\text{propane}}} U_{\dot{m}_{\text{propane}}} \right)^2$$

Eq. (A.2) simplifies by differentiation to:

$$U_{i_{\text{propane},3}}^2 = U_{i_{\text{propane},1}}^2 + \left(-\frac{U_{\dot{Q}_{\text{pre}}}}{\dot{m}_{\text{propane}}} \right)^2 + \left(-\frac{U_{\dot{Q}_{\text{loss,2-to-3}}}}{\dot{m}_{\text{propane}}} \right)^2 + \left(\frac{\dot{Q}_{\text{pre}} + \dot{Q}_{\text{loss,2-to-3}}}{\dot{m}_{\text{propane}}^2} U_{\dot{m}_{\text{propane}}} \right)^2$$

The uncertainty in the ambient loss calculation is taken to be $\pm 25\%$, therefore

$U_{\dot{Q}_{\text{loss,2-to-3}}} = \pm 0.22 \text{ W}$. The enthalpy of the superheated vapor at the inlet of the pre-

condenser is a function of temperature and pressure. The partial derivative with respect to

pressure is two orders of magnitude smaller than the partial derivative with respect to

temperature. When multiplied by the associated uncertainties and squared, this

relationship is maintained. Therefore, for the sake of the current example, the uncertainty

due to pressure is considered negligible and the uncertainty in the propane enthalpy at the

inlet is estimated as follows:

$$U_{i_{\text{propane},1}}^2 = \left(\frac{\partial i_{\text{propane},1}}{\partial T_{\text{propane},1}} U_{T_{\text{propane},1}} \right)^2 = \left(c_{P,\text{propane}} U_{T_{\text{propane},1}} \right)^2 \qquad \text{(A.3)}$$

The uncertainty associated with the RTD temperature measurement is $\pm 0.2°\text{C}$; therefore,

the uncertainty in $i_{\text{propane},1}$ is ± 0.45 kJ kg^{-1}.

The pre-condenser heat duty is calculated from the increase in enthalpy on the air-side of the heat exchanger: $\dot{Q}_{pre} = \dot{m}_{air,pre}\left(i_{air,pre,out} - i_{air,pre,in}\right) + \dot{Q}_{1\text{-to-pre,loss}} + \dot{Q}_{pre,loss}$. The uncertainty in the pre-condenser heat duty is then:

$$U_{\dot{Q}_{pre}}^2 = \left(\frac{\partial\dot{Q}_{pre}}{\partial\dot{m}_{air,pre}}U_{\dot{m}_{air,pre}}\right)^2 + \left(\frac{\partial\dot{Q}_{pre}}{\partial i_{air,pre,in}}U_{i_{air,in}}\right)^2 \\ + \left(\frac{\partial\dot{Q}_{pre}}{\partial i_{air,pre,out}}U_{i_{air,in}}\right)^2 + \left(\frac{\partial\dot{Q}_{pre}}{\partial\dot{Q}_{losses}}U_{\dot{Q}_{losses}}\right)^2 \tag{A.4}$$

Eq. (A.4) simplifies by differentiation to:

$$U_{\dot{Q}_{pre}}^2 = \left(\Delta i_{air,pre}U_{\dot{m}_{air,pre}}\right)^2 + \left(-\dot{m}_{air,pre}U_{i_{air,in}}\right)^2 + \left(\dot{m}_{air,pre}U_{i_{air,in}}\right)^2 + U_{\dot{Q}_{losses}}^2$$

The uncertainty in the ambient losses is assumed to be ±25% or ±0.17 W. The dominant uncertainty in the air enthalpy is due to the temperature measurement. Therefore the uncertainty in the pre-condenser air inlet and outlet enthalpies takes a form similar to that of Eq. (A.3).

$$U_{i_{air,pre,in}}^2 = \left(c_{P,air}U_{T_{air,pre,in}}\right)^2 \tag{A.5}$$

$$U_{i_{air,pre,out}}^2 = \left(c_{P,air}U_{T_{air,pre,out}}\right)^2 \tag{A.6}$$

Because the air inlet and outlet temperatures in the pre-condenser are determined to be the average of an RTD measurement (±0.20°C uncertainty) and a thermocouple measurement (±0.50°C uncertainty), the overall uncertainty in the air temperature measurement is ±0.27°C as shown in Eq. (A.7).

$$U_{T_{air,pre}}^2 = \frac{1}{4}\left(U_{T_{air,pre,RTD}}^2 + U_{T_{air,pre,TC}}^2\right) \tag{A.7}$$

The air mass flow rate is calculated from the density and volumetric flow rate:
$\dot{m}_{air,pre} = \dot{V}_{air,pre}\rho_{air,pre}$. The uncertainty in the air mass flow rate is then:

$$U^2_{\dot{m}_{air,pre}} = \left(\frac{\partial \dot{m}_{air,pre}}{\partial \dot{V}_{air,pre}}U_{\dot{V}_{air,pre}}\right)^2 + \left(\frac{\partial \dot{m}_{air,pre}}{\partial \rho_{air,pre}}U_{\rho_{air,pre}}\right)^2 \tag{A.8}$$

By differentiation, Eq. (A.8) reduces to:

$$U^2_{\dot{m}_{air,pre}} = \left(\rho_{air,pre}U_{\dot{V}_{air,pre}}\right)^2 + \left(\dot{V}_{air,pre}U_{\rho_{air,pre}}\right)^2$$

The uncertainty in the volumetric flow rate is ±0.3% of the measurement or $\pm 5.903 \times 10^{-6}$ m^3 s^{-1}. The uncertainty in the air density at the flow meter is ±0.024 kg m^{-3} and is due to the contributions of temperature and pressure:

$$U^2_{\rho_{air,pre}} = \left(\frac{\partial \rho_{air,pre}}{\partial T_{air,pre}}U_{T_{air,pre}}\right)^2 + \left(\frac{\partial \rho_{air,pre}}{\partial P_{air,pre}}U_{P_{air,pre}}\right)^2 \tag{A.9}$$

The partial derivatives can be approximated by the following method, based on the change in density due to a small change in temperature and pressure δT and δP respectively.

$$\frac{\partial \rho}{\partial T} \approx \frac{\rho(T+\delta T, P) - \rho(T-\delta T, P)}{2\delta T} \tag{A.10}$$

$$\frac{\partial \rho}{\partial P} \approx \frac{\rho(T, P+\delta P) - \rho(T, P-\delta P)}{2\delta P} \tag{A.11}$$

Thus, the air mass flow rate uncertainty can be evaluated in Eq. (A.8) as $\pm 4.8 \times 10^{-5}$ kg s^{-1} (2.0%).

The uncertainties calculated in Eq. (A.2) to (A.9) can be used to determine the uncertainty in the test section inlet enthalpy:

$$U_{i_{\text{propane},3}} = \sqrt{U_{i_{\text{propane},1}}^2 + \left(-\frac{U_{\dot{Q}_{\text{pre}}}}{\dot{m}_{\text{propane}}}\right)^2 + \left(-\frac{U_{\dot{Q}_{\text{loss,2-to-3}}}}{\dot{m}_{\text{propane}}}\right)^2 + \left(\frac{\dot{Q}_{\text{pre}}+\dot{Q}_{\text{loss,2-to-3}}}{\dot{m}_{\text{propane}}^2}U_{\dot{m}_{\text{propane}}}\right)^2}$$

$$= \sqrt{\begin{array}{c}\left(0.45 \text{ kJ kg}^{-1}\right)^2 + \left(-\dfrac{1.33 \text{ W}}{2.932\times10^{-4} \text{ kg s}^{-1}}\right)^2 + \left(-\dfrac{0.22 \text{ W}}{2.932\times10^{-4} \text{ kg s}^{-1}}\right)^2 \\ + \left(\dfrac{46.71 \text{ W}+0.89 \text{ W}}{\left(2.932\times10^{-4} \text{ kg s}^{-1}\right)^2}\left(5.6\times10^{-7} \text{ kg s}^{-1}\right)\right)^2\end{array}}$$

$$= 4.64 \text{ kJ kg}^{-1}$$

The uncertainty in the test section outlet enthalpy is calculated in the same manner, replacing the pre-condenser terms with post-condenser terms. From this method, the uncertainty in the outlet enthalpy, $i_{\text{propane},4}$, is determined to be ±7.27 kJ kg^{-1}.

The uncertainty in the test section heat duty can then be evaluated from Eq. (A.1):

$$U_{\dot{Q}_{\text{test}}} = \sqrt{\left(\Delta i_{\text{propane,test}}U_{\dot{m}_{\text{propane}}}\right)^2 + \left(\dot{m}_{\text{propane}}U_{i_{\text{propane},3}}\right)^2 + \left(-\dot{m}_{\text{propane}}U_{i_{\text{propane},4}}\right)^2}$$

$$= \sqrt{\begin{array}{c}\underbrace{\left((77.12 \text{ kJ kg}^{-1})(5.6\times10^{-7} \text{ kg s}^{-1})\right)^2}_{0.03\%} + \underbrace{\left((2.932\times10^{-4} \text{ kg s}^{-1})(4.64 \text{ kJ kg}^{-1})\right)^2}_{29\%} \\ + \underbrace{\left((-2.932\times10^{-4} \text{ kg s}^{-1})(7.27 \text{ kJ kg}^{-1})\right)^2}_{71\%}\end{array}}$$

$$= 2.54 \text{ W } (11.2\%)$$

The uncertainty in the test section inlet and outlet qualities are determined from Eq. (A.12).

$$U_x^2 = \left(\frac{\partial x}{\partial i_{\text{propane}}}U_{i_{\text{ref}}}\right)^2 + \left(\frac{\partial x}{\partial P_{\text{propane}}}U_{P_{\text{propane}}}\right)^2 \tag{A.12}$$

The partial derivatives are approximated using an approach similar to that of Eq. (A.10) and (A.11). Thus the uncertainty in the test section inlet quality is ±0.02, and the

uncertainty in the outlet quality is ±0.02. The uncertainty in the average test section quality is then ±0.01 from Eq. (A.13):

$$U_{x_{\text{avg}}}^2 = \frac{1}{4}\left(U_{x_3}^2 + U_{x_4}^2\right) \tag{A.13}$$

A.2. **Uncertainty in Heat Transfer Coefficient**

The uncertainty in the heat transfer coefficient is a function of the LMTD, test section heat duty and the coupling fluid thermal resistance. The heat transfer coefficient can be expressed as $h_{\text{test,propane}} = 1/(R_{\text{test, propane}} A_{\text{HT}})$; therefore, the uncertainty can be expressed as:

$$U_{h_{\text{test,propane}}}^2 = \left(\frac{\partial h_{\text{test,propane}}}{\partial R_{\text{test,propane}}} U_{R_{\text{test,propane}}}\right)^2 \tag{A.14}$$

which simplifies by differentiation to:

$$U_{h_{\text{test,propane}}}^2 = \left(-\frac{1}{R_{\text{test,propane}}^2 A_{\text{HT}}} U_{R_{\text{test,propane}}}\right)^2$$

The thermal resistance of the condensing propane can be expressed as: $R_{\text{test,propane}} = \dot{Q}_{\text{test}} / \Delta T_{\text{LM}} - R_{\text{wall\&coupling}}$. The uncertainty is therefore calculated as in Eq. (A.15).

$$U_{R_{\text{test,propane}}}^2 = \left(\frac{\partial R_{\text{test,propane}}}{\partial \dot{Q}_{\text{test}}} U_{\dot{Q}_{\text{test}}}\right)^2$$
$$+ \left(\frac{\partial R_{\text{test,propane}}}{\partial \Delta T_{\text{LM}}} U_{\Delta T_{\text{LM}}}\right)^2 + \left(\frac{\partial R_{\text{test,propane}}}{\partial R_{\text{wall\&coupling}}} U_{R_{\text{wall\&coupling}}}\right)^2 \tag{A.15}$$

or when differentiated,

$$U^2_{R_{\text{test,propane}}} = \underbrace{\left(-\frac{\Delta T_{\text{LM}}}{\dot{Q}^2_{\text{test}}}U_{\dot{Q}_{\text{test}}}\right)^2}_{84\%} + \underbrace{\left(\frac{1}{\dot{Q}_{\text{test}}}U_{\Delta T_{\text{LM}}}\right)^2}_{3\%} + \underbrace{\left(-U_{R_{\text{wall\&coupling}}}\right)^2}_{33\%}$$

The uncertainty in the test section heat duty was calcualted in the previous section. The wall and coupling fluid resistances were assigned a combined uncertainty of $\pm25\%$ or ±0.02 K W^{-1}. The uncertainty in the LMTD can be expressed in terms of the two propane and two water RTD temperature measurements, each with uncertainties of $\pm0.20°$C. The uncertainty of the LMTD is then $\pm0.20°$C as well. The uncertainty in the propane thermal resistance is then ±0.08 K W^{-1}. Thus, Eq. (A.14) can be evaluated to yield the heat transfer coefficient uncertainty of ±457 W m^{-2} K^{-1} (13.6% of the calculated value, which is 3346 W m^{-2} K^{-1}).

A.3. **Pressure Drop Uncertainty**

The uncertainty in the frictional pressure drop is a function of the measured differential pressure, the minor losses, and the static head terms. The frictional pressure drop is calculated from Eq. (4.97).

$$\Delta P_{\text{frictional}} = \Delta P_{\text{measured}} - \Delta P_{\text{contraction}} + \Delta P_{\text{expansion}} + \left|\Delta P_{\text{deceleration}}\right| + \Delta P_{\text{static,test}} - \Delta P_{\text{static,line}}$$

Because this expression is a simple summation, the uncertainty can be expressed as:

$$U^2_{\Delta P_{\text{frictional}}} = U^2_{\Delta P_{\text{measured}}} + U^2_{\Delta P_{\text{contraction}}} + U^2_{\Delta P_{\text{expansion}}} + U^2_{\Delta P_{\text{deceleration}}} + U^2_{\Delta P_{\text{static,test}}} + U^2_{\Delta P_{\text{static,line}}} \qquad \text{(A.16)}$$

The uncertainty of the measured differential pressure is $\pm$ 0.0035 kPa. A $\pm$ 25% uncertainty is assumed for the contraction, expansion and deceleration pressure drop terms; therefore, $U_{\Delta P_{\text{contraction}}} = \pm32.25$ Pa, $U_{\Delta P_{\text{expansion}}} = \pm7.39$ Pa, and $U_{\Delta P_{\text{deceleration}}} = \pm20.85$ Pa .

The uncertainty in the static head in the pressure tap lines from the test section to the transducer is given in Eq. (A.17).

$$U^2_{\Delta P_{\text{static,line}}} = \left(\frac{\partial \Delta P_{\text{static,line}}}{\partial \Delta z} U_{\Delta z} \right)^2 + \left(\frac{\partial \Delta P_{\text{static,line}}}{\partial \rho_{\text{in}}} U_{\rho_{\text{in}}} \right)^2 + \left(\frac{\partial \Delta P_{\text{static,line}}}{\partial \rho_{\text{out}}} U_{\rho_{\text{out}}} \right)^2 \quad (A.17)$$

which simplifies to:

$$U^2_{\Delta P_{\text{static,line}}} = \left(g \left(\rho_{\text{propane,line,in,vertical,down}} - \rho_{\text{propane,line,out,vertical,down}} \right) U_{\Delta z} \right)^2$$
$$+ \left(g \Delta z_{\Delta P_3} U_{\rho_{\text{in}}} \right)^2 + \left(g \Delta z_{\Delta P_4} U_{\rho_{\text{out}}} \right)^2$$

The uncertainty in the height measurement is $\pm$ 1 mm, while the uncertainty in the density measurements is assumed to be 3% of the value ($\pm$ 14.3 kg m^{-3} and $\pm$ 14.5 kg m^{-3} for the inlet and outlet pressure tap lines respectively). Thus, the uncertainty in the pressure tap line static head is estimated to be $\pm$ 50.1 Pa.

The uncertainty in the two-phase static head in the test section is a function of the void fraction, liquid and vapor density and elevation change in the condensing sections and adiabatic inlet and outlet regions. Eq. (A.18) summarizes these contributions.

$$U^2_{\Delta P_{\text{static,test}}} = U^2_{\Delta P_{\text{static,test,in}}} + U^2_{\Delta P_{\text{static,test,HX}}} + U^2_{\Delta P_{\text{static,test,out}}} \quad (A.18)$$

The static head in the inlet adiabatic region is given by: $\Delta P_{\text{static,test,in}} = g \left(\alpha_{\text{test,in}} \rho_{\text{propane,test,in,v}} + (1 - \alpha_{\text{test,in}}) \rho_{\text{propane,test,in,l}} \right) L_{\text{test,entrance}}$. Therefore, the uncertainty can be expressed as in Eq. (A.19),

$$U^2_{\Delta P_{\text{static,test,in}}} = \left(\frac{\partial \Delta P_{\text{static,test,in}}}{\partial \alpha} U_{\alpha_{\text{in}}} \right)^2 + \left(\frac{\partial \Delta P_{\text{static,test,in}}}{\partial \rho_{\text{propane,test,l}}} U_{\rho_{\text{propane,test,in,l}}} \right)^2$$
$$+ \left(\frac{\partial \Delta P_{\text{static,test,in}}}{\partial \rho_{\text{propane,test,in,v}}} U_{\rho_{\text{propane,test,in,v}}} \right)^2 + \left(\frac{\partial \Delta P_{\text{static,test,in}}}{\partial L_{\text{entrance}}} U_{L_{\text{entrance}}} \right)^2 \quad (A.19)$$

which simplifies by differentiation to:

$$U^2{}_{\Delta P_{\text{static,test,in}}} = \underbrace{\left(g \left(\rho_{\text{propane,test,in,v}} - \rho_{\text{propane,test,in,l}} \right) L_{\text{test,entrance}} U_{\alpha_{\text{in}}} \right)^2}_{99.3\%}$$

$$+ \underbrace{\left(g \left(1 - \alpha_{\text{test,in}} \right) L_{\text{test,entrance}} U_{\rho_{\text{propane,test,in,l}}} \right)^2}_{0.6\%} + \underbrace{\left(g \alpha_{\text{test,in}} L_{\text{test,entrance}} U_{\rho_{\text{propane,test,in,v}}} \right)^2}_{0.07\%}$$

$$+ \underbrace{\left(g \left(\alpha_{\text{test,in}} \rho_{\text{propane,test,in,v}} + (1 - \alpha_{\text{test,in}}) \rho_{\text{propane,test,in,l}} \right) U_{L_{\text{entrance}}} \right)^2}_{0.03\%}$$

The uncertainty in the void fraction is assumed to be $\pm$ 25% of the calculated value, while the uncertainties of the density and length are $\pm$ 3% and $\pm$ 1 mm as before. As noted in the above equation, the void fraction is the dominant uncertainty in this calculation. Evaluating Eq. (A.19) yields an uncertainty of $\pm$ 84.0 Pa for the test section inlet static head. Similarly, the uncertainty in the static head in the outlet region of the test section is $\pm$ 81.2 Pa.

The uncertainty in the static head in the condensing region of the test section follows the same form as Eq. (A.19). The equation is simplified to only include the uncertainty due to the void fraction, and the uncertainty of the inlet void fraction is used.

$$U^2{}_{\Delta P_{\text{static,test,HX}}} = \left(\frac{\partial \Delta P_{\text{static,test,HX}}}{\partial \alpha} U_{\alpha} \right)^2 + \left(\frac{\partial \Delta P_{\text{static,test,HX}}}{\partial \rho_{\text{propane,test,l}}} U_{\rho_{\text{propane,test,l}}} \right)^2$$

$$+ \left(\frac{\partial \Delta P_{\text{static,test,HX}}}{\partial \rho_{\text{propane,test,v}}} U_{\rho_{\text{propane,test,v}}} \right)^2 + \left(\frac{\partial \Delta P_{\text{static,test,HX}}}{\partial \Delta z} U_{\Delta z} \right)^2$$

$$\approx \left(\frac{\partial \Delta P_{\text{static,test,HX}}}{\partial \alpha} U_{\alpha_{\text{in}}} \right)^2$$

$$= \left(g \left(\rho_{\text{propane,test,v}} - \rho_{\text{propane,test,l}} \right) L_{\text{test,annulus}} U_{\alpha_{\text{in}}} \right)^2$$

Therefore, the uncertainty in the static head in the condensing region is ± 49.1 Pa, and the overall uncertainty of the two-phase static head is ± 126.7 Pa. Thus Eq. (A.16) can be evaluated, resulting in an uncertainty in the frictional pressure drop of ± 142 Pa (19%).

Finally, the uncertainty in the frictional pressure gradient is calculated using Eq. (A.20).

$$U^2{}_{dP/dz} = \left(\frac{\partial (dP/dz)}{\partial \Delta P_{\mathrm{f}}} U_{\Delta P_{\mathrm{test,f}}} \right)^2 + \left(\frac{\partial (dP/dz)}{\partial L_{\mathrm{test},\Delta P}} U_{L_{\mathrm{test},\Delta P}} \right)^2 \qquad (A.20)$$

Eq. (A.20) simplifies by differentiation to:

$$U^2{}_{dP/dz} = \left(\frac{1}{L_{\mathrm{test},\Delta P}} U_{\Delta P_{\mathrm{test,f}}} \right)^2 + \left(-\frac{\Delta P_{\mathrm{test,f}}}{L_{\mathrm{test},\Delta P}^2} U_{L_{\mathrm{test},\Delta P}} \right)^2$$

The uncertainty in the test section length is ± 1 mm as before. The frictional pressure gradient uncertainty is calculated to be ± 0.743 kPa m^{-1} (19% of the measured value).

APPENDIX B:

COMPRESSED AIR HUMIDITY

The compressed air used as the coupling fluid for the pre- and post-condensers is outdoor air delivered through a compressor and dryer, and is cooled through the large shell-and-tube heat exchanger and a second dryer before being delivered to the pre- and post-condeners. Figure B.1 shows a schematic of the compressed air line. The following analysis describes an approximation of the upper bound of the humidity ratio at the pre- and post-condenser inlets.

The outside air conditions are approximated at 25°C, 100 kPa and 0.8 relative humidity. The humidity ratio, the mass fraction of water vapor to total air mass, is a function of these three quanities: $\omega_{outside} = 0.0162$. This ambient air passes through the compressor in which the back pressure can be varied depending on the desired load. The compressor back pressure is set at 100 psi (689 kPa). Because the humidity ratio is a mass fraction, this quantity remains constant through the compressor based on continuity. Assuming an isothermal process, the relative humidity of the compressed air is: $\phi_{compressor} = f(25°C, 689 \text{ kPa}, \omega_{outside} = 0.0162) = 5.52$. It is assumed that the excess water condenses out in the compressor, therefore the new relative humidity is $\phi_{compressor,out} = 1$.
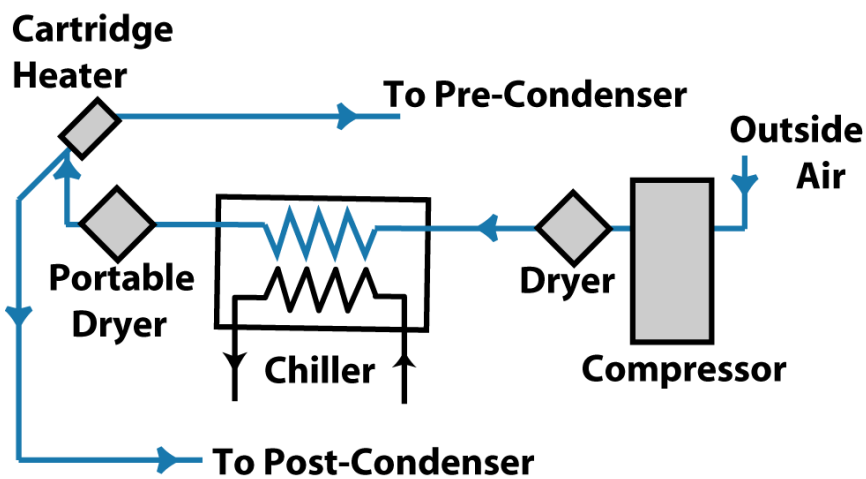
Figure B.1: Schematic showing the compressed air cooling loop

Therefore, the humidity ratio downstream of the compressor is $\omega_{\text{compressed-air}} = f(25°C, 689 \text{ kPa}, \phi_{\text{compressor,out}} = 1) = 0.0029$. The dew point of the air under these conditions is 24.98°C, therefore, more humidity condenses out with cooling.

An outlet temperature of 0°C at a pressure of about 250 kPa for the air exiting the large heat exchanger is considered here for the purpose of illustration. The dewpoint at these conditions is 9°C and the relative humidity is 1.88. Assuming the water condenses out in the heat exchanger leaving saturated air, the relative humidity is then $\phi_{\text{HX,out}} = 1$ and the dew point is reduced to 0°C. Therefore, the humidity ratio of the compressed air leaving the cooling heat exchanger is 0.00152. This is true regardless of the outside humidity because the analysis assumes that the excess water vapor condenses out at the condenser leaving saturated air. The result is insensitive to the assumed outlet pressure. While the humidity ratio does change to some extent with varying outlet temperature, the pressure drop and heat transfer coefficient data are relatively insensitive to this value. For the purpose of illustration, if a value of 0.006 is used for ω, the pressure drop and heat transfer coefficients calculated in the analysis change by less than 1% (well within the range of experimental uncertainty). Therefore, the value of $\omega = 0.00152$ was assumed to apply to all compressed air inlet conditions.

APPENDIX C:

SAMPLE CALCULATION

C.1. Calculation of Condensation Heat Duty and Average Quality

C.1.1 Pre-Condenser Energy Balance

Propane In-Tube Condensation, 9 September 2013, Run 7		
Inputs	**Equations**	**Results**
$\dot{m}_{propane} = 2.932\times10^{-4}\ \text{kg s}^{-1}$ $D_{test,in} = 1.93\ \text{mm}$	$G_{propane} = \dfrac{\dot{m}_{propane}}{\pi D_{test,in}^{\ 2}/4}$	$G_{propane} = 100.2\ \text{kg m}^{-2}\ \text{s}^{-1}$
Pre-Condenser Energy Balance (Figure 4.1)		
$T_{air,pre,in,RTD} = 31.52°C$ $T_{air,pre,in,TC} = 31.27°C$ $T_{air,pre,out,RTD} = 48.36°C$ $T_{air,pre,out,TC} = 48.32°C$	$T_{air,pre,in} = \dfrac{T_{air,pre,in,RTD} + T_{air,pre,in,TC}}{2}$ $T_{air,pre,out} = \dfrac{T_{air,pre,out,RTD} + T_{air,pre,out,TC}}{2}$	$T_{air,pre,in} = 31.39°C$ $T_{air,pre,out} = 48.34°C$
Fluid = air $T_{air,pre,flow} = 31.23°C$ $T_{air,pre,in} = 31.39°C$ $T_{air,pre,out} = 48.34°C$ $P_{air,pre} = 119.40\ \text{kPa}$ $P_{amb} = 93\ \text{kPa}$ $\omega = 0.00152$	$\rho_{air,pre,flow} = f\left(P_{air,pre}, T_{air,pre,flow}, \omega\right)$ $i_{air,pre,in} = f\left(P_{air,pre}, T_{air,pre,in}, \omega\right)$ $i_{air,pre,out} = f\left(P_{amb}, T_{air,pre,out}, \omega\right)$	$\rho_{air,pre,flow} = 1.365\ \text{kg m}^{-3}$ $i_{air,pre,in} = 308.3\ \text{kJ kg}^{-1}$ $i_{air,pre,out} = 325.4\ \text{kJ kg}^{-1}$

Propane In-Tube Condensation, 9 September 2013, Run 7		
Inputs	**Equations**	**Results**
$\dot{V}_{\text{air,pre}} = 1.968 \times 10^{-3} \text{ m}^3 \text{ s}^{-1}$ $\rho_{\text{air,pre,flow}} = 1.365 \text{ kg m}^{-3}$	$\dot{m}_{\text{air,pre}} = \dot{V}_{\text{air,pre}} \rho_{\text{air,pre,flow}}$	$\dot{m}_{\text{air,pre}} = 2.686 \times 10^{-3} \text{ kg s}^{-1}$
$i_{\text{air,pre,in}} = 291.1 \text{ kJ kg}^{-1}$ $i_{\text{air,pre,out}} = 314.1 \text{ kJ kg}^{-1}$ $\dot{m}_{\text{air,pre}} = 2.686 \times 10^{-3} \text{ kg s}^{-1}$ $\dot{Q}_{\text{1-to-pre,loss}} = 0.21 \text{ W}$ $\dot{Q}_{\text{pre,loss}} = 0.45 \text{ W}$	$\dot{Q}_{\text{pre}} = \dot{m}_{\text{air,pre}} \left(i_{\text{air,pre,out}} - i_{\text{air,pre,in}} \right) + \dot{Q}_{\text{1-to-pre,loss}} + \dot{Q}_{\text{pre,loss}}$	$\dot{Q}_{\text{pre,air}} = 46.71 \text{ W}$
Fluid = Propane $P_{\text{propane,1}} = 1615.7 \text{ kPa}$ $T_{\text{propane,1}} = 82.91°\text{C}$ $\dot{m}_{\text{propane}} = 2.932 \times 10^{-4} \text{ kg s}^{-1}$ $\dot{Q}_{\text{pre,air}} = 46.71 \text{ W}$ $\dot{Q}_{\text{loss,2-to-3}} = 0.89 \text{ W}$	$T_{\text{sat,propane,1}} = f\left(P_{\text{propane,1}}\right)$ $\Delta T_{\text{sup}} = T_{\text{propane,1}} - T_{\text{sat,propane,1}}$ $i_{\text{propane,1}} = f\left(T_{\text{propane,1}}, P_{\text{propane,1}}\right)$ $i_{\text{propane,2}} = i_{\text{propane,1}} - \dfrac{\dot{Q}_{\text{pre}}}{\dot{m}_{\text{propane}}}$ $i_{\text{propane,3}} = i_{\text{propane,2}} - \dfrac{\dot{Q}_{\text{loss,2-to-3}}}{\dot{m}_{\text{propane}}}$	$T_{\text{sat,propane,1}} = 47.32°\text{C}$ $\Delta T_{\text{sup}} = 35.58°\text{C}$ $i_{\text{propane,1}} = 700.8 \text{ kJ kg}^{-1}$ $i_{\text{propane,2}} = 541.5 \text{ kJ kg}^{-1}$ $i_{\text{propane,3}} = 538.5 \text{ kJ kg}^{-1}$
Fluid = Propane $P_{\text{propane,3}} = 1607.1 \text{ kPa}$ $\Delta z_{P3} = 202 \text{ mm}$	$\rho_{\text{propane,v,3}} = f\left(P_{\text{propane,3,adj.}}, x = 1\right)$ $P_{\text{propane,3,adj.}} = P_{\text{propane,3}} + \rho_{\text{propane,v,3}} g \Delta z_{P_3}$	$P_{\text{propane,adj,3}} = 1607.2 \text{ kPa}$ $\rho_{\text{propane,v,3}} = 35.95 \text{ kg m}^{-3}$

Propane In-Tube Condensation, 9 September 2013, Run 7		
Inputs	**Equations**	**Results**
$g = 9.81$ m s^{-2}		
$i_{\text{propane},3} = 538.5$ kJ kg^{-1} $P_{\text{propane,adj},3} = 1607.2$ kPa	$x_3 = f\left(i_{\text{propane},3}, P_{\text{propane,adj},3}\right)$	$x_3 = 0.72$
Heat Loss Between Propane Measurement 1 and the Pre-Condenser (Figure 4.4)		
Fluid = Propane $P_{\text{propane},1} = 1615.7$ kPa $T_{\text{propane},1} = 82.91°C$	$\mu_{\text{propane,pre,in}}, k_{\text{propane,pre,in}}, \text{Pr}_{\text{propane,pre,in}} = f\left(P_{\text{propane},1}, T_{\text{propane},1}\right)$	$\mu_{\text{propane,pre,in}} = 1.01 \times 10^{-5}$ kg m^{-1} s^{-1} $k_{\text{propane,pre,in}} = 0.027$ W m^{-1} K^{-1} $\text{Pr}_{\text{propane,pre,in}} = 0.835$
$G_{\text{propane}} = 100.2$ kg m^{-2} s^{-1} $D_{\text{line,in}} = 4.57$ mm $\mu_{\text{propane,pre,in}} = 1.01 \times 10^{-5}$ kg m^{-1} s^{-1}	$\text{Re}_{\text{1-to-pre,propane}} = \dfrac{G_{\text{propane}} D_{\text{line,in}}}{\mu_{\text{propane,pre,in}}}$	$\text{Re}_{\text{1-to-pre,propane}} = 8094$

Propane In-Tube Condensation, 9 September 2013, Run 7		
Inputs	**Equations**	**Results**
$\mathrm{Re}_{\text{1-to-pre,propane}} = 8094$ $e = 0.0015$ mm $D_{\text{line,in}} = 4.57$ mm	$$f = 8\left(\left(\frac{8}{\mathrm{Re}_{\text{1-to-pre,propane}}}\right)^{12} + \frac{1}{(B+C)^{1.5}}\right)^{1/12}$$ where $B = \left(2.457\ln\dfrac{1}{(7/\mathrm{Re}_{\text{1-to-pre,propane}})^{0.9} + 0.27(e/D_{\text{line,in}})}\right)^{16}$ and $$C = \left(\frac{37530}{\mathrm{Re}_{\text{1-to-pre,propane}}}\right)^{16}$$ (Churchill, 1977b)	$f = 0.033$
$\mathrm{Re}_{\text{1-to-pre,propane}} = 8094$ $\mathrm{Pr}_{\text{propane,pre,in}} = 0.835$ $f = 0.033$ $k_{\text{propane,pre,in}} = 0.027$ W m^{-1} K^{-1} $D_{\text{line,in}} = 4.57$ mm	$$\mathrm{Nu} = \left(4.364^{10} + \left(\frac{e^{\frac{2200-\mathrm{Re}}{365}}}{4.364^2} + \frac{1}{\left(6.3 + \dfrac{0.079\left(\frac{f}{8}\right)^{0.5}\mathrm{Re}\,\mathrm{Pr}}{\left(1+\mathrm{Pr}^{0.8}\right)^{5/6}}\right)^2}\right)^{-5}\right)^{1/10}$$ $$h_{\text{propane,1-to-pre}} = \frac{Nu_{\text{propane,1-to-pre}}k_{\text{propane,pre,in}}}{D_{\text{line,in}}}$$	$\mathrm{Nu} = 26.82$ $h_{\text{propane,1-to-pre}} = 157.2$ W m^{-2} K^{-1}

Propane In-Tube Condensation, 9 September 2013, Run 7		
Inputs	**Equations**	**Results**
	(Churchill, 1977a)	
$h_{\text{propane,1-to-pre}} = 157.2 \text{ W m}^{-2} \text{ K}^{-1}$ $D_{\text{line,in}} = 4.57 \text{ mm}$ $L_{\text{1-to-pre}} = 65 \text{ mm}$	$$R_{\text{1-to-pre,ref}} = \frac{1}{h_{\text{propane,1-to-pre}} \pi D_{\text{line,in}} L_{\text{1-to-pre}}}$$	$R_{\text{1-to-pre,propane}} = 6.81 \text{ K W}^{-1}$
$D_{\text{line,in}} = 4.57 \text{ mm}$ $D_{\text{line,out}} = 6.35 \text{ mm}$ $L_{\text{1-to-pre}} = 65 \text{ mm}$ $T_{\text{line,wall,out}} = 81.49°\text{C}^{*}$	Tube wall conduction resistance: $$k_{\text{SS316}} = f\left(T_{\text{line,wall,out}}\right)$$ $$R_{\text{1-to-pre,wall}} = \frac{\ln(D_{\text{line,out}} / D_{\text{line,in}})}{2\pi k_{\text{SS316}} L_{\text{1-to-pre}}}$$	$k_{\text{SS316}} = 14.4 \text{ W m}^{-1} \text{ K}^{-1}$ $R_{\text{1-to-pre,wall}} = 0.0559 \text{ K W}^{-1}$
$D_{\text{insulation,tube,in}} = 25 \text{ mm}$ $D_{\text{line,out}} = 6.35 \text{ mm}$ $k_{\text{insulation,wrap}} = 0.0432 \text{ W m}^{-1} \text{ K}^{-1}$ $L_{\text{1-to-pre}} = 65 \text{ mm}$	Soft wrap insulation conduction resistance: $$R_{\text{1-to-pre,insulation,wrap}} = \frac{\ln(D_{\text{insulation,tube,in}} / D_{\text{line,out}})}{2\pi k_{\text{insulation,wrap}} L_{\text{1-to-pre}}}$$	$R_{\text{1-to-pre,insulation,wrap}} = 77.67 \text{ K W}^{-1}$
$D_{\text{insulation,tube,out}} = 87 \text{ mm}$ $D_{\text{insulation,tube,in}} = 25 \text{ mm}$ $k_{\text{insulation,tube}} = 0.019 \text{ W m}^{-1} \text{ K}^{-1}$ $L_{\text{1-to-pre}} = 65 \text{ mm}$	Tube insulation conduction resistance: $$R_{\text{1-to-pre,insulation,tube}} = \frac{\ln(D_{\text{insulation,tube,out}} / D_{\text{insulation,tube,in}})}{2\pi k_{\text{insulation,tube}} L_{\text{1-to-pre}}}$$	$R_{\text{1-to-pre,insulation,tube}} = 160.7 \text{ K W}^{-1}$

Propane In-Tube Condensation, 9 September 2013, Run 7		
Inputs	**Equations**	**Results**
$\epsilon_{ins} = 0.9$ $\sigma = 5.67 \times 10^{-8}$ W m^{-2} K^{-4} $T_{amb} = 303.86$ K $T_{1\text{-to-pre,insulation,surface}} = 305.31$ K* $D_{insulation,tube,out} = 87$ mm $L_{1\text{-to-pre}} = 65$ mm	Radiation resistance: $$h_{rad} = \epsilon_{ins}\sigma\left(T_{insulation,surface}^2 + T_{amb}^2\right)\left(T_{insulation,surface} + T_{amb}\right)$$ $$R_{1\text{-to-pre,rad}} = \frac{1}{\pi D_{insulation,tube,out} L_{1\text{-to-pre}} h_{1\text{-to-pre,rad}}}$$	$h_{1\text{-to-pre,rad}} = 5.77$ W m^{-2} K^{-1} $R_{1\text{-to-pre,rad}} = 9.76$ K W^{-1}
$T_{amb} = 30.71°C$ $T_{1\text{-to-pre,insulation,surface}} = 32.16°C^{*}$ $R_{1\text{-to-pre,rad}} = 9.76$ K W^{-1}	$$\dot{Q}_{1\text{-to-pre,rad}} = \frac{T_{amb} - T_{1\text{-to-pre,insulation,surface}}}{R_{1\text{-to-pre,rad}}}$$	$\dot{Q}_{1\text{-to-pre,rad}} = 0.15$ W
Fluid = air $T_{amb} = 30.71°C$ $T_{1\text{-to-pre,insulation,surface}} = 32.16°C^{*}$ $P_{amb} = 101$ kPa	$$T_{film} = \frac{T_{amb} + T_{insulation,surface}}{2}$$ $\rho_{air}, \mu_{air}, c_{p,air}, k_{air} = f\left(T_{film}, P_{amb}\right)$ $\beta_{air} = f\left(T_{film}\right)$ $$\alpha_{air} = \frac{k_{air}}{\rho_{air} c_{p,air}}$$ $$\text{Pr}_{air} = \frac{c_{p,air}\mu_{air}}{k_{air}}$$	$T_{1\text{-to-pre,film}} = 31.43°C$ $\rho_{air} = 1.16$ kg m^{-3} $\mu_{air} = 1.88 \times 10^{-5}$ kg m^{-1} s^{-1} $c_{p,air} = 1007$ J kg^{-1} K^{-1} $k_{air} = 0.026$ W m^{-1} K^{-1} $\beta_{air} = 3.3 \times 10^{-3}$ K^{-1} $\alpha_{air} = 2.26 \times 10^{-5}$ m^2 s^{-1} $\text{Pr}_{air} = 0.719$

Propane In-Tube Condensation, 9 September 2013, Run 7		
Inputs	**Equations**	**Results**
$\rho_{air} = 1.16$ kg m^{-3} $\mu_{air} = 1.88 \times 10^{-5}$ kg m^{-1} s^{-1} $\beta_{air} = 3.3 \times 10^{-3}$ K^{-1} $\alpha_{air} = 2.26 \times 10^{-5}$ m^2 s^{-1} $T_{amb} = 30.71$°C $T_{1\text{-to-pre,insulation,surface}} = 32.16$°C* $D_{insulation,tube,out} = 87$ mm $g = 9.81$ m s^{-2}	$$\mathrm{Ra}_D = \frac{\rho_{air}\, g\, \beta_{air}\, \left| T_{insulation,surface} - T_{amb} \right| D_{insulation,tube,out}^3}{\mu_{air}\,\alpha_{air}}$$	$\mathrm{Ra}_{D,1\text{-to-pre}} = 84136$
$\mathrm{Ra}_{D,1\text{-to-pre}} = 84136$ $\mathrm{Pr}_{air} = 0.719$ $k_{air} = 0.026$ W m^{-1} K^{-1} $D_{insulation,tube,out} = 87$ mm	Natural convection from horizontal tube $$\mathrm{Nu}_{nat.conv.} = \left(0.60 + \frac{0.387\mathrm{Ra}_D^{1/6}}{\left(1 + \left(\frac{0.559}{\mathrm{Pr}} \right)^{9/16} \right)^{8/27}} \right)^2$$ $$h_{nat.conv.} = \frac{\mathrm{Nu}_{nat.conv.} \cdot k_{air}}{D_{insulation,tube,out}}$$ (Churchill and Chu, 1975a)	$\mathrm{Nu}_{nc,1\text{-to-pre}} = 7.45$ $h_{nc,1\text{-to-pre}} = 2.25$ W m^{-2} K^{-1}
$D_{insulation,tube,out} = 87$ mm	Natural Convection Resistance	$R_{1\text{-to-pre,nc}} = 24.98$ K W^{-1}

Propane In-Tube Condensation, 9 September 2013, Run 7		
Inputs	**Equations**	**Results**
$L_{\text{1-to-pre}} = 65$ mm $h_{\text{nc,1-to-pre}} = 2.25$ W m^{-2} K^{-1}	$R_{\text{1-to-pre,nc}} = \dfrac{1}{\pi D_{\text{insulation,tube,out}} L_{\text{1-to-pre}} h_{\text{1-to-pre,nc}}}$	
$T_{\text{amb}} = 30.71°C$ $T_{\text{1-to-pre,insulation,surface}} = 32.16°C^{*}$ $R_{\text{1-to-pre,nc}} = 24.98$ K W^{-1}	$\dot{Q}_{\text{1-to-pre,nc}} = \dfrac{T_{\text{amb}} - T_{\text{1-to-pre,insulation,surface}}}{R_{\text{1-to-pre,nc}}}$	$\dot{Q}_{\text{1-to-pre,nc}} = 0.06$ W
$T_{\text{propane,1}} = 82.91°C$ $T_{\text{amb}} = 30.71°C$ $R_{\text{1-to-pre,propane}} = 6.81$ K W^{-1} $R_{\text{1-to-pre,wall}} = 0.0559$ K W^{-1} $R_{\text{1-to-pre,insulation,wrap}} = 77.67$ K W^{-1} $R_{\text{1-to-pre,insulation,tube}} = 160.7$ K W^{-1} $R_{\text{1-to-pre,rad}} = 9.76$ K W^{-1} $R_{\text{1-to-pre,nc}} = 24.98$ K W^{-1}	$\dot{Q}_{\text{1-to-pre,loss}} = \dfrac{T_{\text{ref,1}} - T_{\text{1-to-pre,insulation,surface}}}{\begin{array}{c} R_{\text{1-to-pre,ref}} + R_{\text{1-to-pre,wall}} \\ + R_{\text{1-to-pre,insulation,wrap}} + R_{\text{1-to-pre,insulation,tube}} \end{array}}$ $\dot{Q}_{\text{1-to-pre,loss}} = \left(T_{\text{1-to-pre,insulation,surface}} - T_{\text{amb}} \right) \left(\dfrac{1}{R_{\text{1-to-pre,rad}}} + \dfrac{1}{R_{\text{1-to-pre,nc}}} \right)$	$T_{\text{1-to-pre,insulation,surface}} = 32.16°C^{*}$ $\dot{Q}_{\text{1-to-pre,loss}} = 0.21$ W

Propane In-Tube Condensation, 9 September 2013, Run 7		
Inputs	**Equations**	**Results**
Heat Loss from the Pre-Condenser (Figure 4.5)		
Fluid = Air $T_{air,pre,in} = 31.39°C$ $T_{air,pre,out} = 48.34°C$ $P_{air,pre} = 119.40 \text{ kPa}$ $P_{amb} = 93 \text{ kPa}$ $\omega = 0.00152$	$T_{air,pre,avg} = \dfrac{T_{air,pre,in} + T_{air,pre,out}}{2}$ $\mu_{air,pre,in}, k_{air,pre,in}, \text{Pr}_{air,pre,in} = f\left(P_{air,pre}, T_{air,pre,in}, \omega\right)$ $\mu_{air,pre,out}, k_{air,pre,out}, \text{Pr}_{air,pre,out} = f\left(P_{amb}, T_{air,pre,out}, \omega\right)$ $\mu_{air,pre}, k_{air,pre}, \text{Pr}_{air,pre} = f\left(P_{air,pre}, T_{air,pre,avg}, \omega\right)$	$T_{air,pre,avg} = 39.87°C$ $\mu_{air,pre,in} = 1.88 \times 10^{-5} \text{ kg m}^{-1} \text{ s}^{-1}$ $k_{air,pre,in} = 0.026 \text{ W m}^{-1} \text{ K}^{-1}$ $\text{Pr}_{air,pre,in} = 0.716$ $\mu_{air,pre,out} = 1.96 \times 10^{-5} \text{ kg m}^{-1} \text{ s}^{-1}$ $k_{air,pre,out} = 0.028 \text{ W m}^{-1} \text{ K}^{-1}$ $\text{Pr}_{air,pre,out} = 0.714$ $\mu_{air,pre} = 1.92 \times 10^{-5} \text{ kg m}^{-1} \text{ s}^{-1}$ $k_{air,pre} = 0.027 \text{ W m}^{-1} \text{ K}^{-1}$ $\text{Pr}_{air,pre} = 0.715$
$\dot{m}_{air,pre} = 2.686 \times 10^{-3} \text{ kg s}^{-1}$ $D_{Cu,line,in} = 14.25 \text{ mm}$ $\mu_{air,pre,in} = 1.88 \times 10^{-5} \text{ kg m}^{-1} \text{ s}^{-1}$ $\mu_{air,pre,out} = 1.96 \times 10^{-5} \text{ kg m}^{-1} \text{ s}^{-1}$	$\text{Re}_{air,pre,in/out} = \dfrac{4\dot{m}_{air,pre}}{\pi \mu_{ref,pre,in/out} D_{Cu,line,in}}$	$\text{Re}_{air,pre,in} = 12775$ $\text{Re}_{air,pre,in} = 12253$

Propane In-Tube Condensation, 9 September 2013, Run 7		
Inputs	**Equations**	**Results**
$\mathrm{Re}_{air,pre,in}= 12775$ $\mathrm{Re}_{air,pre,in}= 12253$ $e = 0.005$ mm $D_{Cu,line,in} = 14.25$ mm	$$f = 8\left(\left(\frac{8}{\mathrm{Re}}\right)^{12} + \frac{1}{(B+C)^{1.5}}\right)^{1/12}$$ where $B = \left(2.457\ln\dfrac{1}{(7/\mathrm{Re})^{0.9}+0.27(e/D_{line,in})}\right)^{16}$ and $$C = \left(\frac{37530}{\mathrm{Re}}\right)^{16}$$ (Churchill, 1977b)	$f_{air,pre,in} = 0.030$ $f_{air,pre,out} = 0.030$
$\mathrm{Re}_{air,pre,in}= 12775$ $\mathrm{Re}_{air,pre,in}= 12253$ $f_{air,pre,in} = 0.030$ $f_{air,pre,out} = 0.030$ $k_{air,pre,in} = 0.026$ W m^{-1} K^{-1} $k_{air,pre,out} = 0.028$ W m^{-1} K^{-1} $D_{Cu,line,in} = 14.25$ mm	$$\mathrm{Nu} = \left(4.364^{10} + \left(\frac{e^{\frac{2200-\mathrm{Re}}{365}}}{4.364^2} + \frac{1}{\left(6.3 + \frac{0.079\left(\frac{f}{8}\right)^{0.5}\mathrm{Re}\,\mathrm{Pr}}{\left(1+\mathrm{Pr}^{0.8}\right)^{5/6}}\right)^2}\right)^{-5}\right)^{1/10}$$ $$h_{air,pre,in/out} = \frac{Nu_{air,pre,in/out}\, k_{air,pre,in/out}}{D_{Cu,line,in}}$$	$\mathrm{Nu}_{air,pre,in} = 33.71$ $\mathrm{Nu}_{air,pre,out} = 32.67$ $h_{air,pre,in} = 62.62$ W m^{-2} K^{-1} $h_{air,pre,out} = 63.49$ W m^{-2} K^{-1}

Propane In-Tube Condensation, 9 September 2013, Run 7		
Inputs	**Equations**	**Results**
	(Churchill, 1977a)	
$p_{t,pre} = 4.58$ mm $D_{pre,tube,o} = 3.82$ mm $L_{pre} = 275$ mm $N_{b,pre} = 14$ $D_{pre,shell,in} = 22.9$ mm	Exergy 00540-5 Shell and Tube Heat Exchanger $C_{pre} = p_{t,pre} - D_{pre,tube,o}$ $B_{pre} = L_{pre} / N_{b,pre}$ $A_{pre,s} = \dfrac{D_{pre,shell,in} C_{pre} B_{pre}}{p_{t,pre}}$ $D_{pre,e} = \dfrac{3.44 p_{t,pre}^{2}}{\pi D_{pre,tube,o}} - D_{pre,tube,o}$	$C_{pre} = 0.76$ mm $B_{pre} = 19.6$ mm $A_{pre,s} = 74.6$ mm^2 $D_{pre,e} = 2.2$ mm
$\dot{m}_{air,pre} = 2.686 \times 10^{-3}$ kg s^{-1} $A_{pre,s} = 74.6$ mm^2 $D_{pre,e} = 2.2$ mm $\mu_{air,pre} = 1.92 \times 10^{-5}$ kg m^{-1} s^{-1}	$\mathrm{Re}_{pre,shell} = \dfrac{\dot{m}_{air,pre} D_{pre,e}}{\mu_{air} A_{pre,s}}$	$\mathrm{Re}_{pre,shell} = 4111$
$\mathrm{Re}_{pre,shell} = 4111$ $\mathrm{Pr}_{air,pre} = 0.715$ $k_{air,pre} = 0.027$ W m^{-1} K^{-1} $D_{pre,e} = 2.2$ mm	$\mathrm{Nu}_{pre,shell} = 0.36 \, \mathrm{Re}_{pre,shell}^{0.55} \, \mathrm{Pr}_{air,pre}^{1/3}$ $h_{pre,shell} = \dfrac{\mathrm{Nu}_{pre,shell} k_{air,pre}}{D_{pre,e}}$	$\mathrm{Nu}_{pre,shell} = 31.29$ $h_{pre,shell} = 386.5$ W m^{-2} K^{-1}
$h_{air,pre,in} = 62.62$ W m^{-2} K^{-1} $h_{pre,shell} = 386.5$ W m^{-2} K^{-1}	$R_{air} = \dfrac{1}{h_{air} \pi D_{wall,in} L}$	$R_{pre,in,air} = 2.34$ K W^{-1} $R_{pre,HX,air} = 0.13$ K W^{-1}

Propane In-Tube Condensation, 9 September 2013, Run 7		
Inputs	**Equations**	**Results**
$h_{\text{air,pre,out}} = 63.49 \text{ W m}^{-2} \text{ K}^{-1}$ $D_{\text{Cu,line,in}} = 14.25 \text{ mm}$ $D_{\text{pre,shell,in}} = 22.9 \text{ mm}$ $L_{\text{pre,air}} = 154.2 \text{ mm}$ $L_{\text{pre}} = 275 \text{ mm}$		$R_{\text{pre,out,air}} = 2.31 \text{ K W}^{-1}$
$D_{\text{Cu,line,in}} = 14.25 \text{ mm}$ $D_{\text{Cu,line,out}} = 15.88 \text{ mm}$ $D_{\text{pre,shell,in}} = 22.9 \text{ mm}$ $D_{\text{pre,shell,out}} = 25.4 \text{ mm}$ $L_{\text{pre,air}} = 154.2 \text{ mm}$ $L_{\text{pre}} = 275 \text{ mm}$ $T_{\text{pre,in,wall,out}} = 31.38°\text{C}^{*}$ $T_{\text{pre,shell,wall,out}} = 39.84°\text{C}^{*}$ $T_{\text{pre,in,wall,out}} = 47.86°\text{C}^{*}$	Tube wall conduction resistance: $k_{\text{Cu,in/out}} = f\left(T_{\text{wall,out}}\right)$ $R_{\text{wall}} = \dfrac{\ln(D_{\text{wall,out}} / D_{\text{wall,in}})}{2\pi k_{\text{wall}} L}$	$k_{\text{Cu,in}} = 396.0 \text{ W m}^{-1} \text{ K}^{-1}$ $k_{\text{Cu,out}} = 395.0 \text{ W m}^{-1} \text{ K}^{-1}$ $k_{\text{SS316}} = 13.67 \text{ W m}^{-1} \text{ K}^{-1}$ $R_{\text{pre,in,wall}} = 2.84 \times 10^{-4} \text{ K W}^{-1}$ $R_{\text{pre,HX,wall}} = 4.47 \times 10^{-3} \text{ K W}^{-1}$ $R_{\text{pre,out,wall}} = 2.85 \times 10^{-4} \text{ K W}^{-1}$
$D_{\text{insulation,tube,in}} = 25 \text{ mm}$ $D_{\text{Cu,line,out}} = 15.88 \text{ mm}$ $k_{\text{insulation,wrap}} = 0.0432 \text{ W m}^{-1} \text{ K}^{-1}$ $L_{\text{pre,air}} = 154.2 \text{ mm}$	Soft wrap insulation conduction resistance: $R_{\text{insulation,wrap}} = \dfrac{\ln(D_{\text{insulation,tube,in}} / D_{\text{wall,out}})}{2\pi k_{\text{insulation,wrap}} L}$	$R_{\text{pre,air,insulation,wrap}} = 10.98 \text{ K W}^{-1}$

Propane In-Tube Condensation, 9 September 2013, Run 7		
Inputs	**Equations**	**Results**
$D_{\text{insulation,tube,out}} = 87$ mm $D_{\text{insulation,tube,in}} = 25$ mm $k_{\text{insulation,tube}} = 0.019$ W m^{-1} K^{-1} $L_{\text{pre,air}} = 154.2$ mm $L_{\text{pre}} = 275$ mm	Tube insulation conduction resistance: $$R_{\text{insulation,tube}} = \frac{\ln(D_{\text{insulation,tube,out}} / D_{\text{insulation,tube,in}})}{2\pi k_{\text{insulation,tube}} L}$$	$R_{\text{pre,air,insulation,tube}} = 68.54$ K W^{-1} $R_{\text{pre,HX,insulation,tube}} = 37.98$ K W^{-1}
$\epsilon_{\text{ins}} = 0.9$ $\sigma = 5.67 \times 10^{-8}$ W m^{-2} K^{-4} $T_{\text{amb}} = 303.86$ K $T_{\text{pre,in,insulation,surface}} = 303.88$ K* $T_{\text{pre,HX,insulation,surface}} = 304.27$ K* $T_{\text{pre,out,insulation,surface}} = 304.49$ K* $D_{\text{insulation,tube,out}} = 87$ mm $L_{\text{pre,air}} = 154.2$ mm $L_{\text{pre}} = 275$ mm	Radiation resistance: $$h_{\text{rad}} = \epsilon_{\text{ins}} \sigma \left(T_{\text{insulation,surface}}^2 + T_{\text{amb}}^2 \right) \left(T_{\text{insulation,surface}} + T_{\text{amb}} \right)$$ $$R_{\text{rad}} = \frac{1}{\pi D_{\text{insulation,tube,out}} L h_{\text{rad}}}$$	$h_{\text{pre,in,rad}} = 5.73$ W m^{-2} K^{-1} $h_{\text{pre,HX,rad}} = 5.74$ W m^{-2} K^{-1} $h_{\text{pre,out,rad}} = 5.74$ W m^{-2} K^{-1} $R_{\text{pre,in,rad}} = 4.19$ K W^{-1} $R_{\text{pre,HX,rad}} = 2.32$ K W^{-1} $R_{\text{pre,out,rad}} = 4.18$ K W^{-1}

Propane In-Tube Condensation, 9 September 2013, Run 7		
Inputs	**Equations**	**Results**
$T_{amb} = 30.71°C$ $T_{pre,in,insulation,surface} = 30.73°C^{*}$ $T_{pre,HX,insulation,surface} = 31.12°C^{*}$ $T_{pre,out,insulation,surface} = 31.34°C^{*}$ $R_{pre,in,rad} = 4.19$ K W^{-1} $R_{pre,HX,rad} = 2.32$ K W^{-1} $R_{pre,out,rad} = 4.18$ K W^{-1}	$$\dot{Q}_{pre,in,rad} = \frac{T_{amb} - T_{pre,in,insulation,surface}}{R_{pre,in,rad}}$$ $$\dot{Q}_{pre,HX,rad} = \frac{T_{amb} - T_{pre,HX,insulation,surface}}{R_{pre,HX,rad}}$$ $$\dot{Q}_{pre,out,rad} = \frac{T_{amb} - T_{pre,in,insulation,surface}}{R_{pre,out,rad}}$$	$\dot{Q}_{pre,in,rad} = 0.01$ W $\dot{Q}_{pre,HX,rad} = 0.18$ W $\dot{Q}_{pre,out,rad} = 0.15$ W
Fluid = air $T_{amb} = 30.71°C$ $T_{pre,in,insulation,surface} = 30.73°C^{*}$ $T_{pre,HX,insulation,surface} = 31.12°C^{*}$ $T_{pre,out,insulation,surface} = 31.34°C^{*}$ $P_{amb} = 101$ kPa	$$T_{film} = \frac{T_{amb} + T_{insulation,surface}}{2}$$ $$\rho_{air}, \mu_{air}, c_{p,air}, k_{air} = f\left(T_{film}, P_{amb}\right)$$ $$\beta_{air} = f\left(T_{film}\right)$$ $$\alpha_{air} = \frac{k_{air}}{\rho_{air} c_{p,air}}$$ $$Pr_{air} = \frac{c_{p,air} \mu_{air}}{k_{air}}$$	$T_{pre,in,film} = 30.73°C^{*}$ $T_{pre,HX,film} = 30.91°C^{*}$ $T_{pre,out,film} = 31.02°C^{*}$ $\rho_{air} = 1.16$ kg m^{-3} $\mu_{air} = 1.88 \times 10^{-5}$ kg m^{-1} s^{-1} $c_{p,air} = 1007$ J kg^{-1} K^{-1} $k_{air} = 0.026$ W m^{-1} K^{-1} $\beta_{air} = 3.29 \times 10^{-3}$ K^{-1} $\alpha_{air} = 2.25 \times 10^{-5}$ m^{2} s^{-1} $Pr_{air} = 0.719$

Propane In-Tube Condensation, 9 September 2013, Run 7		
Inputs	**Equations**	**Results**
$\rho_{air} = 1.16$ kg m^{-3} $\mu_{air} = 1.88 \times 10^{-5}$ kg m^{-1} s^{-1} $\beta_{air} = 3.29 \times 10^{-3}$ K^{-1} $\alpha_{air} = 2.25 \times 10^{-5}$ m^2 s^{-1} $T_{amb} = 30.71$°C $T_{pre,in,insulation,surface} = 30.73$°C* $T_{pre,HX,insulation,surface} = 31.12$°C* $T_{pre,out,insulation,surface} = 31.34$°C* $D_{insulation,tube,out} = 87$ mm $L_{pre,air} = 154.2$ mm $g = 9.81$ m s^{-2}	$$\mathrm{Ra}_D = \frac{\rho_{air}\, g\, \beta_{air}\, \left| T_{insulation,surface} - T_{amb} \right|\, D_{insulation,tube,out}^3}{\mu_{air}\, \alpha_{air}}$$ $$\mathrm{Ra}_L = \frac{\rho_{air}\, g\, \beta_{air}\, \left| T_{insulation,surface} - T_{amb} \right|\, L_{pre,air}^3}{\mu_{air}\, \alpha_{air}}$$	$\mathrm{Ra}_{D,pre,HX} = 24164$ $\mathrm{Ra}_{L,pre,in} = 8845$ $\mathrm{Ra}_{L,pre,out} = 198128$
$\mathrm{Ra}_{D,pre,HX} = 24164$ $\mathrm{Pr}_{air} = 0.719$	Natural convection from horizontal tube $$\mathrm{Nu}_{nat.conv.} = \left(0.60 + \frac{0.387 \mathrm{Ra}_D^{1/6}}{\left(1 + \left(\frac{0.559}{\mathrm{Pr}} \right)^{9/16} \right)^{8/27}} \right)^2$$ (Churchill and Chu, 1975a)	$\mathrm{Nu}_{nc,pre,HX} = 5.43$

Propane In-Tube Condensation, 9 September 2013, Run 7		
Inputs	**Equations**	**Results**
$Ra_{L,pre,in} = 8845$ $Ra_{L,pre,out} = 198128$ $Pr_{air} = 0.719$ $Nu_{nc,plate,pre,in} = 5.11$ $Nu_{nc,plate,pre,in} = 10.49$ $D_{insulation,tube,out} = 87$ mm $L_{pre,air} = 154.2$ mm	Natural convection from vertical plate $$Nu_{nat.conv.,plate} = \left(0.825 + \frac{0.387 Ra_L^{1/6}}{\left(1 + \left(\frac{0.492}{Pr} \right)^{9/16} \right)^{8/27}} \right)^2$$ (Churchill and Chu, 1975b)	$Nu_{nc,plate,pre,in} = 5.30$ $Nu_{nc,plate,pre,in} = 10.92$
	$$Gr_L = \frac{Ra_L}{Pr}$$ $$\zeta = \frac{1.8}{Nu_{nat.conv.,plate}} \frac{L}{D}$$ $$Nu_{nat.conv.,vertical,cylinder} = \begin{cases} Nu_{nat.conv.,plate} & \text{if } \dfrac{D}{L} > \dfrac{35}{Gr_L^{0.25}} \\ Nu_{nat.conv.,plate} \dfrac{\zeta}{\ln(1+\zeta)} & \text{if } \dfrac{D}{L} \leq \dfrac{35}{Gr_L^{0.25}} \end{cases}$$ (Sparrow and Gregg, 1956)	$Gr_{L,pre,in} = 12300$ $Gr_{L,pre,out} = 275522$ $(D/L)_{pre,in} = 0.57 < 3.47$ $(D/L)_{pre,out} = 0.57 < 1.59$ $\zeta_{pre,in} = 0.62$ $\zeta_{pre,out} = 0.30$ $Nu_{nc,pre,in} = 6.75$ $Nu_{nc,pre,out} = 12.43$

Propane In-Tube Condensation, 9 September 2013, Run 7		
Inputs	**Equations**	**Results**
$Nu_{nc,pre,in} = 6.75$ $Nu_{nc,pre,HX} = 5.43$ $Nu_{nc,pre,out} = 12.43$ $k_{air} = 0.026$ W m^{-1} K^{-1} $D_{insulation,tube,out} = 87$ mm $L_{pre,air} = 154.2$ mm	$h_{nc,pre,in/out} = \dfrac{Nu_{nat.conv.} \cdot k_{air}}{L_{pre,air}}$ $h_{nc,pre,HX} = \dfrac{Nu_{nat.conv.} \cdot k_{air}}{D_{insulation,tube,out}}$	$h_{nc,pre,in} = 1.16$ W m^{-2} K^{-1} $h_{nc,pre,HX} = 1.64$ W m^{-2} K^{-1} $h_{nc,pre,out} = 2.14$ W m^{-2} K^{-1}
$D_{insulation,tube,out} = 87$ mm $L_{pre,air} = 154.2$ mm $L_{pre} = 275$ mm $h_{nc,pre,in} = 1.16$ W m^{-2} K^{-1} $h_{nc,pre,HX} = 1.64$ W m^{-2} K^{-1} $h_{nc,pre,out} = 2.14$ W m^{-2} K^{-1}	Natural Convection Resistance $R_{nc} = \dfrac{1}{\pi D_{insulation,tube,out} L h_{nc}}$	$R_{pre,in,nc} = 20.62$ K W^{-1} $R_{pre,HX,nc} = 8.12$ K W^{-1} $R_{pre,out,nc} = 11.20$ K W^{-1}
$T_{amb} = 30.71°C$ $T_{pre,in,insulation,surface} = 30.73°C^*$ $T_{pre,HX,insulation,surface} = 31.12°C^*$ $T_{pre,out,insulation,surface} = 31.34°C^*$ $R_{pre,in,nc} = 20.62$ K W^{-1} $R_{pre,HX,nc} = 8.12$ K W^{-1}	$\dot{Q}_{pre,in,nc} = \dfrac{T_{amb} - T_{pre,in,insulation,surface}}{R_{pre,in,nc}}$ $\dot{Q}_{pre,HX,nc} = \dfrac{T_{amb} - T_{pre,HX,insulation,surface}}{R_{pre,HX,nc}}$ $\dot{Q}_{pre,out,nc} = \dfrac{T_{amb} - T_{pre,out,insulation,surface}}{R_{pre,out,nc}}$	$\dot{Q}_{pre,in,nc} = 0.001$ W $\dot{Q}_{pre,HX,nc} = 0.05$ W $\dot{Q}_{pre,out,nc} = 0.06$ W

Propane In-Tube Condensation, 9 September 2013, Run 7		
Inputs	**Equations**	**Results**
$R_{\text{pre,out,nc}} = 11.20 \text{ K W}^{-1}$		
$T_{\text{air,pre,in}} = 31.39°\text{C}$ $T_{\text{amb}} = 30.71°\text{C}$ $R_{\text{pre,in,air}} = 2.34 \text{ K W}^{-1}$ $R_{\text{pre,in,wall}} = 2.85 \times 10^{-4} \text{ K W}^{-1}$ $R_{\text{pre,air,insulation,wrap}} = 10.98 \text{ K W}^{-1}$ $R_{\text{pre,air,insulation,tube}} = 68.54 \text{ K W}^{-1}$ $R_{\text{pre,in,rad}} = 4.19 \text{ K W}^{-1}$ $R_{\text{pre,in,nc}} = 20.62 \text{ K W}^{-1}$	$\dot{Q}_{\text{pre,in,loss}} = \dfrac{T_{\text{air,pre,in}} - T_{\text{pre,in,insulation,surface}}}{R_{\text{pre,in,air}} + R_{\text{pre,in,wall}} + R_{\text{pre,air,insulation,wrap}} + R_{\text{pre,air,insulation,tube}}}$ $\dot{Q}_{\text{pre,in,loss}} = \left(T_{\text{pre,in,insulation,surface}} - T_{\text{amb}}\right)\left(\dfrac{1}{R_{\text{pre,in,rad}}} + \dfrac{1}{R_{\text{pre,in,nc}}}\right)$	$T_{\text{pre,in,insulation,surface}} = 30.73°\text{C}^{*}$ $\dot{Q}_{\text{pre,in,loss}} = 0.01 \text{ W}$
$T_{\text{air,pre,avg}} = 39.87°\text{C}$ $T_{\text{amb}} = 30.71°\text{C}$ $R_{\text{pre,HX,air}} = 0.13 \text{ K W}^{-1}$ $R_{\text{pre,HX,wall}} = 4.39 \times 10^{-3} \text{ K W}^{-1}$ $R_{\text{pre,HX,insulation,tube}} = 37.98 \text{ K W}^{-1}$ $R_{\text{pre,HX,rad}} = 2.32 \text{ K W}^{-1}$ $R_{\text{pre,HX,nc}} = 8.12 \text{ K W}^{-1}$	$\dot{Q}_{\text{pre,HX,loss}} = \dfrac{T_{\text{air,pre,avg}} - T_{\text{pre,HX,insulation,surface}}}{R_{\text{pre,HX,air}} + R_{\text{pre,HX,wall}} + R_{\text{pre,HX,insulation,tube}}}$ $\dot{Q}_{\text{pre,HX,loss}} = \left(T_{\text{pre,HX,insulation,surface}} - T_{\text{amb}}\right)\left(\dfrac{1}{R_{\text{pre,HX,rad}}} + \dfrac{1}{R_{\text{pre,HX,nc}}}\right)$	$T_{\text{pre,HX,insulation,surface}} = 31.12°\text{C}^{*}$ $\dot{Q}_{\text{pre,HX,loss}} = 0.23 \text{ W}$

Propane In-Tube Condensation, 9 September 2013, Run 7		
Inputs	**Equations**	**Results**
$T_{\text{air,pre,out}} = 48.34°C$ $T_{\text{amb}} = 30.71°C$ $R_{\text{pre,out,air}} = 2.31 \text{ K W}^{-1}$ $R_{\text{pre,out,wall}} = 2.86 \times 10^{-4} \text{ K W}^{-1}$ $R_{\text{pre,air,insulation,wrap}} = 10.98 \text{ K W}^{-1}$ $R_{\text{pre,air,insulation,tube}} = 68.54 \text{ K W}^{-1}$ $R_{\text{pre,out,rad}} = 4.18 \text{ K W}^{-1}$ $R_{\text{pre,out,nc}} = 11.20 \text{ K W}^{-1}$	$\dot{Q}_{\text{pre,out,loss}} = \dfrac{T_{\text{air,pre,out}} - T_{\text{pre,out,insulation,surface}}}{R_{\text{pre,out,air}} + R_{\text{pre,out,wall}} + R_{\text{pre,air,insulation,wrap}} + R_{\text{pre,air,insulation,tube}}}$ $\dot{Q}_{\text{pre,out,loss}} = \left(T_{\text{pre,out,insulation,surface}} - T_{\text{amb}}\right)\left(\dfrac{1}{R_{\text{pre,out,rad}}} + \dfrac{1}{R_{\text{pre,out,nc}}}\right)$	$T_{\text{pre,out,insulation,surface}} = 31.34°C^{*}$ $\dot{Q}_{\text{pre,out,loss}} = 0.21 \text{ W}$
$\dot{Q}_{\text{pre,in,loss}} = 0.01 \text{ W}$ $\dot{Q}_{\text{pre,HX,loss}} = 0.23 \text{ W}$ $\dot{Q}_{\text{pre,out,loss}} = 0.21 \text{ W}$	$\dot{Q}_{\text{pre,loss}} = \dot{Q}_{\text{pre,in,loss}} + \dot{Q}_{\text{pre,HX,loss}} + \dot{Q}_{\text{pre,out,loss}}$	$\dot{Q}_{\text{pre,loss}} = 0.45 \text{ W}$
Heat Loss Between the Pre-Condenser and Test Section (Figures 4.1, 4,4)		
$T_{\text{propane,2}} = 47.31°C$ $T_{\text{propane,3}} = 47.01°C$	Assuming negligible convective resistance: $T_{\text{23,wall,in}} = \dfrac{T_{\text{propane,2}} + T_{\text{propane,3}}}{2}$	$T_{\text{23,wall,in}} = 47.16°C$
$D_{\text{line,in}} = 4.57 \text{ mm}$ $D_{\text{line,out}} = 6.35 \text{ mm}$ $s_{\text{h,valve,out}} = 19.0 \text{ mm}$	Detailed analysis shown for one segment ("2-to-3" tube); other segments calculated similarly. Tube wall conduction resistance:	$D_{\text{h,valve,out}} = 19.0 \text{ mm}$ $k_{\text{SS316}} = 13.80 \text{ W m}^{-1} \text{ K}^{-1}$ $R_{\text{2-to-3,wall}} = 9.62 \times 10^{-3} \text{ K W}^{-1}$

Propane In-Tube Condensation, 9 September 2013, Run 7		
Inputs	**Equations**	**Results**
$D_{\text{filter,in}} = 19.1$ mm $D_{\text{filter,out}} = 25.4$ mm $L_{\text{2-to-3}} = 394$ mm $L_{\text{valve}} = 50$ mm $L_{\text{filter}} = 18.2$ mm $T_{\text{line,wall,out}} = 47.16°\text{C}^*$	$D_{\text{h,valve,out}} = \dfrac{4A_{\text{square}}}{P_{\text{square}}} = \dfrac{4s_{\text{h,valve,out}}^2}{4s_{\text{h,valve,out}}} = s_{\text{h,valve,out}}$ $k_{\text{SS316}} = f\left(T_{\text{line,wall,out}}\right)$ $R_{\text{wall}} = \dfrac{\ln(D_{\text{wall,out}} / D_{\text{wall,in}})}{2\pi k_{\text{SS316}}L}$	
$D_{\text{insulation,tube,in}} = 25$ mm $D_{\text{line,out}} = 6.35$ mm $k_{\text{insulation,wrap}} = 0.0432$ W m^{-1} K^{-1} $L_{\text{2-to-3}} = 394$ mm	Soft wrap insulation conduction resistance: $R_{\text{insulation,wrap}} = \dfrac{\ln(D_{\text{insulation,tube,in}} / D_{\text{wall,out}})}{2\pi k_{\text{insulation,wrap}}L}$	$R_{\text{2-to-3,insulation,wrap}} = 12.82$ K W^{-1}
$D_{\text{insulation,tube,out}} = 87$ mm $D_{\text{insulation,tube,in}} = 25$ mm $k_{\text{insulation,tube}} = 0.019$ W m^{-1} K^{-1} $L_{\text{2-to-3}} = 394$ mm	Tube insulation conduction resistance: $R_{\text{insulation,tube}} = \dfrac{\ln(D_{\text{insulation,tube,out}} / D_{\text{insulation,tube,in}})}{2\pi k_{\text{insulation,tube}}L}$	$R_{\text{2-to-3,insulation,tube}} = 26.53$ K W^{-1}
$\epsilon_{\text{ins}} = 0.9$ $\sigma = 5.67 \times 10^{-8}$ W m^{-2} K^{-4} $T_{\text{amb}} = 303.86$ K $T_{\text{2-to-3,insulation,surface}} = 304.36$ K*	Radiation resistance: $h_{\text{rad}} = \epsilon_{\text{ins}}\sigma\left(T_{\text{insulation,surface}}^2 + T_{\text{amb}}^2\right)\left(T_{\text{insulation,surface}} + T_{\text{amb}}\right)$ $R_{\text{rad}} = \dfrac{1}{\pi D_{\text{insulation,tube,out}}Lh_{\text{rad}}}$	$h_{\text{2-to-3,rad}} = 5.74$ W m^{-2} K^{-1} $R_{\text{2-to-3,rad}} = 1.62$ K W^{-1}

Propane In-Tube Condensation, 9 September 2013, Run 7		
Inputs	**Equations**	**Results**
$D_{\text{insulation,tube,out}} = 87$ mm $L_{\text{2-to-3}} = 394$ mm		
$T_{\text{amb}} = 30.71°C$ $T_{\text{2-to-3,insulation,surface}} = 31.21°C^{*}$ $R_{\text{2-to-3,rad}} = 1.62$ K W^{-1}	$\dot{Q}_{\text{rad}} = \dfrac{T_{\text{amb}} - T_{\text{insulation,surface}}}{R_{\text{rad}}}$	$\dot{Q}_{\text{2-to-3,rad}} = 0.31$ W
Fluid = air $T_{\text{amb}} = 30.71°C$ $T_{\text{2-to-3,insulation,surface}} = 31.21°C^{*}$ $P_{\text{amb}} = 101$ kPa $D_{\text{insulation,tube,out}} = 87$ mm $g = 9.81$ m s^{-2}	$T_{\text{film}} = \dfrac{T_{\text{amb}} + T_{\text{insulation,surface}}}{2}$ $\rho_{\text{air}}, \mu_{\text{air}}, c_{\text{p,air}}, k_{\text{air}} = f\left(T_{\text{film}}, P_{\text{amb}}\right)$ $\beta_{\text{air}} = f\left(T_{\text{film}}\right)$ $\alpha_{\text{air}} = \dfrac{k_{\text{air}}}{\rho_{\text{air}} c_{\text{p,air}}}$ $\mathrm{Pr}_{\text{air}} = \dfrac{c_{\text{p,air}} \mu_{\text{air}}}{k_{\text{air}}}$	$T_{\text{2-to-3,film}} = 30.96°C$ $\rho_{\text{air}} = 1.16$ kg m^{-3} $\mu_{\text{air}} = 1.88 \times 10^{-5}$ kg m^{-1} s^{-1} $c_{\text{p,air}} = 1007$ J kg^{-1} K^{-1} $k_{\text{air}} = 0.026$ W m^{-1} K^{-1} $\beta_{\text{air}} = 3.29 \times 10^{-3}$ K^{-1} $\alpha_{\text{air}} = 2.25 \times 10^{-5}$ m^{2} s^{-1} $\mathrm{Pr}_{\text{air}} = 0.719$
	$\mathrm{Ra}_{D} = \dfrac{\rho_{\text{air}} g \beta_{\text{air}} \left| T_{\text{insulation,surface}} - T_{\text{amb}} \right| D_{\text{insulation,tube,out}}^{3}}{\mu_{\text{air}} \alpha_{\text{air}}}$	$\mathrm{Ra}_{D,\text{2-to-3}} = 29441$
$\mathrm{Ra}_{D,\text{2-to-3}} = 29441$ $\mathrm{Pr}_{\text{air}} = 0.719$ $k_{\text{air}} = 0.026$ W m^{-1} K^{-1}	Natural convection from horizontal tube	$\mathrm{Nu}_{\text{nc,2-to-3}} = 5.70$ $h_{\text{nc,2-to-3}} = 1.72$ W m^{-2} K^{-1}

Propane In-Tube Condensation, 9 September 2013, Run 7		
Inputs	**Equations**	**Results**
$D_{\text{insulation,tube,out}} = 87$ mm	$$\mathrm{Nu}_{\text{nat.conv.}} = \left(0.60 + \frac{0.387\mathrm{Ra}_{\mathrm{D}}^{1/6}}{\left(1 + \left(\frac{0.559}{\mathrm{Pr}} \right)^{9/16} \right)^{8/27}} \right)^{2}$$ $$h_{\text{nat.conv.}} = \frac{\mathrm{Nu}_{\text{nat.conv.}} \cdot k_{\text{air}}}{D_{\text{insulation,tube,out}}}$$ (Churchill and Chu, 1975a)	
$D_{\text{insulation,tube,out}} = 87$ mm $L_{\text{2-to-3}} = 394$ mm $h_{\text{nc,2-to-3}} = 1.72$ W m^{-2} K^{-1}	Natural Convection Resistance $$R_{\text{nc}} = \frac{1}{\pi D_{\text{insulation,tube,out}} L h_{\text{nc}}}$$	$R_{\text{2-to-3,nc}} = 5.40$ K W^{-1}
$T_{\text{amb}} = 30.71°\text{C}$ $T_{\text{2-to-3,insulation,surface}} = 31.21°\text{C}^{*}$ $R_{\text{2-to-3,nc}} = 5.40$ K W^{-1}	$$\dot{Q}_{\text{nc}} = \frac{T_{\text{amb}} - T_{\text{insulation,surface}}}{R_{\text{nc}}}$$	$\dot{Q}_{\text{2-to-3,nc}} = 0.09$ W
$T_{\text{23,wall,in}} = 47.16°\text{C}$ $T_{\text{amb}} = 30.71°\text{C}$ $R_{\text{2-to-3,wall}} = 9.62 \times 10^{-3}$ K W^{-1} $R_{\text{2-to-3,insulation,wrap}} = 12.82$ K W^{-1}	$$\dot{Q}_{\text{2-to-3,line,loss}} = \frac{T_{\text{propane,23,wall,in}} - T_{\text{2-to-3,insulation,surface}}}{R_{\text{2-to-3,wall}} + R_{\text{2-to-3,insulation,wrap}} + R_{\text{2-to-3,insulation,tube}}}$$ $$\dot{Q}_{\text{2-to-3,line,loss}} = \left(T_{\text{2-to-3,insulation,surface}} - T_{\text{amb}} \right) \left(\frac{1}{R_{\text{2-to-3,rad}}} + \frac{1}{R_{\text{2-to-3,nc}}} \right)$$	$T_{\text{2-to-3,insulation,surface}} = 31.22°\text{C}^{*}$ $\dot{Q}_{\text{2-to-3,line,loss}} = 0.41$ W

Propane In-Tube Condensation, 9 September 2013, Run 7		
Inputs	**Equations**	**Results**
$R_{\text{2-to-3,insulation,tube}} = 26.53 \text{ K W}^{-1}$ $R_{\text{2-to-3,rad}} = 1.62 \text{ K W}^{-1}$ $R_{\text{2-to-3,nc}} = 5.40 \text{ K W}^{-1}$		
$T_{\text{23,wall,in}} = 47.16°C$ $T_{\text{amb}} = 30.71°C$ $R_{\text{valve,23,wall}} = 0.329 \text{ K W}^{-1}$ $R_{\text{valve,23, insulation,wrap}} = 20.22 \text{ K W}^{-1}$ $R_{\text{valve,23, insulation,tube}} = 208.9 \text{ K W}^{-1}$ $R_{\text{valve,23, rad}} = 12.74 \text{ K W}^{-1}$ $R_{\text{valve,23, nc}} = 39.68 \text{ K W}^{-1}$	$\dot{Q}_{\text{valve,23,loss}} = \dfrac{T_{\text{propane,23,wall,in}} - T_{\text{valve,23,insulation,surface}}}{R_{\text{valve,23,wall}} + R_{\text{valve,23,insulation,wrap}} + R_{\text{valve,23,insulation,tube}}}$ $\dot{Q}_{\text{valve,23,loss}} = \left(T_{\text{valve,23,insulation,surface}} - T_{\text{amb}}\right)\left(\dfrac{1}{R_{\text{valve,23,rad}}} + \dfrac{1}{R_{\text{valve,23,nc}}}\right)$	$T_{\text{valve,23,insulation,surface}} = 31.38°C^{*}$ $\dot{Q}_{\text{valve,23,loss}} = 0.07 \text{ W}$
$T_{\text{23,wall,in}} = 47.16°C$ $T_{\text{amb}} = 30.71°C$ $R_{\text{filter,wall}} = 0.181 \text{ K W}^{-1}$ $R_{\text{filter, insulation,tube}} = 573.9 \text{ K W}^{-1}$ $R_{\text{filter, rad}} = 34.98 \text{ K W}^{-1}$ $R_{\text{filter, nc}} = 106.7 \text{ K W}^{-1}$	$\dot{Q}_{\text{filter,loss}} = \dfrac{T_{\text{propane,23,wall,in}} - T_{\text{filter,insulation,surface}}}{R_{\text{filter,wall}} + R_{\text{filter,insulation,tube}}}$ $\dot{Q}_{\text{filter,loss}} = \left(T_{\text{filter,insulation,surface}} - T_{\text{amb}}\right)\left(\dfrac{1}{R_{\text{filter,rad}}} + \dfrac{1}{R_{\text{filter,nc}}}\right)$	$T_{\text{filter,insulation,surface}} = 31.44°C^{*}$ $\dot{Q}_{\text{filter,loss}} = 0.03 \text{ W}$

Propane In-Tube Condensation, 9 September 2013, Run 7		
Inputs	**Equations**	**Results**
Heat Losses from Test Section Inlet Pressure Tap (Figure 4.2)		
$T_{\text{propane,3}} = 47.01°C$	Assuming negligible convective resistance: $T_{\text{test,line,in,1h,wall,in}} = T_{\text{ref,3}}$	$T_{\text{test,line,in,1h,wall,in}} = 47.01°C$
Measured wall surface temperatures: $T_{\text{wall,line,1}} = 39.29°C$ $T_{\text{wall,line,2}} = 30.06°C$ $T_{\text{wall,line,3}} = 31.35°C$	$T_{\text{line,in,2h,wall,out}} = T_{\text{wall,line,1}}$ $T_{\text{line,in,3h,wall,out}} = \dfrac{T_{\text{wall,line,1}} + T_{\text{wall,line,2}}}{2}$ $T_{\text{line,in,4v,wall,out}} = T_{\text{wall,line,2}}$ $T_{\text{line,in,5v,wall,out}} = \dfrac{T_{\text{wall,line,1}} + T_{\text{wall,line,3}}}{2}$ $T_{\text{line,in,6h,wall,out}} = T_{\text{line,in,7h,wall,out}} = T_{\text{wall,line,3}}$	$T_{\text{line,in,2h,wall,out}} = 39.29°C$ $T_{\text{line,in,3h,wall,out}} = 34.67°C$ $T_{\text{line,in,4v,wall,out}} = 30.06°C$ $T_{\text{line,in,5v,wall,out}} = 35.32°C$ $T_{\text{line,in,6h,wall,out}} = 31.35°C$ $T_{\text{line,in,7v,wall,out}} = 31.35°C$
$D_{\text{line,in}} = 4.57$ mm $D_{\text{line,out}} = 6.35$ mm $T_{\text{line,in,1h,wall,out}} = 47.01°C^{*}$ $L_{\text{line,in,1h}} = 63.5$ mm	Detailed analysis given for one segment; analysis is similar for all others: Tube wall conduction resistance: $k_{\text{SS316}} = f\left(T_{\text{test,line,in,}j\text{,wall,out}}\right)$ $R_{\text{line,in,}j\text{,wall}} = \dfrac{\ln(D_{\text{line,out}} / D_{\text{line,in}})}{2\pi k_{\text{SS316}} L_{\text{test,line,in,}j}}$	$k_{\text{SS316}} = 13.80$ W m^{-1} K^{-1} $R_{\text{line,in,1h,wall}} = 5.97 \times 10^{-2}$ K W^{-1}
$D_{\text{insulation,tube,out}} = 73.7$ mm	Soft wrap insulation conduction resistance:	$R_{\text{line,in,1h,insulation,wrap}} = 79.51$ K W$^-$

Propane In-Tube Condensation, 9 September 2013, Run 7		
Inputs	**Equations**	**Results**
$D_{\text{insulation,tube,in}} = 25$ mm $D_{\text{line,out}} = 6.35$ mm $k_{\text{insulation,wrap}} = 0.0432$ W m^{-1} K^{-1} $k_{\text{insulation,tube}} = 0.019$ W m^{-1} K^{-1} $L_{\text{line,in,1h}} = 63.5$ mm	$R_{\text{line,in},j,\text{insulation,wrap}} = \dfrac{\ln(D_{\text{insulation,wrap,in}} / D_{\text{line,out}})}{2\pi k_{\text{insulation,wrap}} L_{\text{test,line,in},j}}$	[1]
	Tube insulation conduction resistance: $R_{\text{line,in},j,\text{insulation,tube}} = \dfrac{\ln(D_{\text{insulation,tube,out}} / D_{\text{insulation,tube,in}})}{2\pi k_{\text{insulation,tube}} L_{\text{test,line,in},j}}$	$R_{\text{line,in,1h,insulation,tube}} = 142.5$ K W^{-1}
$\epsilon_{\text{ins}} = 0.9$ $\sigma = 5.67 \times 10^{-8}$ W m^{-2} K^{-4} $D_{\text{insulation,tube,out}} = 73.7$ mm $T_{\text{amb}} = 303.86$ K $T_{\text{line,in,1h,insulation,surface}} = 304.48$ K[*] $L_{\text{line,in,1h}} = 63.5$ mm	Radiation resistance: $h_{\text{rad}} = \epsilon_{\text{ins}}\sigma\left(T_{\text{insulation,surface}}^2 + T_{\text{amb}}^2\right)\left(T_{\text{insulation,surface}} + T_{\text{amb}}\right)$ $R_{\text{line,in},j,\text{rad}} = \dfrac{1}{\pi D_{\text{insulation,tube,out}} L_{\text{test,line,in},j} h_{\text{test,line,in},j,\text{rad}}}$	$h_{\text{line,in,1h,rad}} = 5.74$ W m^{-2} K^{-1} $R_{\text{line,in,1h,rad}} = 11.85$ K W^{-1}
	$\dot{Q}_{\text{test,line,in},j,\text{rad}} = \dfrac{T_{\text{amb}} - T_{\text{test,line,in},j,\text{insulation,surface}}}{R_{\text{test,line,in},j,\text{rad}}}$	$\dot{Q}_{\text{test,line,in,1h,rad}} = 0.05$ W

Propane In-Tube Condensation, 9 September 2013, Run 7		
Inputs	**Equations**	**Results**
Fluid = air $T_{amb} = 30.71°C$ $T_{line,in,1h,insulation,surface} = 31.33°C^*$ $P_{amb} = 101 \text{ kPa}$ $D_{insulation,tube,out} = 73.7 \text{ mm}$ $g = 9.81 \text{ m s}^{-2}$ $T_{line,in,4v,insulation,surface} = 30.68°C^*$ $L_{line,in,4v} = 196.9 \text{ mm}$	$T_{film} = \dfrac{T_{amb} + T_{insulation,surface}}{2}$ $\rho_{air}, \mu_{air}, c_{p,air}, k_{air} = f\left(T_{film}, P_{amb}\right)$ $\beta_{air} = f\left(T_{film}\right)$ $\alpha_{air} = \dfrac{k_{air}}{\rho_{air} c_{p,air}}$ $Pr_{air} = \dfrac{c_{p,air} \mu_{air}}{k_{air}}$	$T_{line,in,1h,film} = 31.02°C$ $T_{line,in,4v,film} = 30.69°C$ $\rho_{air} = 1.16 \text{ kg m}^{-3}$ $\mu_{air} = 1.88 \times 10^{-5} \text{ kg m}^{-1} \text{ s}^{-1}$ $c_{p,air} = 1007 \text{ J kg}^{-1} \text{ K}^{-1}$ $k_{air} = 0.026 \text{ W m}^{-1} \text{ K}^{-1}$ $\beta_{air} = 3.29 \times 10^{-3} \text{ K}^{-1}$ $\alpha_{air} = 2.25 \times 10^{-5} \text{ m}^2 \text{ s}^{-1}$ $Pr_{air} = 0.719$
	$Ra_D = \dfrac{\rho_{air} g \beta_{air} \left|T_{insulation,surface} - T_{amb}\right| D_{insulation,tube,out}^3}{\mu_{air} \alpha_{air}}$	$Ra_{D,line,in,1h} = 22239$
	$Ra_L = \dfrac{\rho_{air} g \beta_{air} \left|T_{insulation,surface} - T_{amb}\right| L_{test,line,in,jv}^3}{\mu_{air} \alpha_{air}}$	$Ra_{L, line,in,4v} = 18914$
$Ra_{D,line,in,1h} = 22239$ $Pr_{air} = 0.719$	Natural convection from horizontal tube	$Nu_{line,in,1h} = 5.32$

Propane In-Tube Condensation, 9 September 2013, Run 7		
Inputs	**Equations**	**Results**
	$$\mathrm{Nu}_{\mathrm{nat.conv.}} = \left(0.60 + \frac{0.387 \mathrm{Ra}_D^{1/6}}{\left(1 + \left(\frac{0.559}{\mathrm{Pr}}\right)^{9/16}\right)^{8/27}} \right)^2$$ (Churchill and Chu, 1975a)	
$\mathrm{Ra}_{\mathrm{L, line,in,4v}} = 18914$ $\mathrm{Pr}_{\mathrm{air}} = 0.719$	Natural convection from vertical plate $$\mathrm{Nu}_{\mathrm{nat.conv.,plate}} = \left(0.825 + \frac{0.387 \mathrm{Ra}_L^{1/6}}{\left(1 + \left(\frac{0.492}{\mathrm{Pr}}\right)^{9/16}\right)^{8/27}} \right)^2$$ (Churchill and Chu, 1975b)	$\mathrm{Nu}_{\mathrm{line,in,4v,plate}} = 6.26$

Propane In-Tube Condensation, 9 September 2013, Run 7		
Inputs	**Equations**	**Results**
$Ra_{L,\,line,in,4v} = 18914$ $Pr_{air} = 0.719$ $Nu_{line,in,4v,plate} = 6.26$ $D_{insulation,tube,out} = 73.7$ mm $L_{line,in,4v} = 196.9$ mm	$$Gr_L = \frac{Ra_L}{Pr}$$ $$\zeta = \frac{1.8}{Nu_{nat.conv.,plate}}\frac{L}{D}$$ $$Nu_{nat.conv.,vertical,cylinder} = \begin{cases} Nu_{nat.conv.,plate} & \text{if } \dfrac{D}{L} > \dfrac{35}{Gr_L^{0.25}} \\[2em] Nu_{nat.conv.,plate}\,\dfrac{\zeta}{\ln(1+\zeta)} & \text{if } \dfrac{D}{L} \le \dfrac{35}{Gr_L^{0.25}} \end{cases}$$ (Sparrow and Gregg, 1956)	$Gr_{L,\,line,in,4v} = 26302$ $(D\,/\,L)_{line,in,4v} = 0.37 < 2.9$ $\zeta_{line,in,4v} = 0.80$ $Nu_{line,in,4v} = 8.43$
$Nu_{line,in,1h} = 5.32$ $Nu_{line,in,4v} = 8.43$ $k_{air} = 0.026$ W m^{-1} K^{-1} $D_{insulation,tube,out} = 73.7$ mm $L_{line,in,4v} = 196.9$ mm	$$h_{nat.conv.} = \frac{Nu_{nat.conv.}\cdot k_{air}}{D_{insulation,tube,out}}$$	$h_{nc,line,in,1h} = 1.90$ W m^{-2} K^{-1} $h_{nc,\,line,in,4v} = 1.13$ W m^{-2} K^{-1}
$D_{insulation,tube,out} = 73.7$ mm $L_{line,in,1h} = 63.5$ mm $h_{nc,line,in,1h} = 1.90$ W m^{-2} K^{-1}	Natural Convection Resistance $$R_{test,line,in,j,nc} = \frac{1}{\pi D_{insulation,tube,out}L_{test,line,in,j}h_{test,line,in,j,nc}}$$	$R_{line,in,1h,nc} = 35.87$ K W^{-1}

Propane In-Tube Condensation, 9 September 2013, Run 7		
Inputs	**Equations**	**Results**
$T_{\text{amb}} = 30.71°C$ $T_{\text{line,in,1h,insulation,surface}} = 31.33°C^*$ $R_{\text{line,in,1h,nc}} = 35.87$ K W^{-1}	$$\dot{Q}_{\text{test,line,in},j,\text{nc}} = \frac{T_{\text{amb}} - T_{\text{test,line,in},j,\text{insulation,surface}}}{R_{\text{test,line,in},j,\text{nc}}}$$	$\dot{Q}_{\text{test,line,in,1h,nc}} = 0.02$ W
$T_{\text{test,line,in,1h,wall,in}} = 47.01°C$ $T_{\text{amb}} = 30.71°C$ $R_{\text{line,in,1h,wall}} = 5.97 \times 10^{-2}$ K W^{-1} $R_{\text{line,in,1h,insulation,wrap}} = 79.51$ K W^{-1} $R_{\text{line,in,1h,insulation,tube}} = 142.5$ K W^{-1} $R_{\text{line,in,1h,rad}} = 11.85$ K W^{-1} $R_{\text{line,in,1h,nc}} = 35.87$ K W^{-1}	$$\dot{Q}_{\text{test,line,in},j,\text{loss}} = \frac{T_{\text{ref,test,wall,in},j} - T_{\text{test,line,in},j,\text{wall,out}}}{R_{\text{test,line,in},j,\text{wall}}}$$ $$\dot{Q}_{\text{test,line,in},j,\text{loss}} = \frac{T_{\text{test,line,in},j,\text{wall,out}} - T_{\text{test,line,in},j,\text{insulation,surface}}}{R_{\text{test,line},j,\text{in,insulation,wrap}} + R_{\text{test,line,in},j,\text{insulation,tube}}}$$ $$\dot{Q}_{\text{test,line,in},j,\text{loss}} = \frac{T_{\text{test,line,in},j,\text{insulation,surface}} - T_{\text{amb}}}{\left(\dfrac{1}{R_{\text{test,line,in},j,\text{rad}}} + \dfrac{1}{R_{\text{test,line,in},j,\text{nc}}}\right)^{-1}}$$	$T_{\text{test,line,in,1h,wall,out}} = 47.01°C$ $T_{\text{line,in,1h,insulation,surface}} = 31.33°C^*$ $\dot{Q}_{\text{test,line,in,1h,loss}} = 0.07$ W

Propane In-Tube Condensation, 9 September 2013, Run 7		
Inputs	**Equations**	**Results**
$\dot{Q}_{test,line,in,1h,loss} = 0.07$ W $\dot{Q}_{test,line,in,2h,loss} = 0.04$ W $\dot{Q}_{test,line,in,3h,loss} = 0.12$ W $\dot{Q}_{test,line,in,4v,loss} = -0.01$ W $\dot{Q}_{test,line,in,5v,loss} = 0.14$ W $\dot{Q}_{test,line,in,6h,loss} = 0.01$ W $\dot{Q}_{test,line,in,7v,loss} = 0.01$ W	$\dot{Q}_{test,line,in,loss} = \sum\limits_{j=1}^{7} \dot{Q}_{test,line,in,j,loss}$	$\dot{Q}_{test,line,in,loss} = 0.38$ W
$\dot{Q}_{2\text{-to-}3,line,loss} = 0.41$ W $\dot{Q}_{valve23,loss} = 0.07$ W $\dot{Q}_{filter,loss} = 0.03$ W $\dot{Q}_{test,line,in,loss} = 0.38$ W	$\dot{Q}_{loss,2\text{-to-}3} = \dot{Q}_{2\text{-to-}3,line,loss} + \dot{Q}_{valve,23,loss} + \dot{Q}_{filter,loss} + \dot{Q}_{test,line,in,loss}$	$\dot{Q}_{loss,2\text{-to-}3} = 0.89$ W

C.2.1 Post-Condenser Energy Balance

<table>
<tr><td colspan="3">Propane In-Tube Condensation, 9 September 2013, Run 7</td></tr>
<tr><td>Inputs</td><td>Equations</td><td>Results</td></tr>
<tr>
<td>

$T_{\text{air,post,in,RTD}} = 18.93°C$

$T_{\text{air,post,in,TC}} = 18.63°C$

$T_{\text{air,post,out,RTD}} = 29.32°C$

$T_{\text{air,post,out,TC}} = 29.17°C$

</td>
<td>

$$T_{\text{air,post,in}} = \frac{T_{\text{air,post,in,RTD}} + T_{\text{air,post,in,TC}}}{2}$$

$$T_{\text{air,post,out}} = \frac{T_{\text{air,post,out,RTD}} + T_{\text{air,post,out,TC}}}{2}$$

</td>
<td>

$T_{\text{air,post,in}} = 18.78°C$

$T_{\text{air,post,out}} = 29.24°C$

</td>
</tr>
<tr>
<td>

Fluid = air

$T_{\text{air,post,flow}} = 17.65°C$

$T_{\text{air,post,in}} = 18.78°C$

$T_{\text{air,post,out}} = 29.24°C$

$P_{\text{air,post}} = 154.03 \text{ kPa}$

$P_{\text{amb}} = 93 \text{ kPa}$

$\omega = 0.00152$

</td>
<td>

$\rho_{\text{air,post,flow}} = f\left(P_{\text{air,post}}, T_{\text{air,post,flow}}, \omega\right)$

$i_{\text{air,post,in}} = f\left(P_{\text{air,post}}, T_{\text{air,post,in}}, \omega\right)$

$i_{\text{air,post,out}} = f\left(P_{\text{amb}}, T_{\text{air,post,out}}, \omega\right)$

</td>
<td>

$\rho_{\text{air,post,flow}} = 1.844 \text{ kg m}^{-3}$

$i_{\text{air,post,in}} = 295.5 \text{ kJ kg}^{-1}$

$i_{\text{air,post,out}} = 306.2 \text{ kJ kg}^{-1}$

</td>
</tr>
<tr>
<td>

$\dot{V}_{\text{air,post}} = 2.765 \times 10^{-3} \text{ m}^3 \text{ s}^{-1}$

$\rho_{\text{air,post,flow}} = 1.844 \text{ kg m}^{-3}$

</td>
<td>

$\dot{m}_{\text{air,post}} = \dot{V}_{\text{air,post}} \rho_{\text{air,post,flow}}$

</td>
<td>

$\dot{m}_{\text{air,post}} = 5.099 \times 10^{-3} \text{ kg s}^{-1}$

</td>
</tr>
</table>

Propane In-Tube Condensation, 9 September 2013, Run 7		
Inputs	**Equations**	**Results**
$i_{\text{air,post,in}} = 295.5 \text{ kJ kg}^{-1}$ $i_{\text{air,post,out}} = 306.2 \text{ kJ kg}^{-1}$ $\dot{m}_{\text{air,post}} = 5.099 \times 10^{-3} \text{ kg s}^{-1}$ $\dot{Q}_{\text{post-to-6,loss}} = -0.01 \text{ W}$ $\dot{Q}_{\text{post,loss}} = -0.30 \text{ W}$	$\dot{Q}_{\text{post}} = \dot{m}_{\text{air,post}} \left(i_{\text{air,post,out}} - i_{\text{air,post,in}} \right) + \dot{Q}_{\text{post-to-6,loss}} + \dot{Q}_{\text{post,loss}}$	$\dot{Q}_{\text{post}} = 54.18 \text{ W}$
Fluid = Propane $P_{\text{propane,6}} = 1604.1 \text{ kPa}$ $T_{\text{propane,6}} = 28.33°\text{C}$ $\dot{m}_{\text{propane}} = 2.932 \times 10^{-4} \text{ kg s}^{-1}$ $\dot{Q}_{\text{post}} = 54.18 \text{ W}$ $\dot{Q}_{\text{loss,4-to-5}} = 0.70 \text{ W}$	$T_{\text{sat,propane,6}} = f\left(P_{\text{propane,6}} \right)$ $\Delta T_{\text{sub}} = T_{\text{sat,propane,6}} - T_{\text{propane,6}}$ $i_{\text{propane,6}} = f\left(T_{\text{propane,6}}, P_{\text{propane,6}} \right)$ $i_{\text{propane,5}} = i_{\text{propane,6}} + \dfrac{\dot{Q}_{\text{post}}}{\dot{m}_{\text{propane}}}$ $i_{\text{propane,4}} = i_{\text{propane,5}} + \dfrac{\dot{Q}_{\text{loss,4-to-5}}}{\dot{m}_{\text{propane}}}$	$T_{\text{sat,propane,6}} = 47.00°\text{C}$ $\Delta T_{\text{sub}} = 18.67°\text{C}$ $i_{\text{propane,4}} = 461.4 \text{ kJ kg}^{-1}$ $i_{\text{propane,5}} = 459.0 \text{ kJ kg}^{-1}$ $i_{\text{propane,6}} = 274.2 \text{ kJ kg}^{-1}$
Fluid = Propane $P_{\text{propane,4}} = 1604.0 \text{ kPa}$ $T_{\text{propane,test,line,out,2v}} = 32.06°\text{C}$ $\Delta z_{P4} = 83 \text{ mm}$ $g = 9.81 \text{ m s}^{-2}$	$\rho_{\text{propane,line,out}} = f\left(P_{\text{propane,4,adj.}}, T_{\text{propane,test,line,out,2v}} \right)$ $P_{\text{propane,4,adj.}} = P_{\text{propane,4}} - \rho_{\text{propane,line,out}} \, g \Delta z_{P_4}$	$P_{\text{propane,adj,4}} = 1603.6 \text{ kPa}$ $\rho_{\text{propane,line,out}} = 482.7 \text{ kg m}^{-3}$

Propane In-Tube Condensation, 9 September 2013, Run 7		
Inputs	**Equations**	**Results**
$i_{propane,4} = 461.4 \text{ kJ kg}^{-1}$ $P_{propane,adj,4} = 1603.6 \text{ kPa}$	$x_4 = f\left(i_{propane,4}, P_{propane,adj,4}\right)$	$x_4 = 0.46$
Heat Loss Between Propane Measurement 6 and the Post-Condenser (Figures 4.3, 4,4)		
Fluid = Propane $P_{propane,6} = 1604.1 \text{ kPa}$ $T_{propane,6} = 28.33°C$	$\mu_{propane,post,out}, k_{propane,post,out}, \text{Pr}_{propane,post,out} = f\left(P_{propane,6}, T_{propane,6}\right)$	$\mu_{propane,post,out} = 9.50 \times 10^{-5} \text{ kg m}^{-1} \text{ s}^{-1}$ $k_{propane,post,out} = 0.093 \text{ W m}^{-1} \text{ K}^{-1}$ $\text{Pr}_{propane,post,out} = 2.81$
$G_{propane} = 100.2 \text{ kg m}^{-2} \text{ s}^{-1}$ $D_{line,in} = 4.57 \text{ mm}$ $\mu_{propane,post,out} = 9.50 \times 10^{-5} \text{ kg m}^{-1} \text{ s}^{-1}$	$\text{Re}_{post\text{-}to\text{-}6,propane} = \dfrac{G_{propane} D_{line,in}}{\mu_{propane,post,out}}$	$\text{Re}_{post\text{-}to\text{-}6,propane} = 859.5$

Propane In-Tube Condensation, 9 September 2013, Run 7		
Inputs	**Equations**	**Results**
$\mathrm{Re}_{\text{post-to-6,propane}} = 859.5$ $e = 0.0015$ mm $D_{\text{line,in}} = 4.57$ mm	$$f = 8\left(\left(\frac{8}{\mathrm{Re}_{\text{post-to-6,propane}}}\right)^{12} + \frac{1}{(B+C)^{1.5}}\right)^{1/12}$$ where $B = \left(2.457\ln\dfrac{1}{(7/\mathrm{Re}_{\text{post-to-6,propane}})^{0.9} + 0.27(e/D_{\text{line,in}})}\right)^{16}$ and $$C = \left(\frac{37530}{\mathrm{Re}_{\text{post-to-6,propane}}}\right)^{16}$$ (Churchill, 1977b)	$f = 0.074$

Propane In-Tube Condensation, 9 September 2013, Run 7		
Inputs	**Equations**	**Results**
$\text{Re}_{\text{post-to-6,propane}} = 859.5$ $\text{Pr}_{\text{propane,post,out}} = 2.81$ $f = 0.074$ $k_{\text{propane,post,out}} = 0.093 \text{ W m}^{-1}\text{ K}^{-1}$ $D_{\text{line,in}} = 4.57 \text{ mm}$	$$\text{Nu} = \left(4.364^{10} + \left(\frac{e^{\frac{2200-\text{Re}}{365}}}{4.364^2} + \frac{1}{\left(6.3 + \frac{0.079 \left(\frac{f}{8} \right)^{0.5} \text{Re}\,\text{Pr}}{\left(1 + \text{Pr}^{0.8} \right)^{5/6}} \right)^2} \right)^{-5} \right)^{1/10}$$ $$h_{\text{propane,post-to-6}} = \frac{Nu_{\text{propane,post-to-6}} k_{\text{propane,pre,out}}}{D_{\text{line,in}}}$$ (Churchill, 1977a)	$\text{Nu} = 4.36$ $h_{\text{propane,post-to-6}} = 88.61 \text{ W m}^{-2}\text{ K}^{-1}$
$h_{\text{propane,post-to-6}} = 88.61 \text{ W m}^{-2}\text{ K}^{-1}$ $D_{\text{line,in}} = 4.57 \text{ mm}$ $L_{\text{post-to-6}} = 67 \text{ mm}$	$$R_{\text{1-to-pre,propane}} = \frac{1}{h_{\text{propane,1-to-pre}} \pi D_{\text{line,in}} L_{\text{1-to-pre}}}$$	$R_{\text{post-to-6,propane}} = 11.73 \text{ K W}^{-1}$
$D_{\text{line,in}} = 4.57 \text{ mm}$ $D_{\text{line,out}} = 6.35 \text{ mm}$ $L_{\text{post-to-6}} = 67 \text{ mm}$ $T_{\text{line,wall,out}} = 28.44°\text{C}^{*}$	Tube wall conduction resistance: $$k_{\text{SS316}} = f\left(T_{\text{line,wall,out}} \right)$$ $$R_{\text{post-to-6,wall}} = \frac{\ln(D_{\text{line,out}} / D_{\text{line,in}})}{2\pi k_{\text{SS316}} L_{\text{post-to-6}}}$$	$k_{\text{SS316}} = 13.47 \text{ W m}^{-1}\text{ K}^{-1}$ $R_{\text{post-to-6,wall}} = 0.0579 \text{ K W}^{-1}$

Propane In-Tube Condensation, 9 September 2013, Run 7		
Inputs	**Equations**	**Results**
$D_{\text{insulation,tube,in}} = 25$ mm $D_{\text{line,out}} = 6.35$ mm $k_{\text{insulation,wrap}} = 0.0432$ W m^{-1} K^{-1} $L_{\text{post-to-6}} = 67$ mm	Soft wrap insulation conduction resistance: $R_{\text{post-to-6,insulation,wrap}} = \dfrac{\ln(D_{\text{insulation,tube,in}} / D_{\text{line,out}})}{2\pi k_{\text{insulation,wrap}} L_{\text{post-to-6}}}$	$R_{\text{post-to-6,insulation,wrap}} = 75.36$ K W^{-1}
$D_{\text{insulation,tube,out}} = 87$ mm $D_{\text{insulation,tube,in}} = 25$ mm $k_{\text{insulation,tube}} = 0.019$ W m^{-1} K^{-1} $L_{\text{post-to-6}} = 67$ mm	Tube insulation conduction resistance: $R_{\text{post-to-6,insulation,tube}} = \dfrac{\ln(D_{\text{insulation,tube,out}} / D_{\text{insulation,tube,in}})}{2\pi k_{\text{insulation,tube}} L_{\text{post-to-6}}}$	$R_{\text{post-to-6,insulation,tube}} = 155.9$ K W^{-1}
$\epsilon_{\text{ins}} = 0.9$ $\sigma = 5.67 \times 10^{-8}$ W m^{-2} K^{-4} $T_{\text{amb}} = 303.86$ K $T_{\text{post-to-6,insulation,surface}} = 303.78$ K* $D_{\text{insulation,tube,out}} = 87$ mm $L_{\text{post-to-6}} = 67$ mm	Radiation resistance: $h_{\text{rad}} = \epsilon_{\text{ins}}\sigma\left(T_{\text{insulation,surface}}^2 + T_{\text{amb}}^2\right)\left(T_{\text{insulation,surface}} + T_{\text{amb}}\right)$ $R_{\text{post-to-6,rad}} = \dfrac{1}{\pi D_{\text{insulation,tube,out}} L_{\text{post-to-6}} h_{\text{post-to-6,rad}}}$	$h_{\text{post-to-6,rad}} = 5.72$ W m^{-2} K^{-1} $R_{\text{post-to-6,rad}} = 9.54$ K W^{-1}
$T_{\text{amb}} = 30.71$°C $T_{\text{post-to-6,insulation,surface}} = 30.63$°C* $R_{\text{post-to-6,rad}} = 9.54$ K W^{-1}	$\dot{Q}_{\text{post-to-6,rad}} = \dfrac{T_{\text{amb}} - T_{\text{post-to-6,insulation,surface}}}{R_{\text{post-to-6,rad}}}$	$\dot{Q}_{\text{post-to-6,rad}} = -0.01$ W

Propane In-Tube Condensation, 9 September 2013, Run 7		
Inputs	**Equations**	**Results**
Fluid = air $T_{amb} = 30.71°C$ $T_{post-to-6,insulation,surface} = 30.63°C^{*}$ $P_{amb} = 101$ kPa	$T_{film} = \dfrac{T_{amb} + T_{insulation,surface}}{2}$ $\rho_{air}, \mu_{air}, c_{p,air}, k_{air} = f\left(T_{film}, P_{amb}\right)$ $\beta_{air} = f\left(T_{film}\right)$ $\alpha_{air} = \dfrac{k_{air}}{\rho_{air} c_{p,air}}$ $Pr_{air} = \dfrac{c_{p,air} \mu_{air}}{k_{air}}$	$T_{post-to-6,film} = 30.67°C$ $\rho_{air} = 1.16$ kg m^{-3} $\mu_{air} = 1.88 \times 10^{-5}$ kg m^{-1} s^{-1} $c_{p,air} = 1007$ J kg^{-1} K^{-1} $k_{air} = 0.026$ W m^{-1} K^{-1} $\beta_{air} = 3.29 \times 10^{-3}$ K^{-1} $\alpha_{air} = 2.25 \times 10^{-5}$ m^2 s^{-1} $Pr_{air} = 0.719$
$\rho_{air} = 1.16$ kg m^{-3} $\mu_{air} = 1.88 \times 10^{-5}$ kg m^{-1} s^{-1} $\beta_{air} = 3.29 \times 10^{-3}$ K^{-1} $\alpha_{air} = 2.25 \times 10^{-5}$ m^2 s^{-1} $T_{amb} = 30.71°C$ $T_{post-to-6,insulation,surface} = 30.63°C^{*}$ $D_{insulation,tube,out} = 87$ mm $g = 9.81$ m s^{-2}	$Ra_{D} = \dfrac{\rho_{air} g \beta_{air} \left\|T_{insulation,surface} - T_{amb}\right\| D_{insulation,tube,out}^{3}}{\mu_{air} \alpha_{air}}$	$Ra_{D,post-to-6} = 4441$

Propane In-Tube Condensation, 9 September 2013, Run 7		
Inputs	**Equations**	**Results**
$Ra_{D,\text{post-to-6}} = 4441$ $Pr_{air} = 0.719$ $k_{air} = 0.026$ W m^{-1} K^{-1} $D_{\text{insulation,tube,out}} = 87$ mm	Natural convection from horizontal tube $$Nu_{nat.conv.} = \left(0.60 + \frac{0.387 Ra_D^{1/6}}{\left(1 + \left(\frac{0.559}{Pr} \right)^{9/16} \right)^{8/27}} \right)^2$$ $$h_{nat.conv.} = \frac{Nu_{nat.conv.} \cdot k_{air}}{D_{\text{insulation,tube,out}}}$$ (Churchill and Chu, 1975a)	$Nu_{nc,\text{post-to-6}} = 3.63$ $h_{nc,\text{post-to-6}} = 1.09$ W m^{-2} K^{-1}
$D_{\text{insulation,tube,out}} = 87$ mm $L_{\text{post-to-6}} = 67$ mm $h_{nc,\text{post-to-6}} = 1.09$ W m^{-2} K^{-1}	Natural Convection Resistance $$R_{\text{post-to-6,nc}} = \frac{1}{\pi D_{\text{insulation,tube,out}} L_{\text{post-to-6}} h_{\text{post-to-6,nc}}}$$	$R_{\text{post-to-6,nc}} = 49.90$ K W^{-1}
$T_{amb} = 30.71°C$ $T_{\text{post-to-6,insulation,surface}} = 30.63°C^*$ $R_{\text{post-to-6,nc}} = 49.90$ K W^{-1}	$$\dot{Q}_{\text{post-to-6,nc}} = \frac{T_{amb} - T_{\text{post-to-6,insulation,surface}}}{R_{\text{post-to-6,nc}}}$$	$\dot{Q}_{\text{post-to-6,nc}} = -0.001$ W

Propane In-Tube Condensation, 9 September 2013, Run 7		
Inputs	**Equations**	**Results**
$T_{\text{propane},6} = 28.33°C$ $T_{\text{amb}} = 30.71°C$ $R_{\text{post-to-6,propane}} = 11.73\ \text{K W}^{-1}$ $R_{\text{post-to-6,wall}} = 0.0579\ \text{K W}^{-1}$ $R_{\text{post-to-6,insulation,wrap}} = 75.36\ \text{K W}^{-1}$ $R_{\text{post-to-6,insulation,tube}} = 155.9\ \text{K W}^{-1}$ $R_{\text{post-to-6,rad}} = 9.54\ \text{K W}^{-1}$ $R_{\text{post-to-6,nc}} = 51.82\ \text{K W}^{-1}$	$$\dot{Q}_{\text{post-to-6,loss}} = \frac{T_{\text{propane},1} - T_{\text{post-to-6,insulation,surface}}}{\begin{array}{c} R_{\text{post-to-6,ref}} + R_{\text{post-to-6,wall}} \\ + R_{\text{post-to-6,insulation,wrap}} + R_{\text{post-to-6,insulation,tube}} \end{array}}$$ $$\dot{Q}_{\text{post-to-6,loss}} = \left(T_{\text{post-to-6,insulation,surface}} - T_{\text{amb}}\right)\left(\frac{1}{R_{\text{post-to-6,rad}}} + \frac{1}{R_{\text{post-to-6,nc}}}\right)$$	$T_{\text{post-to-6,insulation,surface}} = 30.63°C^{*}$ $\dot{Q}_{\text{post-to-6,loss}} = -0.01\ \text{W}$

Propane In-Tube Condensation, 9 September 2013, Run 7		
Inputs	**Equations**	**Results**
Heat Loss from the Post-Condenser (Figures 4.4, 4.5)		
Fluid = Air $T_{air,post,in} = 18.78°C$ $T_{air,post,out} = 29.24°C$ $P_{air,post} = 154.03$ kPa $P_{amb} = 93$ kPa $\omega = 0.00152$	$T_{air,post,avg} = \dfrac{T_{air,post,in} + T_{air,post,out}}{2}$ $\mu_{air,post,in}, k_{air,post,in}, Pr_{air,post,in} = f\left(P_{air,post}, T_{air,post,in}, \omega\right)$ $\mu_{air,post,out}, k_{air,post,out}, Pr_{air,post,out} = f\left(P_{amb}, T_{air,post,out}, \omega\right)$ $\mu_{air,post}, k_{air,post}, Pr_{air,post} = f\left(P_{air,post}, T_{air,post,avg}, \omega\right)$	$T_{air,post,avg} = 24.01°C$ $\mu_{air,post,in} = 1.82 \times 10^{-5}$ kg m^{-1} s^{-1} $k_{air,post,in} = 0.026$ W m^{-1} K^{-1} $Pr_{air,post,in} = 0.718$ $\mu_{air,post,out} = 1.87 \times 10^{-5}$ kg m^{-1} s^{-1} $k_{air,post,out} = 0.026$ W m^{-1} K^{-1} $Pr_{air,post,out} = 0.716$ $\mu_{air,post} = 1.84 \times 10^{-5}$ kg m^{-1} s^{-1} $k_{air,post} = 0.026$ W m^{-1} K^{-1} $Pr_{air,post} = 0.717$
$\dot{m}_{air,post} = 5.099 \times 10^{-3}$ kg s^{-1} $D_{Cu,line,in} = 14.25$ mm $\mu_{air,post,in} = 1.82 \times 10^{-5}$ kg m^{-1} s^{-1} $\mu_{air,post,out} = 1.87 \times 10^{-5}$ kg m^{-1} s^{-1}	$Re_{air,pre,in/out} = \dfrac{4\dot{m}_{air,pre}}{\pi \mu_{ref,pre,in/out} D_{Cu,line,in}}$	$Re_{air,post,in} = 25055$ $Re_{air,post,in} = 24387$

Propane In-Tube Condensation, 9 September 2013, Run 7		
Inputs	**Equations**	**Results**
$Re_{air,post,in} = 25055$ $Re_{air,post,in} = 24387$ $e = 0.005$ mm $D_{Cu,line,in} = 14.25$ mm	$$f = 8\left(\left(\frac{8}{Re}\right)^{12} + \frac{1}{(B+C)^{1.5}}\right)^{1/12}$$ where $B = \left(2.457\ln\frac{1}{(7/Re)^{0.9} + 0.27(e/D_{line,in})}\right)^{16}$ and $$C = \left(\frac{37530}{Re}\right)^{16}$$ (Churchill, 1977b)	$f_{air,post,in} = 0.025$ $f_{air,post,out} = 0.025$
$Re_{air,post,in} = 25055$ $Re_{air,post,in} = 24387$ $f_{air,post,in} = 0.025$ $f_{air,post,out} = 0.025$ $k_{air,post,in} = 0.026$ W m^{-1} K^{-1} $k_{air,post,out} = 0.026$ W m^{-1} K^{-1} $D_{Cu,line,in} = 14.25$ mm	$$Nu = \left(4.364^{10} + \left(\frac{e^{\frac{2200-Re}{365}}}{4.364^2} + \frac{1}{\left(6.3 + \frac{0.079\left(\frac{f}{8}\right)^{0.5} Re\, Pr}{\left(1+Pr^{0.8}\right)^{5/6}}\right)^2}\right)^{-5}\right)^{1/10}$$ $$h_{air,post,in/out} = \frac{Nu_{air,post,in/out}\, k_{air,post,in/out}}{D_{Cu,line,in}}$$ (Churchill, 1977a)	$Nu_{air,post,in} = 56.11$ $Nu_{air,post,out} = 54.83$ $h_{air,post,in} = 100.6$ W m^{-2} K^{-1} $h_{air,post,out} = 101.2$ W m^{-2} K^{-1}

Propane In-Tube Condensation, 9 September 2013, Run 7		
Inputs	**Equations**	**Results**
$p_{t,post} = 4.58$ mm $D_{post,tube,o} = 3.82$ mm $L_{post} = 275$ mm $N_{b,post} = 14$ $D_{post,shell,in} = 22.9$ mm	Exergy 00540-5 Shell and Tube Heat Exchanger $C_{post} = p_{t,post} - D_{post,tube,o}$ $B_{post} = L_{post} / N_{b,post}$ $A_{post,s} = \dfrac{D_{pre,shell,in} C_{post} B_{post}}{p_{t,pre}}$ $D_{post,e} = \dfrac{3.44 p_{t,post}^{\,2}}{\pi D_{post,tube,o}} - D_{post,tube,o}$	$C_{post} = 0.76$ mm $B_{post} = 19.6$ mm $A_{post,s} = 74.6$ mm^2 $D_{post,e} = 2.2$ mm
$\dot{m}_{air,post} = 5.099 \times 10^{-3}$ kg s^{-1} $A_{post,s} = 74.6$ mm^2 $D_{post,e} = 2.2$ mm $\mu_{air,post} = 1.84 \times 10^{-5}$ kg m^{-1} s^{-1}	$\mathrm{Re}_{post,shell} = \dfrac{\dot{m}_{air,post} D_{post,e}}{\mu_{air} A_{post,s}}$	$\mathrm{Re}_{post,shell} = 8124$
$\mathrm{Re}_{post,shell} = 8124$ $k_{air,post} = 0.026$ W m^{-1} K^{-1} $\mathrm{Pr}_{air,post} = 0.717$ $D_{post,e} = 2.2$ mm	$\mathrm{Nu}_{post,shell} = 0.36 \mathrm{Re}_{post,shell}^{\,0.55} \mathrm{Pr}_{post,pre}^{\,1/3}$ $h_{post,shell} = \dfrac{\mathrm{Nu}_{post,shell} k_{air,post}}{D_{post,e}}$	$\mathrm{Nu}_{post,shell} = 45.56$ $h_{post,shell} = 538.8$ W m^{-2} K^{-1}

Propane In-Tube Condensation, 9 September 2013, Run 7		
Inputs	**Equations**	**Results**
$h_{air,post,in} = 100.6$ W m^{-2} K^{-1} $h_{post,shell} = 538.8$ W m^{-2} K^{-1} $h_{air,post,out} = 101.2$ W m^{-2} K^{-1} $D_{Cu,line,in} = 14.25$ mm $D_{post,shell,in} = 22.9$ mm $L_{post,air} = 127$ mm $L_{post} = 275$ mm	$$R_{air} = \frac{1}{h_{air}\pi D_{wall,in}L}$$	$R_{post,in,air} = 1.75$ K W^{-1} $R_{post,HX,air} = 0.09$ K W^{-1} $R_{post,out,air} = 1.74$ K W^{-1}
$D_{Cu,line,in} = 14.25$ mm $D_{Cu,line,out} = 15.88$ mm $D_{post,shell,in} = 22.9$ mm $D_{post,shell,out} = 25.4$ mm $L_{post,air} = 127$ mm $L_{post} = 275$ mm $T_{post,in,wall,out} = 18.99°C^{*}$ $T_{post,shell,wall,out} = 24.03°C^{*}$ $T_{post,in,wall,out} = 29.27°C^{*}$	Tube wall conduction resistance: $$k_{wall} = f\left(T_{wall,out}\right)$$ $$R_{wall} = \frac{\ln(D_{wall,out} / D_{wall,in})}{2\pi k_{wall}L}$$	$k_{Cu,in} = 397.0$ W m^{-1} K^{-1} $k_{Cu,out} = 396.1$ W m^{-1} K^{-1} $k_{SS316} = 13.39$ W m^{-1} K^{-1} $R_{post,in,wall} = 3.41 \times 10^{-4}$ K W^{-1} $R_{post,HX,wall} = 4.48 \times 10^{-3}$ K W^{-1} $R_{post,out,wall} = 3.42 \times 10^{-4}$ K W^{-1}

Propane In-Tube Condensation, 9 September 2013, Run 7		
Inputs	**Equations**	**Results**
$D_{\text{insulation,tube,in}} = 25$ mm $D_{\text{Cu,line,out}} = 15.88$ mm $k_{\text{insulation,wrap}} = 0.0432$ W m^{-1} K^{-1} $L_{\text{post,air}} = 127$ mm	Soft wrap insulation conduction resistance: $R_{\text{insulation,wrap}} = \dfrac{\ln(D_{\text{insulation,tube,in}} / D_{\text{wall,out}})}{2\pi k_{\text{insulation,wrap}} L}$	$R_{\text{post,air,insulation,wrap}} = 13.17$ K W^{-1}
$D_{\text{insulation,tube,out}} = 87$ mm $D_{\text{insulation,tube,in}} = 25$ mm $k_{\text{insulation,tube}} = 0.019$ W m^{-1} K^{-1} $L_{\text{post,air}} = 127$ mm $L_{\text{post}} = 275$ mm	Tube insulation conduction resistance: $R_{\text{insulation,tube}} = \dfrac{\ln(D_{\text{insulation,tube,out}} / D_{\text{insulation,tube,in}})}{2\pi k_{\text{insulation,tube}} L}$	$R_{\text{post,air,insulation,tube}} = 82.25$ K W^{-1} $R_{\text{post,HX,insulation,tube}} = 37.98$ K W^{-1}
$\epsilon_{\text{ins}} = 0.9$ $\sigma = 5.67 \times 10^{-8}$ W m^{-2} K^{-4} $T_{\text{amb}} = 303.86$ K $T_{\text{post,in,insulation,surface}} = 303.40$ K* $T_{\text{post,HX,insulation,surface}} = 303.55$ K* $T_{\text{post,out,insulation,surface}} = 303.79$ K* $D_{\text{insulation,tube,out}} = 87$ mm $L_{\text{post,air}} = 127$ mm $L_{\text{post}} = 275$ mm	Radiation resistance: $h_{\text{rad}} = \epsilon_{\text{ins}}\sigma\left(T_{\text{insulation,surface}}^2 + T_{\text{amb}}^2\right)\left(T_{\text{insulation,surface}} + T_{\text{amb}}\right)$ $R_{\text{rad}} = \dfrac{1}{\pi D_{\text{insulation,tube,out}} L h_{\text{rad}}}$	$h_{\text{post,in,rad}} = 5.71$ W m^{-2} K^{-1} $h_{\text{post,HX,rad}} = 5.72$ W m^{-2} K^{-1} $h_{\text{post,in,rad}} = 5.72$ W m^{-2} K^{-1} $R_{\text{post,in,rad}} = 5.04$ K W^{-1} $R_{\text{post,HX,rad}} = 2.33$ K W^{-1} $R_{\text{post,out,rad}} = 5.03$ K W^{-1}

Propane In-Tube Condensation, 9 September 2013, Run 7		
Inputs	**Equations**	**Results**
$T_{amb} = 30.71°C$ $T_{post,in,insulation,surface} = 30.25°C^*$ $T_{post,HX,insulation,surface} = 30.40°C^*$ $T_{post,out,insulation,surface} = 30.64°C^*$ $R_{post,in,rad} = 5.04$ K W^{-1} $R_{post,HX,rad} = 2.33$ K W^{-1} $R_{post,out,rad} = 5.03$ K W^{-1}	$\dot{Q}_{post,in,rad} = \dfrac{T_{amb} - T_{post,in,insulation,surface}}{R_{post,in,rad}}$ $\dot{Q}_{post,HX,rad} = \dfrac{T_{amb} - T_{post,HX,insulation,surface}}{R_{post,HX,rad}}$ $\dot{Q}_{post,out,rad} = \dfrac{T_{amb} - T_{post,in,insulation,surface}}{R_{post,out,rad}}$	$\dot{Q}_{post,in,rad} = -0.09$ W $\dot{Q}_{post,HX,rad} = -0.13$ W $\dot{Q}_{post,out,rad} = -0.01$ W
Fluid = air $T_{amb} = 30.71°C$ $T_{post,in,insulation,surface} = 30.25°C^*$ $T_{post,HX,insulation,surface} = 30.40°C^*$ $T_{post,out,insulation,surface} = 30.64°C^*$ $P_{amb} = 93$ kPa	$T_{film} = \dfrac{T_{amb} + T_{insulation,surface}}{2}$ $\rho_{air}, \mu_{air}, c_{p,air}, k_{air} = f\left(T_{film}, P_{amb}\right)$ $\beta_{air} = f\left(T_{film}\right)$ $\alpha_{air} = \dfrac{k_{air}}{\rho_{air} c_{p,air}}$ $\text{Pr}_{air} = \dfrac{c_{p,air} \mu_{air}}{k_{air}}$	$T_{post,in,film} = 30.47°C^*$ $T_{post,HX,film} = 30.55°C^*$ $T_{post,out,film} = 30.68°C^*$ $\rho_{air} = 1.16$ kg m^{-3} $\mu_{air} = 1.88 \times 10^{-5}$ kg m^{-1} s^{-1} $c_{p,air} = 1007$ J kg^{-1} K^{-1} $k_{air} = 0.026$ W m^{-1} K^{-1} $\beta_{air} = 3.29 \times 10^{-3}$ K^{-1} $\alpha_{air} = 2.24 \times 10^{-5}$ m^2 s^{-1} $\text{Pr}_{air} = 0.719$

Propane In-Tube Condensation, 9 September 2013, Run 7		
Inputs	**Equations**	**Results**
$\rho_{air} = 1.16 \text{ kg m}^{-3}$ $\mu_{air} = 1.88 \times 10^{-5} \text{ kg m}^{-1} \text{ s}^{-1}$ $\beta_{air} = 3.29 \times 10^{-3} \text{ K}^{-1}$ $\alpha_{air} = 2.24 \times 10^{-5} \text{ m}^2 \text{ s}^{-1}$ $T_{amb} = 30.71°C$ $T_{post,in,insulation,surface} = 30.25°C^*$ $T_{post,HX,insulation,surface} = 30.40°C^*$ $T_{post,out,insulation,surface} = 30.64°C^*$ $D_{insulation,tube,out} = 87 \text{ mm}$ $g = 9.81 \text{ m s}^{-2}$	$$\text{Ra}_D = \frac{\rho_{air} \, g \, \beta_{air} \left| T_{insulation,surface} - T_{amb} \right| D_{insulation,tube,out}^3}{\mu_{air} \alpha_{air}}$$	$\text{Ra}_{D,post,in} = 27011$ $\text{Ra}_{D,post,HX} = 18087$ $\text{Ra}_{D,post,out} = 3603$
$\text{Ra}_{D,post,in} = 27011$ $\text{Ra}_{D,post,HX} = 18087$ $\text{Ra}_{D,post,out} = 3603$ $\text{Pr}_{air} = 0.719$	Natural convection from horizontal tube $$\text{Nu}_{nat.conv.} = \left(0.60 + \frac{0.387 \text{Ra}_D^{1/6}}{\left(1 + \left(\frac{0.559}{\text{Pr}} \right)^{9/16} \right)^{8/27}} \right)^2$$ (Churchill and Chu, 1975a)	$\text{Nu}_{nc,post,in} = 5.58$ $\text{Nu}_{nc,post,HX} = 5.05$ $\text{Nu}_{nc,post,out} = 3.46$

Propane In-Tube Condensation, 9 September 2013, Run 7		
Inputs	**Equations**	**Results**
$Nu_{nc,post,in} = 5.58$ $Nu_{nc,post,HX} = 5.05$ $Nu_{nc,post,out} = 3.46$ $k_{air} = 0.026$ W m^{-1} K^{-1} $D_{insulation,tube,out} = 87$ mm	$$h_{nc} = \frac{Nu_{nat.conv.} \cdot k_{air}}{D_{insulation,tube,out}}$$	$h_{nc,post,in} = 1.68$ W m^{-2} K^{-1} $h_{nc,post,HX} = 1.53$ W m^{-2} K^{-1} $h_{nc,post,out} = 1.04$ W m^{-2} K^{-1}
$D_{insulation,tube,out} = 87$ mm $L_{post,air} = 127$ mm $L_{post} = 275$ mm $h_{nc,post,in} = 1.68$ W m^{-2} K^{-1} $h_{nc,post,HX} = 1.53$ W m^{-2} K^{-1} $h_{nc,post,out} = 1.04$ W m^{-2} K^{-1}	Natural Convection Resistance $$R_{nc} = \frac{1}{\pi D_{insulation,tube,out} L h_{nc}}$$	$R_{post,in,nc} = 17.12$ K W^{-1} $R_{post,HX,nc} = 8.73$ K W^{-1} $R_{post,out,nc} = 27.60$ K W^{-1}
$T_{amb} = 30.71°C$ $T_{post,in,insulation,surface} = 30.25°C^*$ $T_{post,HX,insulation,surface} = 30.40°C^*$ $T_{post,out,insulation,surface} = 30.64°C^*$ $R_{post,in,nc} = 17.12$ K W^{-1} $R_{post,HX,nc} = 8.73$ K W^{-1} $R_{post,out,nc} = 27.60$ K W^{-1}	$$\dot{Q}_{post,in,nc} = \frac{T_{amb} - T_{post,in,insulation,surface}}{R_{post,in,nc}}$$ $$\dot{Q}_{post,HX,nc} = \frac{T_{amb} - T_{post,HX,insulation,surface}}{R_{post,HX,nc}}$$ $$\dot{Q}_{post,out,nc} = \frac{T_{amb} - T_{post,out,insulation,surface}}{R_{post,out,nc}}$$	$\dot{Q}_{post,in,nc} = -0.03$ W $\dot{Q}_{post,HX,nc} = -0.04$ W $\dot{Q}_{post,out,nc} = -0.002$ W

Propane In-Tube Condensation, 9 September 2013, Run 7		
Inputs	**Equations**	**Results**
$T_{\text{air,post,in}} = 18.78°C$ $T_{\text{amb}} = 30.71°C$ $R_{\text{post,in,air}} = 1.75 \text{ K W}^{-1}$ $R_{\text{post,in,wall}} = 3.41 \times 10^{-4} \text{ K W}^{-1}$ $R_{\text{post,air,insulation,wrap}} = 13.17 \text{ K W}^{-1}$ $R_{\text{post,air,insulation,tube}} = 82.25 \text{ K W}^{-1}$ $R_{\text{post,in,rad}} = 5.04 \text{ K W}^{-1}$ $R_{\text{post,in,nc}} = 17.12 \text{ K W}^{-1}$	$\dot{Q}_{\text{post,in,loss}} = \dfrac{T_{\text{air,post,in}} - T_{\text{post,in,insulation,surface}}}{R_{\text{post,in,air}} + R_{\text{post,in,wall}} + R_{\text{post,air,insulation,wrap}} + R_{\text{post,air,insulation,tube}}}$ $\dot{Q}_{\text{post,in,loss}} = \left(T_{\text{post,in,insulation,surface}} - T_{\text{amb}} \right)\left(\dfrac{1}{R_{\text{post,in,rad}}} + \dfrac{1}{R_{\text{post,in,nc}}} \right)$	$T_{\text{post,in,insulation,surface}} = 30.25°C^{*}$ $\dot{Q}_{\text{post,in,loss}} = -0.12 \text{ W}$
$T_{\text{air,post,avg}} = 24.01°C$ $T_{\text{amb}} = 30.71°C$ $R_{\text{post,HX,air}} = 0.09 \text{ K W}^{-1}$ $R_{\text{post,HX,wall}} = 4.48 \times 10^{-3} \text{ K W}^{-1}$ $R_{\text{post,HX,insulation,tube}} = 37.98 \text{ K W}^{-1}$ $R_{\text{post,HX,rad}} = 2.33 \text{ K W}^{-1}$ $R_{\text{post,HX,nc}} = 8.73 \text{ K W}^{-1}$	$\dot{Q}_{\text{post,HX,loss}} = \dfrac{T_{\text{air,post,avg}} - T_{\text{post,HX,insulation,surface}}}{R_{\text{post,HX,air}} + R_{\text{post,HX,wall}} + R_{\text{post,HX,insulation,tube}}}$ $\dot{Q}_{\text{post,HX,loss}} = \left(T_{\text{post,HX,insulation,surface}} - T_{\text{amb}} \right)\left(\dfrac{1}{R_{\text{post,HX,rad}}} + \dfrac{1}{R_{\text{post,HX,nc}}} \right)$	$T_{\text{post,HX,insulation,surface}} = 30.40°C^{*}$ $\dot{Q}_{\text{post,HX,loss}} = -0.17 \text{ W}$

Propane In-Tube Condensation, 9 September 2013, Run 7		
Inputs	**Equations**	**Results**
$T_{air,post,out} = 29.24°C$ $T_{amb} = 30.71°C$ $R_{post,out,air} = 1.74 \text{ K W}^{-1}$ $R_{post,out,wall} = 3.42 \times 10^{-4} \text{ K W}^{-1}$ $R_{post,air,insulation,wrap} = 13.17 \text{ K W}^{-1}$ $R_{post,air,insulation,tube} = 82.25 \text{ K W}^{-1}$ $R_{post,out,rad} = 5.03 \text{ K W}^{-1}$ $R_{post,out,nc} = 27.60 \text{ K W}^{-1}$	$$\dot{Q}_{post,out,loss} = \frac{T_{air,post,out} - T_{post,out,insulation,surface}}{\begin{array}{c} R_{post,out,air} + R_{post,out,wall} \\ + R_{post,air,insulation,wrap} + R_{post,air,insulation,tube} \end{array}}$$ $$\dot{Q}_{postout,loss} = \left(T_{post,out,insulation,surface} - T_{amb}\right)\left(\frac{1}{R_{post,out,rad}} + \frac{1}{R_{post,out,nc}}\right)$$	$T_{post,out,insulation,surface} = 30.64°C^*$ $\dot{Q}_{post,out,loss} = -0.01 \text{ W}$
$\dot{Q}_{post,in,loss} = -0.12 \text{ W}$ $\dot{Q}_{post,HX,loss} = -0.17 \text{ W}$ $\dot{Q}_{post,out,loss} = -0.01 \text{ W}$	$$\dot{Q}_{post,loss} = \dot{Q}_{post,in,loss} + \dot{Q}_{post,HX,loss} + \dot{Q}_{post,out,loss}$$	$\dot{Q}_{post,loss} = -0.30 \text{ W}$
Heat Loss Between the Post-Condenser and Test Section (Figures 4.3, 4.4)		
$T_{propane,4} = 46.52°C$ $T_{propane,5} = 46.75°C$	Assuming negligible convective resistance: $$T_{45,wall,in} = \frac{T_{propane,4} + T_{propane,5}}{2}$$	$T_{45,wall,in} = 46.64°C$

Propane In-Tube Condensation, 9 September 2013, Run 7		
Inputs	**Equations**	**Results**
$D_{line,in} = 4.57$ mm $D_{line,out} = 6.35$ mm $L_{4\text{-}to\text{-}5} = 299$ mm $T_{line,wall,out} = 46.63°C^{*}$	Detailed analysis shown for one segment ("4-to-5" tube); other segments calculated similarly. Tube wall conduction resistance: $$k_{SS316} = f\left(T_{line,wall,out}\right)$$ $$R_{wall} = \frac{\ln(D_{wall,out} / D_{wall,in})}{2\pi k_{SS316}L}$$	$k_{SS316} = 13.79$ W m^{-1} K^{-1} $R_{4\text{-}to\text{-}5,wall} = 0.013$ K W^{-1}
$D_{insulation,tube,in} = 25$ mm $D_{line,out} = 6.35$ mm $k_{insulation,wrap} = 0.0432$ W m^{-1} K^{-1} $L_{4\text{-}to\text{-}5} = 299$ mm	Soft wrap insulation conduction resistance: $$R_{insulation,wrap} = \frac{\ln(D_{insulation,tube,in} / D_{wall,out})}{2\pi k_{insulation,wrap}L}$$	$R_{4\text{-}to\text{-}5,insulation,wrap} = 16.89$ K W^{-1}
$D_{insulation,tube,out} = 87$ mm $D_{insulation,tube,in} = 25$ mm $k_{insulation,tube} = 0.019$ W m^{-1} K^{-1} $L_{4\text{-}to\text{-}5} = 299$ mm	Tube insulation conduction resistance: $$R_{insulation,tube} = \frac{\ln(D_{insulation,tube,out} / D_{insulation,tube,in})}{2\pi k_{insulation,tube}L}$$	$R_{4\text{-}to\text{-}5,insulation,tube} = 34.94$ K W^{-1}

Propane In-Tube Condensation, 9 September 2013, Run 7		
Inputs	**Equations**	**Results**
$\epsilon_{ins} = 0.9$ $\sigma = 5.67 \times 10^{-8}$ W m^{-2} K^{-4} $T_{amb} = 303.86$ K $T_{4\text{-to-}5,insulation,surface} = 304.35$ K* $D_{insulation,tube,out} = 87$ mm $L_{4\text{-to-}5} = 299$ mm	Radiation resistance: $h_{rad} = \epsilon_{ins}\sigma\left(T^2_{insulation,surface} + T^2_{amb}\right)\left(T_{insulation,surface} + T_{amb}\right)$ $R_{rad} = \dfrac{1}{\pi D_{insulation,tube,out} L h_{rad}}$	$h_{4\text{-to-}5,rad} = 5.74$ W m^{-2} K^{-1} $R_{4\text{-to-}5,rad} = 2.13$ K W^{-1}
$T_{amb} = 30.71$°C $T_{4\text{-to-}5,insulation,surface} = 31.20$°C* $R_{4\text{-to-}5,rad} = 2.13$ K W^{-1}	$\dot{Q}_{rad} = \dfrac{T_{amb} - T_{insulation,surface}}{R_{rad}}$	$\dot{Q}_{4\text{-to-}5,rad} = 0.23$ W
Fluid = air $T_{amb} = 30.71$°C $T_{4\text{-to-}5,insulation,surface} = 31.20$°C* $P_{amb} = 101$ kPa $D_{insulation,tube,out} = 87$ mm $g = 9.81$ m s^{-2}	$T_{film} = \dfrac{T_{amb} + T_{insulation,surface}}{2}$ $\rho_{air}, \mu_{air}, c_{p,air}, k_{air} = f\left(T_{film}, P_{amb}\right)$ $\beta_{air} = f\left(T_{film}\right)$ $\alpha_{air} = \dfrac{k_{air}}{\rho_{air} c_{p,air}}$ $Pr_{air} = \dfrac{c_{p,air} \mu_{air}}{k_{air}}$	$T_{4\text{-to-}5,film} = 30.95$°C $\rho_{air} = 1.16$ kg m^{-3} $\mu_{air} = 1.88 \times 10^{-5}$ kg m^{-1} s^{-1} $c_{p,air} = 1007$ J kg^{-1} K^{-1} $k_{air} = 0.026$ W m^{-1} K^{-1} $\beta_{air} = 3.29 \times 10^{-3}$ K^{-1} $\alpha_{air} = 2.25 \times 10^{-5}$ m^2 s^{-1} $Pr_{air} = 0.719$

Propane In-Tube Condensation, 9 September 2013, Run 7		
Inputs	**Equations**	**Results**
	$$\mathrm{Ra}_D = \frac{\rho_{air}\, g\, \beta_{air} \left| T_{insulation,surface} - T_{amb} \right| D^3_{insulation,tube,out}}{\mu_{air}\, \alpha_{air}}$$	$\mathrm{Ra}_{D,4\text{-to-}5} = 28557$
$\mathrm{Ra}_{D,4\text{-to-}5} = 28557$ $\mathrm{Pr}_{air} = 0.719$ $k_{air} = 0.026$ W m^{-1} K^{-1} $D_{insulation,tube,out} = 87$ mm	Natural convection from horizontal tube $$\mathrm{Nu}_{nat.conv.} = \left(0.60 + \frac{0.387\,\mathrm{Ra}_D^{1/6}}{\left(1 + \left(\frac{0.559}{\mathrm{Pr}} \right)^{9/16} \right)^{8/27}} \right)^2$$ $$h_{nat.conv.} = \frac{\mathrm{Nu}_{nat.conv.} \cdot k_{air}}{D_{insulation,tube,out}}$$ (Churchill and Chu, 1975a)	$\mathrm{Nu}_{nc,4\text{-to-}5} = 5.66$ $h_{nc,4\text{-to-}5} = 1.71$ W m^{-2} K^{-1}
$D_{insulation,tube,out} = 87$ mm $L_{4\text{-to-}5} = 299$ mm $h_{nc,4\text{-to-}5} = 1.71$ W m^{-2} K^{-1}	Natural Convection Resistance $$R_{nc} = \frac{1}{\pi D_{insulation,tube,out} L h_{nc}}$$	$R_{4\text{-to-}5,nc} = 7.16$ K W^{-1}
$T_{amb} = 30.71°C$ $T_{4\text{-to-}5,insulation,surface} = 31.20°C^{*}$ $R_{4\text{-to-}5,nc} = 7.16$ K W^{-1}	$$\dot{Q}_{nc} = \frac{T_{amb} - T_{insulation,surface}}{R_{nc}}$$	$\dot{Q}_{4\text{-to-}5,nc} = 0.07$ W

Propane In-Tube Condensation, 9 September 2013, Run 7		
Inputs	**Equations**	**Results**
$T_{23,\text{wall,in}} = 46.64°C$ $T_{\text{amb}} = 30.71°C$ $R_{4\text{-to-5,wall}} = 0.013 \text{ K W}^{-1}$ $R_{4\text{-to-5,insulation,wrap}} = 16.89 \text{ K W}^{-1}$ $R_{4\text{-to-5,insulation,tube}} = 34.94 \text{ K W}^{-1}$ $R_{4\text{-to-5,rad}} = 2.13 \text{ K W}^{-1}$ $R_{4\text{-to-5,nc}} = 7.16 \text{ K W}^{-1}$	$\dot{Q}_{4\text{-to-5,line,loss}} = \dfrac{T_{\text{propane,45,wall,in}} - T_{4\text{-to-5,insulation,surface}}}{R_{4\text{-to-5,wall}} + R_{4\text{-to-5,insulation,wrap}} + R_{4\text{-to-5,insulation,tube}}}$ $\dot{Q}_{4\text{-to-5,line,loss}} = \left(T_{4\text{-to-5,insulation,surface}} - T_{\text{amb}}\right)\left(\dfrac{1}{R_{4\text{-to-5,rad}}} + \dfrac{1}{R_{4\text{-to-5,nc}}}\right)$	$T_{4\text{-to-5,insulation,surface}} = 31.20°C^{*}$ $\dot{Q}_{4\text{-to-5,line,loss}} = 0.30 \text{ W}$
$T_{23,\text{wall,in}} = 46.64°C$ $T_{\text{amb}} = 30.71°C$ $R_{\text{valve,23,wall}} = 0.329 \text{ K W}^{-1}$ $R_{\text{valve,23, insulation,wrap}} = 20.22 \text{ K W}^{-1}$ $R_{\text{valve,23, insulation,tube}} = 208.9 \text{ K W}^{-1}$ $R_{\text{valve,23, rad}} = 12.74 \text{ K W}^{-1}$ $R_{\text{valve,23, nc}} = 39.99 \text{ K W}^{-1}$	$\dot{Q}_{\text{valve,45,loss}} = \dfrac{T_{\text{propane,45,wall,in}} - T_{\text{valve,45,insulation,surface}}}{R_{\text{valve,45,wall}} + R_{\text{valve,45,insulation,wrap}} + R_{\text{valve,45,insulation,tube}}}$ $\dot{Q}_{\text{valve,45,loss}} = \left(T_{\text{valve,45,insulation,surface}} - T_{\text{amb}}\right)\left(\dfrac{1}{R_{\text{valve,45,rad}}} + \dfrac{1}{R_{\text{valve,45,nc}}}\right)$	$T_{\text{valve,45,insulation,surface}} = 31.36°C^{*}$ $\dot{Q}_{\text{valve,45,loss}} = 0.07 \text{ W}$
Heat Losses from Test Section Inlet Pressure Tap (Figures 4.2, 4.4)		
$T_{\text{propane,4}} = 46.52°C$	Assuming negligible convective resistance: $T_{\text{test,line,out,1h,wall,in}} = T_{\text{propane,4}}$	$T_{\text{test,line,out,1h,wall,in}} = 46.52°C$

Propane In-Tube Condensation, 9 September 2013, Run 7		
Inputs	**Equations**	**Results**
Measured wall surface temperatures: $T_{\text{wall,line,4}} = 32.45°C$ $T_{\text{wall,line,5}} = 31.67°C$	$$T_{\text{line,out,2v,wall,out}} = \frac{T_{\text{wall,line,4}} + T_{\text{wall,line,5}}}{2}$$ $T_{\text{line,in,3h,wall,out}} = T_{\text{line,in,4h,wall,out}} = T_{\text{wall,line,5}}$ $T_{\text{line,in,5v,wall,out}} = T_{\text{line,in,6v,wall,out}} = T_{\text{wall,line,5}}$	$T_{\text{line,out,2h,wall,out}} = 32.06°C$ $T_{\text{line,out,3h,wall,out}} = 31.67°C$ $T_{\text{line,out,4v,wall,out}} = 31.67°C$ $T_{\text{line,out,5v,wall,out}} = 31.67°C$ $T_{\text{line,out,6h,wall,out}} = 31.67°C$
$D_{\text{line,in}} = 4.57$ mm $D_{\text{line,out}} = 6.35$ mm $T_{\text{line,out,1h,wall,out}} = 46.52°C^{*}$ $L_{\text{line,out,1h}} = 241.3$ mm	Detailed analysis given for one segment; analysis is similar for all others: Tube wall conduction resistance: $$k_{\text{SS316}} = f\left(T_{\text{test,line,out,}j\text{,wall,out}}\right)$$ $$R_{\text{line,out,}j\text{,wall}} = \frac{\ln(D_{\text{line,out}} / D_{\text{line,in}})}{2\pi k_{\text{SS316}} L_{\text{test,line,out,}j}}$$	$k_{\text{SS316}} = 13.79$ W m^{-1} K^{-1} $R_{\text{line,out,1h,wall}} = 0.016$ K W^{-1}
$D_{\text{insulation,tube,out}} = 73.7$ mm $D_{\text{insulation,tube,in}} = 25$ mm $D_{\text{line,out}} = 6.35$ mm $k_{\text{insulation,wrap}} = 0.0432$ W m^{-1} K^{-1}	Soft wrap insulation conduction resistance: $$R_{\text{line,out,}j\text{,insulation,wrap}} = \frac{\ln(D_{\text{insulation,wrap,in}} / D_{\text{line,out}})}{2\pi k_{\text{insulation,wrap}} L_{\text{test,line,out,}j}}$$	$R_{\text{line,out,1h,insulation,wrap}} = 20.9$ K W^{-1}
$k_{\text{insulation,tube}} = 0.019$ W m^{-1} K^{-1} $L_{\text{line,out,1h}} = 241.3$ mm	Tube insulation conduction resistance: $$R_{\text{line,out,}j\text{,insulation,tube}} = \frac{\ln(D_{\text{insulation,tube,out}} / D_{\text{insulation,tube,in}})}{2\pi k_{\text{insulation,tube}} L_{\text{test,line,out,}j}}$$	$R_{\text{line,out,1h,insulation,tube}} = 37.5$ K W^{-1}

Propane In-Tube Condensation, 9 September 2013, Run 7		
Inputs	**Equations**	**Results**
$\epsilon_{\text{ins}} = 0.9$ $\sigma = 5.67 \times 10^{-8}$ W m^{-2} K^{-4} $D_{\text{insulation,tube,out}} = 73.7$ mm $T_{\text{amb}} = 303.86$ K $T_{\text{line,out,1h,insulation,surface}} = 304.47$ K* $L_{\text{line,out,1h}} = 241.3$ mm	Radiation resistance: $$h_{\text{rad}} = \epsilon_{\text{ins}}\sigma\left(T^2_{\text{insulation,surface}} + T^2_{\text{amb}}\right)\left(T_{\text{insulation,surface}} + T_{\text{amb}}\right)$$ $$R_{\text{line,out},j,\text{rad}} = \frac{1}{\pi D_{\text{insulation,tube,out}} L_{\text{test,line,out},j} h_{\text{test,line,out},j,\text{rad}}}$$	$h_{\text{line,out,1h,rad}} = 5.74$ W m^{-2} K^{-1} $R_{\text{line,out,1h,rad}} = 3.12$ K W^{-1}
	$$\dot{Q}_{\text{test,line,out},j,\text{rad}} = \frac{T_{\text{amb}} - T_{\text{test,line,out},j,\text{insulation,surface}}}{R_{\text{test,line,out},j,\text{rad}}}$$	$\dot{Q}_{\text{test,line,out,1h,rad}} = 0.20$ W
Fluid = air $T_{\text{amb}} = 30.71$°C $T_{\text{line,out,1h,insulation,surface}} = 31.32$°C* $P_{\text{amb}} = 101$ kPa $D_{\text{insulation,tube,out}} = 73.7$ mm $g = 9.81$ m s^{-2} $T_{\text{line,out,2v,insulation,surface}} = 30.76$°C* $L_{\text{line,out,2v}} = 228.6$ mm	$$T_{\text{film}} = \frac{T_{\text{amb}} + T_{\text{insulation,surface}}}{2}$$ $$\rho_{\text{air}}, \mu_{\text{air}}, c_{\text{p,air}}, k_{\text{air}} = f\left(T_{\text{film}}, P_{\text{amb}}\right)$$ $$\beta_{\text{air}} = f\left(T_{\text{film}}\right)$$ $$\alpha_{\text{air}} = \frac{k_{\text{air}}}{\rho_{\text{air}} c_{\text{p,air}}}$$ $$\text{Pr}_{\text{air}} = \frac{c_{\text{p,air}} \mu_{\text{air}}}{k_{\text{air}}}$$	$T_{\text{line,out,1h,film}} = 31.01$°C $T_{\text{line,out,2v,film}} = 30.73$°C $\rho_{\text{air}} = 1.16$ kg m^{-3} $\mu_{\text{air}} = 1.88 \times 10^{-5}$ kg m^{-1} s^{-1} $c_{\text{p,air}} = 1007$ J kg^{-1} K^{-1} $k_{\text{air}} = 0.026$ W m^{-1} K^{-1} $\beta_{\text{air}} = 3.29 \times 10^{-3}$ K^{-1} $\alpha_{\text{air}} = 2.25 \times 10^{-5}$ m^2 s^{-1} $\text{Pr}_{\text{air}} = 0.719$

Propane In-Tube Condensation, 9 September 2013, Run 7		
Inputs	**Equations**	**Results**
	$$\mathrm{Ra}_D = \frac{\rho_{air}\, g\, \beta_{air}\, \left|T_{insulation,surface} - T_{amb}\right|\, D^3_{insulation,tube,out}}{\mu_{air}\alpha_{air}}$$	$\mathrm{Ra}_{D,line,out,1h} = 21613$
	$$\mathrm{Ra}_L = \frac{\rho_{air}\, g\, \beta_{air}\, \left|T_{insulation,surface} - T_{amb}\right|\, L^3_{test,line,in,jv}}{\mu_{air}\alpha_{air}}$$	$\mathrm{Ra}_{L,\,line,out,2v} = 60630$
$\mathrm{Ra}_{D,line,out,1h} = 21613$ $\mathrm{Pr}_{air} = 0.719$	Natural convection from horizontal tube $$\mathrm{Nu}_{nat.conv.} = \left(0.60 + \frac{0.387\mathrm{Ra}_D^{1/6}}{\left(1 + \left(\frac{0.559}{\mathrm{Pr}}\right)^{9/16}\right)^{8/27}}\right)^2$$ (Churchill and Chu, 1975a)	$\mathrm{Nu}_{line,out,1h} = 5.28$
$\mathrm{Ra}_{L,\,line,out,2v} = 60630$ $\mathrm{Pr}_{air} = 0.719$	Natural convection from vertical plate $$\mathrm{Nu}_{nat.conv.,plate} = \left(0.825 + \frac{0.387\mathrm{Ra}_L^{1/6}}{\left(1 + \left(\frac{0.492}{\mathrm{Pr}}\right)^{9/16}\right)^{8/27}}\right)^2$$ (Churchill and Chu, 1975b)	$\mathrm{Nu}_{line,out,2v,plate} = 8.18$

Propane In-Tube Condensation, 9 September 2013, Run 7		
Inputs	**Equations**	**Results**
$Ra_{L, line,out,2v} = 60630$ $Pr_{air} = 0.719$ $Nu_{line,out,2v,plate} = 8.18$ $D_{insulation,tube,out} = 73.7$ mm $L_{line,out,2v} = 228.6$ mm	$$Gr_L = \frac{Ra_L}{Pr}$$ $$\zeta = \frac{1.8}{Nu_{nat.conv.,plate}} \frac{L}{D}$$ $$Nu_{nat.conv.,vertical,cylinder} = \begin{cases} Nu_{nat.conv.,plate} & \text{if } \dfrac{D}{L} > \dfrac{35}{Gr_L^{0.25}} \\ Nu_{nat.conv.,plate} \dfrac{\zeta}{\ln(1+\zeta)} & \text{if } \dfrac{D}{L} \le \dfrac{35}{Gr_L^{0.25}} \end{cases}$$ (Sparrow and Gregg, 1956)	$Gr_{L, line,out,2v} = 84314$ $(D/L)_{line,out,2v} = 0.32 < 2.1$ $\zeta_{line,out,2v} = 0.71$ $Nu_{line,out,2v} = 10.73$
$Nu_{line,out,1h} = 5.28$ $Nu_{line,out,2v} = 10.73$ $k_{air} = 0.026$ W m^{-1} K^{-1} $D_{insulation,tube,out} = 73.7$ mm $L_{line,out,2v} = 196.9$ mm	$$h_{nat.conv.} = \frac{Nu_{nat.conv.} \cdot k_{air}}{D_{insulation,tube,out}}$$ $$h_{nat.conv.,vertical} = \frac{Nu_{nat.conv.} \cdot k_{air}}{L}$$	$h_{nc,line,out,1h} = 1.88$ W m^{-2} K^{-1} $h_{nc, line,out,2v} = 1.23$ W m^{-2} K^{-1}
$D_{insulation,tube,out} = 73.7$ mm $L_{line,out,1h} = 241.3$ mm $h_{nc,line,out,1h} = 1.88$ W m^{-2} K^{-1}	Natural Convection Resistance $$R_{test,line,out,j,nc} = \frac{1}{\pi D_{insulation,tube,out} L_{test,line,out,j} h_{test,line,out,j,nc}}$$	$R_{line,out,1h,nc} = 9.51$ K W^{-1}

Propane In-Tube Condensation, 9 September 2013, Run 7		
Inputs	**Equations**	**Results**
$T_\text{amb} = 30.71°C$ $T_\text{line,out,1h,insulation,surface} = 31.32°C^{*}$ $R_\text{line,out,1h,nc} = 9.51 \text{ K W}^{-1}$	$\dot{Q}_\text{test,line,out,}j\text{,nc} = \dfrac{T_\text{amb} - T_\text{test,line,out,}j\text{,insulation,surface}}{R_\text{test,line,out,}j\text{,nc}}$	$\dot{Q}_\text{test,line,out,1h,nc} = 0.06 \text{ W}$
$T_\text{test,line,out,1h,wall,in} = 46.52°C$ $T_\text{amb} = 30.71°C$ $R_\text{line,out,1h,wall} = 0.016 \text{ K W}^{-1}$ $R_\text{line,out,1h,insulation,wrap} = 20.9 \text{ K W}^{-1}$ $R_\text{line,out,1h,insulation,tube} = 37.5 \text{ K W}^{-1}$ $R_\text{line,out,1h,rad} = 3.11 \text{ K W}^{-1}$ $R_\text{line,out,1h,nc} = 9.51 \text{ K W}^{-1}$	$\dot{Q}_\text{test,line,in,}j\text{,loss} = \dfrac{T_\text{ref,test,wall,in,}j - T_\text{test,line,in,}j\text{,wall,out}}{R_\text{test,line,in,}j\text{,wall}}$ $\dot{Q}_\text{test,line,in,}j\text{,loss} = \dfrac{T_\text{test,line,in,}j\text{,wall,out} - T_\text{test,line,in,}j\text{,insulation,surface}}{R_\text{test,line,}j\text{,in,insulation,wrap} + R_\text{test,line,in,}j\text{,insulation,tube}}$ $\dot{Q}_\text{test,line,in,}j\text{,loss} = \dfrac{T_\text{test,line,in,}j\text{,insulation,surface} - T_\text{amb}}{\left(\dfrac{1}{R_\text{test,line,in,}j\text{,rad}} + \dfrac{1}{R_\text{test,line,in,}j\text{,nc}}\right)^{-1}}$	$T_\text{test,line,out,1h,wall,out} = 46.52°C$ $T_\text{line,out,1h,insulation,surface} = 31.32°C^{*}$ $\dot{Q}_\text{test,line,in,1h,loss} = 0.26 \text{ W}$
$\dot{Q}_\text{test,line,out,1h,loss} = 0.26 \text{ W}$ $\dot{Q}_\text{test,line,out,2v,loss} = 0.02 \text{ W}$ $\dot{Q}_\text{test,line,out,3h,loss} = 0.02 \text{ W}$ $\dot{Q}_\text{test,line,out,4h,loss} = 0.02 \text{ W}$ $\dot{Q}_\text{test,line,out,5v,loss} = 0.01 \text{ W}$ $\dot{Q}_\text{test,line,out,6v,loss} = 0.01 \text{ W}$	$\dot{Q}_\text{test,line,out,loss} = \displaystyle\sum_{j=1}^{6} \dot{Q}_\text{test,line,out,}j\text{,loss}$	$\dot{Q}_\text{test,line,out,loss} = 0.34 \text{ W}$

Propane In-Tube Condensation, 9 September 2013, Run 7		
Inputs	**Equations**	**Results**
$\dot{Q}_{\text{4-to-5,line,loss}} = 0.30 \text{ W}$ $\dot{Q}_{\text{valve,45,loss}} = 0.07 \text{ W}$ $\dot{Q}_{\text{test,line,out,loss}} = 0.34 \text{ W}$	$\dot{Q}_{\text{loss,4-to-5}} = \dot{Q}_{\text{4-to-5,line,loss}} + \dot{Q}_{\text{valve,45,loss}} + \dot{Q}_{\text{test,line,in,loss}}$	$\dot{Q}_{\text{loss,4-to-5}} = 0.71 \text{ W}$

C.2. Test Section Heat Transfer Coefficient

Propane In-Tube Condensation, 9 September 2013, Run 7		
Inputs	**Equations**	**Results**
$\dot{m}_{\text{propane}} = 2.932 \times 10^{-4}$ kg s^{-1} $i_{\text{propane},3} = 538.5$ kJ kg^{-1} $i_{\text{propane},4} = 461.4$ kJ kg^{-1} $x_3 = 0.72$ $x_4 = 0.46$	$\dot{Q}_{\text{test}} = \dot{m}_{\text{propane}}(i_{\text{ref},3} - i_{\text{ref},4})$ $\Delta x = x_3 - x_4$	$\dot{Q}_{\text{test}} = 22.61$ W $\Delta x = 0.26$
$T_{\text{propane},3} = 47.01°C$ $T_{\text{propane},4} = 46.52°C$ $T_{\text{water,test,in}} = 36.80°C$ $T_{\text{water,test,out}} = 36.98°C$	$\Delta T_{\text{LM,test}} = \dfrac{(T_{\text{propane},3} - T_{\text{water,test,out}}) - (T_{\text{propane},4} - T_{\text{water,test,in}})}{\ln \dfrac{T_{\text{propane},3} - T_{\text{water,test,out}}}{T_{\text{propane},4} - T_{\text{water,test,in}}}}$	$\Delta T_{\text{LM,test}} = 9.87$ K
$\dot{Q}_{\text{test}} = 22.61$ W $\Delta T_{\text{LM,test}} = 9.87$ K	$UA_{\text{test}} = \dfrac{\dot{Q}_{\text{test}}}{\Delta T_{\text{LM,test}}} = 2.29$ W K^{-1}	$UA_{\text{test}} = 2.29$ W K^{-1}
$D_{\text{test,in}} = 1.93$ mm $D_{\text{test,out}} = 2.98$ mm $L_{\text{test,HX}} = 135.1$ mm $T_{\text{propane},3} = 47.01°C$ $T_{\text{propane},4} = 46.52°C$	$T_{\text{propane,test,avg}} = \dfrac{T_{\text{propane},3} + T_{\text{propane},4}}{2}$ $k_{\text{Al}} = f\left(T_{\text{propane,test,avg}}\right)$ $R_{\text{test,wall}} = \dfrac{\ln(D_{\text{test,out}} / D_{\text{test,in}})}{2\pi k_{\text{Al}} L_{\text{test,HT}}}$	$T_{\text{propane,test,avg}} = 46.77°C$ $k_{\text{Al}} = 237.0$ W m^{-1} K^{-1} $R_{\text{test,wall}} = 2.1 \times 10^{-3}$ K W^{-1}

Propane In-Tube Condensation, 9 September 2013, Run 7		
Inputs	**Equations**	**Results**
$T_{\text{propane,test,avg}} = 46.77°C$ $P_{\text{propane,adj,3}} = 1607.2 \text{ kPa}$ $P_{\text{propane,adj,4}} = 1603.6 \text{ kPa}$	$P_{\text{sat,avg}} = \dfrac{P_{\text{propane,adj,3}} + P_{\text{propane,adj,4}}}{2}$ $T_{\text{sat,avg}} = f\left(P_{\text{sat,avg}}\right)$ $\Delta T_{\text{p}} = T_{\text{propane,test,avg}} - T_{\text{sat,avg}}$	$P_{\text{sat,avg}} = 1605.4 \text{ kPa}$ $T_{\text{sat,avg}} = 47.03°C$ $\Delta T_{\text{p}} = -0.27°C$
Coupling Fluid Thermal Resistance (Figures 4.6, 4.7, 4.8)		
$D_{\text{test,out}} = 2.98 \text{ mm}$ $D_{\text{OT,in}} = 5.35 \text{ mm}$ $N_{\text{fins}} = 12$ $H_{\text{fin}} = 0.84 \text{ mm}$ $W_{\text{fin}} = 0.46 \text{ mm}$	Annulus flow area $A_{\text{flow}} = \dfrac{\pi}{4}\left(D_{\text{OT,in}}^2 - D_{\text{test,out}}^2\right) - N_{\text{fins}} H_{\text{fin}} W_{\text{fin}}$ $P_{\text{wetted}} = \pi\left(D_{\text{OT,in}} + D_{\text{test,out}}\right) + 2 N_{\text{fins}} H_{\text{fin}}$ $D_{\text{annulus,h}} = \dfrac{4 A_{\text{flow}}}{P_{\text{wetted}}}$ $A_{\text{cross-section}} = \dfrac{\pi}{4} D_{\text{test,out}}^2 + N_{\text{fins}} H_{\text{fin}} W_{\text{fin}}$	$A_{\text{flow}} = 10.99 \text{ mm}^2$ $P_{\text{wetted}} = 46.18 \text{ mm}$ $D_{\text{annulus,h}} = 0.95 \text{ mm}$ $A_{\text{cross-section}} = 11.49 \text{ mm}^2$
$L_{\text{annulus}} = 58.46 \text{ mm}$ $N_{\text{fins}} = 12$ $H_{\text{fin}} = 0.84 \text{ mm}$ $W_{\text{fin}} = 0.46 \text{ mm}$	Test Section Surface Area $A_{\text{fin}} = 2 L_{\text{annulus}} H_{\text{fin}}$ $A_{\text{base}} = \left(\pi D_{\text{test,out}} - N_{\text{fins}} W_{\text{fin}}\right) L_{\text{annulus}}$ $A_{\text{surface}} = A_{\text{base}} + N_{\text{fins}} A_{\text{fin}}$	$A_{\text{fin}} = 97.63 \text{ mm}^2$ $A_{\text{base}} = 226.3 \text{ mm}^2$ $A_{\text{surface}} = 1398 \text{ mm}^2$

Propane In-Tube Condensation, 9 September 2013, Run 7		
Inputs	**Equations**	**Results**
Fluid = Water $T_{\text{water,test,in}} = 36.80°C$ $T_{\text{water,test,out}} = 36.98°C$ $P_{\text{water,test}} = 236.23$ kPa	$$T_{\text{water,test,avg}} = \frac{T_{\text{water,test,in}} + T_{\text{water,test,out}}}{2}$$ $$\rho_{\text{water,test}}, \mu_{\text{water,test}}, k_{\text{water,test}}$$ $$\text{Pr}_{\text{water,test}}, \beta_{\text{water,test}}, \alpha_{\text{water,test}} = f\left(T_{\text{water,test,avg}}, P_{\text{water,test}}\right)$$	$T_{\text{water,test,avg}} = 36.89°C$ $\rho_{\text{water,test}} = 993.4$ kg m^{-3} $\mu_{\text{water,test}} = 6.93 \times 10^{-4}$ kg m^{-1} s^{-1} $k_{\text{water,test}} = 0.626$ W m^{-1} K^{-1} $\text{Pr}_{\text{water,test}} = 4.62$ $\beta_{\text{water,test}} = 3.62 \times 10^{-4}$ K^{-1} $\alpha_{\text{water,test}} = 1.51 \times 10^{-7}$ m^2 s^{-1}
$\rho_{\text{water,test}} = 993.4$ kg m^{-3} $\dot{V}_{\text{water,test}} = 2.398$ L min^{-1}	$$\dot{m}_{\text{water,test}} = \dot{V}_{\text{water,test}} \rho_{\text{water,test}}$$	$\dot{m}_{\text{water,test}} = 0.040$ kg s^{-1}
$\dot{m}_{\text{water,test}} = 0.040$ kg s^{-1} $A_{\text{flow}} = 10.99$ mm^2 $D_{\text{annulus,h}} = 0.95$ mm $\mu_{\text{water,test}} = 6.93 \times 10^{-4}$ kg m^{-1} s^{-1}	$$\text{Re}_{\text{water,test}} = \frac{\dot{m}_{\text{water,test}} D_{\text{annulus,h}}}{A_{\text{flow}} \mu_{\text{water,test}}}$$	$\text{Re}_{\text{water,test}} = 4964$
$\text{Re}_{\text{water,test}} = 4964$ $\text{Pr}_{\text{water,test}} = 4.62$ $D_{\text{annulus,h}} = 0.95$ mm $L_{\text{annulus}} = 58.46$ mm	Flat plate laminar Nusselt number term $$\text{Nu}_{\text{L,a}} = 2.1\left(\text{Re}_{\text{test,annulus}}\, \text{Pr}_{\text{water,test}}\, \frac{D_{\text{annulus,h}}}{L_{\text{test,annulus}}}\right)^{1/3}$$ (Taborek, 1997)	$\text{Nu}_{\text{L,a}} = 15.13$

Propane In-Tube Condensation, 9 September 2013, Run 7		
Inputs	**Equations**	**Results**
$\mathrm{Nu}_\infty = 4.12$ $\mathrm{Nu}_{L,a} = 15.13$	Laminar Nusselt Number $\mathrm{Nu}_L = \left((\mathrm{Nu}_\infty)^3 + \mathrm{Nu}_{L,a}^3 \right)^{1/3}$	$\mathrm{Nu}_L = 15.23$
$\mathrm{Re}_{T15} = 15000$	Turbulent friction factor $f_{T15} = \left(0.79 \ln\left(\mathrm{Re}_{T15} \right) - 1.64 \right)^{-2}$	$f_{T15} = 0.028$
$T_{\text{propane,test,avg}} = 46.77°C$ $\dot{Q}_{\text{test}} = 22.61 \text{ W}$ $R_{\text{test,wall}} = 2.1 \times 10^{-3} \text{ K W}^{-1}$ $R_{\text{test,propane}} = 0.365 \text{ K W}^{-1*}$ $P_{\text{water,test}} = 236.23 \text{ kPa}$	$T_{\text{test,wall,out}} = T_{\text{ref,test,avg}} - \dfrac{\dot{Q}_{\text{test}}}{R_{\text{test,ref}} + R_{\text{test,wall}}}$ $\mu_{\text{water,wall}} = f\left(T_{\text{test,wall,out}}, P_{\text{water,test}} \right)$	$T_{\text{test,wall,out}} = 38.47°C^*$ $\mu_{\text{water,wall}} = 6.82 \times 10^{-4} \text{ kg m}^{-1} \text{ s}^{-1}$
$\mu_{\text{water,test}} = 6.93 \times 10^{-4} \text{ kg m}^{-1} \text{ s}^{-1}$ $\mu_{\text{water,wall}} = 6.82 \times 10^{-4} \text{ kg m}^{-1} \text{ s}^{-1}$	$\phi_{\text{liq}} = \left(\dfrac{\mu_{\text{water,test}}}{\mu_{\text{water,wall}}} \right)^{0.14}$	$\phi_{\text{liq}} = 1.002$
$A_{\text{flow}} = 11.49 \text{ mm}^2$ $D_{\text{OT,in}} = 5.35 \text{ mm}$	$D_{\text{test,out,eq.}} = \sqrt{4 A_{\text{cross-section}} / \pi}$ $r_{\text{test}}^* = \dfrac{D_{\text{test,out,eq.}}}{D_{\text{OT,in}}}$	$D_{\text{test,out,eq.}} = 3.82 \text{ mm}$ $r^*_{\text{test}} = 0.71$

Propane In-Tube Condensation, 9 September 2013, Run 7		
Inputs	**Equations**	**Results**
$Re_{T15} = 15000$ $f_{T15} = 0.028$ $Re_{water,test} = 4964$ $Pr_{water,test} = 4.62$ $\phi_{liq} = 1.002$ $r^*_{test} = 0.71$	Turbulent Nusselt number $$Nu_x = \frac{(f_{T15}/8)\,Re_{T15}\,Pr_{water,test}}{1.07 + 12.7(f_{T15}/8)^{0.5}(Pr_{water,test}^{2/3} - 1)}$$ $$\times \phi_{liq}\left(0.86 r^*_{test}\right)\left(\frac{Re_{test,annulus}}{15{,}000}\right)^{1.25}$$	$Nu_x = 5.19$
$Re_{water,test} = 4964$ $Nu_L = 15.23$ $Nu_x = 5.19$ $\phi_{liq} = 1.002$	Nusselt number interpolation $$z = \max\left[1.2,\ 0.1\,Re_{test,annulus}^{0.4}\right]$$ $$Nu_{test,annulus} = \left(Nu_L^z + Nu_x^z\right)^{1/z}\phi_{liq}$$	$z = 3.01$ $Nu_{test,annulus} = 15.46$
$Nu_{test,annulus} = 15.46$ $k_{water,test} = 0.626\ \text{W m}^{-1}\ \text{K}^{-1}$ $D_{annulus,h} = 0.95\ \text{mm}$	$$h_{test,annulus} = \frac{Nu_{test,annulus}\,k_{water,test}}{D_{test,h}} = 10165\ \text{W m}^{-2}\ \text{K}^{-1}$$	$h_{test,annulus} = 10165\ \text{W m}^{-2}\ \text{K}^{-1}$
$h_{test,annulus} = 10165\ \text{W m}^{-2}\ \text{K}^{-1}$ $k_{Al} = 237.0\ \text{W m}^{-1}\ \text{K}^{-1}$ $H_{fin} = 0.84\ \text{mm}$ $W_{fin} = 0.46\ \text{mm}$	$$m_{fin} = \sqrt{\frac{2h_{test,annulus}}{k_{Al}W_{fin}}}$$ $$\eta_{fin} = \frac{\tanh\left(m_{fin}H_{fin}\right)}{m_{fin}H_{fin}}$$	$m_{fin} = 434.2\ \text{m}^{-1}$ $\eta_{fin} = 0.958$

Propane In-Tube Condensation, 9 September 2013, Run 7		
Inputs	**Equations**	**Results**
$\eta_{fin} = 0.958$ $h_{test,annulus} = 10165$ W m^{-2} K^{-1} $A_{fin} = 97.63$ mm^2 $A_{base} = 226.3$ mm^2 $N_{fins} = 12$	$R_{fin} = \dfrac{1}{\eta_{fin} h_{test,annulus} A_{fin}}$ $R_{unfinned} = \dfrac{1}{h_{test,annulus} A_{base}}$ $R_{test,annulus} = \left(\dfrac{1}{R_{unfinned}} + \dfrac{N_{fins}}{R_{fin}} \right)^{-1}$	$R_{fin} = 1.05$ K W^{-1} $R_{unfinned} = 0.43$ K W^{-1} $R_{test,annulus} = 0.073$ K W^{-1}
$D_{test,out} = 2.98$ mm $D_{tee} = 6.50$ mm $D_{reducer} = 4.42$ mm $T_{water,test,avg} = 36.89°C$ $T_{test,wall,out} = 38.47°C^{*}$ $\rho_{water,test} = 993.4$ kg m^{-3} $\mu_{water,test} = 6.93 \times 10^{-4}$ kg m^{-1} s^{-1} $\beta_{water,test} = 3.62 \times 10^{-4}$ K^{-1} $\alpha_{water,test} = 1.51 \times 10^{-7}$ m^2 s^{-1} $g = 9.81$ m s^{-2}	$Ra^{*}_{fitting} = \dfrac{\left[\ln\left(D_{fitting} / D_{test,out} \right) \right]^{4}}{\left(D_{test,out}^{-3/5} + D_{fitting}^{-3/5} \right)}$ $\times \dfrac{\rho_{water,test}\, g\, \beta_{water,test} \left(T_{wall,out} - T_{water,test,avg} \right)}{\mu_{water,test}\, \alpha_{water,test}}$ (Incropera and DeWitt, 2007)	$Ra^{*}_{tee} = 46.27$ $Ra^{*}_{reducer} = 1.90$

Propane In-Tube Condensation, 9 September 2013, Run 7		
Inputs	**Equations**	**Results**
$\text{Ra}^*_{\text{tee}} = 46.27$ $\text{Ra}^*_{\text{reducer}} = 1.90$ $k_{\text{water,test}} = 0.626 \text{ W m}^{-1} \text{ K}^{-1}$ $\text{Pr}_{\text{water,test}} = 4.62$	$$\frac{k_{\text{eff}}}{k_{\text{water}}} = \begin{cases} 0.386\left(\dfrac{\text{Pr}}{0.861+\text{Pr}}\right)^{0.25}\left(\text{Ra}^*\right)^{0.25} & \text{Ra}^* > 100 \\ 1 & \text{Ra}^* < 100 \end{cases}$$ (Irvine and Hartnett, 1975)	$k_{\text{eff,test,tee}} = 0.626 \text{ W m}^{-1} \text{ K}^{-1}$ $k_{\text{eff,test,reducer}} = 0.626 \text{ W m}^{-1} \text{ K}^{-1}$
$D_{\text{test,out}} = 2.98 \text{ mm}$ $D_{\text{tee}} = 6.50 \text{ mm}$ $D_{\text{reducer}} = 4.42 \text{ mm}$ $k_{\text{eff,test,tee}} = 0.626 \text{ W m}^{-1} \text{ K}^{-1}$ $k_{\text{eff,test,reducer}} = 0.626 \text{ W m}^{-1} \text{ K}^{-1}$ $L_{\text{tee,in}} = 11.41 \text{ mm}$ $L_{\text{tee,out}} = 11.91 \text{ mm}$ $L_{\text{tee,in}} = 26.66 \text{ mm}$	$$R_{\text{test,fitting}} = \frac{\ln\left(D_{\text{fitting}} / D_{\text{test,out}}\right)}{2\pi k_{\text{eff,test,fitting}} L_{\text{fitting}}}$$	$R_{\text{test,tee,1}} = 17.45 \text{ K W}^{-1}$ $R_{\text{test,tee,2}} = 16.71 \text{ K W}^{-1}$ $R_{\text{test,tee,reducer}} = 3.79 \text{ K W}^{-1}$
$T_{\text{water,test,in}} = 36.80°\text{C}$ $T_{\text{water,test,out}} = 36.98°\text{C}$ $T_{\text{test,wall,out}} = 38.47°\text{C}^*$ $R_{\text{test,tee,1}} = 17.45 \text{ K W}^{-1}$ $R_{\text{test,tee,2}} = 16.71 \text{ K W}^{-1}$ $R_{\text{test,tee,reducer}} = 3.79 \text{ K W}^{-1}$	$$\dot{Q}_{\text{test,fitting,}j} = \frac{T_{\text{test,wall,out}} - T_{\text{water,test,}j}}{R_{\text{test,fitting,}j}}$$	$\dot{Q}_{\text{test,tee,in}} = 0.09 \text{ W}$ $\dot{Q}_{\text{test,tee,out}} = 0.10 \text{ W}$ $\dot{Q}_{\text{test,reducer,in}} = 0.39 \text{ W}$ $\dot{Q}_{\text{test,reducer,out}} = 0.44 \text{ W}$

Propane In-Tube Condensation, 9 September 2013, Run 7		
Inputs	**Equations**	**Results**
$R_{\text{test,tee,1}} = 17.45 \text{ K W}^{-1}$ $R_{\text{test,annulus}} = 0.073 \text{ K W}^{-1}$ $R_{\text{test,tee,2}} = 16.71 \text{ K W}^{-1}$ $R_{\text{test,tee,reducer}} = 3.79 \text{ K W}^{-1}$	$\dfrac{1}{R_{\text{test,water}}} = \dfrac{1}{R_{\text{test,tee,1}}} + \dfrac{1}{R_{\text{test,annulus}}} + \dfrac{1}{R_{\text{test,tee,2}}} + 2\left(\dfrac{1}{R_{\text{test,reducer}}}\right)$	$R_{\text{test,water}} = 0.070 \text{ K W}^{-1}$
$UA_{\text{test}} = 2.29 \text{ W K}^{-1}$ $R_{\text{test,wall}} = 2.1 \times 10^{-3} \text{ K W}^{-1}$ $R_{\text{test,water}} = 0.070 \text{ K W}^{-1}$	$R_{\text{test,propane}} = \dfrac{1}{UA_{\text{test}}} - R_{\text{test,wall}} - R_{\text{test,water}}$	$R_{\text{test,propane}} = 0.365 \text{ K W}^{-1}$
$R_{\text{test,propane}} = 0.365 \text{ K W}^{-1}$ $R_{\text{test,wall}} = 2.1 \times 10^{-3} \text{ K W}^{-1}$ $R_{\text{test,water}} = 0.070 \text{ K W}^{-1}$	$R_{\text{ratio,test}} = \dfrac{R_{\text{test,propane}}}{R_{\text{test,wall}} + R_{\text{test,water}}}$ $R_{\text{ratio,test,wall}} = \dfrac{R_{\text{test,propane}}}{R_{\text{test,wall}}}$	$R_{\text{ratio,test}} = 5.08$ $R_{\text{ratio,test,wall}} = 170.3$
$R_{\text{test,propane}} = 0.365 \text{ K W}^{-1}$ $D_{\text{test,in}} = 1.93 \text{ mm}$ $L_{\text{test,HX}} = 135.1 \text{ mm}$	$h_{\text{test,propane}} = \dfrac{1}{R_{\text{test,propane}} \pi D_{\text{test,in}} L_{\text{test,HT}}}$	$h_{\text{test,propane}} = 3346 \text{ W m}^{-2} \text{ K}^{-1}$
$h_{\text{test,propane}} = 3346 \text{ W m}^{-2} \text{ K}^{-1}$ $D_{\text{test,in}} = 1.93 \text{ mm}$ $P_{\text{propane,test,avg}} = 1605.4 \text{ kPa}$	$k_{\text{propane,test,l}} = f\left(P_{\text{propane,test,avg}}, x = 0\right)$ $\text{Nu}_{\text{propane,test}} = \dfrac{h_{\text{propane,ref}} D_{\text{test,in}}}{k_{\text{propane,test,l}}}$	$k_{\text{propane,test,l}} = 0.084 \text{ W m}^{-1} \text{ K}^{-1}$ $\text{Nu}_{\text{propane,test,1}} = 77.0$

C.3. Test Section Pressure Drop

Figure (4.9)

Propane In-Tube Condensation, 9 September 2013, Run 7		
Inputs	**Equations**	**Results**
$P_{propane,adj,3} = 1607.2$ kPa $P_{propane,adj,4} = 1603.6$ kPa	$T_{propane,sat,avg} = f\left(P_{propane,test,avg}\right)$ $P_{propane,test,avg} = \dfrac{P_{propane,adj,3} + P_{propane,adj,4}}{2}$ $\rho_{propane,l} = f\left(P_{propane,adj}, x = 0\right)$ $\rho_{propane,v} = f\left(P_{propane,adj}, x = 1\right)$	$T_{propane,sat,avg} = 47.03°C$ $P_{propane,test,avg} = 1605.4$ kPa $\rho_{propane,l,3} = 454.5$ kg m^{-3} $\rho_{propane,v,3} = 35.95$ kg m^{-3} $\rho_{propane,l,4} = 454.7$ kg m^{-3} $\rho_{propane,v,4} = 35.86$ kg m^{-3} $\rho_{propane,test,l} = 454.6$ kg m^{-3} $\rho_{propane,test,v} = 35.90$ kg m^{-3}
$D_{reducer} = 4.42$ mm $D_{cross} = 4.83$ mm $D_{contraction} = 2.40$ mm $D_{test,in} = 1.93$ mm	$A_{ratio,test.1} = D_{reducer}^{\,2} / D_{cross}^{\,2}$ $A_{ratio,test,2} = D_{contraction}^{\,2} / D_{reducer}^{\,2}$ $A_{ratio,test,3} = D_{test,in}^{\,2} / D_{contraction}^{\,2}$	$A_{ratio,test,1} = 0.839$ $A_{ratio,test,2} = 0.295$ $A_{ratio,test,3} = 0.647$
$G_{propane} = 100.2$ kg m^{-2} s^{-1} $A_{ratio,test,2} = 0.295$ $A_{ratio,test,3} = 0.647$	$G_{propane,contraction} = G_{propane} A_{ratio,test,3}$ $G_{propane,reducer} = G_{propane} A_{ratio,test,3} A_{ratio,test,2}$	$G_{propane,contraction} = 64.8$ kg m^{-2} s^{-1} $G_{propane,reducer} = 19.1$ kg m^{-2} s^{-1}

Propane In-Tube Condensation, 9 September 2013, Run 7		
Inputs	**Equations**	**Results**
$A_{\text{ratio,test},1} = 0.839$ $A_{\text{ratio,test},2} = 0.295$ $A_{\text{ratio,test},3} = 0.647$	$$C_{\text{C}} = \dfrac{1}{0.639\left(1 - A_{\text{ratio,test}}\right)^{1/2} + 1}$$ (Chisholm, 1983)	$C_{\text{C},1} = 0.7958$ $C_{\text{C},1} = 0.6508$ $C_{\text{C},1} = 0.7247$
$\rho_{\text{propane,l},3} = 454.5 \text{ kg m}^{-3}$ $\rho_{\text{propane,v},3} = 35.95 \text{ kg m}^{-3}$ $x_3 = 0.72$	$$\psi_{\text{H}} = 1 + \left(\dfrac{\rho_{\text{propane,l},3}}{\rho_{\text{propane,v},3}} - 1\right)x_3$$ (Hewitt *et al.*, 1994)	$\psi_{\text{H}} = 9.40$

Propane In-Tube Condensation, 9 September 2013, Run 7		
Inputs	**Equations**	**Results**
$G_{propane} = 100.2$ kg m^{-2} s^{-1} $G_{propane,contraction} = 64.8$ kg m^{-2} s^{-1} $G_{propane,reducer} = 19.1$ kg m^{-2} s^{-1} $\rho_{propane,l,3} = 454.5$ kg m^{-3} $A_{ratio,test,1} = 0.839$ $A_{ratio,test,2} = 0.295$ $A_{ratio,test,3} = 0.647$ $C_{C,1} = 0.7958$ $C_{C,1} = 0.6508$ $C_{C,1} = 0.7247$ $\psi_H = 9.40$	$$\Delta P_{contraction,j} = \frac{G_{propane,j}^{2}}{2\rho_{propane,l,3}}\left(1 - A_{ratio,j}^{2} + \left(\frac{1}{C_{C,j}} - 1\right)^{2}\right)\psi_H$$ $$\Delta P_{contraction} = \Delta P_{contraction,1} + \Delta P_{contraction,2} + \Delta P_{contraction,3}$$	$\Delta P_{contraction,1} = 1.37$ Pa $\Delta P_{contraction,2} = 52.18$ Pa $\Delta P_{contraction,3} = 75.44$ Pa $\Delta P_{contraction} = 129.00$ Pa
$\rho_{propane,l,4} = 454.7$ kg m^{-3} $\rho_{propane,v,4} = 35.86$ kg m^{-3} $x_4 = 0.46$ $B = 0.25$	$$\psi_S = 1 + \left(\frac{\rho_{propane,l,4}}{\rho_{propane,v,4}} - 1\right)\left[Bx_4\left(1 - x_4\right) + x_4^{2}\right]$$	$\psi_S = 4.18$

Propane In-Tube Condensation, 9 September 2013, Run 7		
Inputs	**Equations**	**Results**
$G_{\text{propane}} = 100.2 \text{ kg m}^{-2} \text{ s}^{-1}$ $G_{\text{propane,contraction}} = 64.8 \text{ kg m}^{-2} \text{ s}^{-1}$ $G_{\text{propane,reducer}} = 19.1 \text{ kg m}^{-2} \text{ s}^{-1}$ $\rho_{\text{propane,l,4}} = 454.7 \text{ kg m}^{-3}$ $A_{\text{ratio,test,1}} = 0.839$ $A_{\text{ratio,test,2}} = 0.295$ $A_{\text{ratio,test,3}} = 0.647$ $\psi_{\text{S}} = 4.18$	$\Delta P_{\text{expansion},j} = \dfrac{G_{\text{propane},j}^{\;2}}{2\rho_{\text{propane,l,4}}}\left(\left(1 - A_{\text{ratio},j}^{2}\right) - \left(1 - A_{\text{ratio},j}\right)^{2}\right)\psi_{S}$ $\Delta P_{\text{expansion}} = \Delta P_{\text{expansion,1}} + \Delta P_{\text{expansion,2}} + \Delta P_{\text{expansion,3}}$	$\Delta P_{\text{expansion,1}} = 0.45 \text{ Pa}$ $\Delta P_{\text{expansion,2}} = 8.02 \text{ Pa}$ $\Delta P_{\text{expansion,3}} = 21.07 \text{ Pa}$ $\Delta P_{\text{expansion}} = 29.54 \text{ Pa}$

Propane In-Tube Condensation, 9 September 2013, Run 7		
Inputs	**Equations**	**Results**
$G_{propane} = 100.2$ kg m^{-2} s^{-1} $x_3 = 0.72$ $x_4 = 0.46$ $\rho_{propane,l,3} = 454.5$ kg m^{-3} $\rho_{propane,v,3} = 35.95$ kg m^{-3} $\rho_{propane,l,4} = 454.7$ kg m^{-3} $\rho_{propane,v,4} = 35.86$ kg m^{-3}	$$\alpha_{homogeneous} = \left(1 + \left(\frac{1-x}{x}\right)\left(\frac{\rho_v}{\rho_l}\right)\right)^{-1}$$ $$j = \frac{Gx}{\rho_v} + \frac{G(1-x)}{\rho_l}$$ $$\alpha_{Winkler,\ 2012} = \frac{\alpha_{homogeneous}}{1.153 + 0.071 \text{ m s}^{-1}\big/ j}$$ (Winkler *et al.*, 2012)	$\alpha_{test,in,hom.} = 0.97$ $\alpha_{test,out,hom.} = 0.92$ $j_{test,in} = 2.1$ m s^{-1} $j_{test,in} = 1.4$ m s^{-1} $\alpha_{test,in} = 0.76$ $\alpha_{test,out} = 0.82$
	$$\left|\Delta P_{deceleration}\right| = \left\|\left. G_{propane}^{\ 2}\left(\frac{x^2}{\rho_{propane,v,4}\,\alpha} + \frac{(1-x)^2}{\rho_{propane,l,4}(1-\alpha)}\right)\right|_{\substack{\alpha=\alpha_{test,out}\\x=x_4}} \right. \\ \left. - \left|G_{ref}^{\ 2}\left(\frac{x^2}{\rho_{propane,v,3}\,\alpha} + \frac{(1-x)^2}{\rho_{propane,l,3}(1-\alpha)}\right)\right|_{\substack{\alpha=\alpha_{test,in}\\x=x_3}} \right\|$$	$\Delta P_{deceleration} = 83.39$ Pa

Propane In-Tube Condensation, 9 September 2013, Run 7		
Inputs	**Equations**	**Results**
$\alpha_{test,in} = 0.76$ $\alpha_{test,out} = 0.82$ $\rho_{propane,l,3} = 454.5$ kg m^{-3} $\rho_{propane,v,3} = 35.95$ kg m^{-3} $\rho_{propane,l,4} = 454.7$ kg m^{-3} $\rho_{propane,v,4} = 35.86$ kg m^{-3} $\rho_{propane,test,l} = 454.6$ kg m^{-3} $\rho_{propane,test,v} = 35.90$ kg m^{-3} $G_{propane} = 100.2$ kg m^{-2} s^{-1} $T_{propane,sat,avg} = 47.03$°C $x_3 = 0.72$ $L_{annulus} = 58.46$ mm $g = 9.81$ m s^{-2}	$\Delta P_{static,test,in} = g\left(\alpha_{test,in}\rho_{propane,v,3} + (1-\alpha_{test,in})\rho_{propane,l,3}\right)L_{test,entrance}$ $\Delta P_{static,test,out} = g\left(\alpha_{test,out}\rho_{propane,v,4} + (1-\alpha_{test,out})\rho_{propane,l,4}\right)L_{test,exit}$	$\Delta P_{static,test,in} = 110.2$ Pa $\Delta P_{static,test,out} = 139.2$ Pa
	$a_2 = 4.7785 - 0.02459 G_{propane} + 0.01741 T_{sat}$ $a_1 = a_2 L_{test,annulus} + \Delta x / L_{test,annulus}$ $x_i = x_3 - a_1 z_i + a_2 z_i^2$ $\alpha_i = f(x_i)$ $\Delta P_{static,test,HX} \approx \sum_{i=1}^{15} g\left(\alpha_i \rho_{propane,test,v} + (1-\alpha_i)\rho_{propane,test,l}\right)\Delta z$	$a_1 = 4.7$ m^{-1} $a_2 = 3.1$ m^{-2} $\Delta P_{static,test,HX} = 70.6$ Pa
$\Delta P_{static,test,in} = 110.2$ Pa $\Delta P_{static,test,HX} = 70.6$ Pa $\Delta P_{static,test,out} = 139.2$ Pa	$\Delta P_{static,test} = \Delta P_{static,test,in} + \Delta P_{static,test,HX} + \Delta P_{static,test,out}$	$\Delta P_{static,test} = 319.9$ Pa

Propane In-Tube Condensation, 9 September 2013, Run 7		
Inputs	**Equations**	**Results**
$T_{\text{wall,line,1}} = 39.29°C$ $T_{\text{wall,line,3}} = 31.35°C$ $P_{\text{propane,adj,3}} = 1607.2 \text{ kPa}$	Assuming negligible ambient loss in this segment: $T_{\text{propane,line,in,down}} \approx T_{\text{wall,line,in,down}} = \dfrac{T_{\text{wall,line,1}} + T_{\text{wall,line,3}}}{2}$	$T_{\text{propane,line,in,down}} = 35.32°C$
	$\rho_{\text{ref,line,in,down}} = f\left(T_{\text{ref,line,in,down}}, P_{\text{ref,adj,3}}\right)$	$\rho_{\text{propane,line,in,down}} = 477.0 \text{ kg m}^{-3}$
$T_{\text{wall,line,4}} = 32.45°C$ $T_{\text{wall,line,5}} = 31.67°C$ $P_{\text{propane,adj,4}} = 1603.6 \text{ kPa}$	Assuming negligible ambient loss in this segment: $T_{\text{propane,line,out}} \approx T_{\text{wall,line,out}} = \dfrac{T_{\text{wall,line,4}} + T_{\text{wall,line,5}}}{2}$	$T_{\text{propane,line,out}} = 32.06°C$
	$\rho_{\text{propane,line,out}} = f\left(T_{\text{propane,line,out}}, P_{\text{propane,adj,4}}\right)$	$\rho_{\text{propane,line,out}} = 482.7 \text{ kg m}^{-3}$
$g = 9.81 \text{ m s}^{-2}$ $\Delta z_{\Delta P3} = 347 \text{ mm}$ $\Delta z_{\Delta P3} = 83 \text{ mm}$ $\rho_{\text{propane,line,in,down}} = 477.0 \text{ kg m}^{-3}$ $\rho_{\text{propane,line,out}} = 482.7 \text{ kg m}^{-3}$	$\Delta P_{\text{static,line}} = \rho_{\text{propane,line,in,down}} \, g \Delta z_{\Delta P_3} - \rho_{\text{propane,line,out}} \, g \Delta z_{\Delta P_4}$	$\Delta P_{\text{static,line}} = 1230 \text{ Pa}$

Propane In-Tube Condensation, 9 September 2013, Run 7		
Inputs	**Equations**	**Results**
$\Delta P_{\text{measured}} = 1680 \text{ Pa}$ $\Delta P_{\text{contraction}} = 129.00 \text{ Pa}$ $\Delta P_{\text{expansion}} = 29.54 \text{ Pa}$ $\Delta P_{\text{deceleration}} = 83.39 \text{ Pa}$ $\Delta P_{\text{static,test}} = 319.9 \text{ Pa}$ $\Delta P_{\text{static,line}} = 1230 \text{ Pa}$	$\Delta P_{\text{frictional}} = \Delta P_{\text{measured}} - \Delta P_{\text{contraction}} + \Delta P_{\text{expansion}}$ $+ \left| \Delta P_{\text{deceleration}} \right| + \Delta P_{\text{static,test}} - \Delta P_{\text{static,line}}$	$\Delta P_{\text{frictional}} = 0.753 \text{ kPa}$
$\Delta P_{\text{frictional}} = 0.753 \text{ kPa}$ $L_{\text{test},\Delta P} = 191 \text{ mm}$	$\left. \dfrac{dP}{dz} \right|_{\text{frictional}} = \dfrac{\Delta P_{\text{frictional}}}{L_{\text{test},\Delta P}}$	$\left. \dfrac{dP}{dz} \right|_{\text{frictional}} = 3.944 \text{ kPa m}^{-1}$

REFERENCES

Akers, W. W., H. A. Deans and O. K. Crosser (1959), "Condensing Heat Transfer within Horizontal Tubes," *Chemical Engineering Progress Symposium Series* Vol. 55(29) pp. 171-176.

Andresen, U. C. (2006). *Supercritical Gas Cooling and near-Critical-Pressure Condensation of Refrigerant Blends in Microchannels*.

Armand, A. A. (1946). *The Resistance During the Movement of a Two-Phase System in Horizontal Pipes*. Izv Vses Tepl, AERA-Lib/Trans, Vol. 868 pp. 16-23.

Baker, O. (1954), "Design of Pipe Lines for Simultaneous Flow of Oil and Gas," *Oil and Gas Journal* Vol. 26 pp. 185-195.

Bandhauer, T. M., A. Agarwal and S. Garimella (2006), "Measurement and Modeling of Condensation Heat Transfer Coefficients in Circular Microchannels," *Journal of Heat Transfer* Vol. 128(10) pp. 1050-1059.

Barnea, D. (1990), "Effect of Bubble Shape on Pressure Drop Calculations in Vertical Slug Flow," *International Journal of Multiphase Flow* Vol. 16(1) pp. 79-89.

Barnea, D., O. Shoham and Y. Taitel (1982), "Flow Pattern Transition for Vertical Downward Two Phase Flow," *Chemical Engineering Science* Vol. 37(5) pp. 741-744.

Baroczy, C. J. (1965), "Correlation of Liquid Fraction in Two-Phase Flow with Applications to Liquid Metals," *Chem. Eng. Prog. Symp. Series* Vol. 61(57) pp. 179-191.

Baroczy, C. J. (1966), "A Systematic Correlation for Two-Phase Pressure Drop," *Chem. Eng. Prog. Symp. Series* Vol. 62(44) pp. 287-289.

Beattie, D. R. H. and P. B. Whalley (1982), "A Simple Two-Phase Flow Frictional Pressure Drop Calculation Method," *International Journal of Multiphase Flow* Vol. 8 pp. 83-87.

Breber, G., J. W. Palen and J. Taborek (1980), "Prediction of Horizontal Tubeside Condensation of Pure Components Using Flow Regime Criteria," *Journal of Heat Transfer, Transactions ASME* Vol. 102(3) pp. 471-476.

Burdell, G. P. (1930), "How to Succeed at Georgia Tech without Really Trying," *The Tower* Vol. 1.

Carey, V. P. (2008). *Liquid-Vapor Phase-Change Phenomena: An Introduction to the Thermophysics of Vaporization and Condensation Processes in Heat Transfer Equipment*. Second Ed. New York, NY, Taylor and Francis.

Carpenter, F. G. and A. P. Colburn (1951), "The Effect of Vapor Velocity on Condensation inside Tubes," *ASME Proceedings of the General Discussion of Heat Transfer* pp. 20-26.

Cavallini, A., G. Censi, D. Del Col, L. Doretti, G. A. Longo and L. Rossetto (2001), "Experimental Investigation on Condensation Heat Transfer and Pressure Drop of New Hfc Refrigerants (R134a, R125, R32, R410a, R236ea) in a Horizontal Smooth Tube," *International Journal of Refrigeration-Revue Internationale Du Froid* Vol. 24(1) pp. 73-87.

Cavallini, A., G. Censi, D. Del Col, L. Doretti, G. A. Longo and L. Rossetto (2002), "Condensation of Halogenated Refrigerants inside Smooth Tubes," *HVAC&R Research* Vol. 8(4) pp. 429-451.

Cavallini, A., D. Del Col, M. Matkovic and L. Rossetto (2009), "Frictional Pressure Drop During Vapour–Liquid Flow in Minichannels: Modelling and Experimental Evaluation," *International Journal of Heat and Fluid Flow* Vol. 30(1) pp. 131-139.

Cavallini, A. and R. Zecchin (1974), "A Dimensionless Correlation for Heat Transfer in Forced Convective Condensation," *Proceedings of the 5th International Heat transfer Conference, JSME*, pp. 309-313.

Chen, I. Y., K. S. Yang, Y. J. Chang and C. C. Wang (2001), "Two-Phase Pressure Drop of Air-Water and R-410a in Small Horizontal Tubes," *International Journal of Multiphase Flow* Vol. 27(7) pp. 1293-1299.

Chen, L., Y. S. Tian and T. G. Karayiannis (2006), "The Effect of Tube Diameter on Vertical Two-Phase Flow Regimes in Small Tubes," *International Journal of Heat and Mass Transfer* Vol. 49(21–22) pp. 4220-4230.

Chisholm, D. (1967), "A Theoretical Basis for the Lockhart-Martinelli Correlation for Two-Phase Flow," *International Journal of Heat and Mass Transfer* Vol. 10(12) pp. 1767-1778.

Chisholm, D. (1973), "Pressure Gradients Due to Friction During the Flow of Evaporationg Two-Phase Mixtures in Smooth Tubes and Channels," *International Journal of Heat and Mass Transfer* Vol. 16(2) pp. 347-358.

Chisholm, D. (1983). *Two-Phase Flow in Pipelines and Heat Exchangers*. New York, Longman.

Churchill, S. W. (1977a), "Comprehensive Correlating Equations for Heat, Mass and Momentum Transfer in Fully Developed Flow in Smooth Tubes," *Ind. Eng. Chem. Fundamentals* Vol. 16(1) pp. 109-116.

Churchill, S. W. (1977b), "Friction-Factor Equations Spans All Fluid Flow Regimes," *Chem. Eng. Prog.* Vol. 84(24) pp. 91-92.

Churchill, S. W. and H. H. S. Chu (1975a), "Correlating Equations for Laminar and Turbulent Free Convection from a Horizontal Cylinder," *International Journal of Heat and Mass Transfer* Vol. 18(9) pp. 1049-1053.

Churchill, S. W. and H. H. S. Chu (1975b), "Correlating Equations for Laminar and Turbulent Free Convection from a Vertical Plate," *International Journal of Heat and Mass Transfer* Vol. 18(11) pp. 1323-1329.

Colebrook, C. F. (1939), "Turbulent Flow in Pipes with Particular Reference to the Transition Region between the Smooth and Rough Pipe Laws," *J Inst Civil Eng* Vol. 11(4) pp. 133-156.

Coleman, J. W. (2000). *Flow Visualization and Pressure Drop in Small Hydraulic Diameter Geometries During Phase Change of Refrigerants*. Mechanical Engineering. Aimes, Iowa State University, Vol. Ph.D.

Coleman, J. W. and S. Garimella (1999), "Characterization of Two-Phase Flow Patterns in Small Diameter Round and Rectangular Tubes," *International Journal of Heat and Mass Transfer* Vol. 42(15) pp. 2869-2881.

Coleman, J. W. and S. Garimella (2000a), "Two-Phase Flow Regime Transitions in Microchannel Tubes: The Effect of Hydraulic Diameter," *ASME Heat Transfer Division - 2000*, Orlando, FL, American Society of Mechanical Engineers, pp. 71-83.

Coleman, J. W. and S. Garimella (2000b), "Two-Phase Flow Regime Transitions in Microchannel Tubes: The Effect of Hydraulic Diameter," *Procedings of IMECE*, Orlando

Coleman, J. W. and S. Garimella (2000c), "Visualization of Two-Phase Refrigerant Flow During Phase Change.," *Proc. 34th National Heat Transfer Conference*

Coleman, J. W. and S. Garimella (2003), "Two-Phase Flow Regimes in Round, Square and Rectangular Tubes During Condensation of Refrigerant R134a," *International Journal of Refrigeration* Vol. 26(1) pp. 117-128.

Dalkilic, A. S., O. Agra, I. Teke and S. Wongwises (2010), "Comparison of Frictional Pressure Drop Models During Annular Flow Condensation of R600a in a Horizontal Tube at Low Mass Flux and of R134a in a Vertical Tube at High Mass Flux," *International Journal of Heat and Mass Transfer* Vol. 53(9-10) pp. 2052-2064.

Dalkilic, A. S., I. Teke and S. Wongwises (2011), "Experimental Analysis for the Determination of the Convective Heat Transfer Coefficient by Measuring Pressure Drop Directly During Annular Condensation Flow of R134a in a Vertical Smooth Tube," *International Journal of Heat and Mass Transfer* Vol. 54(4) pp. 1008-1014.

Dalkilic, A. S. and S. Wongwises (2010a), "An Investigation of a Model of the Flow Pattern Transition Mechanism in Relation to the Identification of Annular Flow of R134a in a Vertical Tube Using Various Void Fraction Models and Flow Regime Maps," *Experimental Thermal and Fluid Science* Vol. 34(6) pp. 692-705.

Dalkilic, A. S. and S. Wongwises (2010b), "New Experimental Approach on the Determination of Condensation Heat Transfer Coefficient Using Frictional Pressure Drop and Void Fraction Models in a Vertical Tube," *Energy Conversion and Management* Vol. 51(12) pp. 2535-2547.

Derby, M., H. J. Lee, Y. Peles and M. K. Jensen (2012), "Condensation Heat Transfer in Square, Triangular, and Semi-Circular Mini-Channels," *International Journal of Heat and Mass Transfer* Vol. 55(1–3) pp. 187-197.

Dobson, M. K. and J. C. Chato (1998), "Condensation in Smooth Horizontal Tubes.," *Journal of Heat Transfer* Vol. 120(1) pp. 193-213.

El Hajal, J., J. R. Thome and A. Cavallini (2003), "Condensation in Horizontal Tubes, Part 1: Two-Phase Flow Pattern Map," *International Journal of Heat and Mass Transfer* Vol. 46(18) pp. 3349-3363.

EPA (2010). *Transitioning to Low-Gwp Alternatives in Commercial Refrigeration*. U. S. E. P. Agency.

Fernando, P., B. Palm, T. Ameel, P. Lundqvist and E. Granryd (2008), "A Minichannel Aluminium Tube Heat Exchanger - Part Iii: Condenser Performance with Propane," *International Journal of Refrigeration* Vol. 31(4) pp. 696-708.

Friedel, L. (1979), "Improved Friction Pressure Drop Correlation for Horizontal and Vertical Two Phase Flow," *3R International* Vol. 18(7) pp. 485-491.

Garimella, S., A. Agarwal and J. D. Killion (2005), "Condensation Pressure Drop in Circular Microchannels," *Heat Transfer Engineering* Vol. 26(3) pp. 28-35.

Garimella, S., Agarwal, A., Coleman, J.W. (2003), "Two-Phase Pressure Drops in the Annular Flow Regime in Circular Microchannels," *International Congress of Refrigeration*, Washington D.C.

Garimella, S. and T. M. Bandhauer (2001), "Measurement of Condensation Heat Transfer Coefficients in Microchannel Tubes," *Proc. 2001 International Mechanical Engineering Congress and Exposition*, pp. 1-7.

Garimella, S., J. D. Killion and J. W. Coleman (2002), "Experimentally Validated Model for Two-Phase Pressure Drop in the Intermittent Flow Regime for Circular Microchannels," *Journal of Fluids Engineering, Transactions of the ASME* Vol. 124(1) pp. 205-214.

Garimella, S., J. D. Killion and J. W. Coleman (2003), "An Expermentally Validated Model for Two-Phase Pressure Drop in the Intermittent Flow Regime for Noncircular Microchannels," *Journal of Fluids Engineering, Transactions of the ASME* Vol. 125(5) p. 887.

Geiger, G. E. and W. M. Rohrer (1966), "Sudden Contraction Losses in Two-Phases Flow," *American Society of Mechanical Engineers -- Transactions -- Journal of Heat Transfer* Vol. 88(1) pp. 1-9.

Hewitt, G. F. and D. N. Roberts (1969). Studies of Two-Phase Flow Patterns by Simultaneous X-Ray and Flash Photography. UKAEA. Harwell, Berkshire, AERE-M2159.p.

Hewitt, G. F., G. L. Shires and T. R. Bott (1994). *Process Heat Transfer*, CRC Press LLC.

Incropera, F. P. and D. P. DeWitt (2007). *Fundamentals of Heat and Mass Transfer*. 6 Ed., John Wiley and Sons.

Irvine, T. F. J. and J. P. Hartnett (1975). *Advances in Heat Transfer*. New York, Academic Press.

Janna, W. S. (1993). *Design of Fluid Thermal Systems*. Boston :, PWS-Kent Pub. Co.

Julia, J. E., Y. Liu, T. Hibiki and M. Ishii (2013), "Local Flow Regime Analysis in Vertical Co-Current Downward Two-Phase Flow," *Experimental Thermal and Fluid Science* Vol. 44 pp. 345-355.

Jung, D. S., M. McLinden, R. Radermacher and D. Didion (1989), "A Study of Flow Boiling Heat Transfer with Refrigerant Mixtures," *International Journal of Heat and Mass Transfer* Vol. 32(9) pp. 1751-1764.

Kattan, N., J. R. Thome and D. Favrat (1998), "Flow Boiling in Horizontal Tubes: Part 1 - Development of a Diabatic Two-Phase Flow Pattern Map," *Journal of Heat Transfer, Transactions ASME* Vol. 120(1) pp. 140-147.

Kim, S.-M. and I. Mudawar (2012), "Universal Approach to Predicting Two-Phase Frictional Pressure Drop for Adiabatic and Condensing Mini/Micro-Channel Flows," *International Journal of Heat and Mass Transfer* Vol. 55(11-12) pp. 3246-3261.

Klausner, J. F., B. T. Chao and S. L. Soo (1991), "Improved Correlation for Two-Phase Frictional Pressure Drop in Boiling and Adiabatic Downflow in the Annular Flow

Regime," *Proceedings of the Institution of Mechanical Engineers, Part C: Journal of Mechanical Engineering Science* Vol. 205(5) pp. 317-328.

Klein, S. A. (2011). *Engineering Equation Solver*, F-Chart Software.

Kosky, P. G. and F. W. Staub (1971), "Local Condensing Heat Transfer Coefficients in the Annular Flow Regime," *AIChe Journal* Vol. 17(5) pp. 1037-1043.

Lee, H.-S., J.-I. Yoon, J.-D. Kim and P. K. Bansal (2006a), "Characteristics of Condensing and Evaporating Heat Transfer Using Hydrocarbon Refrigerants," *Applied Thermal Engineering* Vol. 26(10) pp. 1054-1062.

Lee, H.-S., J.-I. Yoon, J.-D. Kim and P. K. Bansal (2006b), "Condensing Heat Transfer and Pressure Drop Characteristics of Hydrocarbon Refrigerants," *International Journal of Heat and Mass Transfer* Vol. 49(11-12) pp. 1922-1927.

Lee, H. J. and S. Y. Lee (2001), "Pressure Drop Correlations for Two-Phase Flow within Horizontal Rectangular Channels with Small Heights," *International Journal of Multiphase Flow* Vol. 27(5) pp. 783-796.

Lemmon, E. W., M. L. Huber and M. O. McLinden (2010). *Reference Fluid Thermodynamic and Transport Properties - Refprop Version 9.0*. NIST Standard Reference Database 23. Gaithersburg, National Institute of Standards and Technology, Standard Reference Data Program.

Lips, S. and J. P. Meyer (2012), "Experimental Study of Convective Condensation in an Inclined Smooth Tube. Part Ii: Inclination Effect on Pressure Drops and Void Fractions," *International Journal of Heat and Mass Transfer* Vol. 55(1–3) pp. 405-412.

Liu, H., C. O. Vandu and R. Krishna (2005), "Hydrodynamics of Taylor Flow in Vertical Capillaries: Flow Regimes, Bubble Rise Velocity, Liquid Slug Length, and Pressure Drop," *Industrial and Engineering Chemistry Research* Vol. 44(14) pp. 4884-4897.

Lockhart, R. W. and R. C. Martinelli (1949), "Proposed Correlation of Data for Isothermal Two-Phase Two-Component Flow in a Pipe," *Chem. Eng. Prog. Symp. Series* Vol. 45 p. 39.

Mandane, J. M., G. A. Gregory and K. Aziz (1974), "A Flow Pattern Map for Gas-Liquid Flow in Horizontal Pipes," *International Journal of Multiphase Flow* Vol. 1 pp. 537-553.

McAdams, W. H., W. K. Woods and J. L. C. Heroman (1942), "Vaporization inside Horizontal Tubes -- Ii, Benzene Oil Mixtures," *American Society of Mechanical Engineers -- Transactions* Vol. 64(3) pp. 193-200.

Mishima, K. and T. Hibiki (1996), "Some Characteristics of Air-Water Two-Phase Flow in Small Diameter Vertical Tubes," *International Journal of Multiphase Flow* Vol. 22(4) pp. 703-712.

Mishima, K. and M. Ishii (1984), "Flow Regime Transition Criteria for Upward Two-Phase Flow in Vertical Tubes.," Vol. 27(5) pp. 723-737.

Mitra, B. and S. Garimella (2003), "Heat Transfer and Pressure Drop for Condensation of Refrigerant R410a at near-Critical Pressures," *2003 ASME International Mechanical Engineering Congress, Nov 15-21 2003*, Washington, DC., United States, American Society of Mechanical Engineers, pp. 87-97.

Moser, K. W., R. L. Webb and B. Na (1998), "A New Equivalent Reynolds Number Model for Condensation in Smooth Tubes," *Journal of Heat Transfer* Vol. 120(2) pp. 410-417.

Munson, B. R., D. F. Young and T. H. Okiishi (2006). *Fundamentals of Fluid Mechanics*. 5th Ed.

Nusselt, W. (1916), "Die Oberflaechenkondensation Des Wasserdampfes," *Zeitschrift des Vereines Deutscher Ingenieure* Vol. 60 pp. 541-546.

Paliwoda, A. (1989), "Generalized Method of Pressure Drop and Tube Length Calculation with Boiling and Condensing Refrigerants within the Entire Zone of Saturation," *International Journal of Refrigeration* Vol. 12(6) pp. 314-322.

Park, K.-J., D. Jung and T. Seo (2008), "Flow Condensation Heat Transfer Characteristics of Hydrocarbon Refrigerants and Dimethyl Ether inside a Horizontal Plain Tube," *International Journal of Multiphase Flow* Vol. 34(7) pp. 628-635.

Petukhov, B. S. (1970). Heat Transfer and Friction in Turbulent Pipe Flow with Variable Physical Properties. *Advances in Heat Transfer*. P. H. James and F. I. Thomas, Elsevier, Vol. Volume 6 pp. 503-564.

Reif-Acherman, S. (2012), "The Early Ice Making Systems in the Nineteenth Century," *International Journal of Refrigeration* Vol. 35(5) pp. 1224-1252.

Sardesai, R. G., R. G. Owen and D. J. Pulling (1981), "Flow Regimes for Condensation of a Vapour inside a Horizontal Tube," *Chemical Engineering Science* Vol. 36(7) pp. 1173-1180.

Shah, M. M. (1979), "A General Correlation for Heat Transfer During Film Condensation inside Pipes," *International Journal of Heat and Mass Transfer* Vol. 22 pp. 547-556.

Shah, M. M. (2009), "An Improved and Extended General Correlationfor Heat Transfer During Condensation in Plain Tubes," *HVAC&R Research* Vol. 15(5) pp. 889-913.

Shin, J. S. and M. H. Kim (2004), "An Experimental Study of Condensation Heat Transfer inside a Mini-Channel with a New Measurement Technique," *International Journal of Multiphase Flow* Vol. 30(3) pp. 311-325.

Sloan, M. and W. Wilczewski (2013). 2013 Propane Market Outlook. Propane Education and Research Council. Fairfax, VA, 25 p.

Soliman, H. M. (1986), "The Mist-Annular Transition During Condensation and Its Influence on the Heat Transfer Mechanism," *International Journal of Multiphase Flow* Vol. 12(2) pp. 277-288.

Soliman, H. M., J. R. Schuster and P. J. Berenson (1968), "A General Heat Transfer Correlation for Annular Flow Condensation," *Journal of Heat Transfer* Vol. 90 pp. 267-276.

Sparrow, E. M. and J. L. Gregg (1956), "Laminar-Free-Convection Heat Transfer from Outer Surface of Vertical Circular Cylinder," *American Society of Mechanical Engineers -- Transactions* Vol. 78(8) pp. 1823-1829.

Swagelok (2011). An Installer's Pocket Guide for Swagelok Tube Fittings. Solon, OH, 19 p.

Taborek, J. (1997), "Double-Pipe and Multitube Heat Exchangers with Plain and Longitudinal Finned Tubes," *Heat Transfer Engineering* Vol. 18(2) pp. 34-45.

Taitel, Y., D. Barnea and A. E. Dukler (1980), "Modelling Flow Pattern Transitions for Steady Upward Gas-Liquid Flow in Vertical Tubes," *AIChE Journal* Vol. 26(3) pp. 345-354.

Taitel, Y. and A. E. Dukler (1976), "A Model for Predicting Flow Regime Transitions in Horizontal and near Horizontal Gas-Liquid Flow," *AIChe Journal* Vol. 22(1) pp. 47-54.

Tandon, T. N., H. K. Varma and C. P. Gupta (1982), "A New Flow Regimes Map for Condensation inside Horizontal Tubes," *ASME Journal of Heat Transfer* Vol. 104(4) pp. 763-768.

Tandon, T. N., H. K. Varma and C. P. Gupta (1985), "Prediction of Flow Patterns During Condensation of Binary Mixtures in a Horizontal Tube," *Journal of Heat Transfer, Transactions ASME* Vol. 107(2) pp. 424-430.

Tang, L. (1997). *Empirical Study of New Refrigerant Flow Condensation inside Horizontal Smooth and Micro-Fin Tubes*. College Park, MD, University of Maryland, Vol. Ph.D.

Taylor, B. N. and C. E. Kuyatt (1994). Nat. Inst. Stand. & Technol., Washington, DC, USA, Copyright 1993, IEE, NIST/TN 1297, 15 p.

Thome, J. R. (2005), "Update on Advances in Flow Pattern Based Two-Phase Heat Transfer Models," *Experimental Thermal and Fluid Science* Vol. 29(3) pp. 341-349.

Traviss, D. P., W. M. Rohsenow and A. B. Baron (1973), "Forced-Convection Condensation inside Tubes: A Heat Transfer Equation for Condenser Design," *ASHRAE Transactions* Vol. 79(Part 1) pp. 157-165.

Triplett, K. A., S. M. Ghiaasiaan, S. I. Abdel-Khalik and D. L. Sadowski (1999), "Gas-Liquid Two-Phase Flow in Microchannels Part I: Two-Phase Flow Patterns," *International Journal of Multiphase Flow* Vol. 25(3) pp. 377-394.

von Kármán, T. (1930), "Mechanische Ähnlichkeit Und Turbulenz," *Nachrichten von der Gesellschaft der Wissenschaften zu Göttingen, Fachgruppe 1 (Mathematik)* Vol. 5 pp. 58-76.

Wang, W.-W. W., T. D. Radcliff and R. N. Christensen (2002), "A Condensation Heat Transfer Correlation for Millimeter-Scale Tubing with Flow Regime Transition," *Experimental Thermal and Fluid Science* Vol. 26(5) pp. 473-485.

Wen, M.-Y., C.-Y. Ho and J.-M. Hsieh (2006), "Condensation Heat Transfer and Pressure Drop Characteristics of R-290 (Propane), R-600 (Butane), and a Mixture of R-290/R-600 in the Serpentine Small-Tube Bank," *Applied Thermal Engineering* Vol. 26(16) pp. 2045-2053.

Winkler, J., J. Killion and S. Garimella (2012), "Void Fractions for Condensing Refrigerant Flow in Small Channels. Part Ii: Void Fraction Measurement and Modeling, Langford Lane, Kidlington, Oxford, OX5 1GB, United Kingdom, Elsevier Ltd, pp. 246-262.

Zhang, M. (1998). *A New Equivalent Reynolds Number Model for Vapor Shear-Controlled Condensation inside Smooth and Micro-Fin Tubes*. University Park, PA, The Pennsylvania State University, Vol. Ph.D.

Zhang, W., T. Hibiki and K. Mishima (2010), "Correlations of Two-Phase Frictional Pressure Drop and Void Fraction in Mini-Channel," *International Journal of Heat and Mass Transfer* Vol. 53(1-3) pp. 453-465.

Zivi, S. M. (1964), "Estimation of Steady-State Stream Void-Fraction by Means of the Principle of Minimum Entropy Production," *ASME Journal of Heat Transfer* Vol. 86 pp. 247-252.